

Formulation of the Finite Element Method— Linear Analysis in Solid and Structural Mechanics

4.1 INTRODUCTION

A very important application area for finite element analysis is the linear analysis of solids and structures. This is where the first practical finite element procedures were applied and where the finite element method has obtained its primary impetus of development.

Today many types of linear analyses of structures can be performed in a routine manner. Finite element discretization schemes are well established and are used in standard computer programs. However, there are two areas in which effective finite elements have been developed only recently, namely, the analysis of general plate and shell structures and the solution of (almost) incompressible media.

The standard formulation for the finite element solution of solids is the displacement method, which is widely used and effective except in these two areas of analysis. For the analysis of plate and shell structures and the solution of incompressible solids, mixed formulations are preferable.

In this chapter we introduce the displacement-based method of analysis in detail. The principle of virtual work is the basic relationship used for the finite element formulation. We first establish the governing finite element equations and then discuss the convergence properties of the method. Since the displacement-based solution is not effective for certain applications, we then introduce the use of mixed formulations in which not only the displacements are employed as unknown variables. The use of a mixed method, however, requires a careful selection of appropriate interpolations, and we address this issue in the last part of the chapter.

Various displacement-based and mixed formulations have been presented in the literature, and as pointed out before, our aim is not to survey all these formulations. Instead, we

will concentrate in this chapter on some important useful principles of formulating finite elements. Some efficient applications of the principles discussed in this chapter are then presented in Chapter 5.

4.2 FORMULATION OF THE DISPLACEMENT-BASED FINITE ELEMENT METHOD

The displacement-based finite element method can be regarded as an extension of the displacement method of analysis of beam and truss structures, and it is therefore valuable to review this analysis process. The basic steps in the analysis of a beam and truss structure using the displacement method are the following.

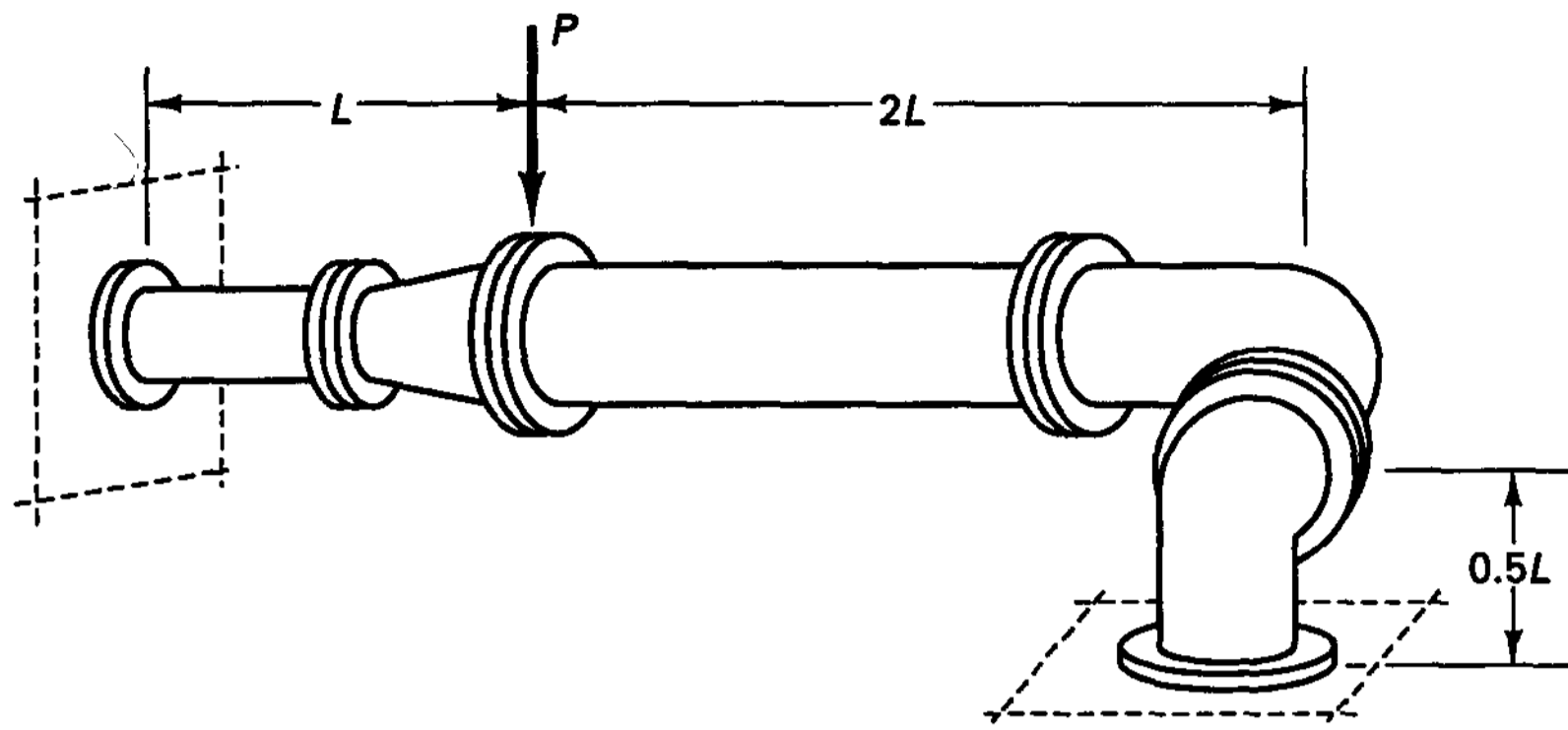
1. Idealize the total structure as an assemblage of beam and truss elements that are interconnected at structural joints.
2. Identify the unknown joint displacements that completely define the displacement response of the structural idealization.
3. Formulate force balance equations corresponding to the unknown joint displacements and solve these equations.
4. With the beam and truss element end displacements known, calculate the internal element stress distributions.
5. Interpret, based on the assumptions used, the displacements and stresses predicted by the solution of the structural idealization.

In practical analysis and design the most important steps of the complete analysis are the proper idealization of the actual problem, as performed in step 1, and the correct interpretation of the results, as in step 5. Depending on the complexity of the actual system to be analyzed, considerable knowledge of the characteristics of the system and its mechanical behavior may be required in order to establish an appropriate idealization, as briefly discussed in Chapter 1.

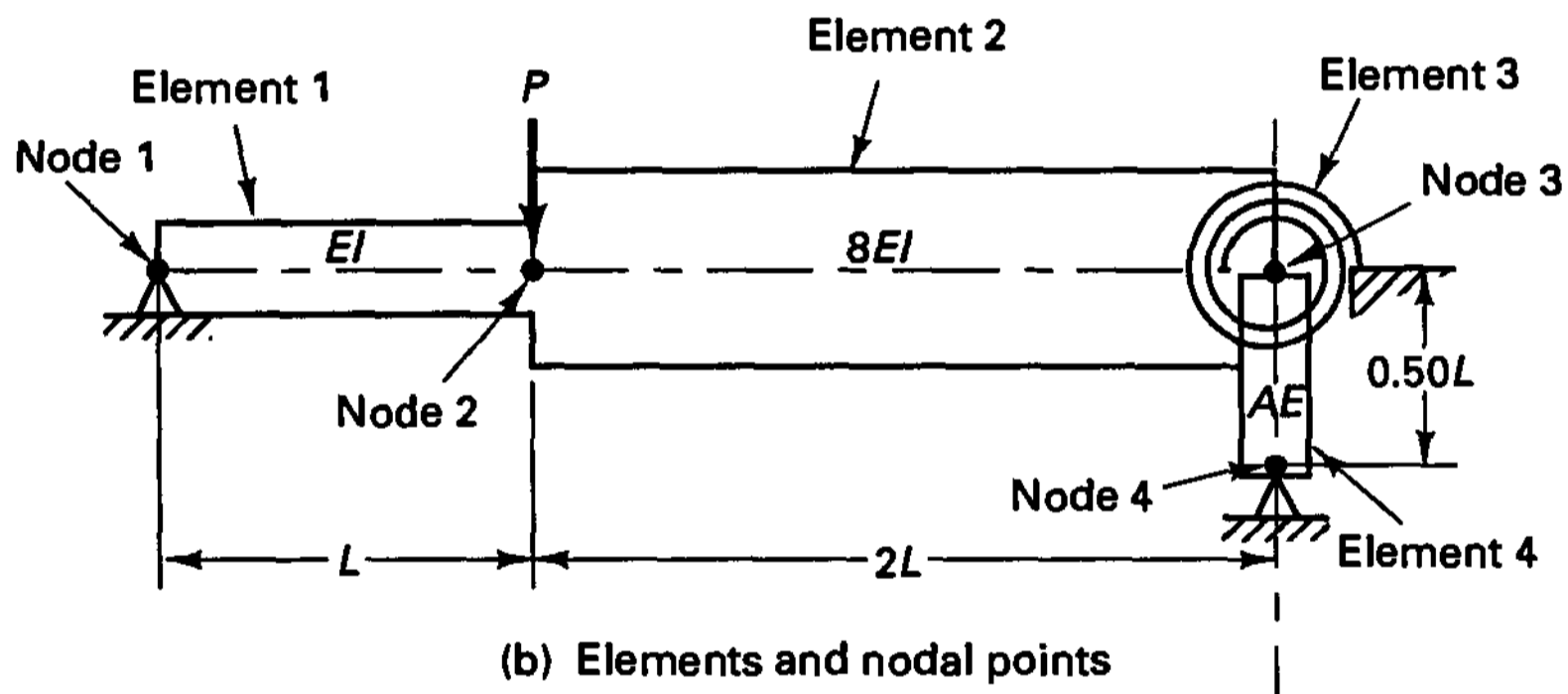
These analysis steps have already been demonstrated to some degree in Chapter 3, but it is instructive to consider another more complex example.

EXAMPLE 4.1: The piping system shown in Fig. E4.1(a) must be able to carry a large transverse load P applied accidentally to the flange connecting the small- and large-diameter pipes. “Analyze this problem.”

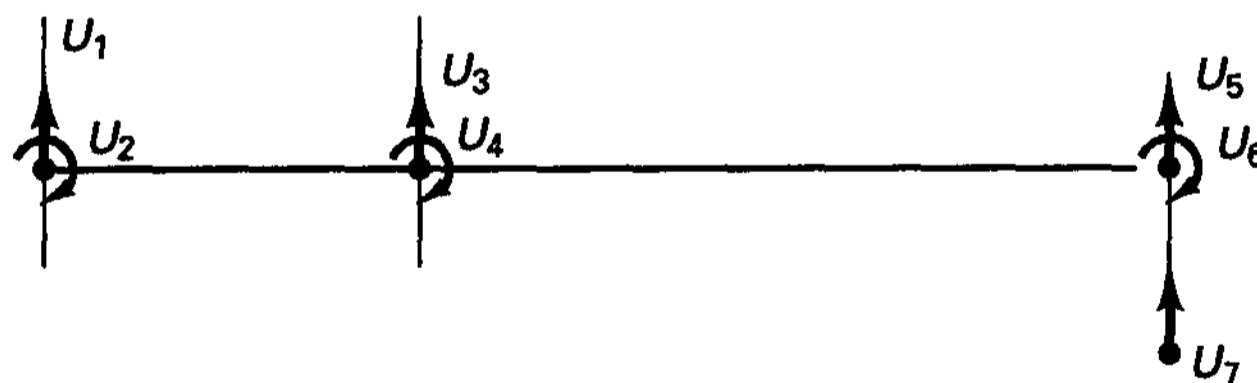
The study of this problem may require a number of analyses in which the local kinematic behavior of the pipe intersection is properly modeled, the nonlinear material and geometric behaviors are taken into account, the characteristics of the applied load are modeled accurately, and so on. In such a study, it is usually most expedient to start with a simple analysis in which gross assumptions are made and then work toward a more refined model as the need arises (see Section 6.8.1).



(a) Piping system



(b) Elements and nodal points



(c) Global degrees of freedom of unrestraint structure

Figure E4.1 Piping system and idealization

Assume that in a first analysis we primarily want to calculate the transverse displacement at the flange when the transverse load is applied slowly. In this case it is reasonable to model the structure as an assemblage of beam, truss, and spring elements and perform a static analysis.

The model chosen is shown in Fig. E4.1(b). The structural idealization consists of two beams, one truss, and a spring element. For the analysis of this idealization we first evaluate the element stiffness matrices that correspond to the global structural degrees of freedom shown in Fig. E4.1(c). For the beam, spring, and truss elements, respectively, we have in this case

$$\mathbf{K}_1^e = \frac{EI}{L} \begin{bmatrix} \frac{12}{L^2} & -\frac{6}{L} & -\frac{12}{L^2} & -\frac{6}{L} \\ & 4 & \frac{6}{L} & 2 \\ \text{symmetric} & & \frac{12}{L^2} & \frac{6}{L} \\ & & & 4 \end{bmatrix}; \quad U_1, U_2, U_3, U_4$$

$$\mathbf{K}_2^e = \frac{EI}{L} \begin{bmatrix} \frac{12}{L^2} & -\frac{12}{L} & -\frac{12}{L^2} & -\frac{12}{L} \\ & 16 & \frac{12}{L} & 8 \\ \text{symmetric} & & \frac{12}{L^2} & \frac{12}{L} \\ & & & 16 \end{bmatrix}; \quad U_3, U_4, U_5, U_6$$

$$\mathbf{K}_3^e = k_s; \quad U_6$$

$$\mathbf{K}_4^e = \frac{EA}{L} \begin{bmatrix} 2 & -2 \\ -2 & 2 \end{bmatrix}; \quad U_5, U_7$$

where the subscript on \mathbf{K}^e indicates the element number, and the global degrees of freedom that correspond to the element stiffnesses are written next to the matrices. It should be noted that in this example the element matrices are independent of direction cosines since the centerlines of the elements are aligned with the global axes. If the local axis of an element is not in the direction of a global axis, the local element stiffness matrix must be transformed to obtain the required global element stiffness matrix (see Example 4.10).

The stiffness matrix of the complete element assemblage is effectively obtained from the stiffness matrices of the individual elements using the *direct stiffness method* (see Examples 3.1 and 4.11). In this procedure the structure stiffness matrix \mathbf{K} is calculated by direct addition of the element stiffness matrices; i.e.,

$$\mathbf{K} = \sum_i \mathbf{K}_i^e$$

where the summation includes all elements. To perform the summation, each element matrix \mathbf{K}_i^e is written as a matrix $\mathbf{K}^{(i)}$ of the same order as the stiffness matrix \mathbf{K} , where all entries in $\mathbf{K}^{(i)}$ are zero except those which correspond to an element degree of freedom. For example, for element 4 we have

$$\mathbf{K}^{(4)} = \begin{matrix} & \begin{matrix} 1 & 2 & 3 & 4 & 5 & 6 & 7 \leftarrow \text{Degree of freedom} \end{matrix} \\ \begin{matrix} 1 \\ 2 \\ 3 \\ 4 \\ 5 \\ 6 \\ 7 \end{matrix} & \begin{bmatrix} 0 & 0 & 0 & 0 & 0 & 0 & 0 \\ 0 & 0 & 0 & 0 & 0 & 0 & 0 \\ 0 & 0 & 0 & 0 & 0 & 0 & 0 \\ 0 & 0 & 0 & 0 & 0 & 0 & 0 \\ 0 & 0 & 0 & 0 & \frac{2AE}{L} & 0 & -\frac{2EA}{L} \\ 0 & 0 & 0 & 0 & 0 & 0 & 0 \\ 0 & 0 & 0 & 0 & -\frac{2AE}{L} & 0 & \frac{2EA}{L} \end{bmatrix} \end{matrix}$$

Therefore, the stiffness matrix of the structure is

$$\mathbf{K} = \begin{bmatrix} \frac{12EI}{L^3} & -\frac{6EI}{L^2} & -\frac{12EI}{L^3} & -\frac{6EI}{L^2} & 0 & 0 & 0 \\ & \frac{4EI}{L} & \frac{6EI}{L^2} & \frac{2EI}{L} & 0 & 0 & 0 \\ & & \frac{24EI}{L^3} & -\frac{6EI}{L^2} & -\frac{12EI}{L^3} & -\frac{12EI}{L^2} & 0 \\ & & & \frac{20EI}{L} & \frac{12EI}{L^2} & \frac{8EI}{L} & 0 \\ & \text{symmetric} & & & \frac{12EI}{L^3} + \frac{2AE}{L} & \frac{12EI}{L^2} & -\frac{2AE}{L} \\ & & & & & \frac{16EI}{L} + k_s & 0 \\ & & & & & & \frac{2AE}{L} \end{bmatrix}$$

and the equilibrium equations for the system are

$$\mathbf{K}\mathbf{U} = \mathbf{R}$$

where \mathbf{U} is a vector of the system global displacements and \mathbf{R} is a vector of forces acting in the direction of these displacements:

$$\mathbf{U}^T = [U_1, \dots, U_7]; \quad \mathbf{R}^T = [R_1, \dots, R_7]$$

Before solving for the displacements of the structure, we need to impose the boundary conditions that $U_1 = 0$ and $U_7 = 0$. This means that we may consider only five equations in five unknown displacements; i.e.,

$$\tilde{\mathbf{K}}\tilde{\mathbf{U}} = \tilde{\mathbf{R}} \quad (\text{a})$$

where $\tilde{\mathbf{K}}$ is obtained by eliminating from \mathbf{K} the first and seventh rows and columns, and

$$\tilde{\mathbf{U}}^T = [U_2 \quad U_3 \quad U_4 \quad U_5 \quad U_6]; \quad \tilde{\mathbf{R}}^T = [0 \quad -P \quad 0 \quad 0 \quad 0]$$

The solution of (a) gives the structure displacements and therefore the element nodal point displacements. The element nodal forces are obtained by multiplying the element stiffness matrices \mathbf{K}_i^e by the element displacements. If the forces at any section of an element are required, we can evaluate them from the element end forces by use of simple statics.

Considering the analysis results it should be recognized, however, that although the structural idealization in Fig. E4.1(b) was analyzed accurately, *the displacements and stresses are only a prediction of the response of the actual physical structure*. Surely this prediction will be accurate only if the model used was appropriate, and in practice a specific model is in general adequate for predicting certain quantities but inadequate for predicting others. For instance, in this analysis the required transverse displacement under the applied load is quite likely predicted accurately using the idealization in Fig. E4.1(b) (provided the load is applied slowly enough, the stresses are small enough not to cause yielding, and so on), but the stresses directly under the load are probably predicted very inaccurately. Indeed, a different and more refined finite element model would need to be used in order to accurately calculate the stresses (see Section 1.2).

This example demonstrates some important aspects of the displacement method of analysis and the finite element method. As summarized previously, the basic process is that

the complete structure is idealized as an assemblage of individual structural elements. The element stiffness matrices corresponding to the global degrees of freedom of the structural idealization are calculated, and the total stiffness matrix is formed by the addition of the element stiffness matrices. The solution of the equilibrium equations of the assemblage of elements yields the element displacements, which are then used to calculate the element stresses. Finally, the element displacements and stresses must be interpreted as an estimate of the actual structural behavior, taking into account that a truss and beam idealization was solved.

Considering the analysis of truss and beam assemblages such as in Example 4.1, originally these solutions were not called finite element analyses because there is one major difference in these solutions when compared to a more general finite element analysis of a two- or three-dimensional problem, namely, in the analysis performed in Example 4.1 the exact element stiffness matrices (“exact” within beam theory) could be calculated. The stiffness properties of a beam element are physically the element end forces that correspond to unit element end displacements. These forces can be evaluated by solving the differential equations of equilibrium of the element when it is subjected to the appropriate boundary conditions. Since by virtue of the solution of the differential equations of equilibrium, all three requirements of an exact solution—namely, the stress equilibrium, the compatibility, and the constitutive requirements—throughout each element are fulfilled, the exact element internal displacements and stiffness matrices are calculated. In an alternative approach, these element end forces could also be evaluated by performing a variational solution based on the Ritz method or Galerkin method, as discussed in Section 3.3.4. Such solutions would give the exact element stiffness coefficients if the exact element internal displacements (as calculated in the solution of the differential equations of equilibrium) are used as trial functions (see Examples 3.22 and 4.8). However, approximate stiffness coefficients are obtained if other trial functions (which may be more suitable in practice) are employed.

When considering more general two- and three-dimensional finite element analyses, we use the variational approach with trial functions that approximate the actual displacements because we do not know the exact displacement functions as in the case of truss and beam elements. The result is that the differential equations of equilibrium are not satisfied in general, but this error is reduced as the finite element idealization of the structure or the continuum is refined.

The general formulation of the displacement-based finite element method is based on the use of the principle of virtual displacements which, as discussed in Section 3.3.4, is equivalent to the use of the Galerkin method, and also equivalent to the use of the Ritz method to minimize the total potential of the system.

4.2.1 General Derivation of Finite Element Equilibrium Equations

In this section we first state the general elasticity problem to be solved. We then discuss the principle of virtual displacements, which is used as the basis of our finite element solution, and we derive the finite element equations. Next we elaborate on some important considerations regarding the satisfaction of stress equilibrium, and finally we discuss some details of the process of assemblage of element matrices.

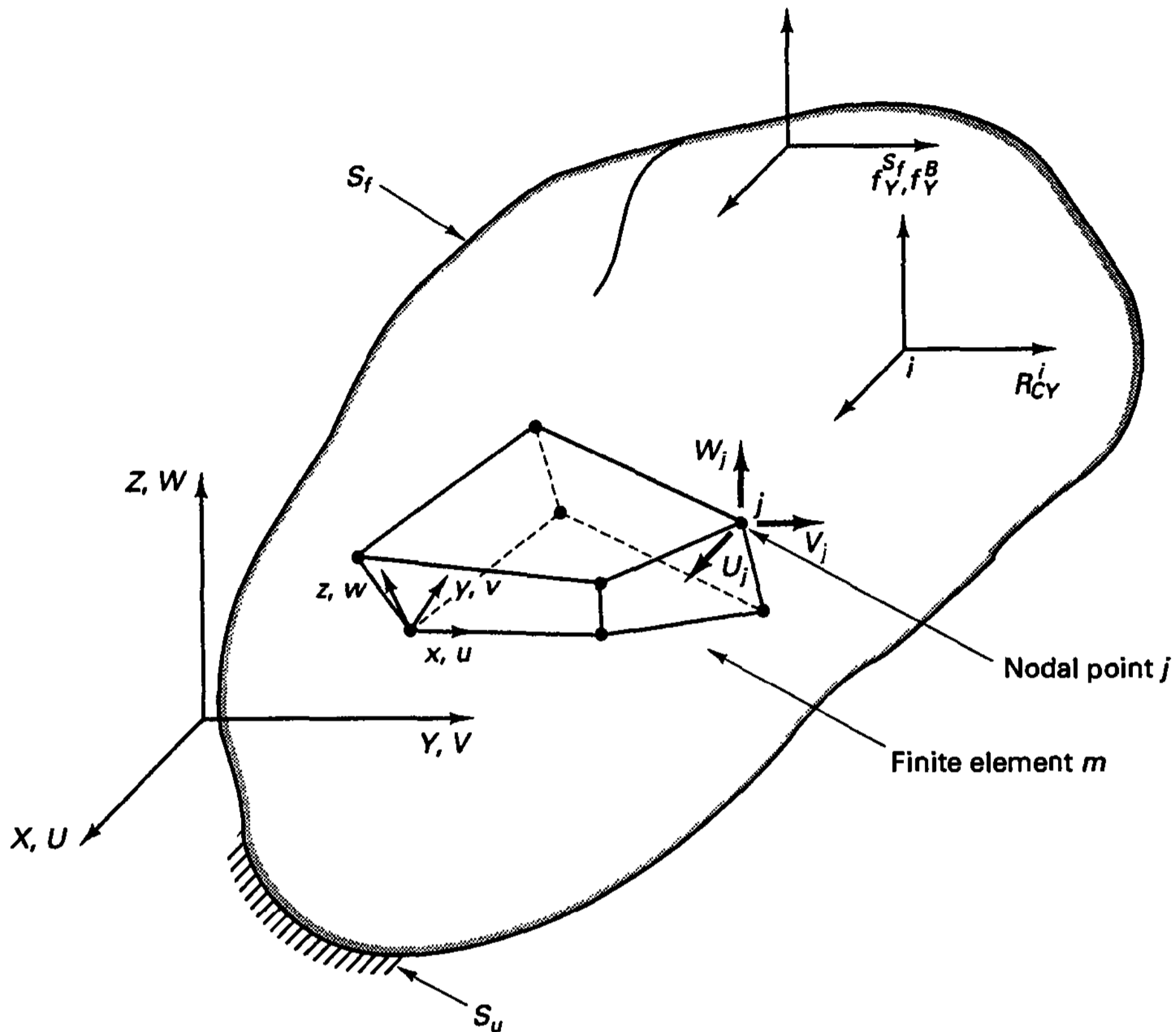


Figure 4.1 General three-dimensional body with an 8-node three-dimensional element

Problem Statement

Consider the equilibrium of a general three-dimensional body such as that shown in Fig. 4.1. The body is located in the fixed (stationary) coordinate system X, Y, Z . Considering the body surface area, the body is supported on the area S_u with prescribed displacements U^{S_u} and is subjected to surface tractions f^{S_f} (forces per unit surface area) on the surface area S_f .¹

¹ We may assume here, for simplicity, that all displacement components on S_u are prescribed, in which case $S_u \cup S_f = S$ and $S_u \cap S_f = 0$. However, in practice, it may well be that at a surface point the displacement(s) corresponding to some direction(s) is (are) imposed, while corresponding to the remaining direction(s) the force component(s) is (are) prescribed. For example, a roller boundary condition on a three-dimensional body would correspond to an imposed zero displacement only in the direction normal to the body surface, while tractions are applied (which are frequently zero) in the remaining directions tangential to the body surface. In such cases, the surface point would belong to S_u and S_f . However, later, in our finite element formulation, we shall first remove all displacement constraints (support conditions) and assume that the reactions are known, and thus consider $S_f = S$ and $S_u = 0$, and then, only after the derivation of the governing finite element equations, impose the displacement constraints. Hence, the assumption that all displacement components on S_u are prescribed may be used here for ease of exposition and does not in any way restrict our formulation.

In addition, the body is subjected to externally applied body forces \mathbf{f}^B (forces per unit volume) and concentrated loads \mathbf{R}_C^i (where i denotes the point of load application). We introduce the forces \mathbf{R}_C^i as separate quantities, although each such force could also be considered surface tractions \mathbf{f}^{S_f} over a very small area (which would usually model the actual physical situation more accurately). In general, the externally applied forces have three components corresponding to the X, Y, Z coordinate axes:

$$\mathbf{f}^B = \begin{bmatrix} f_X^B \\ f_Y^B \\ f_Z^B \end{bmatrix}; \quad \mathbf{f}^{S_f} = \begin{bmatrix} f_X^{S_f} \\ f_Y^{S_f} \\ f_Z^{S_f} \end{bmatrix}; \quad \mathbf{R}_C^i = \begin{bmatrix} R_{CX}^i \\ R_{CY}^i \\ R_{CZ}^i \end{bmatrix} \quad (4.1)$$

where we note that the components of \mathbf{f}^B and \mathbf{f}^{S_f} vary as a function of X, Y, Z (and for \mathbf{f}^{S_f} the specific X, Y, Z coordinates of S_f are considered).

The displacements of the body from the unloaded configuration are measured in the coordinate system X, Y, Z and are denoted by \mathbf{U} , where

$$\mathbf{U}(X, Y, Z) = \begin{bmatrix} U \\ V \\ W \end{bmatrix} \quad (4.2)$$

and $\mathbf{U} = \mathbf{U}^{S_u}$ on the surface area S_u . The strains corresponding to \mathbf{U} are

$$\boldsymbol{\epsilon}^T = [\epsilon_{XX} \quad \epsilon_{YY} \quad \epsilon_{ZZ} \quad \gamma_{XY} \quad \gamma_{YZ} \quad \gamma_{ZX}] \quad (4.3)$$

where

$$\epsilon_{XX} = \frac{\partial U}{\partial X}; \quad \epsilon_{YY} = \frac{\partial V}{\partial Y}; \quad \epsilon_{ZZ} = \frac{\partial W}{\partial Z} \quad (4.4)$$

$$\gamma_{XY} = \frac{\partial U}{\partial Y} + \frac{\partial V}{\partial X}; \quad \gamma_{YZ} = \frac{\partial V}{\partial Z} + \frac{\partial W}{\partial Y}; \quad \gamma_{ZX} = \frac{\partial W}{\partial X} + \frac{\partial U}{\partial Z}$$

The stresses corresponding to $\boldsymbol{\epsilon}$ are

$$\boldsymbol{\tau}^T = [\tau_{XX} \quad \tau_{YY} \quad \tau_{ZZ} \quad \tau_{XY} \quad \tau_{YZ} \quad \tau_{ZX}] \quad (4.5)$$

where

$$\boldsymbol{\tau} = \mathbf{C}\boldsymbol{\epsilon} + \boldsymbol{\tau}^I \quad (4.6)$$

In (4.6), \mathbf{C} is the stress-strain material matrix and the vector $\boldsymbol{\tau}^I$ denotes given initial stresses [with components ordered as in (4.5)].

The analysis problem is now the following.

Given

the geometry of the body, the applied loads $\mathbf{f}^{S_f}, \mathbf{f}^B, \mathbf{R}_C^i, i = 1, 2, \dots$, the support conditions on S_u , the material stress-strain law, and the initial stresses in the body.

Calculate

the displacements \mathbf{U} of the body and the corresponding strains $\boldsymbol{\epsilon}$ and stresses $\boldsymbol{\tau}$.

In the problem solution considered here, we assume linear analysis conditions, which require that

The displacements be infinitesimally small so that (4.4) is valid and the equilibrium of the body can be established (and is solved for) with respect to its unloaded configuration.

The stress-strain material matrix can vary as a function of X, Y, Z but is constant otherwise (e.g., \mathbf{C} does not depend on the stress state).

We consider nonlinear analysis conditions in which one or more of these assumptions are not satisfied in Chapters 6 and 7.

To calculate the response of the body, we could establish the governing differential equations of equilibrium, which then would have to be solved subject to the boundary conditions (see Section 3.3). However, closed-form analytical solutions are possible only when relatively simple geometries are considered.

The Principle of Virtual Displacements

The basis of the displacement-based finite element solution is the principle of virtual displacements (which we also call the principle of virtual work). This principle states that the equilibrium of the body in Fig. 4.1 requires that for any compatible small² virtual displacements (which are zero at and corresponding to the prescribed displacements)³ imposed on the body in its state of equilibrium, the total internal virtual work is equal to the total external virtual work:

Internal virtual work	External virtual work \mathcal{R}
$\int_V \bar{\boldsymbol{\epsilon}}^T \boldsymbol{\tau} dV$	$= \int_V \bar{\mathbf{U}}^T \mathbf{f}^B dV + \int_{S_f} \bar{\mathbf{U}}^{S_f T} \mathbf{f}^{S_f} dS + \sum_i \bar{\mathbf{U}}^{i T} \mathbf{R}_c^i$
\uparrow Virtual strains corresponding to virtual displacements $\bar{\mathbf{U}}$	\uparrow Stresses in equilibrium with applied loads

(4.7)

where the $\bar{\mathbf{U}}$ are the virtual displacements and the $\bar{\boldsymbol{\epsilon}}$ are the *corresponding* virtual strains (the overbar denoting virtual quantities).

The adjective “virtual” denotes that the virtual displacements (and corresponding virtual strains) are not “real” displacements which the body actually undergoes as a consequence of the loading on the body. Instead, the virtual displacements are totally independent

² We stipulate here that the virtual displacements be “small” because the virtual strains corresponding to these displacements are calculated using the small strain measure (see Example 4.2). Actually, provided this small strain measure is used, the virtual displacements can be of any magnitude and indeed we later on choose convenient magnitudes for solution.

³ We use the wording “at and corresponding to the prescribed displacements” to mean “at the points and surfaces and corresponding to the components of displacements that are prescribed at those points and surfaces.”

from the actual displacements and are used by the analyst in a thought experiment to establish the integral equilibrium equation in (4.7).

Let us emphasize that in (4.7),

The stresses $\boldsymbol{\tau}$ are assumed to be known quantities and are the unique stresses⁴ that exactly balance the applied loads.

The virtual strains $\bar{\boldsymbol{\epsilon}}$ are calculated by the differentiations given in (4.4) from the assumed virtual displacements $\bar{\mathbf{U}}$.

The virtual displacements $\bar{\mathbf{U}}$ must represent a continuous virtual displacement field (to be able to evaluate $\bar{\boldsymbol{\epsilon}}$), with $\bar{\mathbf{U}}$ equal to zero at and corresponding to the prescribed displacements on S_u ; also, the components in $\bar{\mathbf{U}}^{S_f}$ are simply the virtual displacements $\bar{\mathbf{U}}$ evaluated on the surface S_f .

All integrations are performed over the original volume and surface area of the body, unaffected by the imposed virtual displacements.

To exemplify the use of the principle of virtual displacements, assume that we believe (but are not sure) to have been given the exact solution displacement field of the body. This given displacement field is continuous and satisfies the displacement boundary conditions on S_u . Then we can calculate $\boldsymbol{\epsilon}$ and $\boldsymbol{\tau}$ (corresponding to this displacement field). The vector $\boldsymbol{\tau}$ lists the correct stresses if and only if the equation (4.7) holds for any arbitrary virtual displacements $\bar{\mathbf{U}}$ that are continuous and zero at and corresponding to the prescribed displacements on S_u . In other words, if we can pick one virtual displacement field $\bar{\mathbf{U}}$ for which the relation in (4.7) is not satisfied, then this is proof that $\boldsymbol{\tau}$ is not the correct stress vector (and hence the given displacement field is not the exact solution displacement field).

We derive and demonstrate the principle of virtual displacements in the following examples.

EXAMPLE 4.2: Derive the principle of virtual displacements for the general three-dimensional body in Fig. 4.1.

To simplify the presentation we use indicial notation with the summation convention (see Section 2.4), with x_i denoting the i th coordinate axis ($x_1 \equiv X, x_2 \equiv Y, x_3 \equiv Z$), u_i denoting the i th displacement component ($u_1 \equiv U, u_2 \equiv V, u_3 \equiv W$), and a comma denoting differentiation.

The given displacement boundary conditions are $u_i^{S_u}$ on S_u , and let us assume that we have no concentrated surface loads, that is, all surface loads are contained in the components $f_i^{S_f}$.

The solution to the problem must satisfy the following differential equations (see, for example, S. Timoshenko and J. N. Goodier [A]):

$$\tau_{ij,j} + f_i^B = 0 \quad \text{throughout the body} \quad (a)$$

with the natural (force) boundary conditions

$$\tau_{ij}n_j = f_i^{S_f} \quad \text{on } S_f \quad (b)$$

and the essential (displacement) boundary conditions

$$u_i = u_i^{S_u} \quad \text{on } S_u \quad (c)$$

where $S = S_u \cup S_f, S_u \cap S_f = \emptyset$, and the n_j are the components of the unit normal vector to the surface S of the body.

⁴For a proof that these stresses are unique, see Section 4.3.4.

Consider now *any* arbitrarily chosen continuous displacements \bar{u}_i satisfying

$$\bar{u}_i = 0 \quad \text{on } S_u \quad (\text{d})$$

Then

$$(\tau_{ij,j} + f_i^p)\bar{u}_i = 0$$

and therefore,

$$\int_V (\tau_{ij,j} + f_i^p)\bar{u}_i dV = 0 \quad (\text{e})$$

We call the \bar{u}_i *virtual displacements*. Note that since the \bar{u}_i are arbitrary, (e) can be satisfied if (and only if) the quantity in the parentheses vanishes. Hence (e) is equivalent to (a).

Using the mathematical identity $(\tau_{ij}\bar{u}_i)_{,j} = \tau_{ij,j}\bar{u}_i + \tau_{ij}\bar{u}_{i,j}$, we obtain from (e),

$$\int_V [(\tau_{ij}\bar{u}_i)_{,j} - \tau_{ij}\bar{u}_{i,j} + f_i^p\bar{u}_i] dV = 0$$

Next, using the identity $\int_V (\tau_{ij}\bar{u}_i)_{,j} dV = \int_S (\tau_{ij}\bar{u}_i)n_j dS$, which follows from the divergence theorem⁵ (see, for example, G. B. Thomas and R. L. Finney [A]), we have

$$\int_V (-\tau_{ij}\bar{u}_{i,j} + f_i^p\bar{u}_i) dV + \int_S (\tau_{ij}\bar{u}_i)n_j dS = 0 \quad (\text{f})$$

In light of (b) and (d), we obtain

$$\int_V (-\tau_{ij}\bar{u}_{i,j} + f_i^p\bar{u}_i) dV + \int_{S_f} f_i^{sf}\bar{u}_i^{sf} dS = 0 \quad (\text{g})$$

Also, because of the symmetry of the stress tensor ($\tau_{ij} = \tau_{ji}$), we have

$$\tau_{ij}\bar{u}_{i,j} = \tau_{ij}\left[\frac{1}{2}(\bar{u}_{i,j} + \bar{u}_{j,i})\right] = \tau_{ij}\bar{\epsilon}_{ij}$$

and hence we obtain from (g) the required result, (4.7),

$$\int_V \tau_{ij}\bar{\epsilon}_{ij} dV = \int_V f_i^p\bar{u}_i dV + \int_{S_f} f_i^{sf}\bar{u}_i^{sf} dS \quad (\text{h})$$

Note that in (h) we use the tensor notation for the strains; hence, the engineering shear strains used in (4.7) are obtained by adding the appropriate tensor shear strain components, e.g., $\bar{\gamma}_{XY} = \bar{\epsilon}_{12} + \bar{\epsilon}_{21}$. Also note that by using (b) [and (d)] in (f), we explicitly introduced the natural boundary conditions into the principle of virtual displacements (h).

EXAMPLE 4.3: Consider the bar shown in Figure E4.3.

- (a) Specialize the equation of the principle of virtual displacements (4.7) to this problem.
- (b) Solve for the exact response of the mechanical model.
- (c) Show that for the exact displacement response the principle of virtual displacements is satisfied with the displacement patterns (i) $\bar{u} = ax$ and (ii) $\bar{u} = ax^2$, where a is a constant.
- (d) Assume that the stress solution is

$$\tau_{xx} = \frac{F}{\frac{3}{2}A_0}$$

⁵The divergence theorem states: Let \mathbf{F} be a vector field in volume V ; then

$$\int_V F_{i,i} dV = \int_S \mathbf{F} \cdot \mathbf{n} dS$$

where \mathbf{n} is the unit outward normal on the surface S of V .

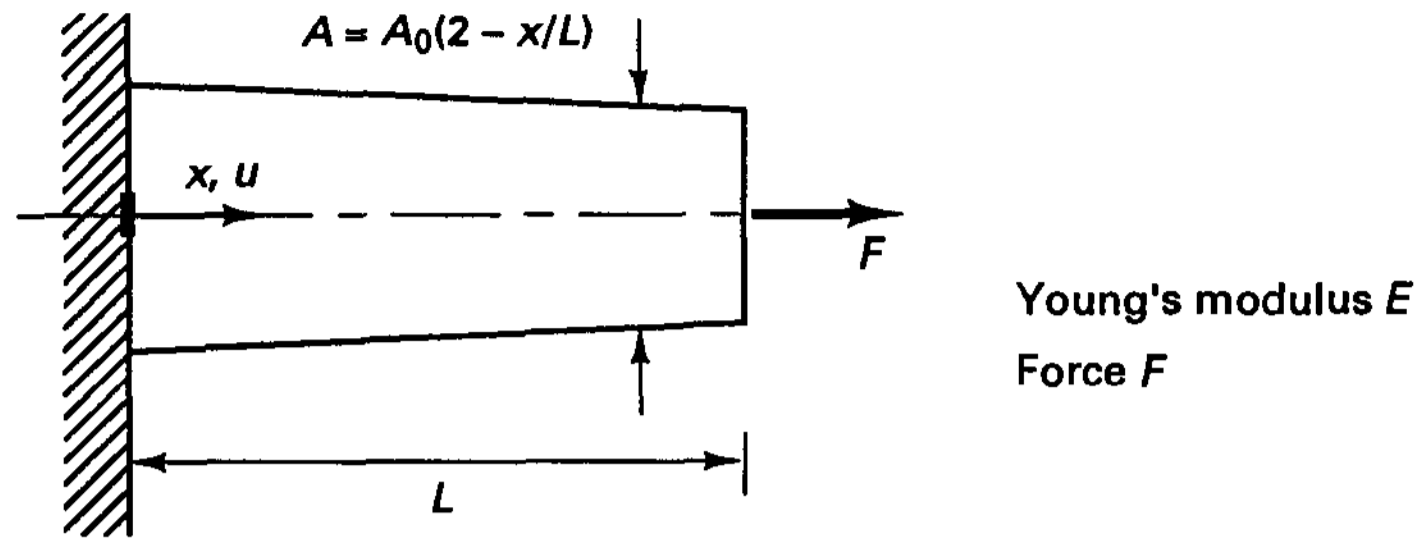


Figure E4.3 Bar subjected to concentrated load F

i.e., that τ_{xx} is the force F divided by the average cross-sectional area, and investigate whether the principle of virtual displacements is satisfied for the displacement patterns given in (c).

The principle of virtual displacements (4.7) specialized to this bar problem gives

$$\int_0^L \frac{d\bar{u}}{dx} EA \frac{du}{dx} dx = \bar{u} \Big|_{x=L} F \tag{a}$$

The governing differential equations are obtained using integration by parts (see Example 3.19):

$$\bar{u} EA \frac{du}{dx} \Big|_0^L - \int_0^L \bar{u} \frac{d}{dx} \left(EA \frac{du}{dx} \right) dx = \bar{u} \Big|_{x=L} F \tag{b}$$

Since $\bar{u}|_{x=0} = 0$ and \bar{u} is arbitrary otherwise, we obtain from (b) (see Example 3.18 for the arguments used),

$$\frac{d}{dx} \left(EA \frac{du}{dx} \right) = 0 \quad \text{differential equation of equilibrium} \tag{c}$$

$$EA \frac{du}{dx} \Big|_{x=L} = F \quad \text{force or natural boundary condition} \tag{d}$$

Of course, in addition we have the displacement boundary condition $u|_{x=0} = 0$. Integrating (c) and using the boundary conditions, we obtain as the exact solution of the mathematical model,

$$u = \frac{FL}{EA_0} \ln \left(\frac{2}{2 - x/L} \right) \tag{e}$$

Next, using (e) and $\bar{u} = ax$ and $\bar{u} = ax^2$ in equation (a), we obtain

$$\int_0^L a \frac{F}{A_0(2 - x/L)} A_0 \left(2 - \frac{x}{L} \right) dx = aLF \tag{f}$$

and

$$\int_0^L 2ax \frac{F}{A_0(2 - x/L)} A_0 \left(2 - \frac{x}{L} \right) dx = aL^2F \tag{g}$$

Equations (f) and (g) show that for the exact displacement /stress response the principle of virtual displacements is satisfied with the assumed virtual displacements.

Now let us employ the principle of virtual displacements with $\tau_{xx} = \frac{2}{3}(F/A_0)$ and use first $\bar{u} = ax$ and then $\bar{u} = ax^2$. We obtain with $\bar{u} = ax$,

$$\int_0^L a \frac{2}{3} \frac{F}{A_0} A_0 \left(2 - \frac{x}{L}\right) dx = aLF$$

which shows that the principle of virtual displacements is satisfied with this virtual displacement field. For $\bar{u} = ax^2$, we obtain

$$\int_0^L 2ax \frac{2}{3} \frac{F}{A_0} A_0 \left(2 - \frac{x}{L}\right) dx \neq aL^2F$$

and this equation shows that $\tau_{xx} = \frac{2}{3}(F/A_0)$ is not the correct stress solution.

The principle of virtual displacements can be directly related to the principle that the total potential Π of the system must be stationary (see Sections 3.3.2 and 3.3.4). We study this relationship in the following example.

EXAMPLE 4.4: Show how for a linear elastic continuum the principle of virtual displacements relates to the principle of stationarity of the total potential.

Assuming a linear elastic continuum with zero initial stresses, the total potential of the body in Fig. 4.1 is

$$\Pi = \frac{1}{2} \int_V \boldsymbol{\epsilon}^T \mathbf{C} \boldsymbol{\epsilon} dV - \int_V \mathbf{U}^T \mathbf{f}^B dV - \int_{S_f} \mathbf{U}^{S_f T} \mathbf{f}^{S_f} dS - \sum_i \mathbf{U}^{i T} \mathbf{R}_C^i \quad (a)$$

where the notation was defined earlier, and we have

$$\boldsymbol{\tau} = \mathbf{C} \boldsymbol{\epsilon}$$

with \mathbf{C} the stress-strain matrix of the material.

Invoking the stationarity of Π , i.e., evaluating $\delta\Pi = 0$ with respect to the displacements (which now appear in the strains) and using the fact that \mathbf{C} is symmetric, we obtain

$$\int_V \delta \boldsymbol{\epsilon}^T \mathbf{C} \boldsymbol{\epsilon} dV = \int_V \delta \mathbf{U}^T \mathbf{f}^B dV + \int_{S_f} \delta \mathbf{U}^{S_f T} \mathbf{f}^{S_f} dS + \sum_i \delta \mathbf{U}^{i T} \mathbf{R}_C^i \quad (b)$$

However, to evaluate Π in (a) the displacements must satisfy the displacement boundary conditions. Hence in (b) we consider any variations on the displacements but with zero values at and corresponding to the displacement boundary conditions, and the corresponding variations in strains. It follows that invoking the stationarity of Π is equivalent to using the principle of virtual displacements, and indeed we may write

$$\delta \boldsymbol{\epsilon} \equiv \bar{\boldsymbol{\epsilon}}; \quad \delta \mathbf{U} \equiv \bar{\mathbf{U}}; \quad \delta \mathbf{U}^{S_f} \equiv \bar{\mathbf{U}}^{S_f}; \quad \delta \mathbf{U}^i \equiv \bar{\mathbf{U}}^i$$

so that (b) reduces to (4.7).

It is important to realize that when the principle of virtual displacements (4.7) is satisfied for all admissible virtual displacements with the stresses $\boldsymbol{\tau}$ “properly obtained” from a continuous displacement field \mathbf{U} that satisfies the displacement boundary conditions on S_u , all three fundamental requirements of mechanics are fulfilled:

1. *Equilibrium* holds because the principle of virtual displacements is an expression of equilibrium as shown in Example 4.2.

2. *Compatibility* holds because the displacement field \mathbf{U} is continuous and satisfies the displacement boundary conditions.
3. *The stress-strain law* holds because the stresses $\boldsymbol{\tau}$ have been calculated using the constitutive relationships from the strains $\boldsymbol{\epsilon}$ (which have been evaluated from the displacements \mathbf{U}).

So far we have assumed that the body being considered is properly supported, i.e., that there are sufficient support conditions for a unique displacement solution. However, the principle of virtual displacements also holds when all displacement supports are removed and the correct reactions (then assumed known) are applied instead. In this case the surface area S_f on which known tractions are applied is equal to the complete surface area S of the body (and S_u is zero)⁶. We use this basic observation in developing the governing finite element equations. That is, it is conceptually expedient to first not consider any displacement boundary conditions, develop the governing finite element equations accordingly, and then prior to solving these equations impose all displacement boundary conditions.

Finite Element Equations

Let us now derive the governing finite element equations. We first consider the response of the general three-dimensional body shown in Fig. 4.1 and later specialize this general formulation to specific problems (see Section 4.2.3).

In the finite element analysis we approximate the body in Fig. 4.1 as an assemblage of discrete finite elements interconnected at nodal points on the element boundaries. The displacements measured in a local coordinate system x, y, z (to be chosen conveniently) within each element are assumed to be a function of the displacements at the N finite element nodal points. Therefore, for element m we have

$$\mathbf{u}^{(m)}(x, y, z) = \mathbf{H}^{(m)}(x, y, z) \hat{\mathbf{U}} \quad (4.8)$$

where $\mathbf{H}^{(m)}$ is the displacement interpolation matrix, the superscript m denotes element m , and $\hat{\mathbf{U}}$ is a vector of the three global displacement components $U_i, V_i,$ and W_i at all nodal points, including those at the supports of the element assemblage; i.e., $\hat{\mathbf{U}}$ is a vector of dimension $3N$,

$$\hat{\mathbf{U}}^T = [U_1 \ V_1 \ W_1 \ U_2 \ V_2 \ W_2 \ \dots \ U_N \ V_N \ W_N] \quad (4.9)$$

We may note here that more generally, we write

$$\hat{\mathbf{U}}^T = [U_1 \ U_2 \ U_3 \ \dots \ U_n] \quad (4.10)$$

where it is understood that U_i may correspond to a displacement in any direction $X, Y,$ or Z , or even in a direction not aligned with these coordinate axes (but aligned with the axes of another local coordinate system), and may also signify a rotation when we consider beams, plates, or shells (see Section 4.2.3). Since $\hat{\mathbf{U}}$ includes the displacements (and rota-

⁶For this reason, and for ease of notation, we shall now mostly (i.e., until Section 4.4.2) no longer use the superscripts S_f and S_u but simply the superscript S on the surface tractions and displacements.

tions) at the supports of the element assemblage, we need to impose, at a later time, the known values of $\hat{\mathbf{U}}$ prior to solving for the unknown nodal point displacements.

Figure 4.1 shows a typical finite element of the assemblage. This element has eight nodal points, one at each of its corners, and can be thought of as a "brick" element. We should imagine that the complete body is represented as an assemblage of such brick elements put together so as to not leave any gaps between the element domains. We show this element here merely as an example; in practice, elements of different geometries and nodal points on faces and in the element interiors may be used.

The choice of element and the construction of the corresponding entries in $\mathbf{H}^{(m)}$ (which depend on the element geometry, the number of element nodes/degrees of freedom, and convergence requirements) constitute the basic steps of a finite element solution and are discussed in detail later.

Although all nodal point displacements are listed in $\hat{\mathbf{U}}$, it should be realized that for a given element only the displacements at the nodes of the element affect the displacement and strain distributions within the element.

With the assumption on the displacements in (4.8) we can now evaluate the corresponding element strains,

$$\boxed{\boldsymbol{\epsilon}^{(m)}(x, y, z) = \mathbf{B}^{(m)}(x, y, z)\hat{\mathbf{U}}} \quad (4.11)$$

where $\mathbf{B}^{(m)}$ is the strain-displacement matrix; the rows of $\mathbf{B}^{(m)}$ are obtained by appropriately differentiating and combining rows of the matrix $\mathbf{H}^{(m)}$.

The purpose of defining the element displacements and strains in terms of the complete array of finite element assemblage nodal point displacements may not be obvious now. However, we will see that by proceeding in this way, the use of (4.8) and (4.11) in the principle of virtual displacements will automatically lead to an effective assemblage process of all element matrices into the governing structure matrices. This assemblage process is referred to as the direct stiffness method.

The stresses in a finite element are related to the element strains and the element initial stresses using

$$\boxed{\boldsymbol{\tau}^{(m)} = \mathbf{C}^{(m)}\boldsymbol{\epsilon}^{(m)} + \boldsymbol{\tau}^{I(m)}} \quad (4.12)$$

where $\mathbf{C}^{(m)}$ is the elasticity matrix of element m and $\boldsymbol{\tau}^{I(m)}$ are the given element initial stresses. The material law specified in $\mathbf{C}^{(m)}$ for each element can be that for an isotropic or an anisotropic material and can vary from element to element.

Using the assumption on the displacements within each finite element, as expressed in (4.8), we can now derive equilibrium equations that correspond to the nodal point displacements of the assemblage of finite elements. First, we rewrite (4.7) as a sum of integrations over the volume and areas of all finite elements:

$$\begin{aligned} \sum_m \int_{V^{(m)}} \bar{\boldsymbol{\epsilon}}^{(m)T} \boldsymbol{\tau}^{(m)} dV^{(m)} &= \sum_m \int_{V^{(m)}} \bar{\mathbf{u}}^{(m)T} \mathbf{f}^{B(m)} dV^{(m)} \\ &+ \sum_m \int_{S_1^{(m)}, \dots, S_q^{(m)}} \bar{\mathbf{u}}^{S(m)T} \mathbf{f}^{S(m)} dS^{(m)} + \sum_i \bar{\mathbf{u}}^i T \mathbf{R}_C^i \end{aligned} \quad (4.13)$$

where $m = 1, 2, \dots, k$, where $k =$ number of elements and $S_1^{(m)}, \dots, S_q^{(m)}$ denotes the element surfaces that are part of the body surface S . For elements totally surrounded by other elements no such surfaces exist, whereas for elements on the surface of the body one or more such element surfaces are included in the surface force integral. Note that we assume in (4.13) that nodal points have been placed at the points where concentrated loads are applied, although a concentrated load can of course also be included in the surface force integrals.

It is important to note that *since the integrations in (4.13) are performed over the element volumes and surfaces, for efficiency we may use a different and any convenient coordinate system for each element in the calculations.* After all, for a given virtual displacement field, the internal virtual work is a number, as is the external virtual work, and this number can be evaluated by integrations in any coordinate system. Of course, it is assumed that for each integral in (4.13) only a single coordinate system for all variables is employed; e.g., $\bar{\mathbf{u}}^{(m)}$ is defined in the same coordinate system as $\mathbf{f}^{B(m)}$. The use of different coordinate systems is in essence the reason why each of the integrals can be evaluated very effectively in general element assemblages.

The relations in (4.8) and (4.11) have been given for the unknown (real) element displacements and strains. In our use of the principle of virtual displacements we employ the same assumptions for the virtual displacements and strains

$$\boxed{\bar{\mathbf{u}}^{(m)}(x, y, z) = \mathbf{H}^{(m)}(x, y, z)\bar{\hat{\mathbf{U}}}} \quad (4.14)$$

$$\boxed{\bar{\boldsymbol{\epsilon}}^{(m)}(x, y, z) = \mathbf{B}^{(m)}(x, y, z)\bar{\hat{\mathbf{U}}}} \quad (4.15)$$

In this way the element stiffness (and mass) matrices will be *symmetric* matrices.

If we now substitute into (4.13), we obtain

$$\begin{aligned} \bar{\hat{\mathbf{U}}}^T \left[\sum_m \int_{V^{(m)}} \mathbf{B}^{(m)T} \mathbf{C}^{(m)} \mathbf{B}^{(m)} dV^{(m)} \right] \hat{\mathbf{U}} = & \bar{\hat{\mathbf{U}}}^T \left[\left\{ \sum_m \int_{V^{(m)}} \mathbf{H}^{(m)T} \mathbf{f}^{B(m)} dV^{(m)} \right\} \right. \\ & + \left\{ \sum_m \int_{S_1^{(m)}, \dots, S_q^{(m)}} \mathbf{H}^{S(m)T} \mathbf{f}^{S(m)} dS^{(m)} \right\} \\ & \left. - \left\{ \sum_m \int_{V^{(m)}} \mathbf{B}^{(m)T} \boldsymbol{\tau}^{I(m)} dV^{(m)} \right\} + \mathbf{R}_C \right] \end{aligned} \quad (4.16)$$

where the surface displacement interpolation matrices $\mathbf{H}^{S(m)}$ are obtained from the displacement interpolation matrices $\mathbf{H}^{(m)}$ in (4.8) by substituting the appropriate element surface coordinates (see Examples 4.7 and 5.12) and \mathbf{R}_C is a vector of concentrated loads applied to the nodes of the element assemblage.

We should note that the i th component in \mathbf{R}_C is the concentrated nodal force that corresponds to the i th displacement component in $\hat{\mathbf{U}}$. In (4.16) the nodal point displacement vectors $\hat{\mathbf{U}}$ and $\bar{\hat{\mathbf{U}}}$ of the element assemblage are independent of element m and are therefore taken out of the summation signs.

To obtain from (4.16) the equations for the unknown nodal point displacements, we apply the principle of virtual displacements n times by imposing unit virtual displacements

in turn for all components of $\hat{\mathbf{U}}$. In the first application $\hat{\mathbf{U}} = \mathbf{e}_1$,⁷ in the second application $\hat{\mathbf{U}} = \mathbf{e}_2$, and so on, until in the n th application $\hat{\mathbf{U}} = \mathbf{e}_n$, so that the result is

$$\boxed{\mathbf{KU} = \mathbf{R}} \quad (4.17)$$

where we do not show the identity matrices \mathbf{I} due to the virtual displacements on each side of the equation and

$$\boxed{\mathbf{R} = \mathbf{R}_B + \mathbf{R}_S - \mathbf{R}_I + \mathbf{R}_C} \quad (4.18)$$

and, as we shall do from now on, we denote the unknown nodal point displacements as \mathbf{U} ; i.e., $\mathbf{U} \equiv \hat{\mathbf{U}}$.

The matrix \mathbf{K} is the stiffness matrix of the element assemblage,

$$\boxed{\mathbf{K} = \sum_m \int_{V^{(m)}} \underbrace{\mathbf{B}^{(m)T} \mathbf{C}^{(m)} \mathbf{B}^{(m)}}_{= \mathbf{K}^{(m)}} dV^{(m)}} \quad (4.19)$$

The load vector \mathbf{R} includes the effect of the element body forces,

$$\boxed{\mathbf{R}_B = \sum_m \int_{V^{(m)}} \underbrace{\mathbf{H}^{(m)T} \mathbf{f}^{B(m)}}_{= \mathbf{R}_B^{(m)}} dV^{(m)}} \quad (4.20)$$

the effect of the element surface forces,

$$\boxed{\mathbf{R}_S = \sum_m \int_{S_1^{(m)}, \dots, S_k^{(m)}} \underbrace{\mathbf{H}^{S(m)T} \mathbf{f}^{S(m)}}_{= \mathbf{R}_S^{(m)}} dS^{(m)}} \quad (4.21)$$

the effect of the element initial stresses,

$$\boxed{\mathbf{R}_I = \sum_m \int_{V^{(m)}} \underbrace{\mathbf{B}^{(m)T} \boldsymbol{\tau}^{I(m)}}_{= \mathbf{R}_I^{(m)}} dV^{(m)}} \quad (4.22)$$

and the nodal concentrated loads \mathbf{R}_C .

⁷For the definition of the vector \mathbf{e}_i , see the text following (2.7).

We note that the summation of the element volume integrals in (4.19) expresses the direct addition of the element stiffness matrices $\mathbf{K}^{(m)}$ to obtain the stiffness matrix of the total element assemblage. In the same way, the assemblage body force vector \mathbf{R}_B is calculated by directly adding the element body force vectors $\mathbf{R}_B^{(m)}$; and \mathbf{R}_S and \mathbf{R}_I are similarly obtained. The process of assembling the element matrices by this direct addition is called the *direct stiffness method*.

This elegant writing of the assemblage process hinges upon two main factors: first, the dimensions of all matrices to be added are the same and, second, the element degrees of freedom are equal to the global degrees of freedom. In practice of course only the nonzero rows and columns of an element matrix $\mathbf{K}^{(m)}$ are calculated (corresponding to the actual element nodal degrees of freedom), and then the assemblage is carried out using for each element a connectivity array LM (see Example 4.11 and Chapter 12). Also, in practice, the element stiffness matrix may first be calculated corresponding to element local degrees of freedom not aligned with the global assemblage degrees of freedom, in which case a transformation is necessary prior to the assemblage [see (4.41)].

Equation (4.17) is a statement of the static equilibrium of the element assemblage. In these equilibrium considerations, the applied forces may vary with time, in which case the displacements also vary with time and (4.17) is a statement of equilibrium for any specific point in time. (In practice, the time-dependent application of loads can thus be used to model multiple-load cases; see Example 4.5.) However, if in actuality the loads are applied rapidly, measured on the natural frequencies of the system, inertia forces need to be considered; i.e., a truly dynamic problem needs to be solved. Using d'Alembert's principle, we can simply include the element inertia forces as part of the body forces. Assuming that the element accelerations are approximated in the same way as the element displacements in (4.8), the contribution from the total body forces to the load vector \mathbf{R} is (with the X, Y, Z coordinate system stationary)

$$\mathbf{R}_B = \sum_m \int_{V^{(m)}} \mathbf{H}^{(m)T} [\mathbf{f}^{B(m)} - \rho^{(m)} \mathbf{H}^{(m)} \ddot{\mathbf{U}}] dV^{(m)} \quad (4.23)$$

where $\mathbf{f}^{B(m)}$ no longer includes inertia forces, $\ddot{\mathbf{U}}$ lists the nodal point accelerations (i.e., is the second time derivative of \mathbf{U}), and $\rho^{(m)}$ is the mass density of element m . The equilibrium equations are, in this case,

$$\mathbf{M} \ddot{\mathbf{U}} + \mathbf{K} \mathbf{U} = \mathbf{R} \quad (4.24)$$

where \mathbf{R} and \mathbf{U} are time-dependent. The matrix \mathbf{M} is the mass matrix of the structure,

$$\mathbf{M} = \sum_m \int_{V^{(m)}} \rho^{(m)} \mathbf{H}^{(m)T} \mathbf{H}^{(m)} dV^{(m)} \quad (4.25)$$

$= \mathbf{M}^{(m)}$

In actually measured dynamic responses of structures it is observed that energy is dissipated during vibration, which in vibration analysis is usually taken account of by introducing velocity-dependent damping forces. Introducing the damping forces as additional contributions to the body forces, we obtain corresponding to (4.23),

$$\mathbf{R}_B = \sum_m \int_{V^{(m)}} \mathbf{H}^{(m)T} [\mathbf{f}^{B(m)} - \rho^{(m)} \mathbf{H}^{(m)} \ddot{\mathbf{U}} - \kappa^{(m)} \mathbf{H}^{(m)} \dot{\mathbf{U}}] dV^{(m)} \quad (4.26)$$

In this case the vectors $\mathbf{f}^{B(m)}$ no longer include inertia and velocity-dependent damping forces, $\dot{\mathbf{U}}$ is a vector of the nodal point velocities (i.e., the first time derivative of \mathbf{U}), and $\kappa^{(m)}$ is the damping property parameter of element m . The equilibrium equations are, in this case,

$$\boxed{\mathbf{M}\ddot{\mathbf{U}} + \mathbf{C}\dot{\mathbf{U}} + \mathbf{K}\mathbf{U} = \mathbf{R}} \quad (4.27)$$

where \mathbf{C} is the damping matrix of the structure; i.e., formally,

$$\mathbf{C} = \sum_m \underbrace{\int_{V^{(m)}} \kappa^{(m)} \mathbf{H}^{(m)T} \mathbf{H}^{(m)} dV^{(m)}}_{= \mathbf{C}^{(m)}} \quad (4.28)$$

In practice it is difficult, if not impossible, to determine for general finite element assemblages the element damping parameters, in particular because the damping properties are frequency dependent. For this reason, the matrix \mathbf{C} is in general not assembled from element damping matrices but is constructed using the mass matrix and stiffness matrix of the complete element assemblage together with experimental results on the amount of damping. Some formulations used to construct physically significant damping matrices are described in Section 9.3.3.

A complete analysis, therefore, consists of calculating the matrix \mathbf{K} (and the matrices \mathbf{M} and \mathbf{C} in a dynamic analysis) and the load vector \mathbf{R} , solving for the response \mathbf{U} from (4.17) [or \mathbf{U} , $\dot{\mathbf{U}}$, $\ddot{\mathbf{U}}$ from (4.24) or (4.27)], and then evaluating the stresses using (4.12). We should emphasize that the stresses are simply obtained using (4.12)—hence only from the initial stresses and element displacements—and that these values are not corrected for externally applied element pressures or body forces, as is common practice in the analysis of frame structures with beam elements (see Example 4.5 and, for example, S. H. Crandall, N. C. Dahl, and T. J. Lardner [A]). In the analysis of beam structures, each element represents a one-dimensional stress situation, and the stress correction due to distributed loading is performed by simple equilibrium considerations. In static analysis, relatively long beam elements can therefore be employed, resulting in the use of only a few elements (and degrees of freedom) to represent a frame structure. However, a similar scheme would require, in general two- and three-dimensional finite element analysis, the solution of boundary value problems for the (large) element domains used, and the use of fine meshes for an accurate prediction of the displacements and strains is more effective. With such fine discretizations, the benefits of even correcting approximately the stress predictions for the effects of distributed element loadings are in general small, although for specific situations of course the use of a rational scheme can result in notable improvements.

To illustrate the above derivation of the finite element equilibrium equations, we consider the following examples.

EXAMPLE 4.5: Establish the finite element equilibrium equations of the bar structure shown in Fig. E4.5. The mathematical model to be used is discussed in Examples 3.17 and 3.22. Use the two-node bar element idealization given and consider the following two cases:

1. Assume that the loads are applied very slowly when measured on the time constants (natural periods) of the structure.
2. Assume that the loads are applied rapidly. The structure is initially at rest.

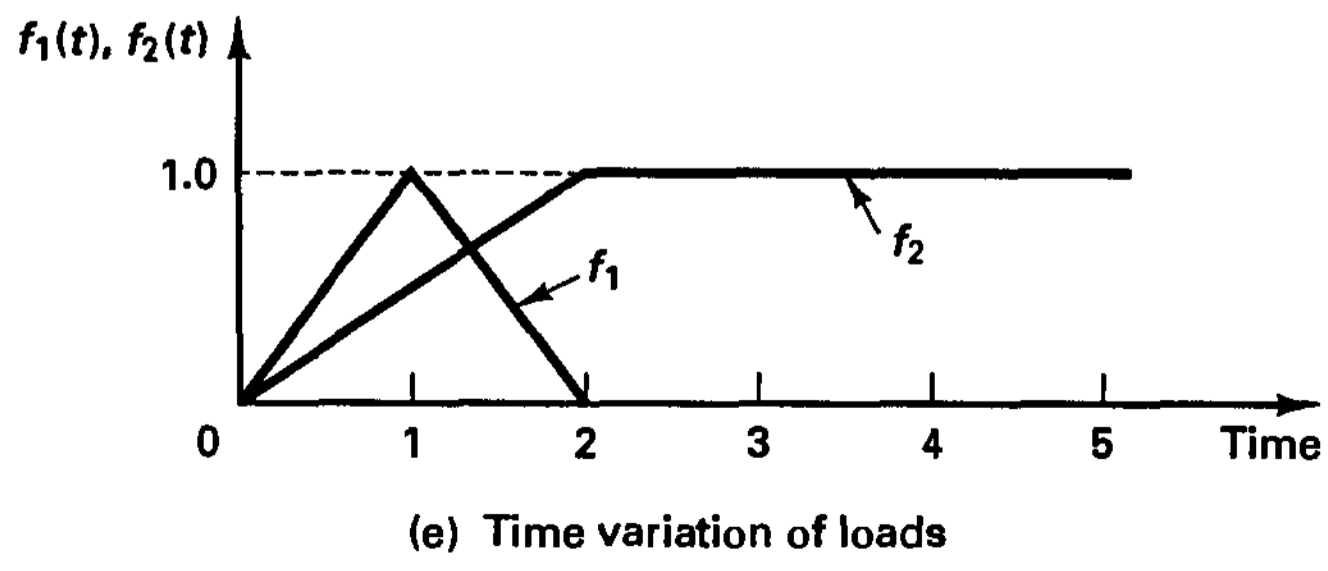
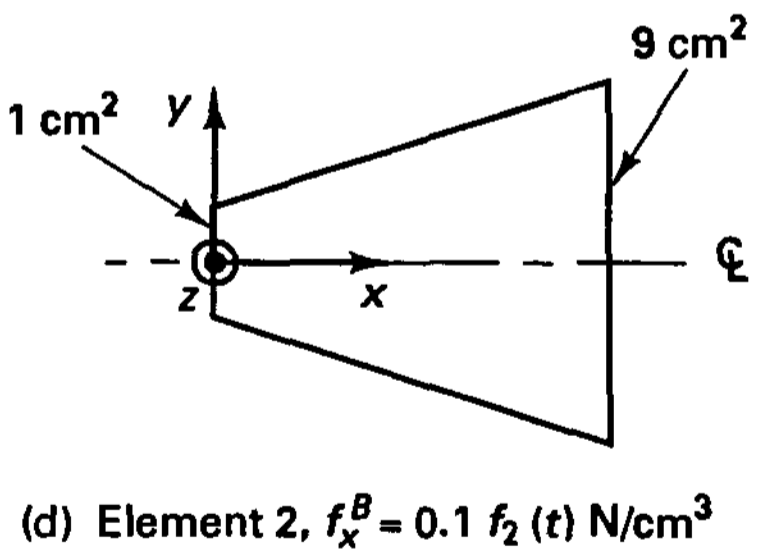
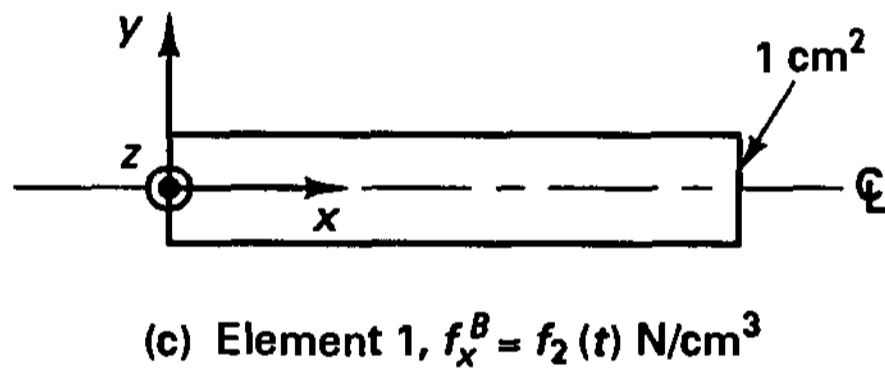
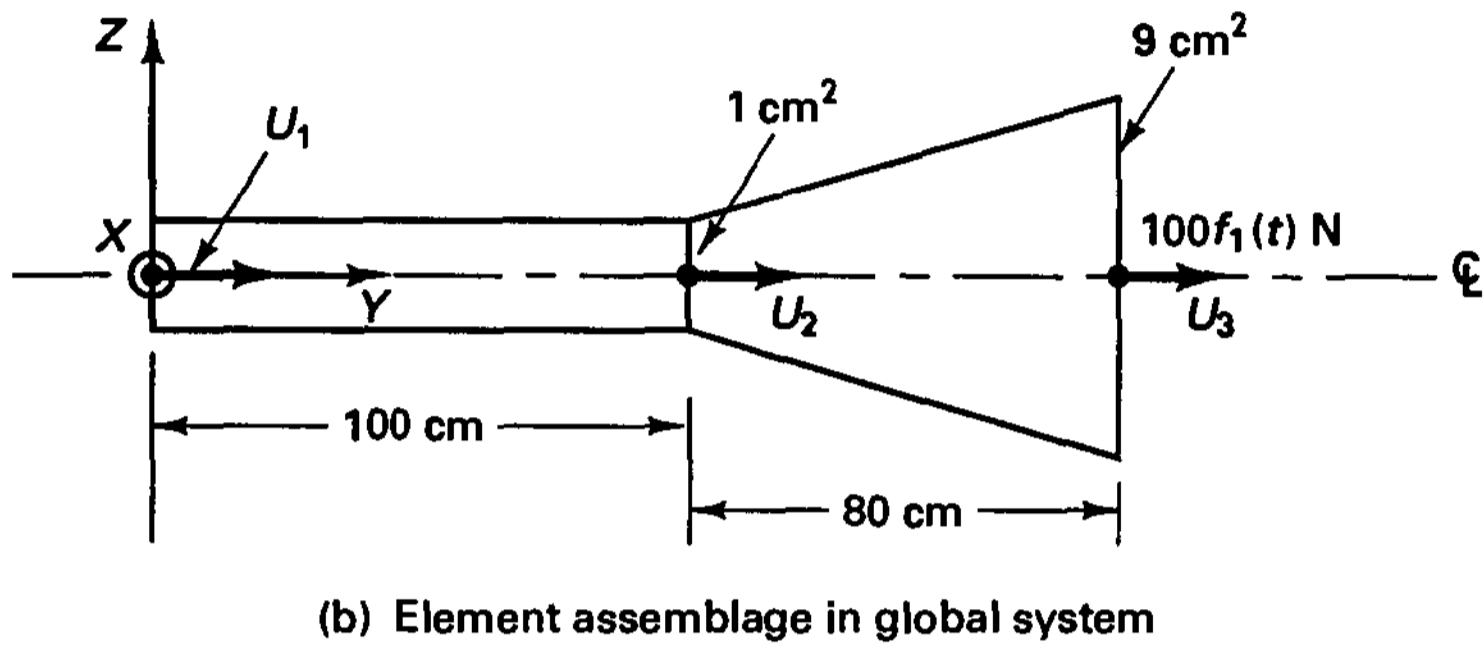
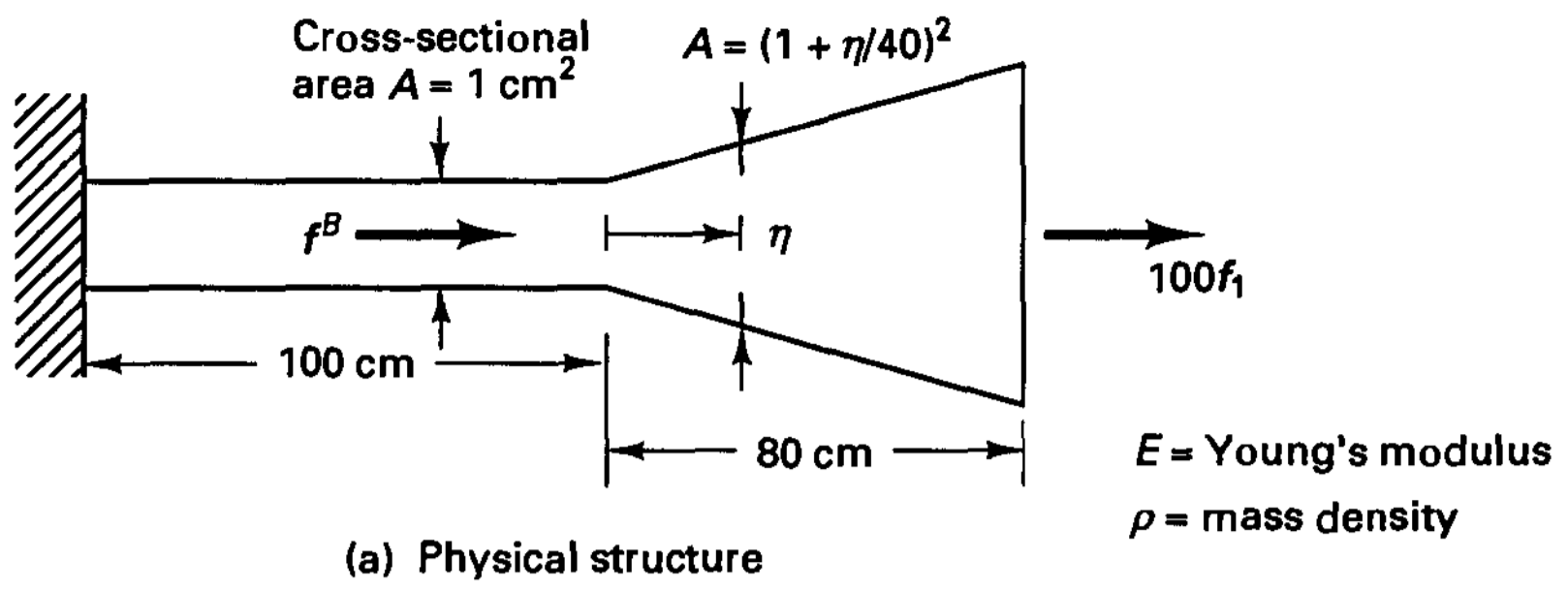


Figure E4.5 Two-element bar assemblage

In the formulation of the finite element equilibrium equations we employ the general equations (4.8) to (4.24) but use that the only nonzero stress is the longitudinal stress in the bar. Furthermore, considering the complete bar as an assemblage of 2 two-node bar elements corresponds to assuming a linear displacement variation between the nodal points of each element.

The first step is to construct the matrices $\mathbf{H}^{(m)}$ and $\mathbf{B}^{(m)}$ for $m = 1, 2$. We recall that although the displacement at the left end of the structure is zero, we first include the displacement at that surface in the construction of the finite element equilibrium equations.

Corresponding to the displacement vector $\mathbf{U}^T = [U_1 \ U_2 \ U_3]$, we have

$$\mathbf{H}^{(1)} = \begin{bmatrix} \left(1 - \frac{x}{100}\right) & \frac{x}{100} & 0 \end{bmatrix}$$

$$\mathbf{B}^{(1)} = \begin{bmatrix} -\frac{1}{100} & \frac{1}{100} & 0 \end{bmatrix}$$

$$\mathbf{H}^{(2)} = \begin{bmatrix} 0 & \left(1 - \frac{x}{80}\right) & \frac{x}{80} \end{bmatrix}$$

$$\mathbf{B}^{(2)} = \begin{bmatrix} 0 & -\frac{1}{80} & \frac{1}{80} \end{bmatrix}$$

The material property matrices are

$$\mathbf{C}^{(1)} = E; \quad \mathbf{C}^{(2)} = E$$

where E is Young's modulus for the material. For the volume integrations we need the cross-sectional areas of the elements. We have

$$A^{(1)} = 1 \text{ cm}^2; \quad A^{(2)} = \left(1 + \frac{x}{40}\right)^2 \text{ cm}^2$$

When the loads are applied very slowly, a static analysis is required in which the stiffness matrix \mathbf{K} and load vector \mathbf{R} must be calculated. The body forces and loads are given in Fig. E4.5. We therefore have

$$\mathbf{K} = (1)E \int_0^{100} \begin{bmatrix} -\frac{1}{100} \\ \frac{1}{100} \\ 0 \end{bmatrix} \begin{bmatrix} -\frac{1}{100} & \frac{1}{100} & 0 \end{bmatrix} dx + E \int_0^{80} \left(1 + \frac{x}{40}\right)^2 \begin{bmatrix} 0 \\ -\frac{1}{80} \\ \frac{1}{80} \end{bmatrix} \begin{bmatrix} 0 & -\frac{1}{80} & \frac{1}{80} \end{bmatrix} dx$$

$$\text{or} \quad \mathbf{K} = \frac{E}{100} \begin{bmatrix} 1 & -1 & 0 \\ -1 & 1 & 0 \\ 0 & 0 & 0 \end{bmatrix} + \frac{13E}{240} \begin{bmatrix} 0 & 0 & 0 \\ 0 & 1 & -1 \\ 0 & -1 & 1 \end{bmatrix}$$

$$= \frac{E}{240} \begin{bmatrix} 2.4 & -2.4 & 0 \\ -2.4 & 15.4 & -13 \\ 0 & -13 & 13 \end{bmatrix} \quad (\text{a})$$

and also,

$$\begin{aligned} \mathbf{R}_B &= \left\{ (1) \int_0^{100} \begin{bmatrix} 1 - \frac{x}{100} \\ \frac{x}{100} \\ 0 \end{bmatrix} (1) dx + \int_0^{80} \left(1 + \frac{x}{40}\right)^2 \begin{bmatrix} 0 \\ 1 - \frac{x}{80} \\ \frac{x}{80} \end{bmatrix} \left(\frac{1}{10}\right) dx \right\} f_2(t) \\ &= \frac{1}{3} \begin{bmatrix} 150 \\ 186 \\ 68 \end{bmatrix} f_2(t) \end{aligned} \quad (b)$$

$$\mathbf{R}_C = \begin{bmatrix} 0 \\ 0 \\ 100 \end{bmatrix} f_1(t) \quad (c)$$

To obtain the solution at a specific time t^* , the vectors \mathbf{R}_B and \mathbf{R}_C must be evaluated corresponding to t^* , and the equation

$$\mathbf{K}\mathbf{U}|_{t=t^*} = \mathbf{R}_B|_{t=t^*} + \mathbf{R}_C|_{t=t^*} \quad (d)$$

yields the displacements at t^* . We should note that in this static analysis the displacements at time t^* depend only on the magnitude of the loads at that time and are independent of the loading history.

Considering now the dynamic analysis, we also need to calculate the mass matrix. Using the displacement interpolations and (4.25), we have

$$\begin{aligned} \mathbf{M} &= (1)\rho \int_0^{100} \begin{bmatrix} 1 - \frac{x}{100} \\ \frac{x}{100} \\ 0 \end{bmatrix} \left[\left(1 - \frac{x}{100}\right) \quad \frac{x}{100} \quad 0 \right] dx \\ &\quad + \rho \int_0^{80} \left(1 + \frac{x}{40}\right)^2 \begin{bmatrix} 0 \\ 1 - \frac{x}{80} \\ \frac{x}{80} \end{bmatrix} \left[0 \quad \left(1 - \frac{x}{80}\right) \quad \frac{x}{80} \right] dx \end{aligned}$$

Hence

$$\mathbf{M} = \frac{\rho}{6} \begin{bmatrix} 200 & 100 & 0 \\ 100 & 584 & 336 \\ 0 & 336 & 1024 \end{bmatrix}$$

Damping was not specified; thus, the equilibrium equations now to be solved are

$$\mathbf{M}\ddot{\mathbf{U}}(t) + \mathbf{K}\mathbf{U}(t) = \mathbf{R}_B(t) + \mathbf{R}_C(t) \quad (e)$$

where the stiffness matrix \mathbf{K} and load vectors \mathbf{R}_B and \mathbf{R}_C have already been given in (a) to (c). Using the initial conditions

$$\mathbf{U}|_{t=0} = \mathbf{0}; \quad \dot{\mathbf{U}}|_{t=0} = \mathbf{0} \quad (f)$$

these dynamic equilibrium equations must be integrated from time 0 to time t^* in order to obtain the solution at time t^* (see Chapter 9).

To actually solve for the response of the structure in Fig. E4.5(a), we need to impose $U_1 = 0$ for all time t . Hence, the equations (d) and (e) must be amended by this condition (see Section 4.2.2). The solution of (d) and (e) then yields $U_2(t)$, $U_3(t)$, and the stresses are obtained using

$$\tau_{xx}^{(m)} = \mathbf{C}^{(m)}\mathbf{B}^{(m)}\mathbf{U}(t); \quad m = 1, 2 \quad (g)$$

These stresses will be discontinuous between the elements because constant element strains are assumed. Of course, in this example, since the exact solution to the mathematical model can be computed, stresses more accurate than those given by (g) could be evaluated within each element.

In static analysis, this increase in accuracy could simply be achieved, as in beam theory, by adding a stress correction for the distributed element loading to the values given in (g). However, such a stress correction is not straightforward in general dynamic analysis (and in any two- and three-dimensional practical analysis), and if a large number of elements is used to represent the structure, the stresses using (g) are sufficiently accurate (see Section 4.3.6).

EXAMPLE 4.6: Consider the analysis of the cantilever plate shown in Fig. E4.6. To illustrate the analysis technique, use the coarse finite element idealization given in the figure (in a practical analysis more finite elements must be employed (see Section 4.3). Establish the matrices $\mathbf{H}^{(2)}$, $\mathbf{B}^{(2)}$, and $\mathbf{C}^{(2)}$.

The cantilever plate is acting in plane stress conditions. For an isotropic linear elastic material the stress-strain matrix is defined using Young's modulus E and Poisson's ratio ν (see Table 4.3),

$$\mathbf{C}^{(2)} = \frac{E}{1 - \nu^2} \begin{bmatrix} 1 & \nu & 0 \\ \nu & 1 & 0 \\ 0 & 0 & \frac{1 - \nu}{2} \end{bmatrix}$$

The displacement transformation matrix $\mathbf{H}^{(2)}$ of element 2 relates the element internal displacements to the nodal point displacements,

$$\begin{bmatrix} u(x, y) \\ v(x, y) \end{bmatrix}^{(2)} = \mathbf{H}^{(2)}\mathbf{U} \quad (a)$$

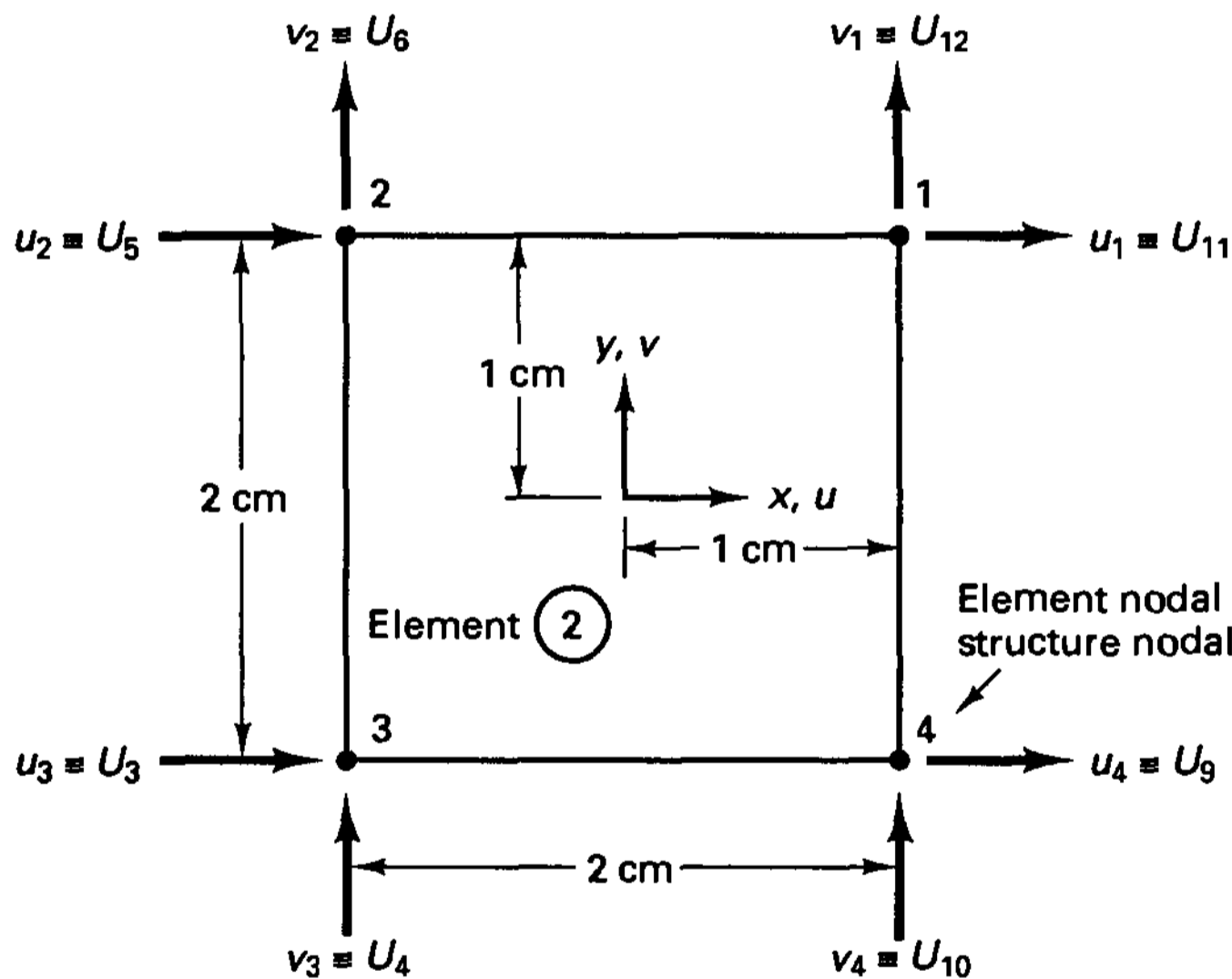
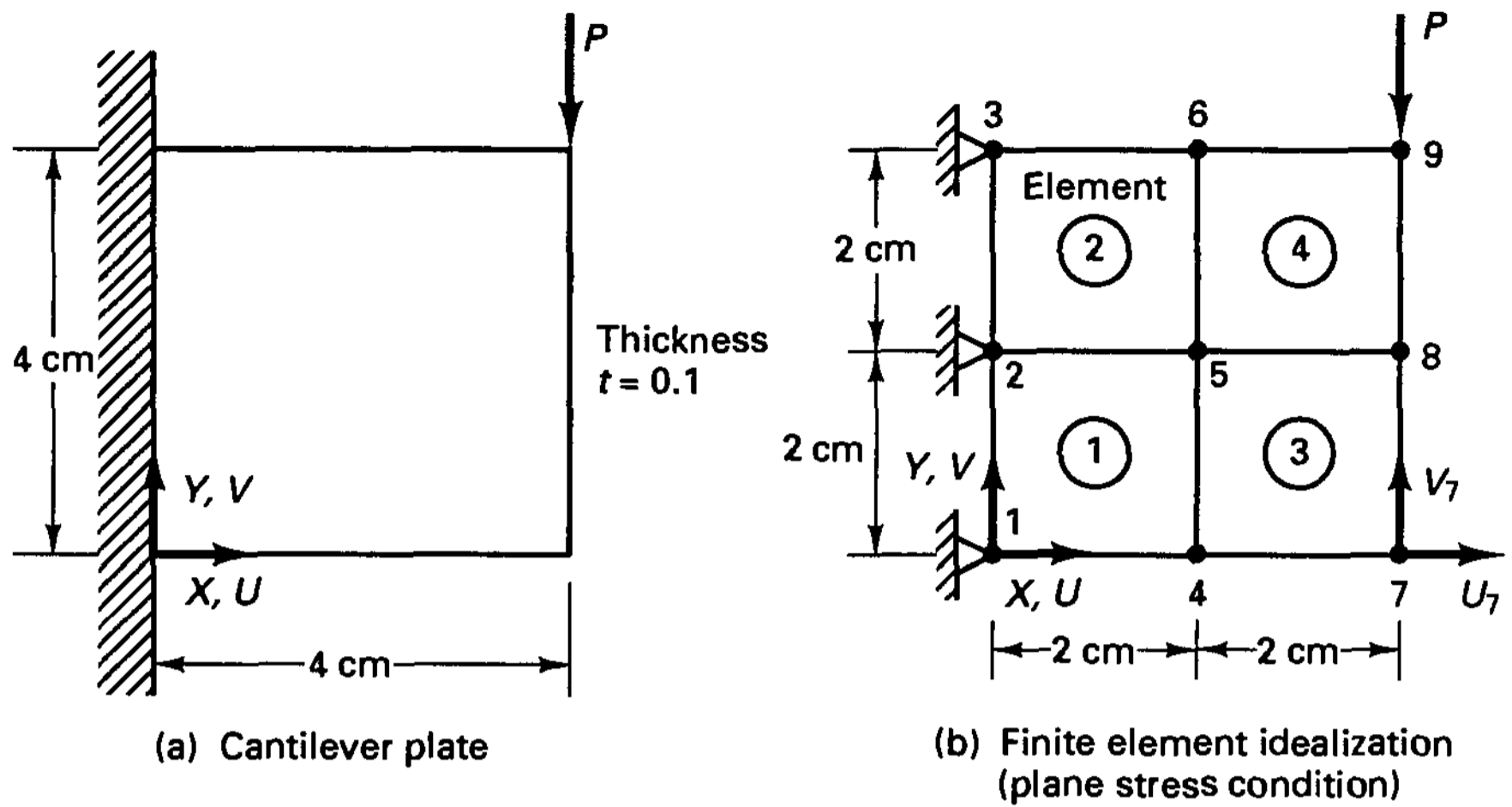
where \mathbf{U} is a vector listing all nodal point displacements of the structure,

$$\mathbf{U}^T = [U_1 \quad U_2 \quad U_3 \quad U_4 \quad \dots \quad U_{17} \quad U_{18}] \quad (b)$$

(As mentioned previously, in this phase of analysis we are considering the structural model without displacement boundary conditions.) In considering element 2, we recognize that only the displacements at nodes 6, 3, 2, and 5 affect the displacements in the element. For computational purposes it is convenient to use a convention to number the element nodal points and corresponding element degrees of freedom as shown in Fig E4.6(c). In the same figure the global structure degrees of freedom of the vector \mathbf{U} in (b) are also given.

To derive the matrix $\mathbf{H}^{(2)}$ in (a) we recognize that there are four nodal point displacements each for expressing $u(x, y)$ and $v(x, y)$. Hence, we can assume that the local element displacements u and v are given in the following form of polynomials in the local coordinate variables x and y :

$$\begin{aligned} u(x, y) &= \alpha_1 + \alpha_2 x + \alpha_3 y + \alpha_4 xy \\ v(x, y) &= \beta_1 + \beta_2 x + \beta_3 y + \beta_4 xy \end{aligned} \quad (c)$$



(c) Typical two-dimensional four-node element defined in local coordinate system

Figure E4.6 Finite element plane stress analysis

The unknown coefficients α_1, \dots, β_4 , which are also called the generalized coordinates, will be expressed in terms of the unknown element nodal point displacements u_1, \dots, u_4 and v_1, \dots, v_4 . Defining

$$\hat{\mathbf{u}}^T = [u_1 \ u_2 \ u_3 \ u_4 \ ; \ v_1 \ v_2 \ v_3 \ v_4] \tag{d}$$

we can write (c) in matrix form:

$$\begin{bmatrix} u(x, y) \\ v(x, y) \end{bmatrix} = \Phi \alpha \tag{e}$$

where
$$\Phi = \begin{bmatrix} \phi & \mathbf{0} \\ \mathbf{0} & \phi \end{bmatrix}; \quad \phi = [1 \quad x \quad y \quad xy]$$

and
$$\alpha^T = [\alpha_1 \quad \alpha_2 \quad \alpha_3 \quad \alpha_4 \quad | \quad \beta_1 \quad \beta_2 \quad \beta_3 \quad \beta_4]$$

Equation (e) must hold for all nodal points of the element; therefore, using (d), we have

$$\hat{\mathbf{u}} = \mathbf{A}\alpha \tag{f}$$

in which

$$\mathbf{A} = \begin{bmatrix} \mathbf{A}_1 & \mathbf{0} \\ \mathbf{0} & \mathbf{A}_1 \end{bmatrix}$$

and

$$\mathbf{A}_1 = \begin{bmatrix} 1 & 1 & 1 & 1 \\ 1 & -1 & 1 & -1 \\ 1 & -1 & -1 & 1 \\ 1 & 1 & -1 & -1 \end{bmatrix}$$

Solving from (f) for α and substituting into (e), we obtain

$$\mathbf{H} = \Phi\mathbf{A}^{-1} \tag{g}$$

where the fact that no superscript is used on \mathbf{H} indicates that the displacement interpolation matrix is defined corresponding to the element nodal point displacements in (d),

$$\mathbf{H} = \frac{1}{4} \begin{bmatrix} (1+x)(1+y) & (1-x)(1+y) & (1-x)(1-y) & (1+x)(1-y) \\ 0 & 0 & 0 & 0 \\ 0 & 0 & 0 & 0 \\ (1+x)(1+y) & (1-x)(1+y) & (1-x)(1-y) & (1+x)(1-y) \end{bmatrix} \tag{h}$$

The displacement functions in \mathbf{H} could also have been established by inspection. Let H_{ij} be the (i, j) th element of \mathbf{H} ; then H_{11} corresponds to a function that varies linearly in x and y [as required in (c)], is unity at $x = 1, y = 1$, and is zero at the other three element nodes. We discuss the construction of the displacement functions in \mathbf{H} based on these thoughts in Section 5.2.

With \mathbf{H} given in (h) we have

$$\mathbf{H}^{(2)} = \begin{bmatrix} U_1 & U_2 & | & U_3 & U_4 & | & U_5 & U_6 & | & U_7 & U_8 & | & U_9 & U_{10} & | & \\ 0 & 0 & | & H_{13} & H_{17} & | & H_{12} & H_{16} & | & 0 & 0 & | & H_{14} & H_{18} & | & \\ 0 & 0 & | & H_{23} & H_{27} & | & H_{22} & H_{26} & | & 0 & 0 & | & H_{24} & H_{28} & | & \\ & & & & & & & & & & & & & & & \end{bmatrix}$$

$u_1 \quad v_1 \leftarrow$ Element degrees of freedom (i)

$$\begin{bmatrix} U_{11} & U_{12} & & U_{13} & U_{14} & & & & & & & & & & & U_{18} \leftarrow \text{Assemblage degrees} \\ | & H_{11} & H_{15} & | & 0 & 0 & | & \dots & \text{zeros} & \dots & 0 & & & & & \text{of freedom} \\ | & H_{21} & H_{25} & | & 0 & 0 & | & \dots & \text{zeros} & \dots & 0 & & & & & \end{bmatrix}$$

The strain-displacement matrix can now directly be obtained from (g). In plane stress conditions the element strains are

$$\epsilon^T = [\epsilon_{xx} \quad \epsilon_{yy} \quad \gamma_{xy}]$$

where
$$\epsilon_{xx} = \frac{\partial u}{\partial x}; \quad \epsilon_{yy} = \frac{\partial v}{\partial y}; \quad \gamma_{xy} = \frac{\partial u}{\partial y} + \frac{\partial v}{\partial x}$$

Using (g) and recognizing that the elements in \mathbf{A}^{-1} are independent of x and y , we obtain

$$\mathbf{B} = \mathbf{E}\mathbf{A}^{-1}$$

where

$$\mathbf{E} = \begin{bmatrix} 0 & 1 & 0 & y & 0 & 0 & 0 & 0 \\ 0 & 0 & 0 & 0 & 0 & 0 & 1 & x \\ 0 & 0 & 1 & x & 0 & 1 & 0 & y \end{bmatrix}$$

Hence, the strain-displacement matrix corresponding to the local element degrees of freedom is

$$\mathbf{B} = \frac{1}{4} \begin{bmatrix} (1+y) & -(1+y) & -(1-y) & (1-y) & 0 & 0 & 0 & 0 \\ 0 & 0 & 0 & 0 & (1+x) & (1-x) & -(1-x) & -(1+x) \\ (1+x) & (1-x) & -(1-x) & -(1+x) & (1+y) & -(1+y) & -(1-y) & (1-y) \end{bmatrix} \quad (j)$$

The matrix \mathbf{B} could also have been calculated directly by operating on the rows of the matrix \mathbf{H} in (h).

Let B_{ij} be the (i, j) th element of \mathbf{B} ; then we now have

$$\mathbf{B}^{(2)} = \begin{bmatrix} 0 & 0 & B_{13} & B_{17} & B_{12} & B_{16} & 0 & 0 & B_{14} & B_{18} & B_{11} & B_{15} & 0 & 0 \\ 0 & 0 & B_{23} & B_{27} & B_{22} & B_{26} & 0 & 0 & B_{24} & B_{28} & B_{21} & B_{25} & 0 & 0 \\ 0 & 0 & B_{33} & B_{37} & B_{32} & B_{36} & 0 & 0 & B_{34} & B_{38} & B_{31} & B_{35} & 0 & 0 \\ \dots & \dots & \dots & \dots & \dots & \dots & \dots & \dots & \dots & \dots & \dots & \dots & \dots & \dots \\ & & & & & & & & & & & & & & 0 \\ & & & & & & & & & & & & & & 0 \\ & & & & & & & & & & & & & & 0 \end{bmatrix}$$

where the element degrees of freedom and assemblage degrees of freedom are ordered as in (d) and (b).

EXAMPLE 4.7: A linearly varying surface pressure distribution as shown in Fig. E4.7 is applied to element (m) of an element assemblage. Evaluate the vector $\mathbf{R}_S^{(m)}$ for this element.

The first step in the calculation of $\mathbf{R}_S^{(m)}$ is the evaluation of the matrix $\mathbf{H}^{S(m)}$. This matrix can be established using the same approach as in Example 4.6. For the surface displacements we assume

$$\begin{aligned} u^S &= \alpha_1 + \alpha_2 x + \alpha_3 x^2 \\ v^S &= \beta_1 + \beta_2 x + \beta_3 x^2 \end{aligned} \quad (a)$$

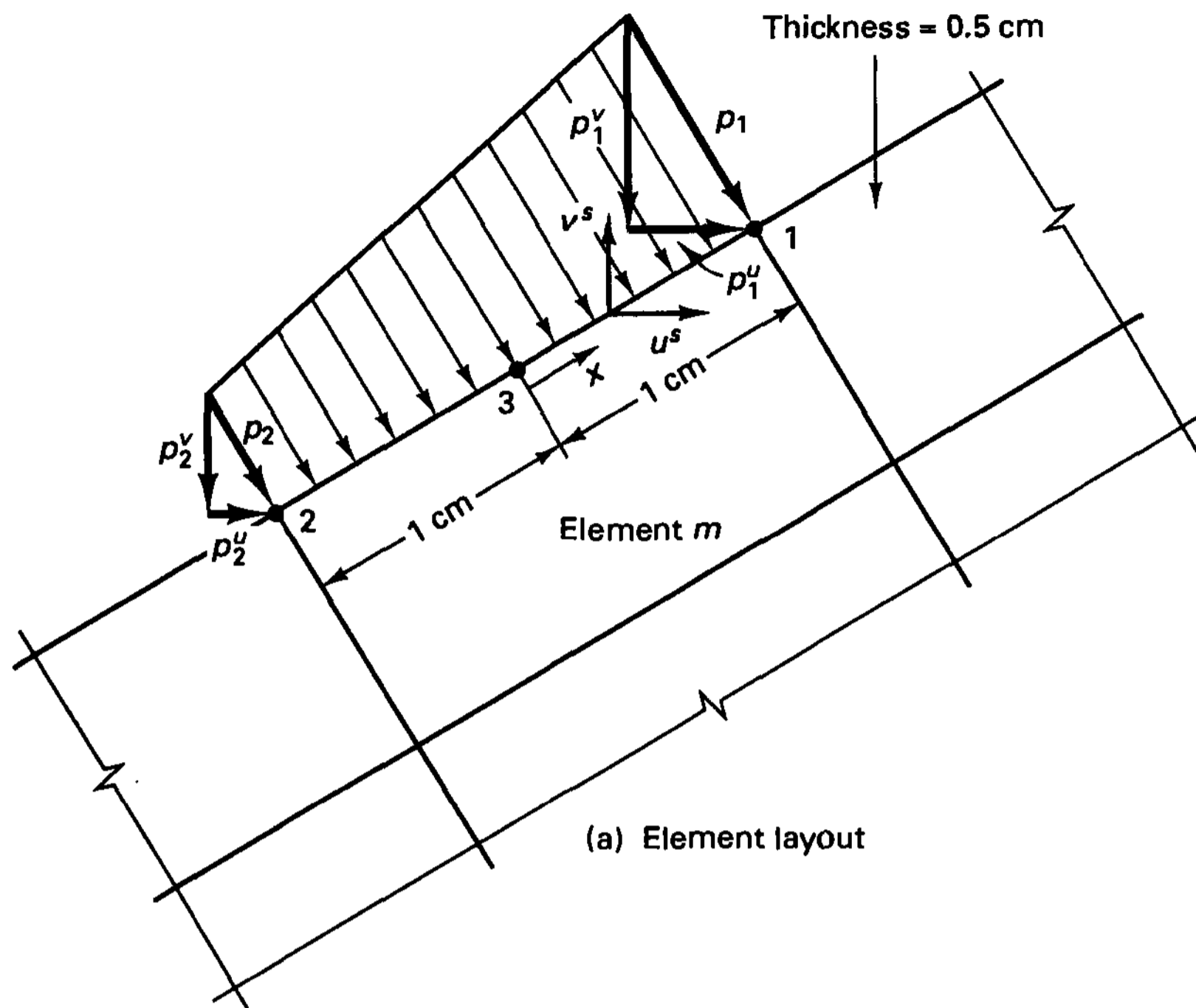
where (as in Example 4.6) the unknown coefficients α_1, \dots, β_3 are evaluated using the nodal point displacements. We thus obtain

$$\begin{bmatrix} u^S(x) \\ v^S(x) \end{bmatrix} = \mathbf{H}^S \hat{\mathbf{u}}$$

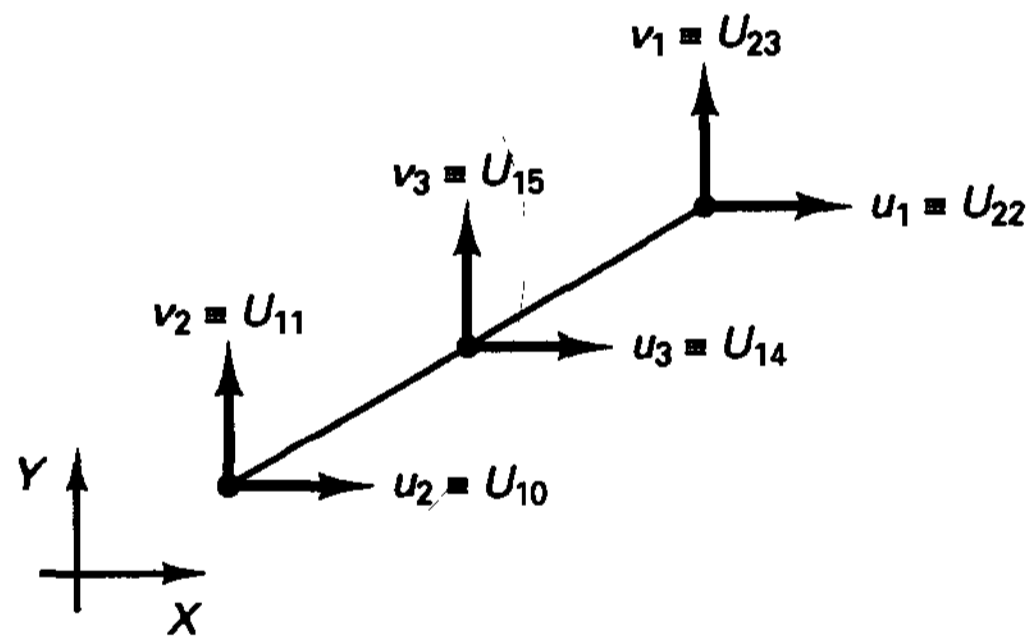
$$\hat{\mathbf{u}}^T = [u_1 \quad u_2 \quad u_3 \quad ; \quad v_1 \quad v_2 \quad v_3]$$

and

$$\mathbf{H}^S = \begin{bmatrix} \frac{1}{2}x(1+x) & -\frac{1}{2}x(1-x) & (1-x^2) & 0 & 0 & 0 \\ 0 & 0 & 0 & \frac{1}{2}x(1+x) & -\frac{1}{2}x(1-x) & (1-x^2) \end{bmatrix}$$



(a) Element layout



(b) Local-global degrees of freedom

Figure E4.7 Pressure loading on element (*m*)

The vector of surface loads is (with p_1 and p_2 positive)

$$\mathbf{f}^s = \begin{bmatrix} \frac{1}{2}(1+x)p_1^u + \frac{1}{2}(1-x)p_2^u \\ -\frac{1}{2}(1+x)p_1^v - \frac{1}{2}(1-x)p_2^v \end{bmatrix}$$

To obtain $\mathbf{R}_S^{(m)}$ we first evaluate

$$\mathbf{R}_S = 0.5 \int_{-1}^{+1} \mathbf{H}^{sT} \mathbf{f}^s dx$$

to obtain

$$\mathbf{R}_s = \frac{1}{3} \begin{bmatrix} p_1^u \\ p_2^u \\ 2(p_1^u + p_2^u) \\ -p_1^v \\ -p_2^v \\ -2(p_1^v + p_2^v) \end{bmatrix}$$

Thus, corresponding to the global degrees of freedom given in Fig. E4.7, we have

$$\mathbf{R}_s^{(m)T} = \frac{1}{3} \begin{bmatrix} 0 & \dots & 0 & \vdots & U_{10} & U_{11} & U_{12} & U_{13} & \vdots & U_{14} & \vdots & U_{15} & \vdots & 0 & \dots \\ & & & & p_2^u & -p_2^u & \vdots & 0 & 0 & \vdots & 2(p_1^u + p_2^u) & -2(p_1^v + p_2^v) & \vdots & 0 & \dots \\ & & & & & & & & & & U_{22} & U_{23} \leftarrow \text{Assemblage degrees of freedom} & & & \\ & & & & & & & & & & \dots & 0 & \vdots & p_1^u & -p_1^v & \vdots & 0 & \dots & 0 \end{bmatrix}$$

The Assumption About Stress Equilibrium

We noted earlier that the analyses of truss and beam assemblages were originally not considered to be finite element analysis because the “exact” element stiffness matrices can be employed in the analyses. These stiffness matrices are obtained in the application of the principle of virtual displacements if the assumed displacement interpolations are in fact the exact displacements that the element undergoes when subjected to the unit nodal point displacements. Here the word “exact” refers to the fact that by imposing these displacements on the element, all pertinent differential equations of equilibrium and compatibility and the constitutive requirements (and also the boundary conditions) are fully satisfied in static analysis.

In considering the analysis of the truss assemblage in Example 4.5, we obtained the exact stiffness matrix of element 1. However, for element 2 an approximate stiffness matrix was calculated as shown in the next example.

EXAMPLE 4.8: Calculate for element 2 in Example 4.5 the exact element internal displacements that correspond to a unit element end displacement u_2 and evaluate the corresponding stiffness matrix. Also, show that using the element displacement assumption in Example 4.5, internal element equilibrium is not satisfied.

Consider element 2 with a unit displacement imposed at its right end as shown in Fig. E4.8. The element displacements are calculated by solving the differential equation (see Example 3.22),

$$E \frac{d}{dx} \left(A \frac{du}{dx} \right) = 0 \tag{a}$$

subject to the boundary conditions $u|_{x=0} = 0$ and $u|_{x=80} = 1.0$. Substituting for the area A and integrating the relation in (a), we obtain

$$u = \frac{3}{2} \left(1 - \frac{1}{1 + x/40} \right) \tag{b}$$

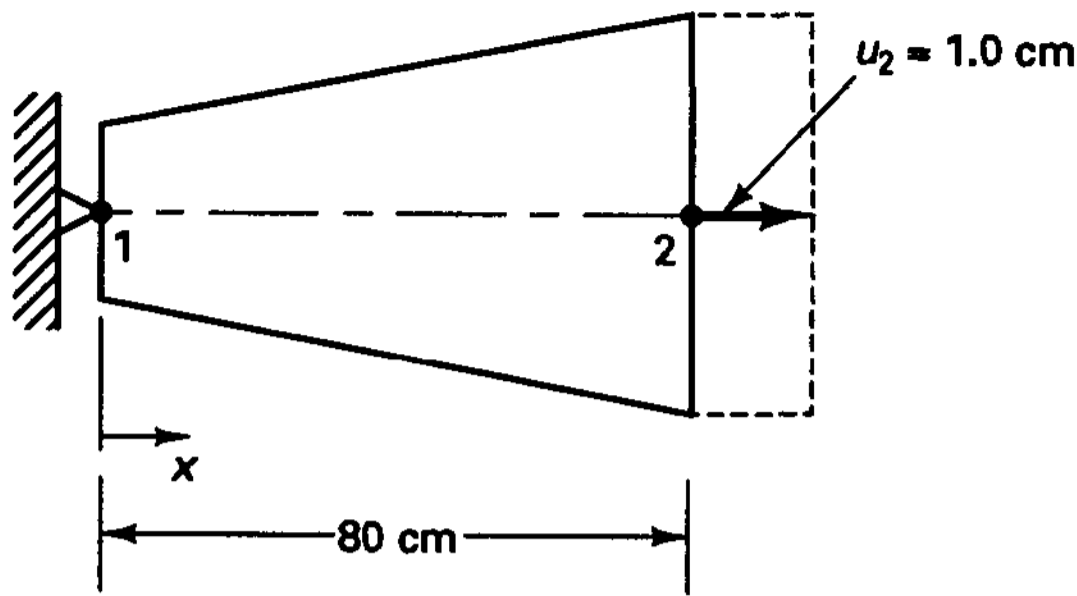


Figure E4.8 Element 2 of bar analyzed in Example 4.5

These are the exact element internal displacements. The element end forces required to subject the bar to these displacements are

$$\begin{aligned} k_{12} &= -EA \left. \frac{du}{dx} \right|_{x=0} \\ k_{22} &= EA \left. \frac{du}{dx} \right|_{x=L} \end{aligned} \quad (c)$$

Substituting from (b) into (c) we have

$$k_{22} = \frac{3E}{80}; \quad k_{12} = -\frac{3E}{80}$$

Hence we have, using the symmetry of the element matrix and equilibrium to establish k_{21} and k_{11} ,

$$\mathbf{K} = \frac{3}{80} E \begin{bmatrix} 1 & -1 \\ -1 & 1 \end{bmatrix} \quad (d)$$

The same result is of course obtained using the principle of virtual displacements with the displacement (b).

We note that the stiffness coefficient in (d) is smaller than the corresponding value obtained in Example 4.5 ($3E/80$ instead of $13E/240$). The finite element solution in Example 4.5 overestimates the stiffness of the structure because the assumed displacements artificially constrain the motion of the material particles (see Section 4.3.4). To check that the internal equilibrium is indeed not satisfied, we substitute the finite element solution (given by the displacement assumption in Example 4.5) into (a) and obtain

$$E \frac{d}{dx} \left\{ \left(1 + \frac{x}{40} \right)^2 \frac{1}{80} \right\} \neq 0$$

The solution of truss and beam structures, using the exact displacements corresponding to unit nodal point displacements and rotations to evaluate the stiffness matrices, gives analysis results that for the selected mathematical model satisfy all three requirements of mechanics exactly: differential equilibrium for every point of the structure (including nodal point equilibrium), compatibility, and the stress-strain relationships. Hence, the exact (unique) solution for the selected mathematical model is obtained.

We may note that such an exact solution is usually pursued in static analysis, in which the exact stiffness relationships are obtained as described in Example 4.8, but an exact

solution is much more difficult to reach in dynamic analysis because in this case the distributed mass and damping effects must be included (see, for example, R. W. Clough and J. Penzien [A]).

However, although in a general (static or dynamic) finite element analysis, differential equilibrium is not exactly satisfied at all points of the continuum considered, two important properties are always satisfied by the finite element solution using a coarse or a fine mesh. These properties are (see Fig. 4.2)

1. Nodal point equilibrium
2. Element equilibrium.

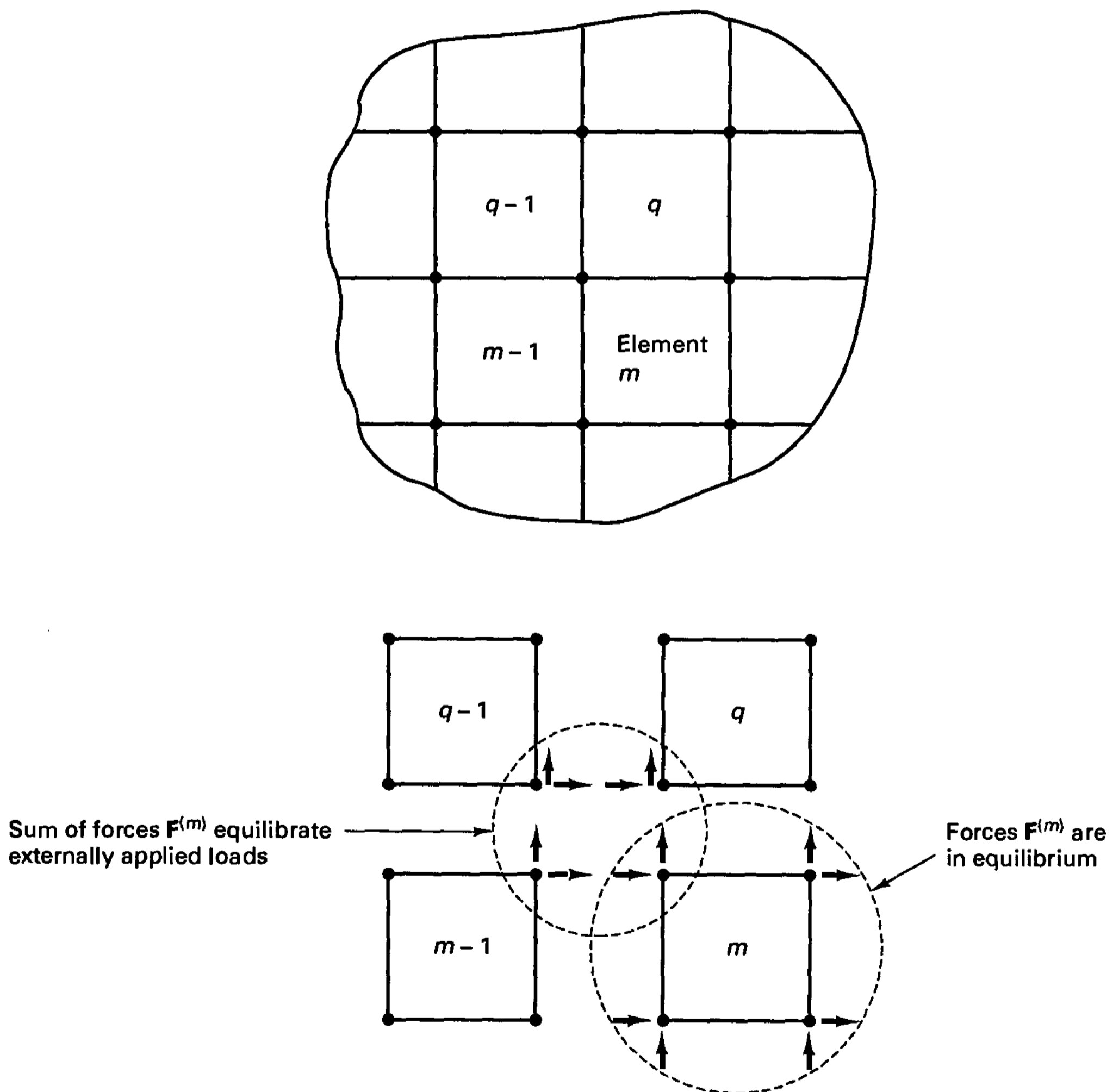


Figure 4.2 Nodal point and element equilibrium in a finite element analysis

Namely, consider that a finite element analysis has been performed and that we calculate for each finite element m the element nodal point force vectors

$$\mathbf{F}^{(m)} = \int_{V^{(m)}} \mathbf{B}^{(m)T} \boldsymbol{\tau}^{(m)} dV^{(m)} \quad (4.29)$$

where $\boldsymbol{\tau}^{(m)} = \mathbf{C}^{(m)} \boldsymbol{\epsilon}^{(m)}$. Then we observe that according to property 1,

At any node, the sum of the element nodal point forces is in equilibrium with the externally applied nodal loads (which include all effects due to body forces, surface tractions, initial stresses, concentrated loads, inertia and damping forces, and reactions).

And according to property 2,

Each element m is in equilibrium under its forces $\mathbf{F}^{(m)}$.

Property 1 follows simply because (4.27) expresses the nodal point equilibrium and we have

$$\sum_m \mathbf{F}^{(m)} = \mathbf{K} \mathbf{U} \quad (4.30)$$

The element equilibrium stated in property 2 is satisfied provided the finite element displacement interpolations in $\mathbf{H}^{(m)}$ satisfy the basic convergence requirements, which include the condition that the element must be able to represent the rigid body motions (see Section 4.3). Namely, let us consider element m subjected to the nodal point forces $\mathbf{F}^{(m)}$ and impose virtual nodal point displacements corresponding to the rigid body motions. Then for each virtual element rigid body motion with nodal point displacements $\bar{\mathbf{u}}$, we have

$$\bar{\mathbf{u}}^T \mathbf{F}^{(m)} = \int_{V^{(m)}} (\mathbf{B}^{(m)} \bar{\mathbf{u}})^T \boldsymbol{\tau}^{(m)} dV^{(m)} = \int_{V^{(m)}} \bar{\boldsymbol{\epsilon}}^{(m)T} \boldsymbol{\tau}^{(m)} dV^{(m)} = 0$$

because here $\bar{\boldsymbol{\epsilon}}^{(m)} = \mathbf{0}$. Using all applicable rigid body motions we therefore find that the forces $\mathbf{F}^{(m)}$ are in equilibrium.

Hence, a finite element analysis can be interpreted as a process in which

1. The structure or continuum is idealized as an assemblage of discrete elements connected at nodes pertaining to the elements.
2. The externally applied forces (body forces, surface tractions, initial stresses, concentrated loads, inertia and damping forces, and reactions) are lumped to these nodes using the virtual work principle to obtain equivalent externally applied nodal point forces.
3. The equivalent externally applied nodal point forces (calculated in 2) are equilibrated by the element nodal point forces that are equivalent (in the virtual work sense) to the element internal stresses; i.e., we have

$$\sum_m \mathbf{F}^{(m)} = \mathbf{R}$$

4. Compatibility and the stress-strain material relationship are satisfied exactly, but instead of equilibrium on the differential level, only global equilibrium for the com-

plete structure, at the nodes, and of each element m under its nodal point forces $\mathbf{F}^{(m)}$ is satisfied.

Consider the following example.

EXAMPLE 4.9: The finite element solution to the problem in Fig. E4.6, with $P = 100$, $E = 2.7 \times 10^6$, $\nu = 0.30$, $t = 0.1$, is given in Fig. E4.9. Clearly, the stresses are not continuous between elements, and equilibrium on the differential level is not satisfied. However,

1. Show that $\sum_m \mathbf{F}^{(m)} = \mathbf{R}$ and calculate the reactions.
2. Show that the element forces $\mathbf{F}^{(4)}$ for element 4 are in equilibrium.

The fact that $\sum_m \mathbf{F}^{(m)} = \mathbf{R}$ follows from the solution of (4.17), and \mathbf{R} consists of the sum of all nodal point forces. Hence, this relation can also be used to evaluate the reactions.

Referring to the nodal point numbering in Fig. E4.6(b), we find for node 1:

$$\begin{aligned} \text{reactions } R_x &= 100.15 \\ R_y &= 41.36 \end{aligned}$$

for node 2:

$$\begin{aligned} \text{reactions } R_x &= 2.58 - 2.88 = -0.30 \\ R_y &= 16.79 + 5.96 = 22.74 \text{ (because of rounding)} \end{aligned}$$

for node 3:

$$\begin{aligned} \text{reactions } R_x &= -99.85 \\ R_y &= 35.90 \end{aligned}$$

for node 4:

$$\begin{aligned} \text{horizontal force equilibrium: } & -42.01 + 42.01 = 0 \\ \text{vertical force equilibrium: } & -22.90 + 22.90 = 0 \end{aligned}$$

for node 5:

$$\begin{aligned} \text{horizontal force equilibrium: } & -60.72 - 12.04 + 44.73 + 28.03 = 0 \\ \text{vertical force equilibrium: } & -35.24 - 35.04 + 19.10 + 51.18 = 0 \end{aligned}$$

for node 6:

$$\begin{aligned} \text{horizontal force equilibrium: } & 57.99 - 57.99 = 0 \\ \text{vertical force equilibrium: } & -6.81 + 6.81 = 0 \end{aligned}$$

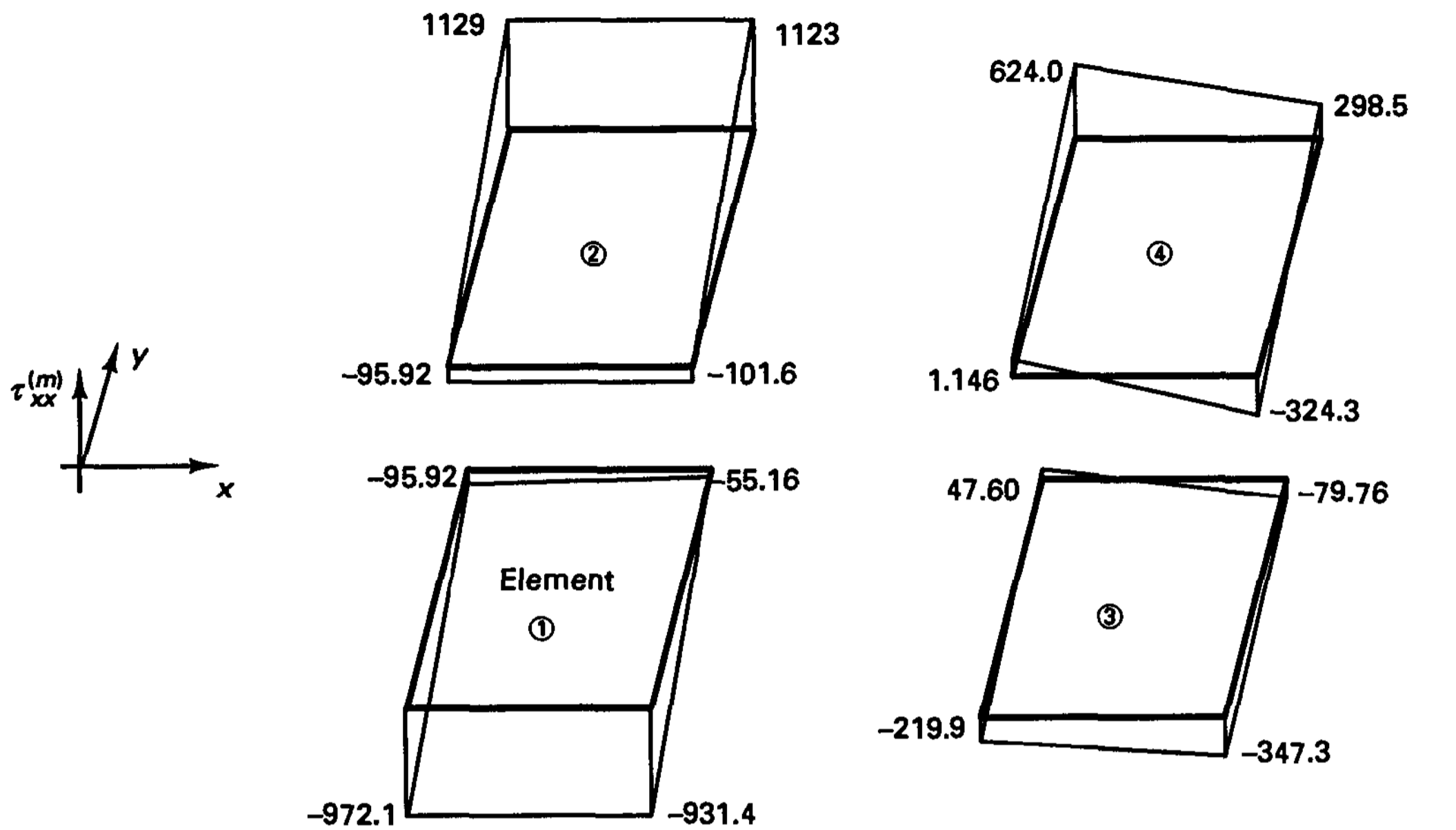
And for nodes 7, 8, and 9, force equilibrium is obviously also satisfied, where at node 9 the element nodal force balances the applied load $P = 100$.

Finally, let us check the overall force equilibrium of the model:
horizontal equilibrium:

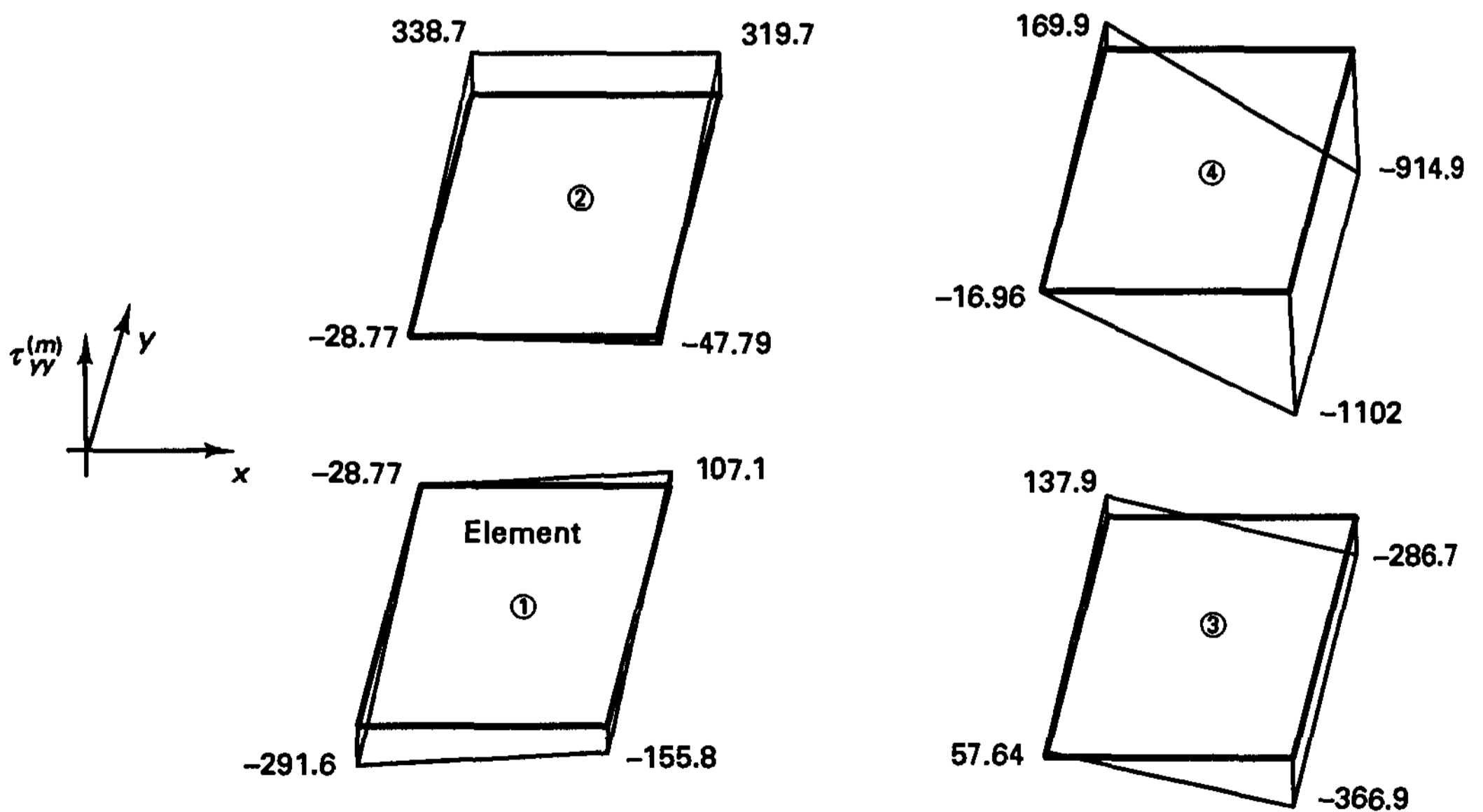
$$100.15 - 0.30 - 99.85 = 0$$

vertical equilibrium:

$$41.36 + 22.74 + 35.90 - 100 = 0$$

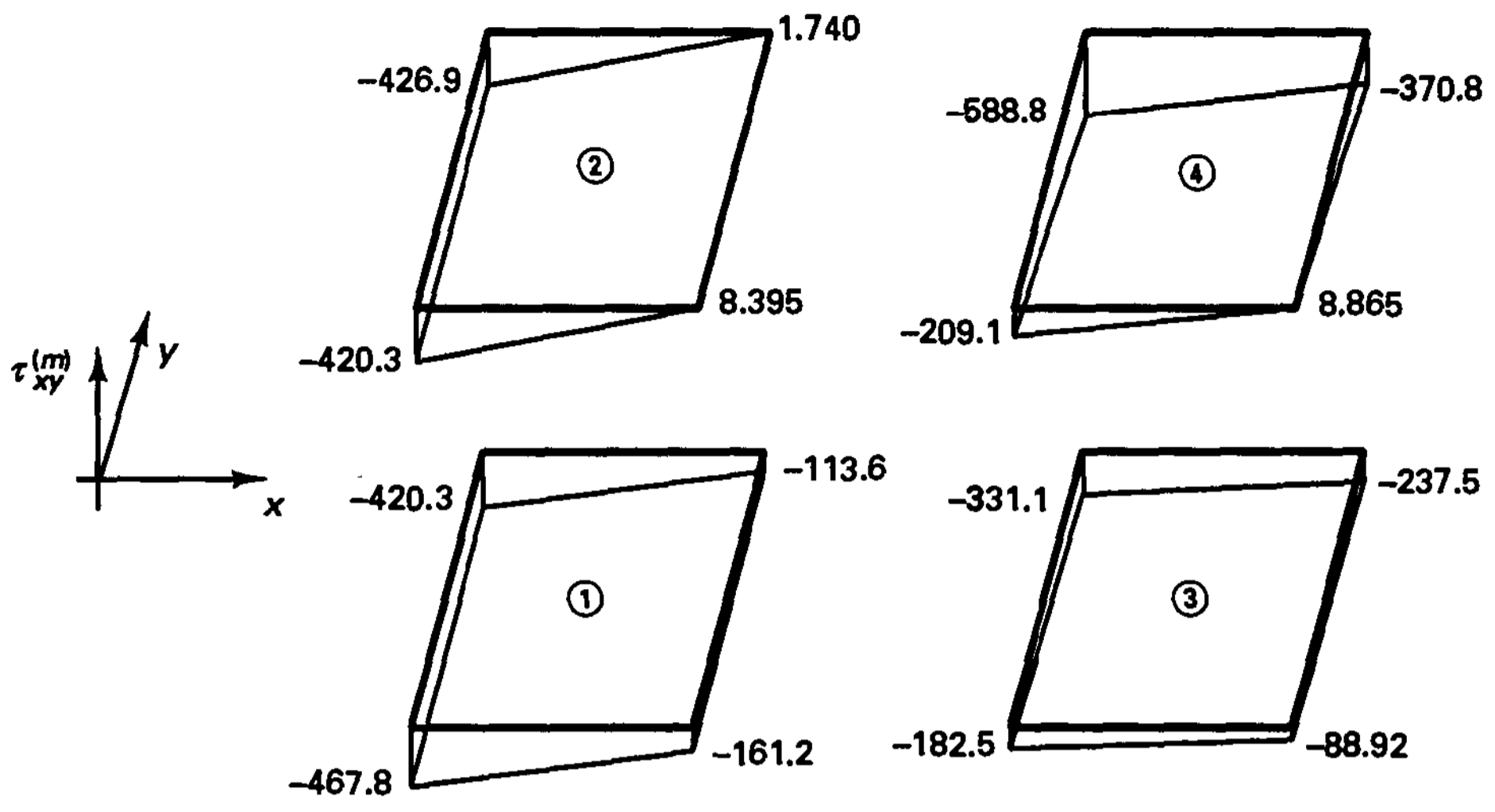


(a) Exploded view of elements showing stresses $\tau_{xx}^{(m)}$. Note the stress discontinuities between elements and the nonzero stresses along the free edges

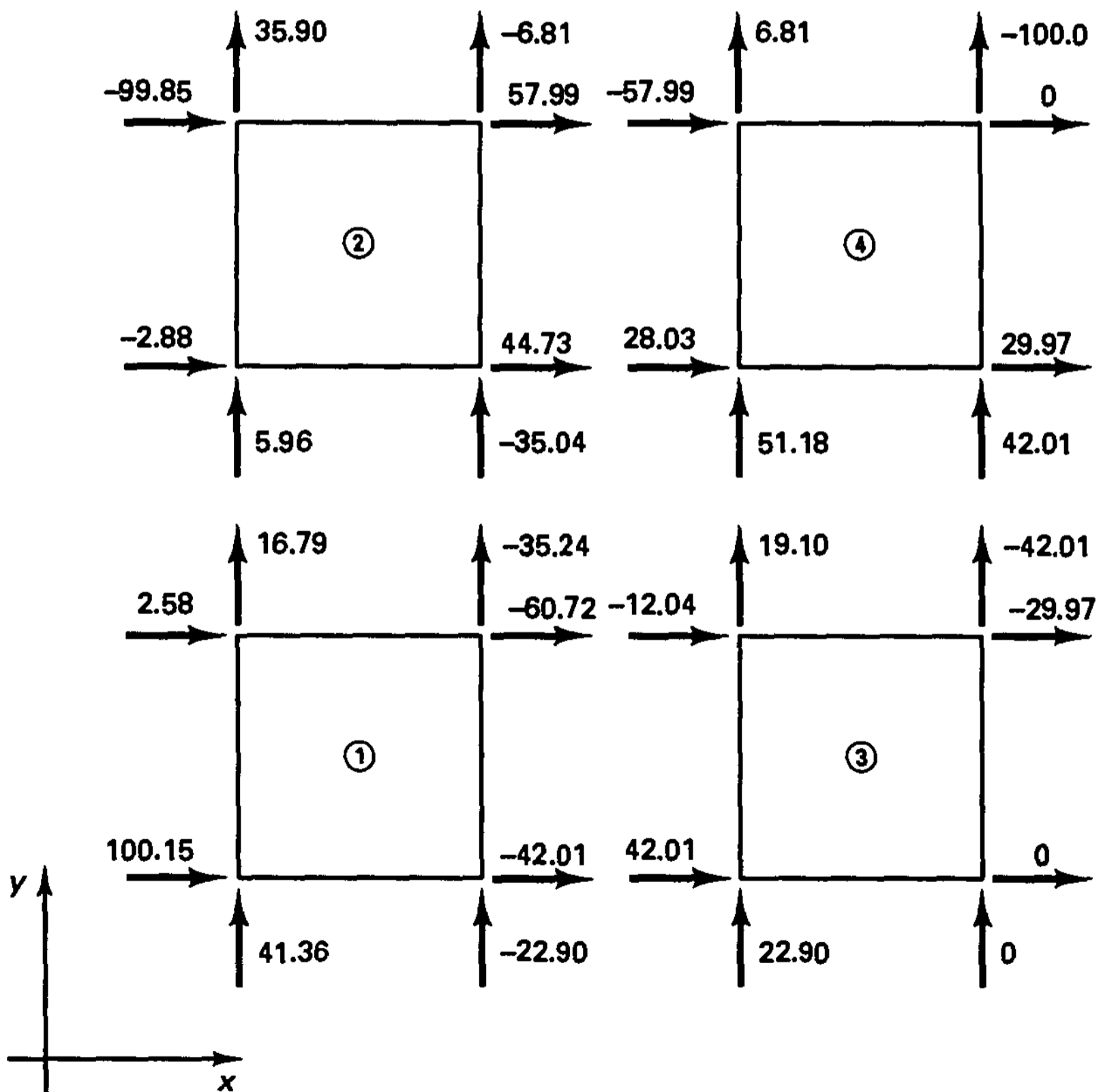


(b) Exploded view of elements showing stresses $\tau_{yy}^{(m)}$

Figure E4.9 Solution results for problem considered in Example 4.6 (rounded to digits shown)



(c) Exploded view of elements showing stresses $\tau_{xy}^{(m)}$



(d) Exploded view of elements showing element nodal point forces equivalent (in the virtual work sense) to the element stresses. The nodal point forces are at each node in equilibrium with the applied forces (including the reactions)

Figure E4.9 (continued)

moment equilibrium (about node 2):

$$-100 \times 4 + 100.15 \times 2 + 99.85 \times 2 = 0$$

It is important to realize that this force equilibrium will hold for *any* finite element mesh, however coarse the mesh may be, provided properly formulated elements are used (see Section 4.3).

Now consider element 4:

horizontal equilibrium:

$$0 - 57.99 + 28.03 + 29.97 = 0 \text{ (because of rounding)}$$

vertical equilibrium:

$$-100 + 6.81 + 51.18 + 42.01 = 0$$

moment equilibrium (about its local node 3):

$$-100 \times 2 + 57.99 \times 2 + 42.01 \times 2 = 0$$

Hence the element nodal forces are in equilibrium.

Element Local and Structure Global Degrees of Freedom

The derivations of the element matrices in Example 4.6 and 4.7 show that it is expedient to first establish the matrices corresponding to the local element degrees of freedom. The construction of the finite element matrices, which correspond to the global assemblage degrees of freedom [used in (4.19) to (4.25)] can then be directly achieved by identifying the global degrees of freedom that correspond to the local element degrees of freedom. However, considering the matrices $\mathbf{H}^{(m)}$, $\mathbf{B}^{(m)}$, $\mathbf{K}^{(m)}$, and so on, corresponding to the global assemblage degrees of freedom, only those rows and columns that correspond to element degrees of freedom have nonzero entries, and the main objective in defining these specific matrices was to be able to express the assemblage process of the element matrices in a theoretically elegant manner. In the practical implementation of the finite element method, this elegance is also present, but all element matrices are calculated corresponding only to the element degrees of freedom and are then directly assembled using the correspondence between the local element and global assemblage degrees of freedom. Thus, with only the element local nodal point degrees of freedom listed in $\hat{\mathbf{u}}$, we now write (as in Example 4.6)

$$\mathbf{u} = \mathbf{H}\hat{\mathbf{u}} \quad (4.31)$$

where the entries in the vector \mathbf{u} are the element displacements measured in any convenient local coordinate system. We then also have

$$\boldsymbol{\epsilon} = \mathbf{B}\hat{\mathbf{u}} \quad (4.32)$$

Considering the relations in (4.31) and (4.32), the fact that no superscript is used on the interpolation matrices indicates that the matrices are defined with respect to the local element degrees of freedom. Using the relations for the element stiffness matrix, mass

matrix, and load vector calculations as before, we obtain

$$\mathbf{K} = \int_V \mathbf{B}^T \mathbf{C} \mathbf{B} dV \quad (4.33)$$

$$\mathbf{M} = \int_V \rho \mathbf{H}^T \mathbf{H} dV \quad (4.34)$$

$$\mathbf{R}_B = \int_V \mathbf{H}^T \mathbf{f}^B dV \quad (4.35)$$

$$\mathbf{R}_S = \int_S \mathbf{H}^{sT} \mathbf{f}^S dS \quad (4.36)$$

$$\mathbf{R}_I = \int_V \mathbf{B}^T \boldsymbol{\tau}^I dV \quad (4.37)$$

where all variables are defined as in (4.19) to (4.25), but corresponding to the local element degrees of freedom. In the derivations and discussions to follow, we shall refer extensively to the relations in (4.33) to (4.37). Once the matrices given in (4.33) to (4.37) have been calculated, they can be assembled directly using the procedures described in Example 4.11 and Chapter 12.

In this assemblage process it is assumed that the directions of the element nodal point displacements $\hat{\mathbf{u}}$ in (4.31) are the same as the directions of the global nodal point displacements \mathbf{U} . However, in some analyses it is convenient to start the derivation with element nodal point degrees of freedom $\tilde{\mathbf{u}}$ that are not aligned with the global assemblage degrees of freedom. In this case we have

$$\mathbf{u} = \tilde{\mathbf{H}} \tilde{\mathbf{u}} \quad (4.38)$$

and

$$\tilde{\mathbf{u}} = \mathbf{T} \hat{\mathbf{u}} \quad (4.39)$$

where the matrix \mathbf{T} transforms the degrees of freedom $\hat{\mathbf{u}}$ to the degrees of freedom $\tilde{\mathbf{u}}$ and (4.39) corresponds to a first-order tensor transformation (see Section 2.4); the entries in column j of the matrix \mathbf{T} are the direction cosines of a unit vector corresponding to the j th degree of freedom in $\hat{\mathbf{u}}$ when measured in the directions of the $\tilde{\mathbf{u}}$ degrees of freedom. Substituting (4.39) into (4.38), we obtain

$$\mathbf{H} = \tilde{\mathbf{H}} \mathbf{T} \quad (4.40)$$

Thus, identifying all finite element matrices corresponding to the degrees of freedom $\tilde{\mathbf{u}}$ with a curl placed over them, we obtain from (4.40) and (4.33) to (4.37),

$$\begin{aligned} \mathbf{K} &= \mathbf{T}^T \tilde{\mathbf{K}} \mathbf{T}; & \mathbf{M} &= \mathbf{T}^T \tilde{\mathbf{M}} \mathbf{T} \\ \mathbf{R}_B &= \mathbf{T}^T \tilde{\mathbf{R}}_B; & \mathbf{R}_S &= \mathbf{T}^T \tilde{\mathbf{R}}_S; & \mathbf{R}_I &= \mathbf{T}^T \tilde{\mathbf{R}}_I \end{aligned} \quad (4.41)$$

We note that such transformations are also used when boundary displacements must be imposed that do not correspond to the global assemblage degrees of freedom (see Section 4.2.2). Table 4.1 summarizes some of the notation that we have employed.

We demonstrate the presented concepts in the following examples.

TABLE 4.1 Summary of some notation used

(a)	$\mathbf{u}^{(m)} = \mathbf{H}^{(m)} \hat{\mathbf{U}}$ or $\mathbf{u}^{(m)} = \mathbf{H}^{(m)} \mathbf{U}$ where $\mathbf{u}^{(m)}$ = displacements within element m as a function of the element coordinates \mathbf{U} = nodal point displacements of the total element assemblage [from equation (4.17) onward we simply use \mathbf{U}].
(b)	$\mathbf{u} = \mathbf{H} \hat{\mathbf{u}}$ where $\mathbf{u} \equiv \mathbf{u}^{(m)}$ and it is implied that a specific element is considered $\hat{\mathbf{u}}$ = nodal point displacements of the element under consideration; the entries of $\hat{\mathbf{u}}$ are those displacements in $\hat{\mathbf{U}}$ that belong to the element.
(c)	$\mathbf{u} = \tilde{\mathbf{H}} \tilde{\mathbf{u}}$ where $\tilde{\mathbf{u}}$ = nodal point displacements of an element in a coordinate system other than the global system (in which $\hat{\mathbf{U}}$ is defined).

EXAMPLE 4.10: Establish the matrix \mathbf{H} for the truss element shown in Fig. E4.10. The directions of local and global degrees of freedom are shown in the figure.

Here we have

$$\begin{bmatrix} u(x) \\ v(x) \end{bmatrix} = \frac{1}{L} \begin{bmatrix} \left(\frac{L}{2} - x\right) & 0 & \left(\frac{L}{2} + x\right) & 0 \\ 0 & \left(\frac{L}{2} - x\right) & 0 & \left(\frac{L}{2} + x\right) \end{bmatrix} \begin{bmatrix} \tilde{u}_1 \\ \tilde{v}_1 \\ \tilde{u}_2 \\ \tilde{v}_2 \end{bmatrix} \quad (a)$$

and

$$\begin{bmatrix} \tilde{u}_1 \\ \tilde{v}_1 \\ \tilde{u}_2 \\ \tilde{v}_2 \end{bmatrix} = \begin{bmatrix} \cos \alpha & \sin \alpha & 0 & 0 \\ -\sin \alpha & \cos \alpha & 0 & 0 \\ 0 & 0 & \cos \alpha & \sin \alpha \\ 0 & 0 & -\sin \alpha & \cos \alpha \end{bmatrix} \begin{bmatrix} u_1 \\ v_1 \\ u_2 \\ v_2 \end{bmatrix}$$

Thus, we have

$$\mathbf{H} = \frac{1}{L} \begin{bmatrix} \left(\frac{L}{2} - x\right) & 0 & \left(\frac{L}{2} + x\right) & 0 \\ 0 & \left(\frac{L}{2} - x\right) & 0 & \left(\frac{L}{2} + x\right) \end{bmatrix} \begin{bmatrix} \cos \alpha & \sin \alpha & 0 & 0 \\ -\sin \alpha & \cos \alpha & 0 & 0 \\ 0 & 0 & \cos \alpha & \sin \alpha \\ 0 & 0 & -\sin \alpha & \cos \alpha \end{bmatrix}$$

It should be noted that for the construction of the strain-displacement matrix \mathbf{B} (in linear analysis), only the first row of \mathbf{H} is required because only the normal strain $\epsilon_{xx} = \partial u / \partial x$ is

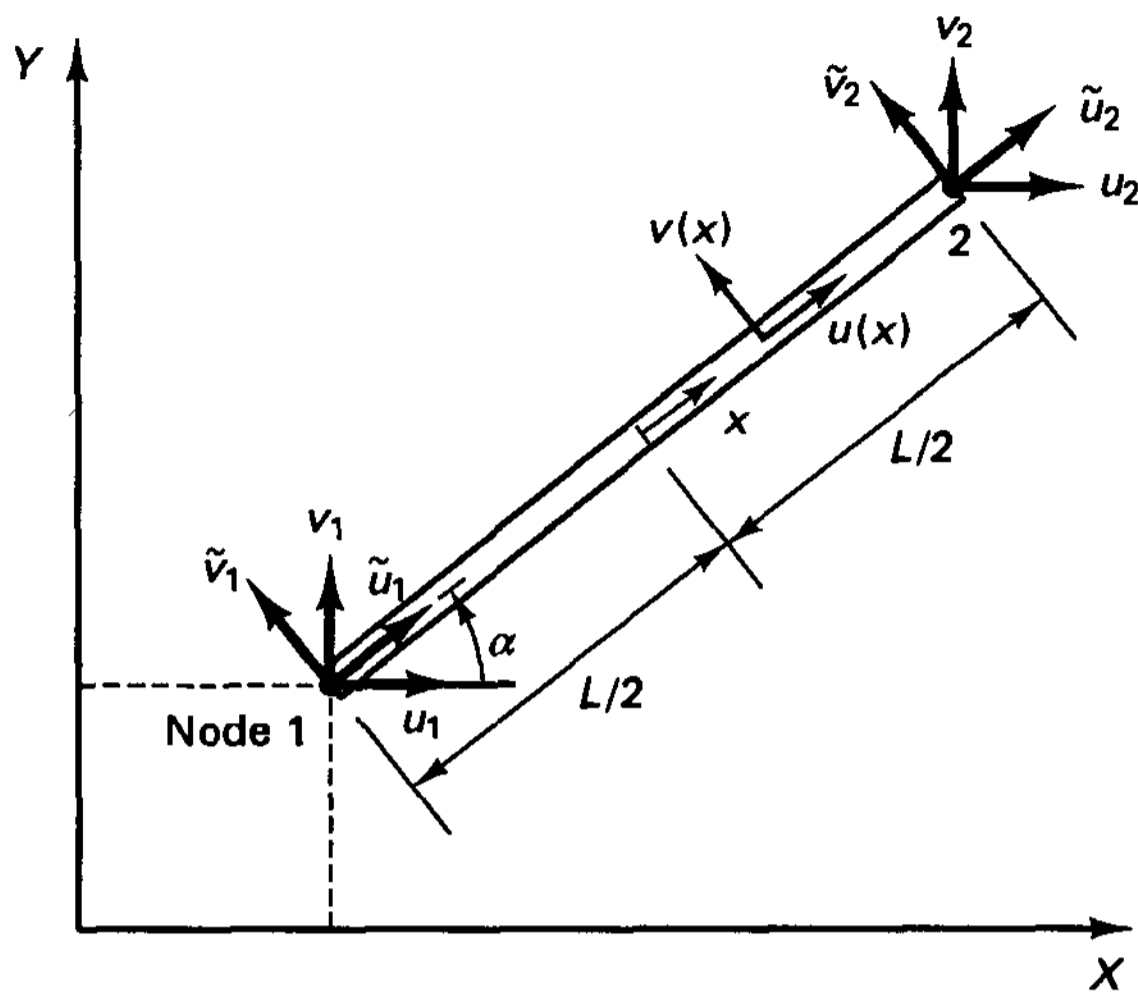


Figure E4.10 Truss element

considered in the derivation of the stiffness matrix. In practice, it is effective to use only the first row of the matrix $\tilde{\mathbf{H}}$ in (a) and then transform the matrix $\tilde{\mathbf{K}}$ as given in (4.41).

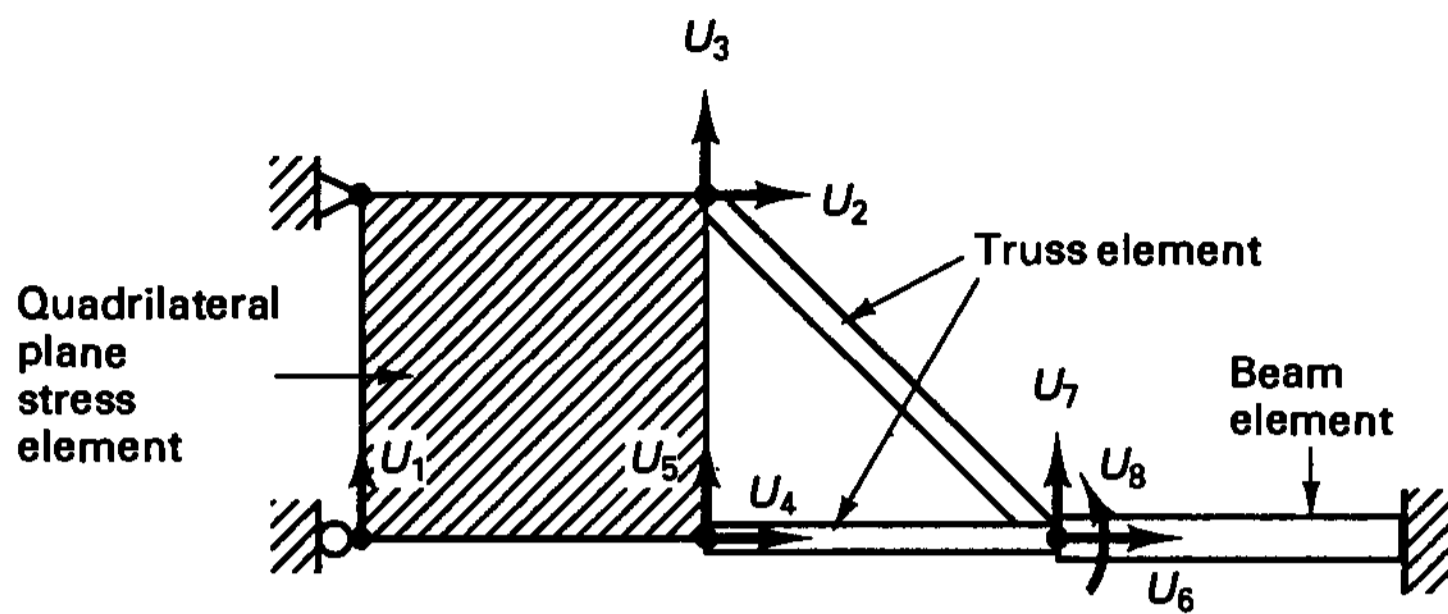
EXAMPLE 4.11: Assume that the element stiffness matrices corresponding to the element displacements shown in Fig. E4.11 have been calculated and denote the elements as shown (A), (B), (C), and (D). Assemble these element matrices directly into the global structure stiffness matrix with the displacement boundary conditions shown in Fig. E4.11(a). Also, give the connectivity arrays LM for the elements.

In this analysis all element stiffness matrices have already been established corresponding to the degrees of freedom aligned with the global directions. Therefore, no transformation as given in (4.41) is required, and we can directly assemble the complete stiffness matrix.

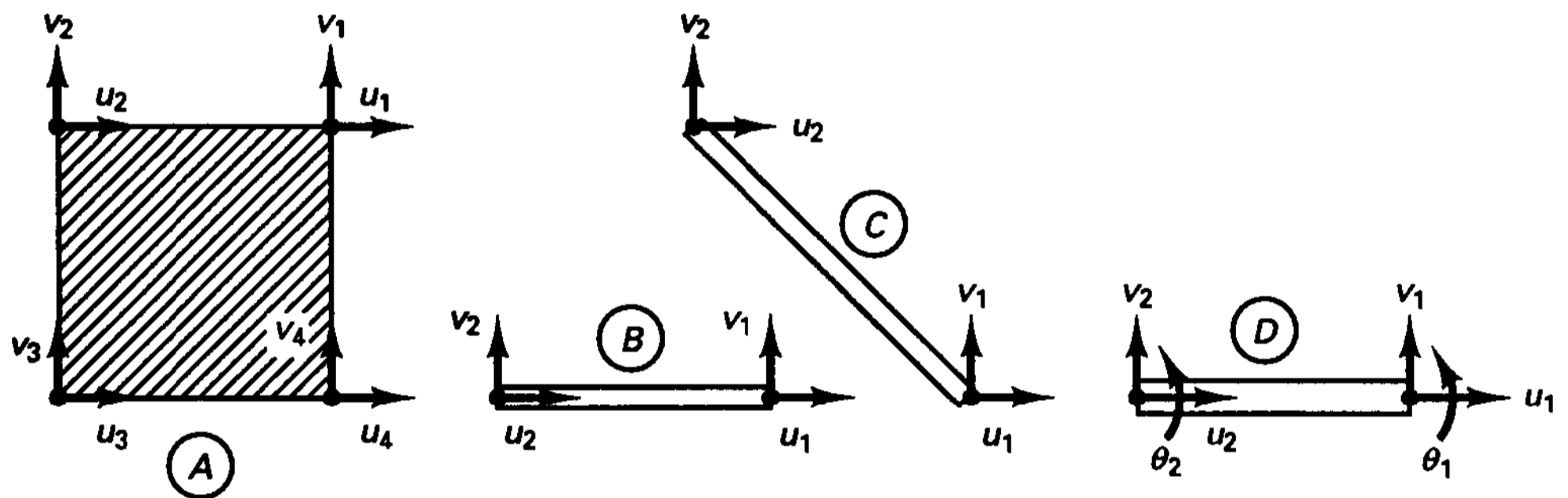
Since the displacements at the supports are zero, we need only assemble the structure stiffness matrix corresponding to the unknown displacement components in \mathbf{U} . The connectivity array (LM array) for each element lists the global structure degrees of freedom in the order of the element local degrees of freedom, with a zero signifying that the corresponding column and row of the element stiffness matrix are not assembled (the column and row correspond to a zero structure degree of freedom) (see also Chapter 12).

	U_2	U_3		U_1	U_4	U_5	← Global displacements		
	u_1	v_1	u_2	v_2	u_3	v_3	u_4	v_4	← Local displacements

$$\mathbf{K}_A = \begin{bmatrix} a_{11} & a_{12} & \cdots & a_{16} & a_{17} & a_{18} \\ a_{21} & a_{22} & \cdots & a_{26} & a_{27} & a_{28} \\ \vdots & \vdots & \cdots & \vdots & \vdots & \vdots \\ \vdots & \vdots & \cdots & \vdots & \vdots & \vdots \\ a_{61} & a_{62} & \cdots & a_{66} & a_{67} & a_{68} \\ a_{71} & a_{72} & \cdots & a_{76} & a_{77} & a_{78} \\ a_{81} & a_{82} & \cdots & a_{86} & a_{87} & a_{88} \end{bmatrix} \begin{matrix} u_1 & U_2 \\ v_1 & U_3 \\ & u_2 \\ & v_2 \\ & u_3 \\ v_3 & U_1 \\ u_4 & U_4 \\ v_4 & U_5 \end{matrix}$$



(a) Structural assemblage and degrees of freedom



(b) Individual elements

Figure E4.11 A simple element assemblage

$$\mathbf{K}_B = \begin{matrix} & U_6 & U_7 & U_4 & U_5 \\ & u_1 & v_1 & u_2 & v_2 \\ \begin{bmatrix} b_{11} & b_{12} & b_{13} & b_{14} \\ b_{21} & b_{22} & b_{23} & b_{24} \\ b_{31} & b_{32} & b_{33} & b_{34} \\ b_{41} & b_{42} & b_{43} & b_{44} \end{bmatrix} & u_1 & U_6 & & \\ & v_1 & U_7 & & \\ & u_2 & U_4 & & \\ & v_2 & U_5 & & \end{matrix} \quad \mathbf{K}_C = \begin{matrix} & U_6 & U_7 & U_2 & U_3 \\ & u_1 & v_1 & u_2 & v_2 \\ \begin{bmatrix} c_{11} & c_{12} & c_{13} & c_{14} \\ c_{21} & c_{22} & c_{23} & c_{24} \\ c_{31} & c_{32} & c_{33} & c_{34} \\ c_{41} & c_{42} & c_{43} & c_{44} \end{bmatrix} & u_1 & U_6 & & \\ & v_1 & U_7 & & \\ & u_2 & U_2 & & \\ & v_2 & U_3 & & \end{matrix}$$

$$\mathbf{K}_D = \begin{matrix} & & & U_6 & U_7 & U_8 \\ & & & u_2 & v_2 & \theta_2 \\ \begin{bmatrix} \dots & \cdot & \cdot & \cdot & \cdot & \dots \\ \dots & \cdot & \cdot & \cdot & \cdot & \dots \\ \dots & \cdot & \cdot & \cdot & \cdot & \dots \\ \dots & \cdot & \dots & d_{44} & d_{45} & d_{46} \\ \dots & \cdot & \dots & d_{54} & d_{55} & d_{56} \\ \dots & \cdot & \dots & d_{64} & d_{65} & d_{66} \end{bmatrix} & u_1 & & & & \\ & v_1 & & & & \\ & \theta_1 & & & & \\ & u_2 & U_6 & & & \\ & v_2 & U_7 & & & \\ & \theta_2 & U_8 & & & \end{matrix}$$

and the equation $\mathbf{K} = \sum_m \mathbf{K}^{(m)}$ gives

$$\mathbf{K} = \begin{bmatrix}
 U_1 & U_2 & U_3 & U_4 & U_5 & U_6 & U_7 & U_8 \\
 a_{66} & a_{61} & a_{62} & a_{67} & a_{68} & \text{zeros} & & \\
 a_{16} & a_{11} + c_{33} & a_{12} + c_{34} & a_{17} & a_{18} & c_{31} & c_{32} & \\
 a_{26} & a_{21} + c_{43} & a_{22} + c_{44} & a_{27} & a_{28} & c_{41} & c_{42} & \\
 a_{76} & a_{71} & a_{72} & a_{77} + b_{33} & a_{78} + b_{34} & b_{31} & b_{32} & \\
 a_{86} & a_{81} & a_{82} & a_{87} + b_{43} & a_{88} + b_{44} & b_{41} & b_{42} & \\
 & c_{13} & c_{14} & b_{13} & b_{14} & b_{11} + c_{11} & b_{12} + c_{12} & d_{46} \\
 & & & & & + d_{44} & + d_{45} & \\
 & c_{23} & c_{24} & b_{23} & b_{24} & b_{21} + c_{21} & b_{22} + c_{22} & d_{56} \\
 & & & & & + d_{54} & + d_{55} & \\
 \text{symmetric about diagonal} & & & & & d_{64} & d_{65} & d_{66} \\
 & & & & & & & U_8
 \end{bmatrix} \begin{matrix} U_1 \\ U_2 \\ U_3 \\ U_4 \\ U_5 \\ U_6 \\ U_7 \\ U_8 \end{matrix}$$

The LM arrays for the elements are

for element A: $\text{LM} = [2 \ 3 \ 0 \ 0 \ 0 \ 1 \ 4 \ 5]$

for element B: $\text{LM} = [6 \ 7 \ 4 \ 5]$

for element C: $\text{LM} = [6 \ 7 \ 2 \ 3]$

for element D: $\text{LM} = [0 \ 0 \ 0 \ 6 \ 7 \ 8]$

We note that if the element stiffness matrices and LM arrays are known, the total structure stiffness matrix can be obtained directly in an automated manner (see also Chapter 12).

4.2.2 Imposition of Displacement Boundary Conditions

We discussed in Section 3.3.2 that in the analysis of a continuum we have displacement (also called essential) boundary conditions and force (also called natural) boundary conditions. Using the displacement-based finite element method, the force boundary conditions are taken into account in evaluating the externally applied nodal point force vector. The vector \mathbf{R}_C assembles the concentrated loads including the reactions, and the vector \mathbf{R}_S contains the effect of the distributed surface loads and distributed reactions.

Assume that the equilibrium equations of a finite element system without the imposition of the displacement boundary conditions as derived in Section 4.2.1 are, neglecting damping,

$$\begin{bmatrix} \mathbf{M}_{aa} & \mathbf{M}_{ab} \\ \mathbf{M}_{ba} & \mathbf{M}_{bb} \end{bmatrix} \begin{bmatrix} \ddot{\mathbf{U}}_a \\ \ddot{\mathbf{U}}_b \end{bmatrix} + \begin{bmatrix} \mathbf{K}_{aa} & \mathbf{K}_{ab} \\ \mathbf{K}_{ba} & \mathbf{K}_{bb} \end{bmatrix} \begin{bmatrix} \mathbf{U}_a \\ \mathbf{U}_b \end{bmatrix} = \begin{bmatrix} \mathbf{R}_a \\ \mathbf{R}_b \end{bmatrix} \quad (4.42)$$

where the \mathbf{U}_a are the unknown displacements and the \mathbf{U}_b are the known, or prescribed, displacements. Solving for \mathbf{U}_a , we obtain

$$\mathbf{M}_{aa}\ddot{\mathbf{U}}_a + \mathbf{K}_{aa}\mathbf{U}_a = \mathbf{R}_a - \mathbf{K}_{ab}\mathbf{U}_b - \mathbf{M}_{ab}\ddot{\mathbf{U}}_b \quad (4.43)$$

Hence, in this solution for \mathbf{U}_a , only the stiffness and mass matrices of the complete assemblage corresponding to the unknown degrees of freedom \mathbf{U}_a need to be assembled (see

Example 4.11), but the load vector \mathbf{R}_a must be modified to include the effect of imposed nonzero displacements. Once the displacements \mathbf{U}_a have been evaluated from (4.43), the reactions can be calculated by first writing [(using (4.18)]

$$\mathbf{R}_b = \mathbf{R}_B^b + \mathbf{R}_S^b - \mathbf{R}_I^b + \mathbf{R}_C^b + \mathbf{R}_r \tag{4.44}$$

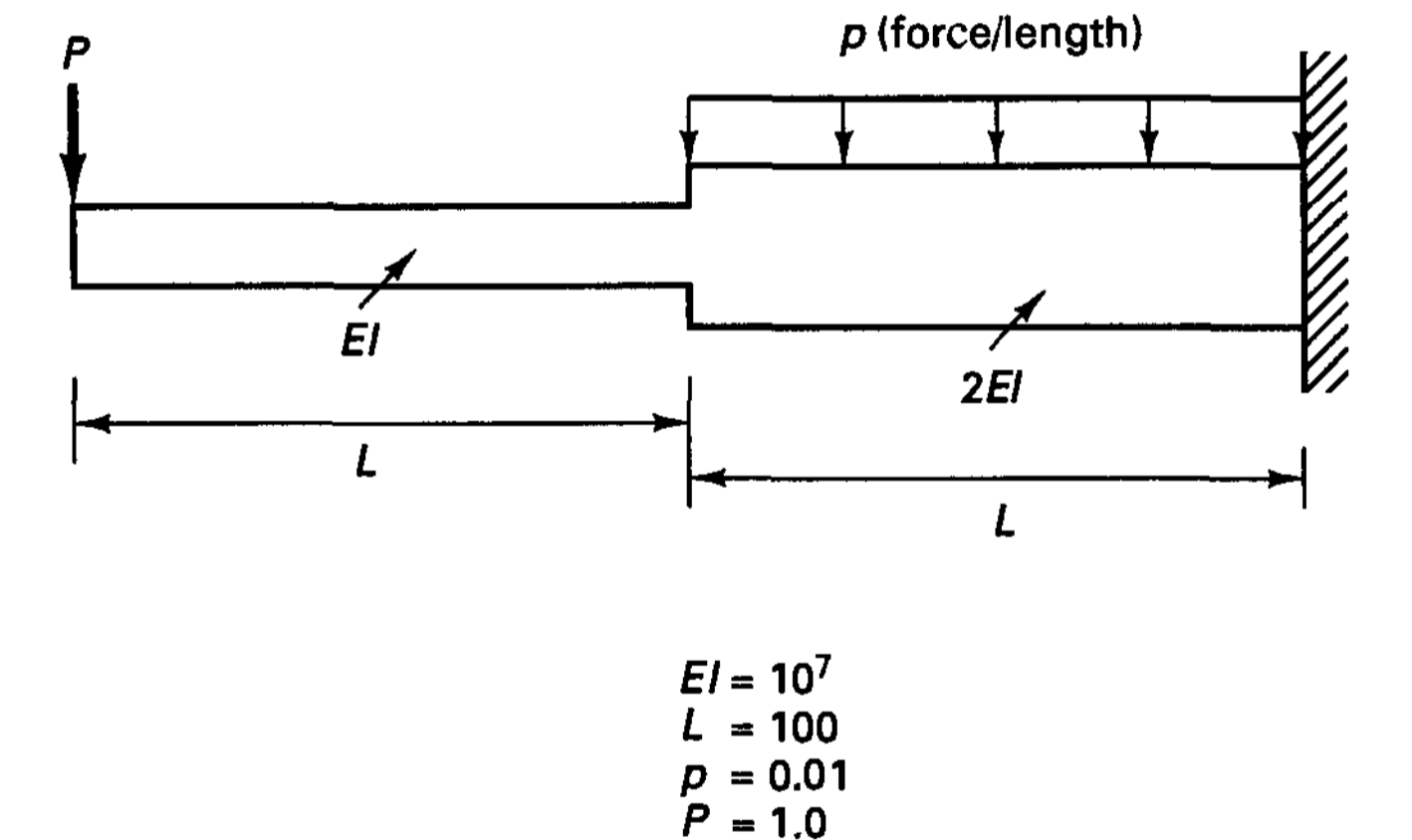
where \mathbf{R}_B^b , \mathbf{R}_S^b , \mathbf{R}_I^b , and \mathbf{R}_C^b are the known externally applied nodal point loads not including the reactions and \mathbf{R}_r denotes the unknown reactions. The superscript b indicates that of \mathbf{R}_B , \mathbf{R}_S , \mathbf{R}_I , and \mathbf{R}_C in (4.17) only the components corresponding to the \mathbf{U}_b degrees of freedom are used in the force vectors. Note that the vector \mathbf{R}_r may be thought of as an unknown correction to the concentrated loads. Using (4.44) and the second set of equations in (4.42), we thus obtain

$$\mathbf{R}_r = \mathbf{M}_{ba}\ddot{\mathbf{U}}_a + \mathbf{M}_{bb}\ddot{\mathbf{U}}_b + \mathbf{K}_{ba}\mathbf{U}_a + \mathbf{K}_{bb}\mathbf{U}_b - \mathbf{R}_B^b - \mathbf{R}_S^b + \mathbf{R}_I^b - \mathbf{R}_C^b \tag{4.45}$$

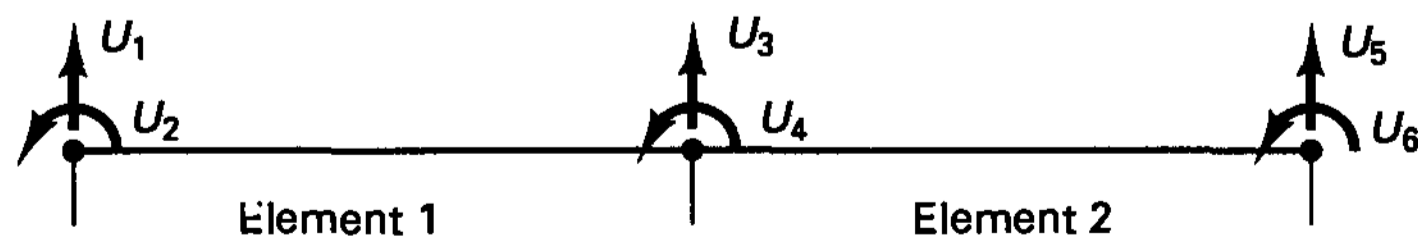
Here, the last four terms are a correction due to known internal and surface element loading and any concentrated loading, all directly applied to the supports.

We demonstrate these relations in the following example.

EXAMPLE 4.12: Consider the structure shown in Fig. E4.12. Solve for the displacement response and calculate the reactions.



(a) Cantilever beam



(b) Discretization

Figure E4.12 Analysis of cantilever beam

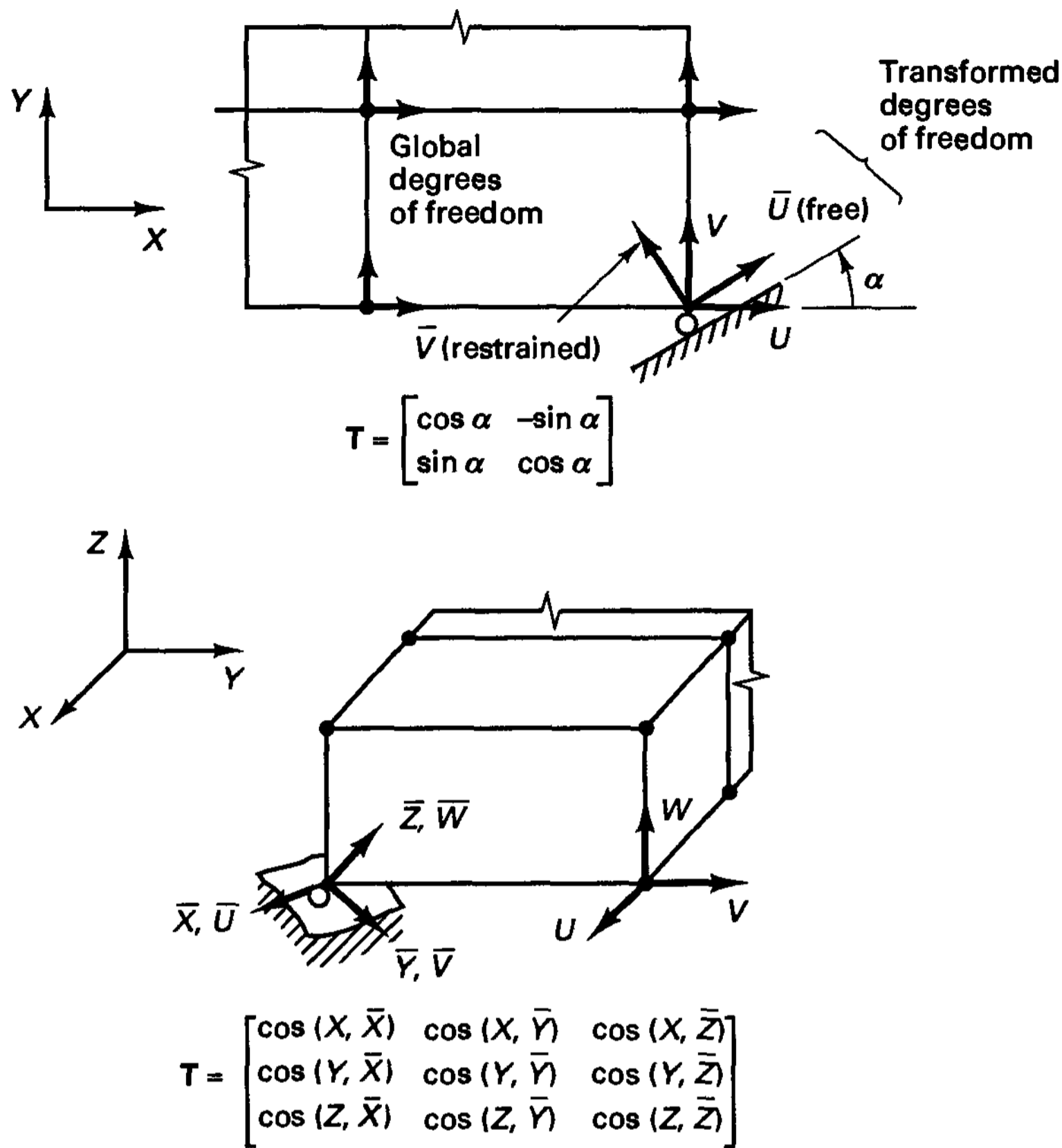


Figure 4.3 Transformation to skew boundary conditions

In an alternative approach, the required displacements can also be imposed by adding to the finite element equilibrium equations (4.47) the constraint equations that express the prescribed displacement conditions. Assume that the displacement is to be specified at degree of freedom i , say $\bar{U}_i = b$; then the constraint equation

$$k\bar{U}_i = kb \tag{4.49}$$

is added to the equilibrium equations (4.47), where $k \gg \bar{k}_{ii}$. Therefore, the solution of the modified equilibrium equations must now give $\bar{U}_i = b$, and we note that because (4.47) was used, only the diagonal element in the stiffness matrix was affected, resulting in a numerically stable solution (see Section 8.2.6). Physically, this procedure can be interpreted as adding at the degree of freedom i a spring of large stiffness k and specifying a load which, because of the relatively flexible element assemblage, produces at this degree of freedom the required displacement b (see Fig. 4.4). Mathematically, the procedure corresponds to an application of the penalty method discussed in Section 3.4.

In addition to specified nodal point displacement conditions, some nodal point displacements may also be subjected to constraint conditions. Considering (4.24), a typical constraint equation would be

$$U_i = \sum_{j=1}^{r_i} \alpha_{q_j} U_{q_j} \tag{4.50}$$

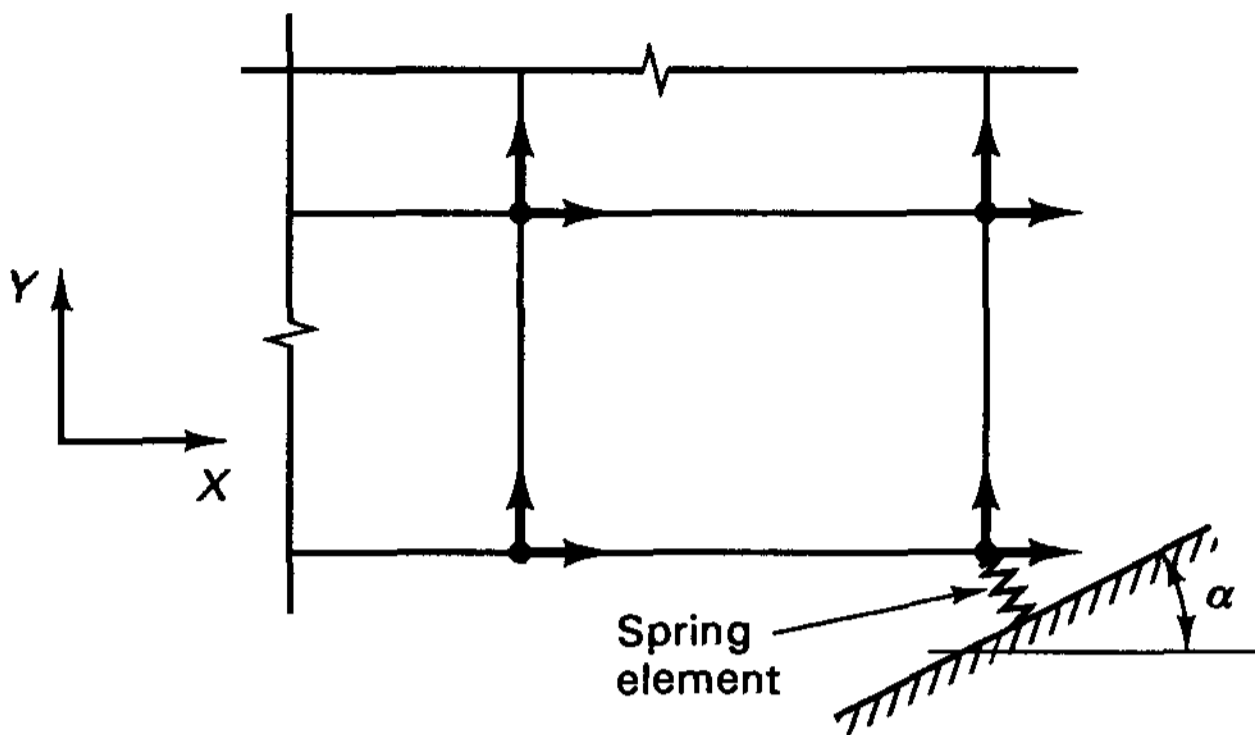


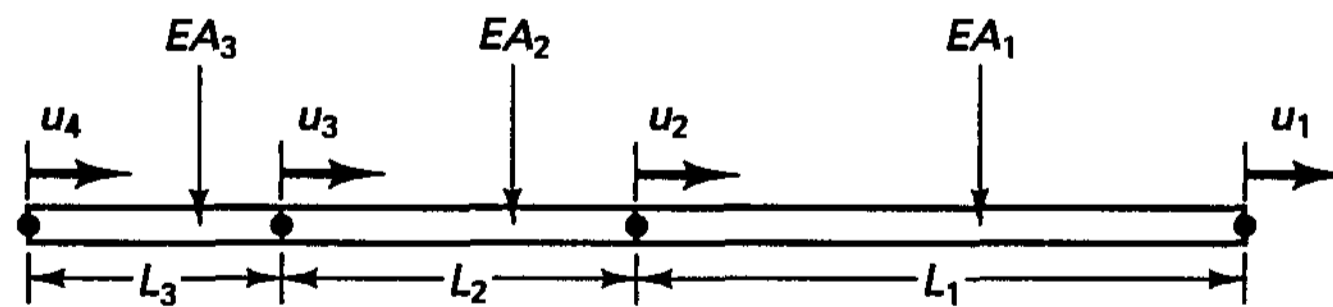
Figure 4.4 Skew boundary condition imposed using spring element

where the U_i is a dependent nodal point displacement and the U_{q_j} are r_i independent nodal point displacements. Using all constraint equations of the form (4.50) and recognizing that these constraints must hold in the application of the principle of virtual work for the actual nodal point displacements as well as for the virtual displacements, the imposition of the constraints corresponds to a transformation of the form (4.46) and (4.47), in which \mathbf{T} is now a rectangular matrix and $\bar{\mathbf{U}}$ contains all independent degrees of freedom. This transformation corresponds to adding α_{q_j} times the i th columns and rows to the q_j th columns and rows, for $j = 1, \dots, r_i$ and all i considered. In the actual implementation the transformation is performed effectively on the element level during the assemblage process.

Finally, it should be noted that combinations of the above displacement boundary conditions are possible, where, for example, in (4.50) an independent displacement component may correspond to a skew boundary condition with a specified displacement. We demonstrate the imposition of displacement constraints in the following examples.

EXAMPLE 4.13: Consider the truss assemblage shown in Fig. E4.13. Establish the stiffness matrix of the structure that contains the constraint conditions given.

The independent degrees of freedom in this analysis are U_1 , U_2 , and U_4 . The element stiffness matrices are given in Fig. E4.13, and we recognize that corresponding to (4.50), we



Displacement conditions: $u_3 = 2u_1$
 $u_4 = \delta$

$$K_i = \frac{EA_i}{L_i} \begin{bmatrix} 1 & -1 \\ -1 & 1 \end{bmatrix}$$

Figure E4.13 Truss assemblage

have $i = 3$, $\alpha_1 = 2$, and $q_1 = 1$. Establishing the complete stiffness matrix directly during the assemblage process, we have

$$\mathbf{K} = \begin{bmatrix} \frac{EA_1}{L_1} & -\frac{EA_1}{L_1} & 0 \\ -\frac{EA_1}{L_1} & \frac{EA_1}{L_1} & 0 \\ 0 & 0 & 0 \end{bmatrix} + \begin{bmatrix} \frac{4EA_2}{L_2} & -\frac{2EA_2}{L_2} & 0 \\ -\frac{2EA_2}{L_2} & \frac{EA_2}{L_2} & 0 \\ 0 & 0 & 0 \end{bmatrix} + \begin{bmatrix} \frac{4EA_3}{L_3} & 0 & -\frac{2EA_3}{L_3} \\ 0 & 0 & 0 \\ -\frac{2EA_3}{L_3} & 0 & \frac{EA_3}{L_3} \end{bmatrix} + \begin{bmatrix} 0 & 0 & 0 \\ 0 & 0 & 0 \\ 0 & 0 & k \end{bmatrix}$$

where

$$k \geq \frac{EA_3}{L_3}$$

EXAMPLE 4.14: The frame structure shown in Fig. E4.14(a) is to be analyzed. Use symmetry and constraint conditions to establish a suitable model for analysis.

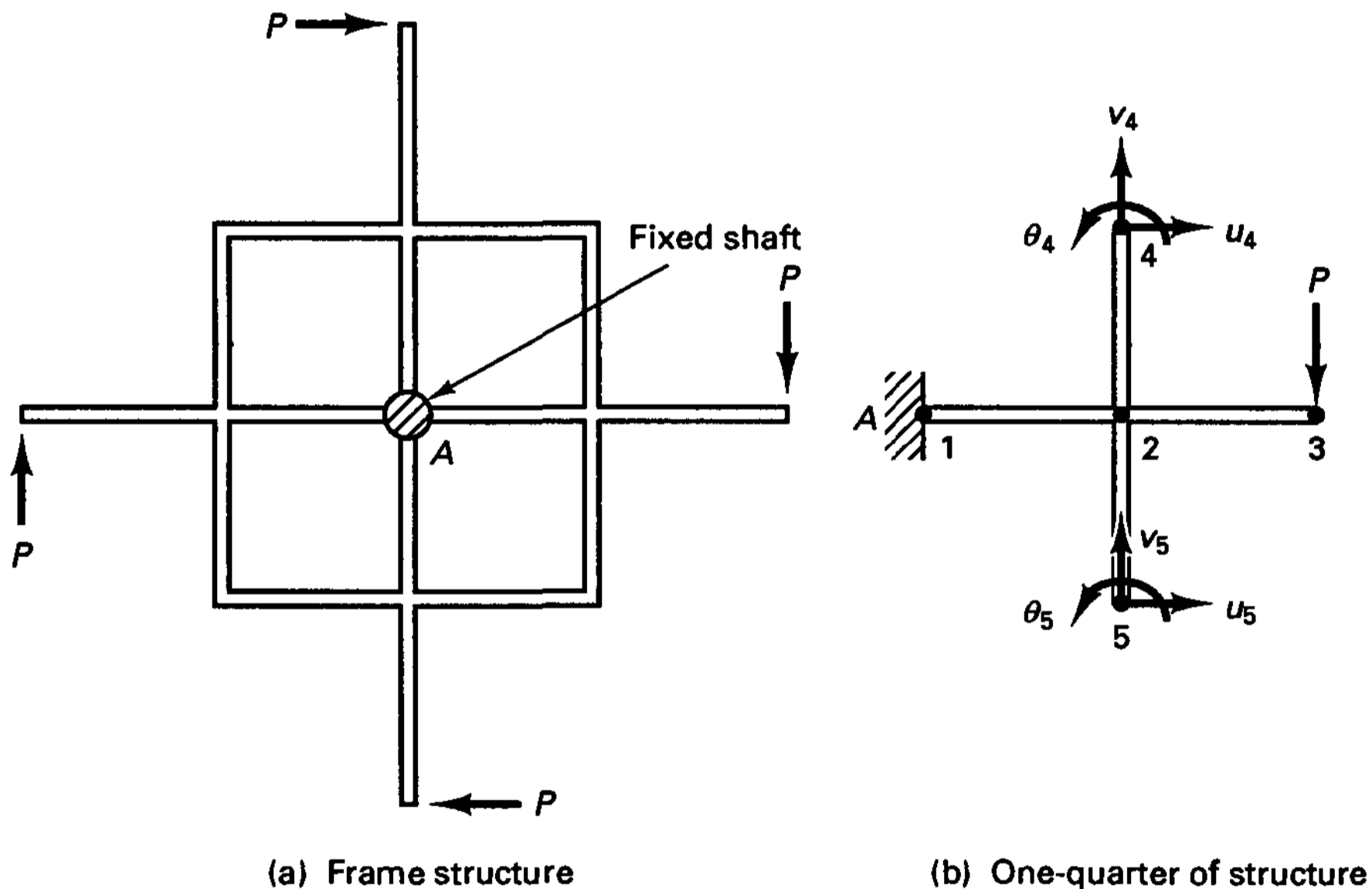


Figure E4.14 Analysis of a cyclicly symmetric structure

The complete structure and applied loading display cyclic symmetry, so that only one-quarter of the structure need be considered, as shown in Fig. E4.14(b), with the following constraint conditions:

$$\begin{aligned} u_5 &= v_4 \\ v_5 &= -u_4 \\ \theta_5 &= \theta_4 \end{aligned}$$

This is a simple example demonstrating how the analysis effort can be reduced considerably through the use of symmetry conditions. In practice, the saving through the use of cyclic symmetry conditions can in some cases be considerable, and indeed only by use of such conditions may the analysis be possible.

In this analysis, the structure *and* loading show cyclic symmetry. An analysis capability can also be developed in which only a part of the structure is modeled for the case of a geometrically cyclic symmetric structure with arbitrary loading (see, for example, W. Zhong and C. Qiu [A]).

4.2.3 Generalized Coordinate Models for Specific Problems

In Section 4.2.1 the finite element discretization procedure and derivation of the equilibrium equations was presented in general; i.e., a general three-dimensional body was considered. As shown in the examples, the general equations derived must be specialized in specific analyses to the specific stress and strain conditions considered. The objective in this section is to discuss and summarize how the finite element matrices that correspond to specific problems can be obtained from the general finite element equations (4.8) to (4.25).

Although in theory any body may be understood to be three-dimensional, for practical analysis it is in many cases imperative to reduce the dimensionality of the problem. The first step in a finite element analysis is therefore to decide what kind of problem⁸ is at hand. This decision is based on the assumptions used in the theory of elasticity mathematical models for specific problems. The classes of problems that are encountered may be summarized as (1) truss, (2) beam, (3) plane stress, (4) plane strain, (5) axisymmetric, (6) plate bending, (7) thin shell, (8) thick shell, and (9) general three-dimensional. For each of these problem cases, the general formulation is applicable; however, only the appropriate displacement, stress, and strain variables must be used. These variables are summarized in Tables 4.2 and 4.3 together with the stress-strain matrices to be employed when considering an isotropic material. Figure 4.5 shows various stress and strain conditions considered in the formulation of finite element matrices.

TABLE 4.2 Corresponding kinematic and static variables in various problems

Problem	Displacement components	Strain vector ϵ^T	Stress vector τ^T
Bar	u	$[\epsilon_{xx}]$	$[\tau_{xx}]$
Beam	w	$[\kappa_{xx}]$	$[M_{xx}]$
Plane stress	u, v	$[\epsilon_{xx} \ \epsilon_{yy} \ \gamma_{xy}]$	$[\tau_{xx} \ \tau_{yy} \ \tau_{xy}]$
Plane strain	u, v	$[\epsilon_{xx} \ \epsilon_{yy} \ \gamma_{xy}]$	$[\tau_{xx} \ \tau_{yy} \ \tau_{xy}]$
Axisymmetric	u, v	$[\epsilon_{xx} \ \epsilon_{yy} \ \gamma_{xy} \ \epsilon_{zz}]$	$[\tau_{xx} \ \tau_{yy} \ \tau_{xy} \ \tau_{zz}]$
Three-dimensional	u, v, w	$[\epsilon_{xx} \ \epsilon_{yy} \ \epsilon_{zz} \ \gamma_{xy} \ \gamma_{yz} \ \gamma_{zx}]$	$[\tau_{xx} \ \tau_{yy} \ \tau_{zz} \ \tau_{xy} \ \tau_{yz} \ \tau_{zx}]$
Plate bending	w	$[\kappa_{xx} \ \kappa_{yy} \ \kappa_{xy}]$	$[M_{xx} \ M_{yy} \ M_{xy}]$

Notation: $\epsilon_{xx} = \frac{\partial u}{\partial x}$, $\epsilon_{yy} = \frac{\partial v}{\partial y}$, $\gamma_{xy} = \frac{\partial u}{\partial y} + \frac{\partial v}{\partial x}$, . . . , $\kappa_{xx} = \frac{\partial^2 w}{\partial x^2}$, $\kappa_{yy} = \frac{\partial^2 w}{\partial y^2}$, $\kappa_{xy} = 2 \frac{\partial^2 w}{\partial x \partial y}$.

In Examples 4.5 to 4.10 we already developed some specific finite element matrices. Referring to Example 4.6, in which we considered a plane stress condition, we used for the u and v displacements simple linear polynomial assumptions, where we identified the

⁸ We use here the parlance commonly used in engineering analysis but recognize that “choice of problem” really corresponds to “choice of mathematical model” (see Section 1.2).

TABLE 4.3 Generalized stress-strain matrices for isotropic materials and the problems in Table 4.2

Problem	Material matrix C
Bar Beam	E EI
Plane stress	$\frac{E}{1-\nu^2} \begin{bmatrix} 1 & \nu & 0 \\ \nu & 1 & 0 \\ 0 & 0 & \frac{1-\nu}{2} \end{bmatrix}$
Plane strain	$\frac{E(1-\nu)}{(1+\nu)(1-2\nu)} \begin{bmatrix} 1 & \frac{\nu}{1-\nu} & 0 \\ \frac{\nu}{1-\nu} & 1 & 0 \\ 0 & 0 & \frac{1-2\nu}{2(1-\nu)} \end{bmatrix}$
Axisymmetric	$\frac{E(1-\nu)}{(1+\nu)(1-2\nu)} \begin{bmatrix} 1 & \frac{\nu}{1-\nu} & 0 & \frac{\nu}{1-\nu} \\ \frac{\nu}{1-\nu} & 1 & 0 & \frac{\nu}{1-\nu} \\ 0 & 0 & \frac{1-2\nu}{2(1-\nu)} & 0 \\ \frac{\nu}{1-\nu} & \frac{\nu}{1-\nu} & 0 & 1 \end{bmatrix}$
Three-dimensional	$\frac{E(1-\nu)}{(1+\nu)(1-2\nu)} \begin{bmatrix} 1 & \frac{\nu}{1-\nu} & \frac{\nu}{1-\nu} & & & \\ \frac{\nu}{1-\nu} & 1 & \frac{\nu}{1-\nu} & & & \\ \frac{\nu}{1-\nu} & \frac{\nu}{1-\nu} & 1 & & & \\ & & & \frac{1-2\nu}{2(1-\nu)} & & \\ & & & & \frac{1-2\nu}{2(1-\nu)} & \\ & & & & & \frac{1-2\nu}{2(1-\nu)} \end{bmatrix}$ <p style="text-align: center;">Elements not shown are zeros</p>
Plate bending	$\frac{Eh^3}{12(1-\nu^2)} \begin{bmatrix} 1 & \nu & 0 \\ \nu & 1 & 0 \\ 0 & 0 & \frac{1-\nu}{2} \end{bmatrix}$

Notation: E = Young's modulus, ν = Poisson's ratio, h = thickness of plate, I = moment of inertia

unknown coefficients in the polynomials as generalized coordinates. The number of unknown coefficients in the polynomials was equal to the number of element nodal point displacements. Expressing the generalized coordinates in terms of the element nodal point displacements, we found that, in general, each polynomial coefficient is not an actual physical displacement but is equal to a linear combination of the element nodal point displacements.

Finite element matrices that are formulated by assuming that the displacements vary in the form of a function whose unknown coefficients are treated as generalized coordinates are referred to as generalized coordinate finite element models. A rather natural class of functions to use for approximating element displacements are polynomials because they are commonly employed to approximate unknown functions, and the higher the degree of the polynomial, the better the approximation that we can expect. In addition, polynomials are easy to differentiate; i.e., if the polynomials approximate the displacements of the structure, we can evaluate the strains with relative ease.

Using polynomial displacement assumptions, a very large number of finite elements for practically all problems in structural mechanics have been developed.

The objective in this section is to describe the formulation of a variety of generalized coordinate finite element models that use polynomials to approximate the displacement fields. Other functions could in principle be used in the same way, and their use can be effective in specific applications (see Example 4.20). In the presentation, emphasis is given to the general formulation rather than to numerically effective finite elements. Therefore, this section serves primarily to enhance our general understanding of the finite element method. More effective finite elements for general application are the isoparametric and related elements described in Chapter 5.

In the following derivations the displacements of the finite elements are always described in the local coordinate systems shown in Fig. 4.5. Also, since we consider one specific element, we shall leave out the superscript (m) used in Section 4.2.1 [see (4.31)].

For one-dimensional bar elements (truss elements) we have

$$u(x) = \alpha_1 + \alpha_2 x + \alpha_3 x^2 + \dots \quad (4.51)$$

where x varies over the length of the element, u is the local element displacement, and $\alpha_1, \alpha_2, \dots$, are the generalized coordinates. The displacement expansion in (4.51) can also be used for the transverse and longitudinal displacements of a beam.

For two-dimensional elements (i.e., plane stress, plane strain, and axisymmetric elements), we have for the u and v displacements as a function of the element x and y coordinates,

$$u(x, y) = \alpha_1 + \alpha_2 x + \alpha_3 y + \alpha_4 xy + \alpha_5 x^2 + \dots \quad (4.52)$$

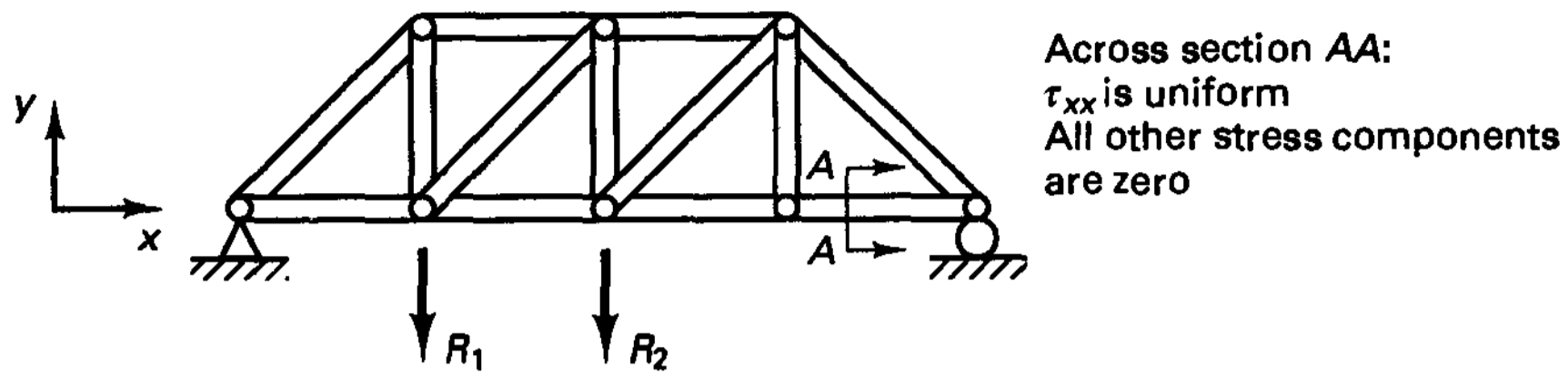
$$v(x, y) = \beta_1 + \beta_2 x + \beta_3 y + \beta_4 xy + \beta_5 x^2 + \dots$$

where $\alpha_1, \alpha_2, \dots$, and β_1, β_2, \dots , are the generalized coordinates.

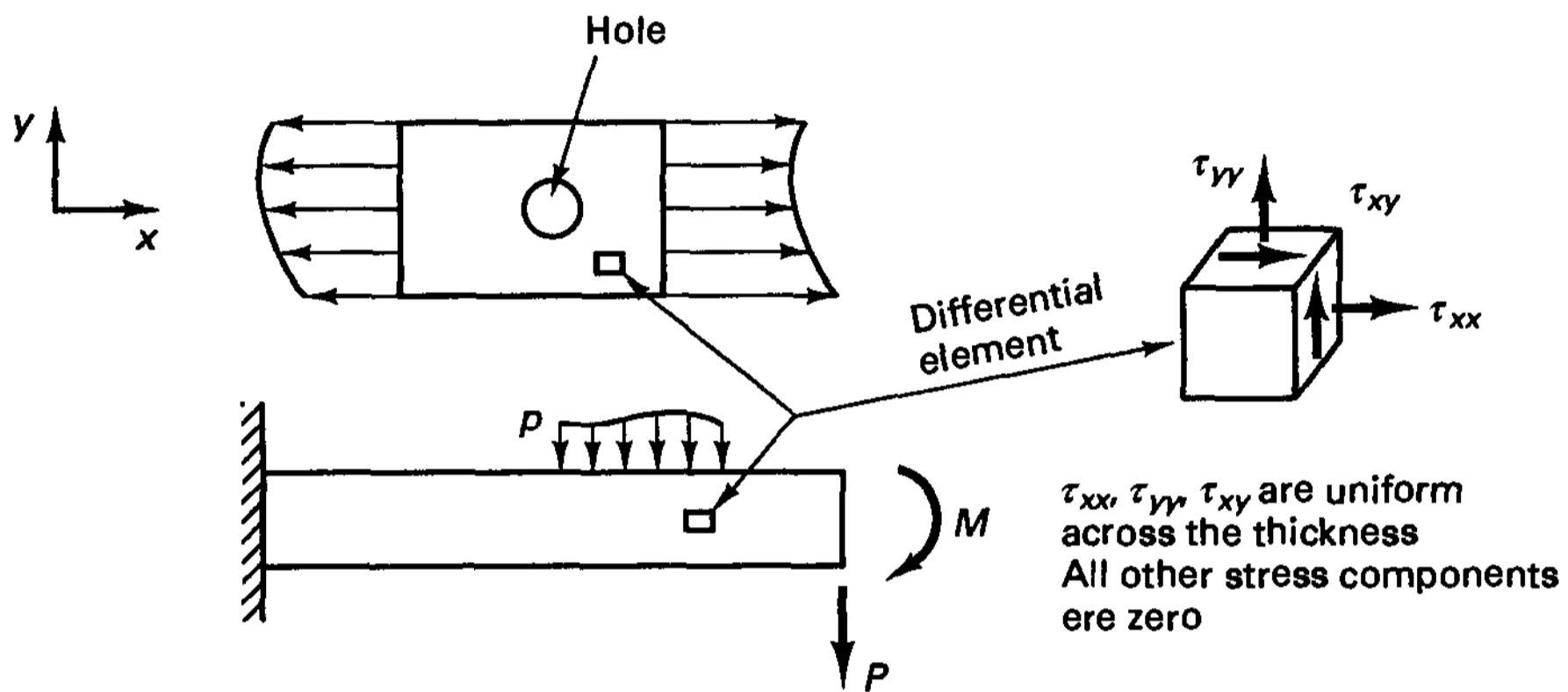
In the case of a plate bending element, the transverse deflection w is assumed as a function of the element coordinates x and y ; i.e.,

$$w(x, y) = \gamma_1 + \gamma_2 x + \gamma_3 y + \gamma_4 xy + \gamma_5 x^2 + \dots \quad (4.53)$$

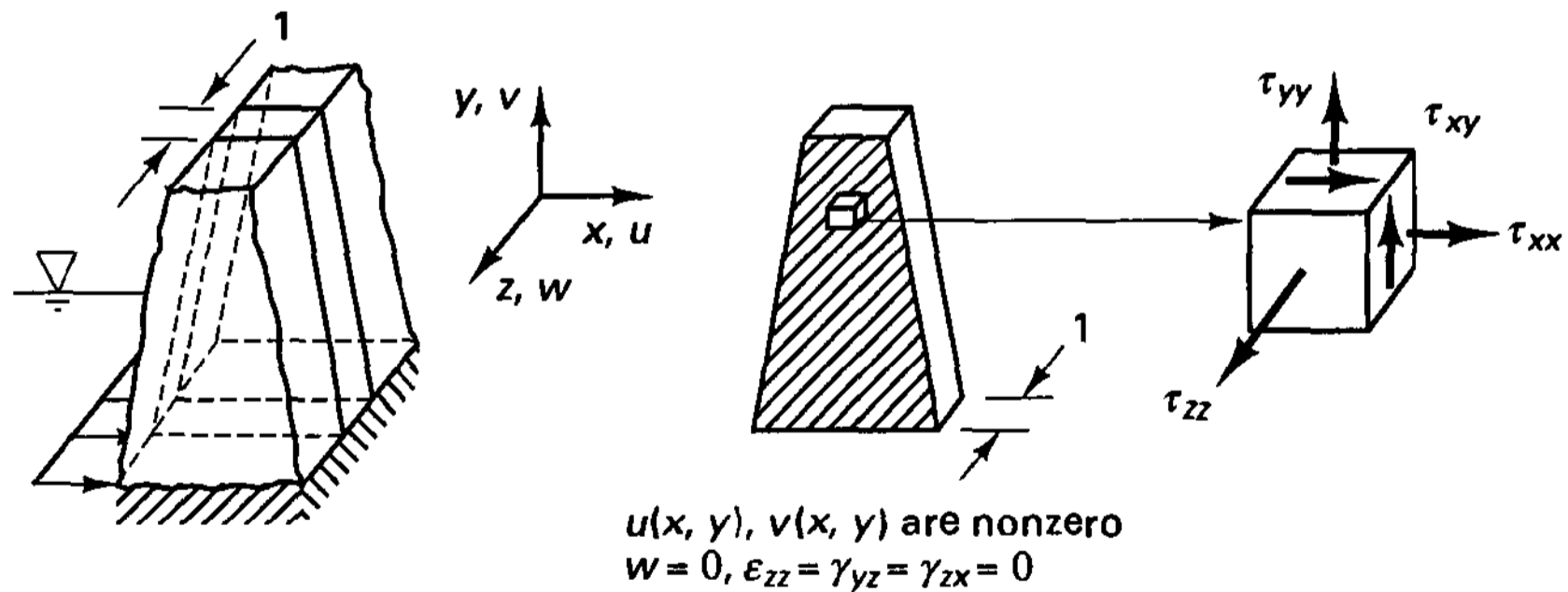
where $\gamma_1, \gamma_2, \dots$, are the generalized coordinates.



(a) Uniaxial stress condition: frame under concentrated loads



(b) Plane stress conditions: membrane and beam under in-plane actions



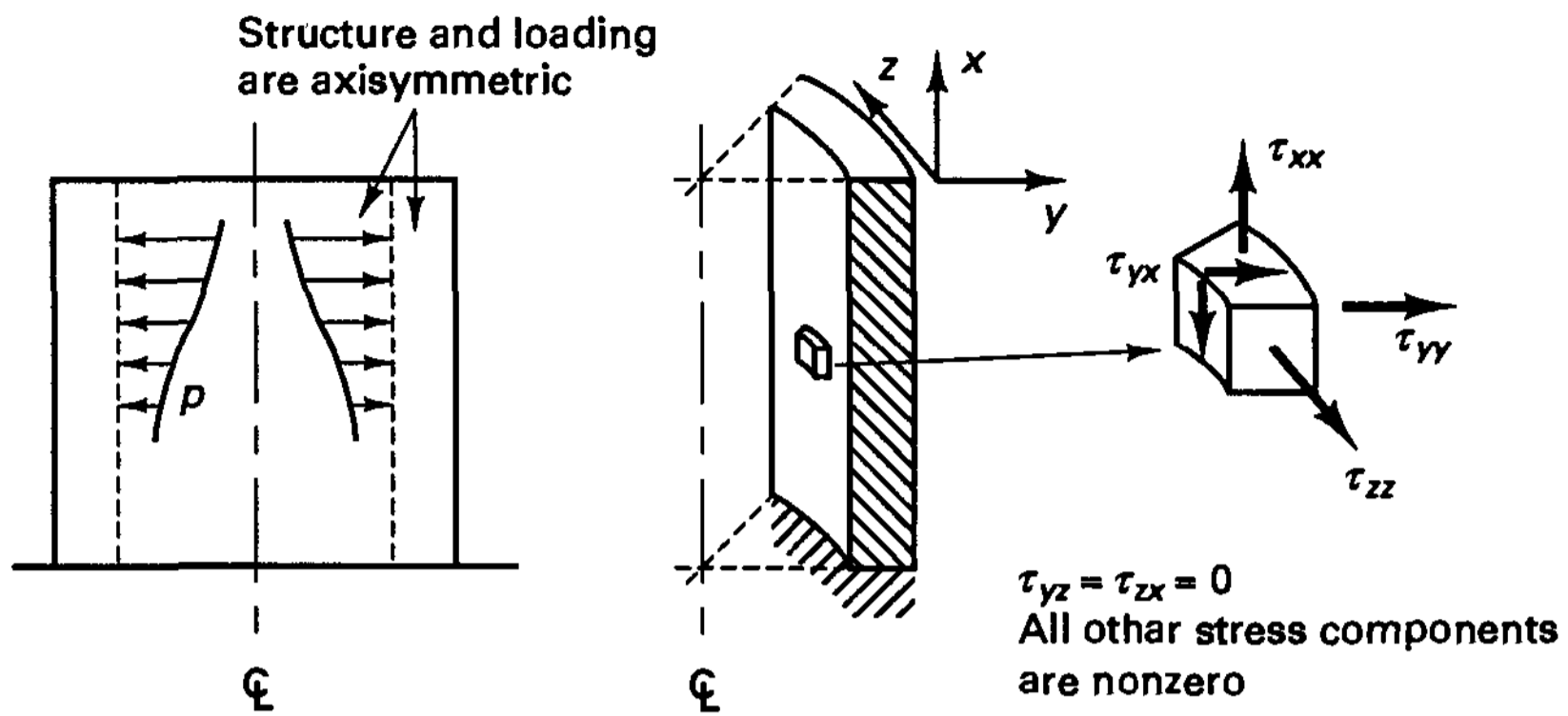
(c) Plane strain condition: long dam subjected to water pressure

Figure 4.5 Various stress and strain conditions with illustrative examples

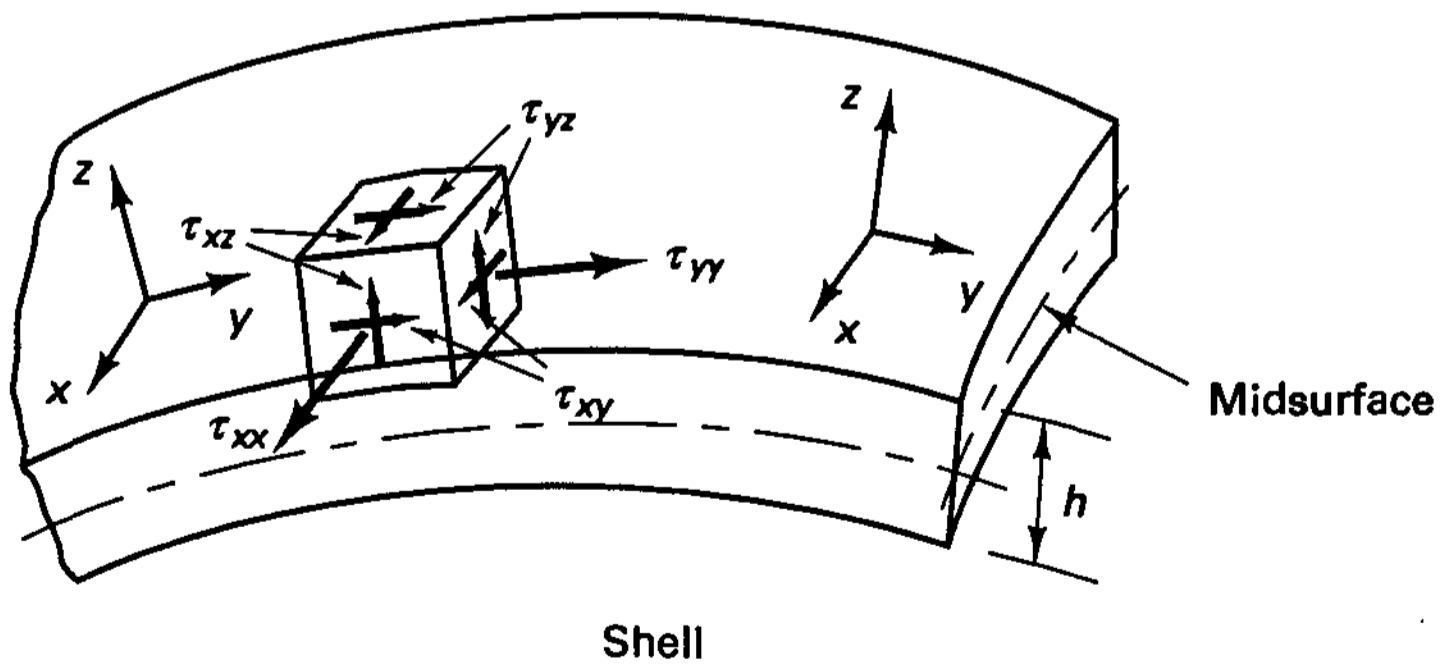
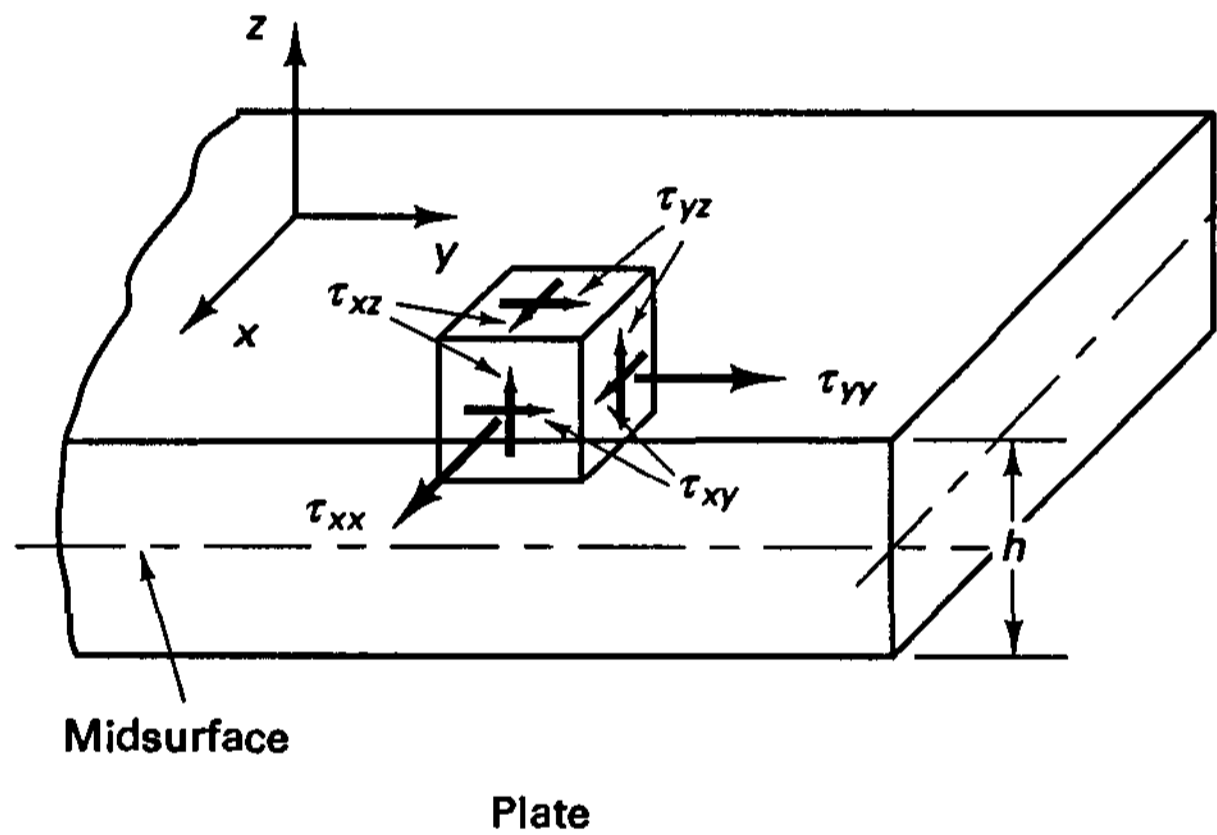
Finally, for elements in which the u , v , and w displacements are measured as a function of the element x , y , and z coordinates, we have, in general,

$$\begin{aligned} u(x, y, z) &= \alpha_1 + \alpha_2 x + \alpha_3 y + \alpha_4 z + \alpha_5 xy + \dots \\ v(x, y, z) &= \beta_1 + \beta_2 x + \beta_3 y + \beta_4 z + \beta_5 xy + \dots \\ w(x, y, z) &= \gamma_1 + \gamma_2 x + \gamma_3 y + \gamma_4 z + \gamma_5 xy + \dots \end{aligned} \tag{4.54}$$

where $\alpha_1, \alpha_2, \dots, \beta_1, \beta_2, \dots$, and $\gamma_1, \gamma_2, \dots$ are now the generalized coordinates.



(d) Axisymmetric condition: cylinder under internal pressure



$\tau_{zz} = 0$
All other stress components are nonzero

(e) Plate and shell structures

Figure 4.5 (continued)

As in the discussion of the plane stress element in Example 4.6, the relations (4.51) to (4.54) can be written in matrix form,

$$\mathbf{u} = \Phi \boldsymbol{\alpha} \quad (4.55)$$

where the vector \mathbf{u} corresponds to the displacements used in (4.51) to (4.54), the elements of Φ are the corresponding polynomial terms, and $\boldsymbol{\alpha}$ is a vector of the generalized coordinates arranged in the appropriate order.

To evaluate the generalized coordinates in terms of the element nodal point displacements, we need to have as many nodal point displacements as assumed generalized coordinates. Then, evaluating (4.55) specifically for the nodal point displacements $\hat{\mathbf{u}}$ of the element, we obtain

$$\hat{\mathbf{u}} = \mathbf{A} \boldsymbol{\alpha} \quad (4.56)$$

Assuming that the inverse of \mathbf{A} exists, we have

$$\boldsymbol{\alpha} = \mathbf{A}^{-1} \hat{\mathbf{u}} \quad (4.57)$$

The element strains to be considered depend on the specific problem to be solved. Denoting by $\boldsymbol{\epsilon}$ a generalized strain vector, whose components are given for specific problems in Table 4.2, we have

$$\boldsymbol{\epsilon} = \mathbf{E} \boldsymbol{\alpha} \quad (4.58)$$

where the matrix \mathbf{E} is established using the displacement assumptions in (4.55). A vector of generalized stresses $\boldsymbol{\tau}$ is obtained using the relation

$$\boldsymbol{\tau} = \mathbf{C} \boldsymbol{\epsilon} \quad (4.59)$$

where \mathbf{C} is a generalized elasticity matrix. The quantities $\boldsymbol{\tau}$ and \mathbf{C} are defined for some problems in Tables 4.2 and 4.3. We may note that except in bending problems, the generalized $\boldsymbol{\tau}$, $\boldsymbol{\epsilon}$, and \mathbf{C} matrices are those that are used in the theory of elasticity. The word "generalized" is employed merely to include curvatures and moments as strains and stresses, respectively. The advantage of using curvatures and moments in bending analysis is that in the stiffness evaluation an integration over the thickness of the corresponding element is not required because this stress and strain variation has already been taken into account (see Example 4.15).

Referring to Table 4.3, it should be noted that all stress-strain matrices can be derived from the general three-dimensional stress-strain relationship. The plane strain and axisymmetric stress-strain matrices are obtained simply by deleting in the three-dimensional stress-strain matrix the rows and columns that correspond to the zero strain components. The stress-strain matrix for plane stress analysis is then obtained from the axisymmetric stress-strain matrix by using the condition that τ_{zz} is zero (see the program QUADS in Section 5.6). To calculate the generalized stress-strain matrix for plate bending analysis, the stress-strain matrix corresponding to plane stress conditions is used, as shown in the following example.

EXAMPLE 4.15: Derive the stress-strain matrix \mathbf{C} used for plate bending analysis (see Table 4.3).

The strains at a distance z measured upward from the midsurface of the plate are

$$\left[-z \frac{\partial^2 w}{\partial x^2} \quad -z \frac{\partial^2 w}{\partial y^2} \quad -z \frac{2\partial^2 w}{\partial x \partial y} \right]$$

In plate bending analysis it is assumed that each layer of the plate acts in plane stress condition and positive curvatures correspond to positive moments (see Section 5.4.2). Hence, integrating the normal stresses in the plate to obtain moments per unit length, the generalized stress-strain matrix is

$$\mathbf{C} = \int_{-h/2}^{+h/2} z^2 \frac{E}{1-\nu^2} \begin{bmatrix} 1 & \nu & 0 \\ \nu & 1 & 0 \\ 0 & 0 & \frac{1-\nu}{2} \end{bmatrix} dz$$

or

$$\mathbf{C} = \frac{Eh^3}{12(1-\nu^2)} \begin{bmatrix} 1 & \nu & 0 \\ \nu & 1 & 0 \\ 0 & 0 & \frac{1-\nu}{2} \end{bmatrix}$$

Considering (4.55) to (4.59), we recognize that, in general terms, all relationships for evaluation of the finite element matrices corresponding to the local finite element nodal point displacements have been defined, and using the notation of Section 4.2.1, we have

$$\mathbf{H} = \Phi \mathbf{A}^{-1} \quad (4.60)$$

$$\mathbf{B} = \mathbf{E} \mathbf{A}^{-1} \quad (4.61)$$

Let us now consider briefly various types of finite elements encountered, which are subject to certain static or kinematic assumptions.

Truss and beam elements. Truss and beam elements are very widely used in structural engineering to model, for example, building frames and bridges [see Fig. 4.5(a) for an assemblage of truss elements].

As discussed in Section 4.2.1, the stiffness matrices of these elements can in many cases be calculated by solving the differential equations of equilibrium (see Example 4.8), and much literature has been published on such derivations. The results of these derivations have been employed in the displacement method of analysis and the corresponding approximate solution techniques, such as the method of moment distribution. However, it can be effective to evaluate the stiffness matrices using the finite element formulation, i.e., the virtual work principle, particularly when considering complex beam geometries and geometric nonlinear analysis (see Section 5.4.1).

Plane stress and plane strain elements. Plane stress elements are employed to model membranes, the in-plane action of beams and plates as shown in Fig. 4.5(b), and so on. In each of these cases a two-dimensional stress situation exists in an xy plane with the stresses τ_{zz} , τ_{yz} , and τ_{zx} equal to zero. Plane strain elements are used to represent a slice (of unit thickness) of a structure in which the strain components ϵ_{zz} , γ_{yz} , and γ_{zx} are zero. This situation arises in the analysis of a long dam as illustrated in Fig. 4.5(c).

Axisymmetric elements. Axisymmetric elements are used to model structural components that are rotationally symmetric about an axis. Examples of application are pressure vessels and solid rings. If these structures are also subjected to axisymmetric loads, a two-dimensional analysis of a unit radian of the structure yields the complete stress and strain distributions as illustrated in Fig. 4.5(d).

On the other hand, if the axisymmetric structure is loaded nonaxisymmetrically, the choice lies between a fully three-dimensional analysis, in which substructuring (see Section 8.2.4) or cyclic symmetry (see Example 4.14) is used, and a Fourier decomposition of the loads for a superposition of harmonic solutions (see Example 4.20).

Plate bending and shell elements. The basic proposition in plate bending and shell analyses is that the structure is thin in one dimension, and therefore the following assumptions can be made [see Fig. 4.5(e)]:

1. The stress through the thickness (i.e., perpendicular to the midsurface) of the plate/shell is zero.
2. Material particles that are originally on a straight line perpendicular to the midsurface of the plate/shell remain on a straight line during deformations. In the Kirchhoff theory, shear deformations are neglected and the straight line remains perpendicular to the midsurface during deformations. In the Reissner/Mindlin theory, shear deformations are included, and therefore the line originally normal to the midsurface in general does not remain perpendicular to the midsurface during the deformations (see Section 5.4.2).

The first finite elements developed to model thin plates in bending and shells were based on the Kirchhoff plate theory (see R. H. Gallagher [A]). The difficulties in these approaches are that the elements must satisfy the convergence requirements *and* be relatively effective in their applications. Much research effort was spent on the development of such elements; however, it was recognized that more effective elements can frequently be formulated using the Reissner/Mindlin plate theory (see Section 5.4.2).

To obtain a shell element a simple approach is to superimpose a plate bending stiffness and a plane stress membrane stiffness. In this way flat shell elements are obtained that can be used to model flat components of shells (e.g., folded plates) and that can also be employed to model general curved shells as an assemblage of flat elements. We demonstrate the development of a plate bending element based on the Kirchhoff plate theory and the construction of an associated flat shell element in Examples 4.18 and 4.19.

EXAMPLE 4.16: Discuss the derivation of the displacement and strain-displacement interpolation matrices of the beam shown in Fig. E4.16.

The exact stiffness matrix (within beam theory) of this beam could be evaluated by solving the beam differential equations of equilibrium, which are for the bending behavior

$$\frac{d^2}{d\xi^2} \left(EI \frac{d^2 w}{d\xi^2} \right) = 0; \quad EI = E \frac{bh^3}{12} \quad (a)$$

and for the axial behavior

$$\frac{d}{d\xi} \left(EA \frac{du}{d\xi} \right) = 0; \quad A = bh \quad (b)$$

where E is Young's modulus. The procedure is to impose a unit end displacement, with all other end displacements equal to zero, and solve the appropriate differential equation of equilibrium of the beam subject to these boundary conditions. Once the element internal displacements for these boundary conditions have been calculated, appropriate derivatives give the element end

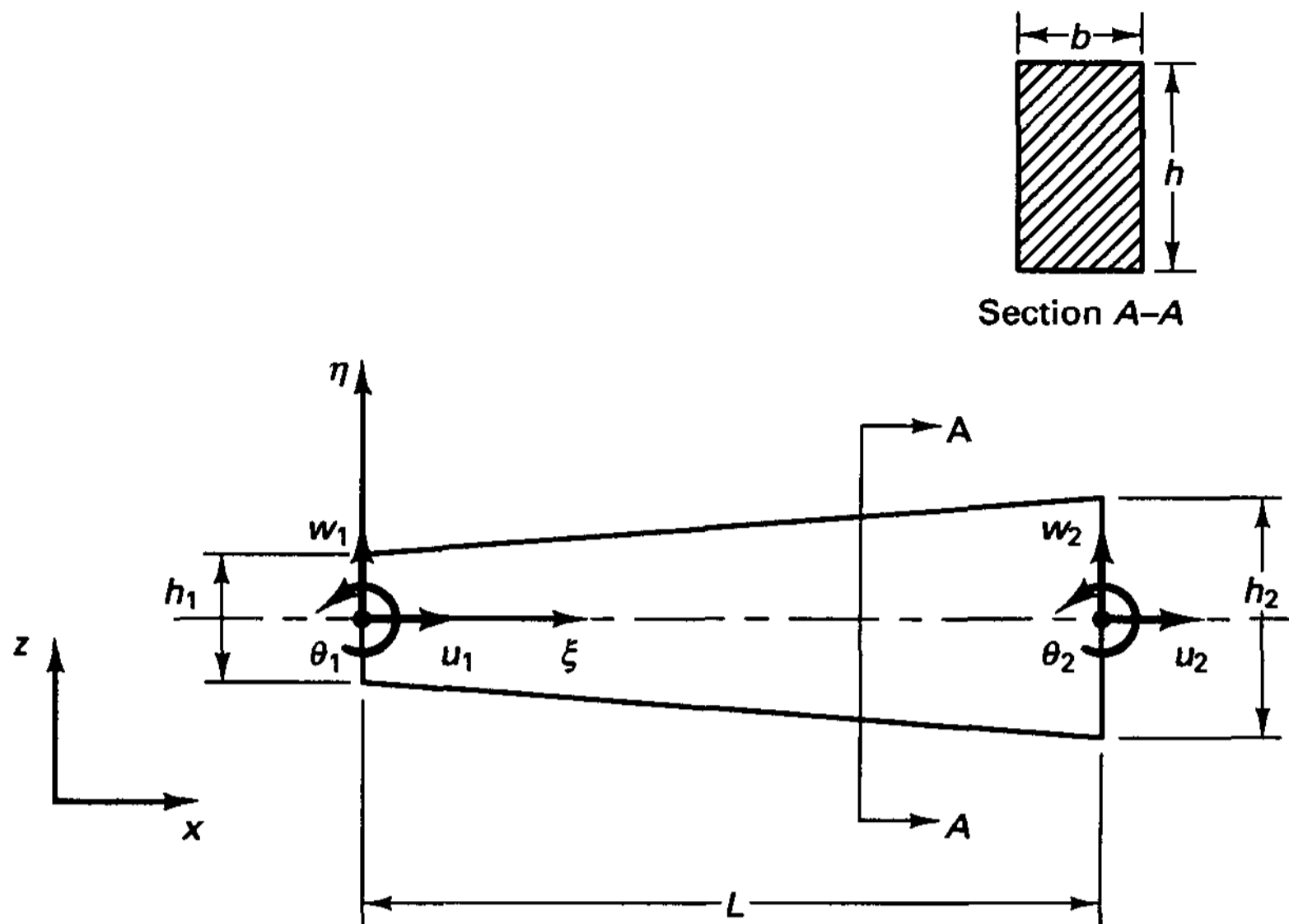


Figure E4.16 Beam element with varying section

forces that together constitute the column of the stiffness matrix corresponding to the imposed end displacement. It should be noted that this stiffness matrix is only “exact” for static analysis because in dynamic analysis the stiffness coefficients are frequency-dependent.

Alternatively, the formulation given in (4.8) to (4.17) can be used. The same stiffness matrix as would be evaluated by the above procedure is obtained if the exact element internal displacements [that satisfy (a) and (b)] are employed to construct the strain-displacement matrix. However, in practice it is frequently expedient to use the displacement interpolations that correspond to a uniform cross-section beam, and this yields an approximate stiffness matrix. The approximation is generally adequate when h_2 is not very much larger than h_1 (hence when a sufficiently large number of beam elements is employed to model the complete structure). The errors encountered in the analysis are those discussed in Section 4.3, because this formulation corresponds to displacement-based finite element analysis.

Using the variables defined in Fig. E4.16 and the “exact” displacements (Hermitian functions) corresponding to a prismatic beam, we have

$$u = \left(1 - \frac{\xi}{L}\right)u_1 + \frac{6\eta}{L}\left(\frac{\xi}{L} - \frac{\xi^2}{L^2}\right)w_1 - \eta\left(1 - 4\frac{\xi}{L} + 3\frac{\xi^2}{L^2}\right)\theta_1 + \frac{\xi}{L}u_2 - \frac{6\eta}{L}\left(\frac{\xi}{L} - \frac{\xi^2}{L^2}\right)w_2 + \eta\left(2\frac{\xi}{L} - 3\frac{\xi^2}{L^2}\right)\theta_2$$

Hence,

$$\mathbf{H} = \left[\begin{array}{cccc} \left(1 - \frac{\xi}{L}\right) & \frac{6\eta}{L}\left(\frac{\xi}{L} - \frac{\xi^2}{L^2}\right) & -\eta\left(1 - 4\frac{\xi}{L} + 3\frac{\xi^2}{L^2}\right) & \frac{\xi}{L} \\ \frac{\xi}{L} & -\frac{6\eta}{L}\left(\frac{\xi}{L} - \frac{\xi^2}{L^2}\right) & \eta\left(2\frac{\xi}{L} - 3\frac{\xi^2}{L^2}\right) & \end{array} \right] \quad (c)$$

For (c) we ordered the nodal point displacements as follows

$$\hat{\mathbf{u}}^T = [u_1 w_1 \theta_1 \quad u_2 w_2 \theta_2]$$

Considering only normal strains and stresses in the beam, i.e., neglecting shearing deformations, we have as the only strain and stress components

$$\epsilon_{\xi\xi} = \frac{du}{d\xi}; \quad \tau_{\xi\xi} = E\epsilon_{\xi\xi}$$

and hence

$$\mathbf{B} = \left[\begin{array}{c|c|c|c|c} -\frac{1}{L} & \frac{6\eta}{L} \left(\frac{1}{L} - \frac{2\xi}{L^2} \right) & -\eta \left(\frac{-4}{L} + \frac{6\xi}{L^2} \right) & \frac{1}{L} & -\frac{6\eta}{L} \left(\frac{1}{L} - \frac{2\xi}{L^2} \right) \\ \hline & & & & \eta \left(\frac{2}{L} - \frac{6\xi}{L^2} \right) \end{array} \right] \quad (d)$$

The relations in (c) and (d) can be used directly to evaluate the element matrices defined in (4.33) to (4.37); e.g.,

$$\mathbf{K} = Eb \int_0^L \int_{-h/2}^{h/2} \mathbf{B}^T \mathbf{B} \, d\eta \, d\xi$$

where

$$h = h_1 + (h_2 - h_1) \frac{\xi}{L}$$

This formulation can be directly extended to develop the element matrices corresponding to the three-dimensional action of the beam element and to include shear deformations (see K. J. Bathe and S. Bolourchi [A]).

EXAMPLE 4.17: Discuss the derivation of the stiffness, mass, and load matrices of the axisymmetric three-node finite element in Fig. E4.17.

This element was one of the first finite elements developed. For most practical applications, much more effective finite elements are presently available (see Chapter 5), but the element is conveniently used for instructional purposes because the equations to be dealt with are relatively simple.

The displacement assumption used is

$$u(x, y) = \alpha_1 + \alpha_2 x + \alpha_3 y$$

$$v(x, y) = \beta_1 + \beta_2 x + \beta_3 y$$

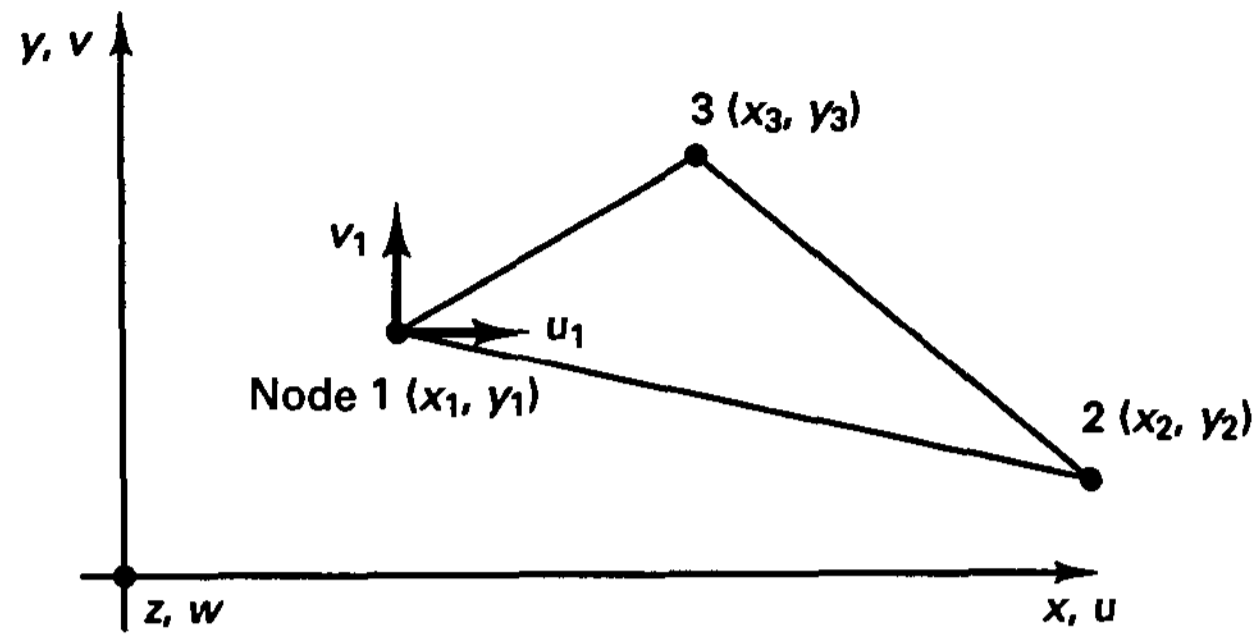
Therefore, a linear displacement variation is assumed, just as for the derivation of the four-node plane stress element considered in Example 4.6 where the fourth node required that the term xy be included in the displacement assumption. Referring to the derivations carried out in Example 4.6, we can directly establish the following relationships:

$$\begin{bmatrix} u(x, y) \\ v(x, y) \end{bmatrix} = \mathbf{H} \begin{bmatrix} u_1 \\ u_2 \\ u_3 \\ v_1 \\ v_2 \\ v_3 \end{bmatrix}$$

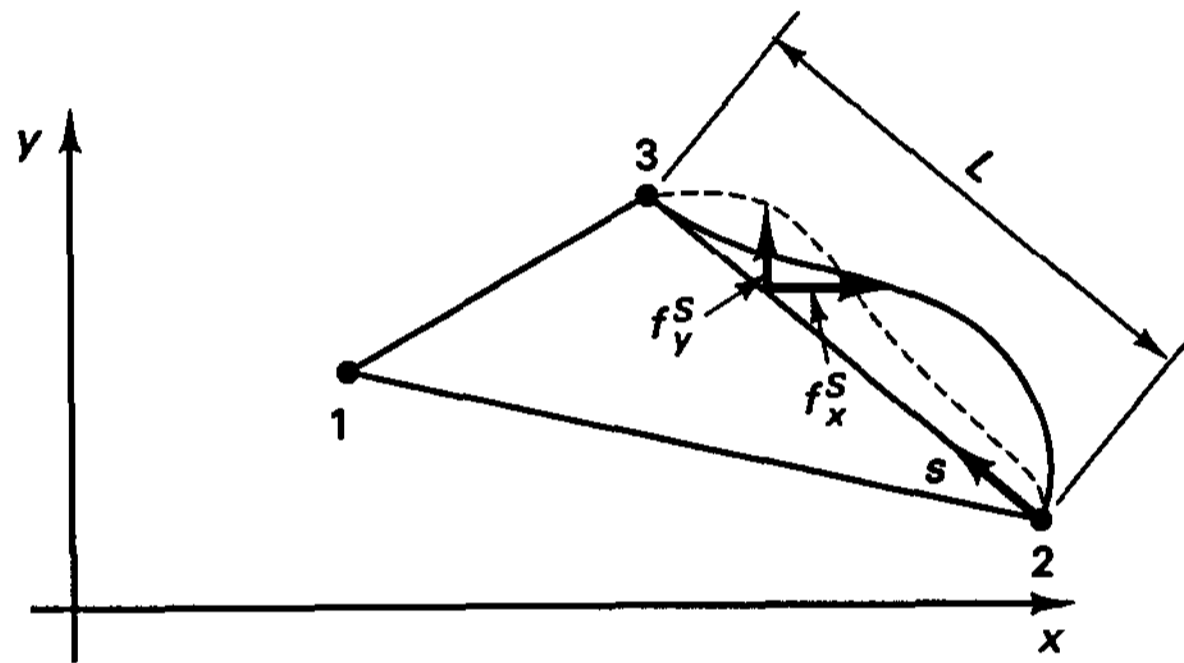
where

$$\mathbf{H} = \begin{bmatrix} 1 & x & y & 0 & 0 & 0 \\ 0 & 0 & 0 & 1 & x & y \end{bmatrix} \mathbf{A}^{-1}$$

$$\mathbf{A}^{-1} = \begin{bmatrix} \mathbf{A}_1^{-1} & \mathbf{0} \\ \mathbf{0} & \mathbf{A}_1^{-1} \end{bmatrix}; \quad \mathbf{A}_1 = \begin{bmatrix} 1 & x_1 & y_1 \\ 1 & x_2 & y_2 \\ 1 & x_3 & y_3 \end{bmatrix}$$



(a) Nodal points



(b) Surface loading

Figure E4.17 Axisymmetric three-node element

Hence

$$\mathbf{A}_1^{-1} = \frac{1}{\det \mathbf{A}_1} \begin{bmatrix} x_2 y_3 - x_3 y_2 & x_3 y_1 - x_1 y_3 & x_1 y_2 - x_2 y_1 \\ y_2 - y_3 & y_3 - y_1 & y_1 - y_2 \\ x_3 - x_2 & x_1 - x_3 & x_2 - x_1 \end{bmatrix}$$

where $\det \mathbf{A}_1 = x_1(y_2 - y_3) + x_2(y_3 - y_1) + x_3(y_1 - y_2)$

We may note that $\det \mathbf{A}_1$ is zero only if the three element nodal points lie on a straight line. The strains are given in Table 4.2 and are

$$\epsilon_{xx} = \frac{\partial u}{\partial x}; \quad \epsilon_{yy} = \frac{\partial v}{\partial y}; \quad \gamma_{xy} = \frac{\partial u}{\partial y} + \frac{\partial v}{\partial x}; \quad \epsilon_{zz} = \frac{\partial w}{\partial z} = \frac{u}{x}$$

Using the assumed displacement polynomials, we obtain

$$\begin{bmatrix} \epsilon_{xx} \\ \epsilon_{yy} \\ \gamma_{xy} \\ \epsilon_{zz} \end{bmatrix} = \mathbf{B} \begin{bmatrix} u_1 \\ u_2 \\ u_3 \\ v_1 \\ v_2 \\ v_3 \end{bmatrix}; \quad \mathbf{B} = \begin{bmatrix} 0 & 1 & 0 & 0 & 0 & 0 \\ 0 & 0 & 0 & 0 & 0 & 1 \\ 0 & 0 & 1 & 0 & 1 & 0 \\ \frac{1}{x} & 1 & \frac{y}{x} & 0 & 0 & 0 \end{bmatrix} \mathbf{A}^{-1} = \mathbf{E} \mathbf{A}^{-1}$$

Using the relations (4.33) to (4.37), we thus have

$$\mathbf{K} = \mathbf{A}^{-T} \left\{ \int_A \frac{E(1-\nu)}{(1+\nu)(1-2\nu)} \begin{bmatrix} 0 & 0 & 0 & \frac{1}{x} \\ 1 & 0 & 0 & 1 \\ 0 & 0 & 1 & \frac{y}{x} \\ 0 & 0 & 0 & 0 \\ 0 & 0 & 1 & 0 \\ 0 & 1 & 0 & 0 \end{bmatrix} \begin{bmatrix} 1 & \frac{\nu}{1-\nu} & 0 & \frac{\nu}{1-\nu} \\ \frac{\nu}{1-\nu} & 1 & 0 & \frac{\nu}{1-\nu} \\ 0 & 0 & \frac{1-2\nu}{2(1-\nu)} & 0 \\ \frac{\nu}{1-\nu} & \frac{\nu}{1-\nu} & 0 & 1 \end{bmatrix} \begin{bmatrix} 0 & 1 & 0 & 0 & 0 & 0 \\ 0 & 0 & 0 & 0 & 0 & 1 \\ 0 & 0 & 1 & 0 & 1 & 0 \\ \frac{1}{x} & 1 & \frac{y}{x} & 0 & 0 & 0 \end{bmatrix} x dx dy \right\} \mathbf{A}^{-1} \quad (\text{a})$$

where 1 radian of the axisymmetric element is considered in the volume integration. Similarly, we have

$$\mathbf{R}_B = \mathbf{A}^{-T} \int_A \begin{bmatrix} 1 & 0 \\ x & 0 \\ y & 0 \\ 0 & 1 \\ 0 & x \\ 0 & y \end{bmatrix} \begin{bmatrix} f_x^B \\ f_y^B \end{bmatrix} x dx dy$$

$$\mathbf{R}_I = \mathbf{A}^{-T} \int_A \begin{bmatrix} 0 & 0 & 0 & \frac{1}{x} \\ 1 & 0 & 0 & 1 \\ 0 & 0 & 1 & \frac{y}{x} \\ 0 & 0 & 0 & 0 \\ 0 & 0 & 1 & 0 \\ 0 & 1 & 0 & 0 \end{bmatrix} \begin{bmatrix} \tau_{xx}^I \\ \tau_{yy}^I \\ \tau_{xy}^I \\ \tau_{zz}^I \end{bmatrix} x dx dy \quad (\text{b})$$

$$\mathbf{M} = \rho \mathbf{A}^{-T} \left\{ \int_A \begin{bmatrix} 1 & 0 \\ x & 0 \\ y & 0 \\ 0 & 1 \\ 0 & x \\ 0 & y \end{bmatrix} \begin{bmatrix} 1 & x & y & 0 & 0 & 0 \\ 0 & 0 & 0 & 1 & x & y \end{bmatrix} x dx dy \right\} \mathbf{A}^{-1}$$

where the mass density ρ is assumed to be constant.

For calculation of the surface load vector \mathbf{R}_S , it is expedient in practice to introduce auxiliary coordinate systems located along the loaded sides of the element. Assume that the side 2-3 of the element is loaded as shown in Fig. E4.17. The load vector \mathbf{R}_S is then evaluated using

as the variable s ,

$$\mathbf{R}_s = \int_s \begin{bmatrix} 0 & 0 \\ 1 - \frac{s}{L} & 0 \\ \frac{s}{L} & 0 \\ 0 & 0 \\ 0 & 1 - \frac{s}{L} \\ 0 & \frac{s}{L} \end{bmatrix} \begin{bmatrix} f_x^s \\ f_y^s \end{bmatrix} \left[x_2 \left(1 - \frac{s}{L} \right) + x_3 \frac{s}{L} \right] ds$$

Considering these finite element matrix evaluations the following observations can be made. First, to evaluate the integrals, it is possible to obtain closed-form solutions; alternatively, numerical integration (discussed in Section 5.5) can be used. Second, we find that the stiffness, mass, and load matrices corresponding to plane stress and plane strain finite elements can be obtained simply by (1) not including the fourth row in the strain-displacement matrix \mathbf{E} used in (a) and (b), (2) employing the appropriate stress-strain matrix \mathbf{C} in (a), and (3) using as the differential volume element $h \, dx \, dy$ instead of $x \, dx \, dy$, where h is the thickness of the element (conveniently taken equal to 1 in plane strain analysis). Therefore, axisymmetric, plane stress, and plane strain analyses can effectively be implemented in a single computer program. Also, the matrix \mathbf{E} shows that constant-strain conditions ϵ_{xx} , ϵ_{yy} , and γ_{xy} are assumed in either analysis.

The concept of performing axisymmetric, plane strain, and plane stress analysis in an effective manner in one computer program is, in fact, presented in Section 5.6, where we discuss the efficient implementation of isoparametric finite element analysis.

EXAMPLE 4.18: Derive the matrices $\Phi(x, y)$, $\mathbf{E}(x, y)$, and \mathbf{A} for the rectangular plate bending element in Fig. E4.18.

This element is one of the first plate bending elements derived, and more effective plate bending elements are already in use (see Section 5.4.2).

As shown in Fig. E4.18, the plate bending element considered has three degrees of freedom per node. Therefore, it is necessary to have 12 unknown generalized coordinates, $\alpha_1, \dots, \alpha_{12}$,

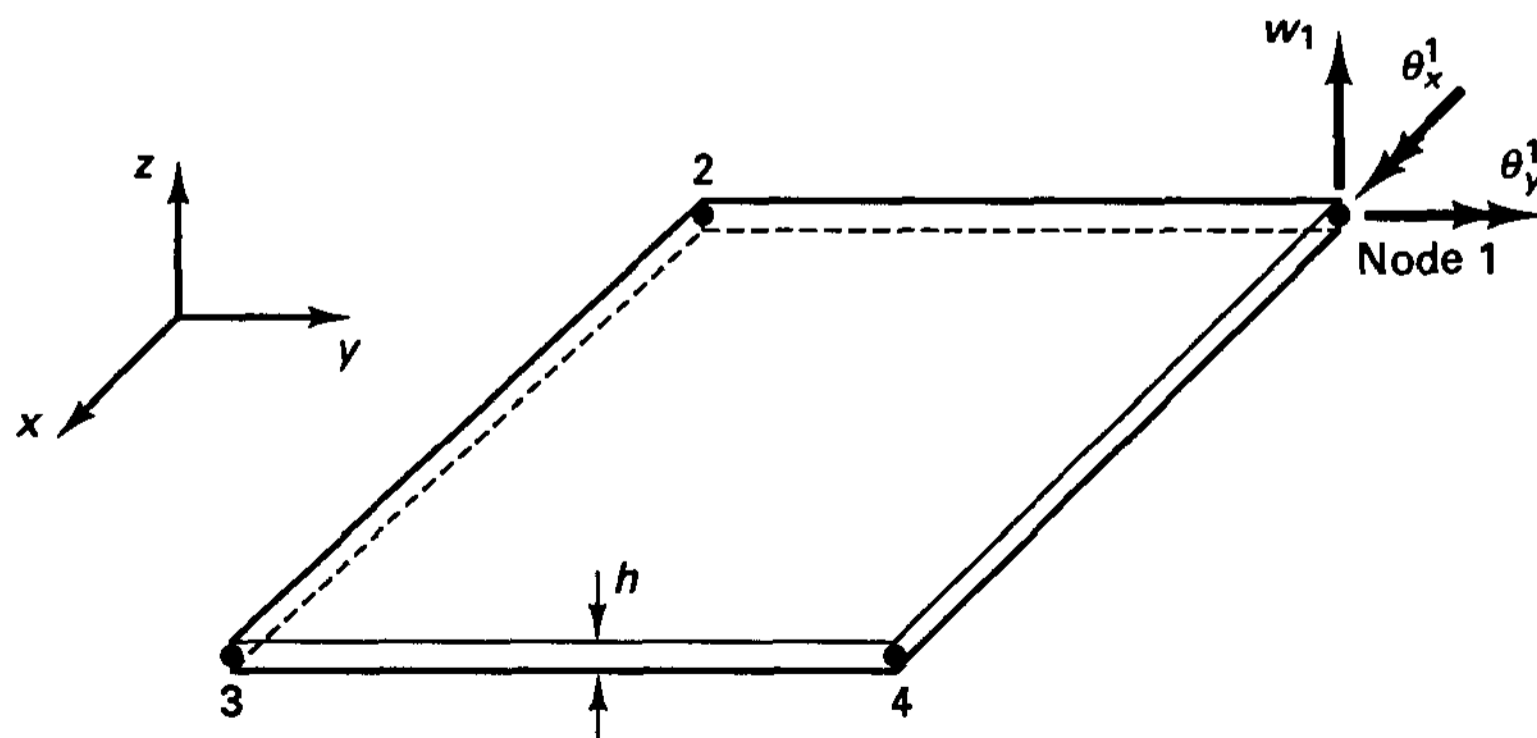


Figure E4.18 Rectangular plate bending element.

in the displacement assumption for w . The polynomial used is

$$w = \alpha_1 + \alpha_2 x + \alpha_3 y + \alpha_4 x^2 + \alpha_5 xy + \alpha_6 y^2 + \alpha_7 x^3 + \alpha_8 x^2 y + \alpha_9 xy^2 + \alpha_{10} y^3 + \alpha_{11} x^3 y + \alpha_{12} xy^3$$

Hence,

$$\Phi(x, y) = [1 \quad x \quad y \quad x^2 \quad xy \quad y^2 \quad x^3 \quad x^2 y \quad xy^2 \quad y^3 \quad x^3 y \quad xy^3] \quad (a)$$

We can now calculate $\partial w/\partial x$ and $\partial w/\partial y$:

$$\frac{\partial w}{\partial x} = \alpha_2 + 2\alpha_4 x + \alpha_5 y + 3\alpha_7 x^2 + 2\alpha_8 xy + \alpha_9 y^2 + 3\alpha_{11} x^2 y + \alpha_{12} y^3 \quad (b)$$

and

$$\frac{\partial w}{\partial y} = \alpha_3 + \alpha_5 x + 2\alpha_6 y + \alpha_8 x^2 + 2\alpha_9 xy + 3\alpha_{10} y^2 + \alpha_{11} x^3 + 3\alpha_{12} xy^2 \quad (c)$$

Using the conditions

$$\left. \begin{aligned} w_i &= (w)_{x_i, y_i}; & \theta_x^i &= \left(\frac{\partial w}{\partial x} \right)_{x_i, y_i} \\ \theta_y^i &= \left(-\frac{\partial w}{\partial y} \right)_{x_i, y_i} \end{aligned} \right\} i = 1, \dots, 4$$

we can construct the matrix A , obtaining

$$\begin{bmatrix} w_1 \\ \vdots \\ w_4 \\ \theta_x^1 \\ \vdots \\ \theta_x^4 \\ \theta_y^1 \\ \vdots \\ \theta_y^4 \end{bmatrix} = A \begin{bmatrix} \alpha_1 \\ \alpha_2 \\ \vdots \\ \alpha_{12} \end{bmatrix}$$

where

$$A = \begin{bmatrix} 1 & x_1 & y_1 & x_1^2 & x_1 y_1 & y_1^2 & x_1^3 & x_1^2 y_1 & x_1 y_1^2 & y_1^3 & x_1^3 y_1 & x_1 y_1^3 \\ \vdots & \vdots & \vdots & \vdots & \vdots & \vdots & \vdots & \vdots & \vdots & \vdots & \vdots & \vdots \\ 1 & x_4 & y_4 & x_4^2 & x_4 y_4 & y_4^2 & x_4^3 & x_4^2 y_4 & x_4 y_4^2 & y_4^3 & x_4^3 y_4 & x_4 y_4^3 \\ 0 & 0 & 1 & 0 & x_1 & 2y_1 & 0 & x_1^2 & 2x_1 y_1 & 3y_1^2 & x_1^3 & 3x_1 y_1^2 \\ \vdots & \vdots & \vdots & \vdots & \vdots & \vdots & \vdots & \vdots & \vdots & \vdots & \vdots & \vdots \\ 0 & 0 & 1 & 0 & x_4 & 2y_4 & 0 & x_4^2 & 2x_4 y_4 & 3y_4^2 & x_4^3 & 3x_4 y_4^2 \\ 0 & -1 & 0 & -2x_1 & -y_1 & 0 & -3x_1^2 & -2x_1 y_1 & -y_1^2 & 0 & -3x_1^2 y_1 & -y_1^3 \\ \vdots & \vdots & \vdots & \vdots & \vdots & \vdots & \vdots & \vdots & \vdots & \vdots & \vdots & \vdots \\ 0 & -1 & 0 & -2x_4 & -y_4 & 0 & -3x_4^2 & -2x_4 y_4 & -y_4^2 & 0 & -3x_4^2 y_4 & -y_4^3 \end{bmatrix} \quad (d)$$

which can be shown to be always nonsingular.

To evaluate the matrix \mathbf{E} , we recall that in plate bending analysis curvatures and moments are used as generalized strains and stresses (see Tables 4.2 and 4.3). Calculating the required derivatives of (b) and (c), we obtain

$$\begin{aligned} \frac{\partial^2 w}{\partial x^2} &= 2\alpha_4 + 6\alpha_7 x + 2\alpha_8 y + 6\alpha_{11} xy \\ \frac{\partial^2 w}{\partial y^2} &= 2\alpha_6 + 2\alpha_9 x + 6\alpha_{10} y + 6\alpha_{12} xy \\ 2 \frac{\partial^2 w}{\partial x \partial y} &= 2\alpha_5 + 4\alpha_8 x + 4\alpha_9 y + 6\alpha_{11} x^2 + 6\alpha_{12} y^2 \end{aligned} \tag{e}$$

Hence we have

$$\mathbf{E} = \begin{bmatrix} 0 & 0 & 0 & 2 & 0 & 0 & 6x & 2y & 0 & 0 & 6xy & 0 \\ 0 & 0 & 0 & 0 & 0 & 2 & 0 & 0 & 2x & 6y & 0 & 6xy \\ 0 & 0 & 0 & 0 & 2 & 0 & 0 & 4x & 4y & 0 & 6x^2 & 6y^2 \end{bmatrix} \tag{f}$$

With the matrices Φ , \mathbf{A} , and \mathbf{E} given in (a), (d), and (f) and the material matrix \mathbf{C} in Table 4.3, the element stiffness matrix, mass matrix, and load vectors can now be calculated.

An important consideration in the evaluation of an element stiffness matrix is whether the element is complete and compatible. The element considered in this example is complete as shown in (e) (i.e., the element can represent constant curvature states), but the element is not compatible. The compatibility requirements are violated in a number of plate bending elements, meaning that convergence in the analysis is in general not monotonic (see Section 4.3).

EXAMPLE 4.19: Discuss the evaluation of the stiffness matrix of a flat rectangular shell element.

A simple rectangular flat shell element can be obtained by superimposing the plate bending behavior considered in Example 4.18 and the plane stress behavior of the element used in Example 4.6. The resulting element is shown in Fig. E4.19. The element can be employed to model assemblages of flat plates (e.g., folded plate structures) and also curved shells. For actual analyses more effective shell elements are available, and we discuss here only the element in Fig. E4.19 in order to demonstrate some basic analysis approaches.

Let $\tilde{\mathbf{K}}_B$ and $\tilde{\mathbf{K}}_M$ be the stiffness matrices, in the local coordinate system, corresponding to the bending and membrane behavior of the element, respectively. Then the shell element stiffness matrix $\tilde{\mathbf{K}}_S$ is

$$\tilde{\mathbf{K}}_S = \begin{bmatrix} \tilde{\mathbf{K}}_B & \mathbf{0} \\ \mathbf{0} & \tilde{\mathbf{K}}_M \end{bmatrix} \tag{a}$$

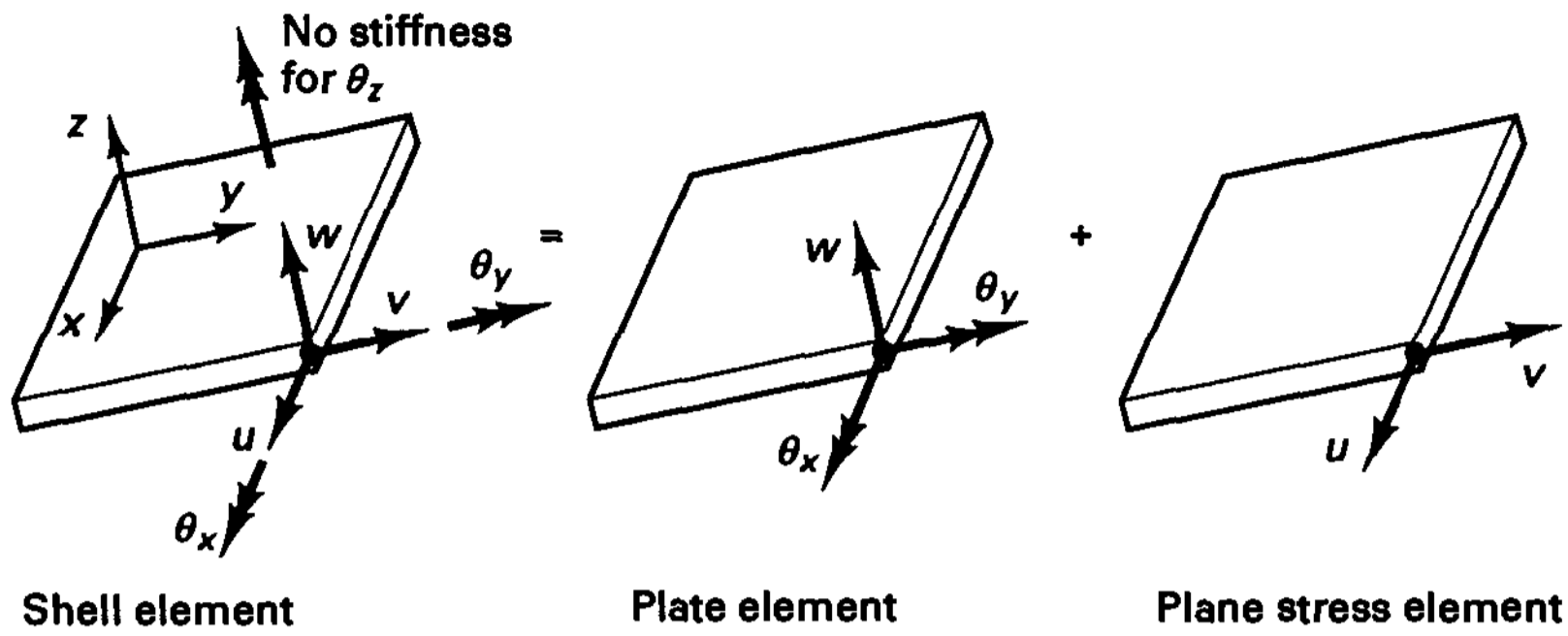
The matrices $\tilde{\mathbf{K}}_M$ and $\tilde{\mathbf{K}}_B$ were discussed in Examples 4.6 and 4.18, respectively.

This shell element can now be directly employed in the analysis of a variety of shell structures. Consider the structures in Fig. E4.19, which might be idealized as shown. Since we deal in these analyses with six degrees of freedom per node, the element stiffness matrices corresponding to the global degrees of freedom are calculated using the transformation given in (4.41)

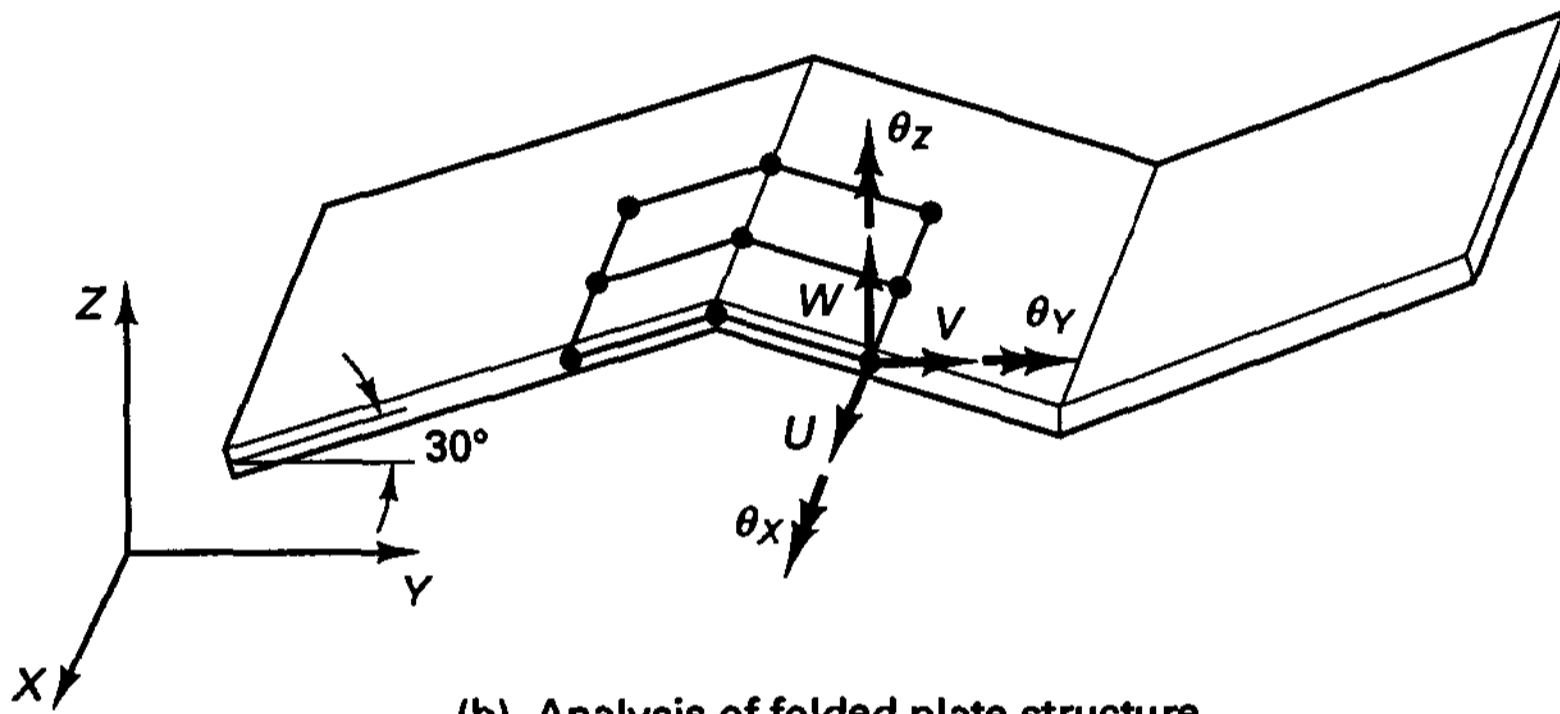
$$\mathbf{K}_S = \mathbf{T}^T \tilde{\mathbf{K}}_S^* \mathbf{T} \tag{b}$$

where

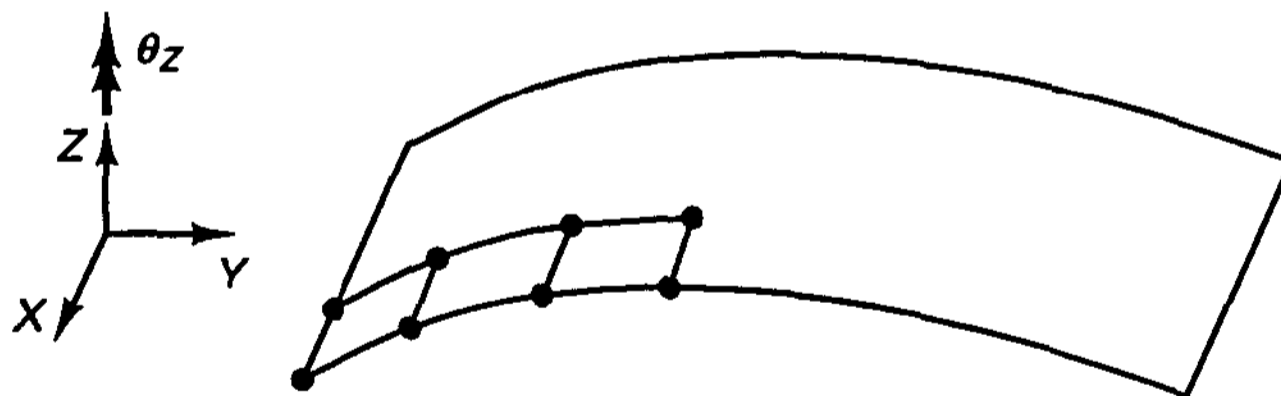
$$\tilde{\mathbf{K}}_S^* = \begin{bmatrix} \tilde{\mathbf{K}}_S & \mathbf{0} \\ \mathbf{0} & \mathbf{0} \end{bmatrix} \tag{c}$$



(a) Basic shell element with local five degrees of freedom at a node



(b) Analysis of folded plate structure



(c) Analysis of slightly curved shell

Figure E4.19 Use of a flat shell element

and T is the transformation matrix between the local and global element degrees of freedom. To define \tilde{K}_S^* corresponding to six degrees of freedom per node, we have amended \tilde{K}_S on the right-hand side of (c) to include the stiffness coefficients corresponding to the local rotations θ_z (rotations about the z -axis) at the nodes. These stiffness coefficients have been set equal to zero in (c). The reason for doing so is that these degrees of freedom have not been included in the formulation of the element; thus the element rotation θ_z at a node is not measured and does not contribute to the strain energy stored in the element.

The solution of a model can be obtained using \tilde{K}_S^* in (c) as long as the elements surrounding a node are not coplanar. This does not hold for the folded plate model, and considering the analysis of the slightly curved shell in Fig. E4.19(c), the elements may be almost coplanar (depending on the curvature of the shell and the idealization used). In these cases, the global

stiffness matrix is singular or ill-conditioned because of the zero diagonal elements in $\tilde{\mathbf{K}}_s^*$ and difficulties arise in solving the global equilibrium equations (see Section 8.2.6). To avoid this problem it is possible to add a small stiffness coefficient corresponding to the θ_z rotation; i.e., instead of $\tilde{\mathbf{K}}_s^*$ in (c) we use

$$\tilde{\mathbf{K}}_s^{*'} = \begin{bmatrix} \tilde{\mathbf{K}}_s & \mathbf{0} \\ \mathbf{0} & k\mathbf{I} \end{bmatrix} \quad (d)$$

20×20 4×4

where k is about one-thousandth of the smallest diagonal element of $\tilde{\mathbf{K}}_s$. The stiffness coefficient k must be large enough to allow accurate solution of the finite element system equilibrium equations and small enough not to affect the system response significantly. Therefore, a large enough number of digits must be used in the floating-point arithmetic (see Section 8.2.6).

A more effective way to circumvent the problem is to use curved shell elements with five degrees of freedom per node where these are defined corresponding to a plane tangent to the midsurface of the shell. In this case the rotation normal to the shell surface is not a degree of freedom (see Section 5.4.2).

In the above element formulations we used polynomial functions to express the displacements. We should briefly note, however, that for certain applications the use of other functions such as trigonometric expressions can be effective. Trigonometric functions, for example, are used in the analysis of axisymmetric structures subjected to nonaxisymmetric loading (see E. L. Wilson [A]), and in the finite strip method (see Y. K. Cheung [A]). The advantage of the trigonometric functions lies in their orthogonality properties. Namely, if sine and cosine products are integrated over an appropriate interval, the integral can be zero. This then means that there is no coupling in the equilibrium equations between the generalized coordinates that correspond to the sine and cosine functions, and the equilibrium equations can be solved more effectively. In this context it may be noted that the best functions that we could use in the finite element analysis would be given by the eigenvectors of the problem because they would give a diagonal stiffness matrix. However, these functions are not known, and for general applications, the use of polynomial, trigonometric, or other assumptions for the finite element displacements is most natural.

The use of special interpolation functions can of course also lead to efficient solution schemes in the analysis of certain fluid flows (see, for example, A. T. Patera [A]).

We demonstrate the use of trigonometric functions in the following example.

EXAMPLE 4.20: Figure E4.20 shows an axisymmetric structure subjected to a nonaxisymmetric loading in the radial direction. Discuss the analysis of this structure using the three-node axisymmetric element in Example 4.17 when the loading is represented as a superposition of Fourier components.

The stress distribution in the structure is three-dimensional and could be calculated using a three-dimensional finite element idealization. However, it is possible to take advantage of the axisymmetric geometry of the structure and, depending on the exact loading applied, reduce the computational effort very significantly.

The key point in this analysis is that we expand the externally applied loads $R_r(\theta, y)$ in the Fourier series:

$$R_r = \sum_{p=1}^{p_c} R_p^c \cos p\theta + \sum_{p=1}^{p_s} R_p^s \sin p\theta \quad (a)$$

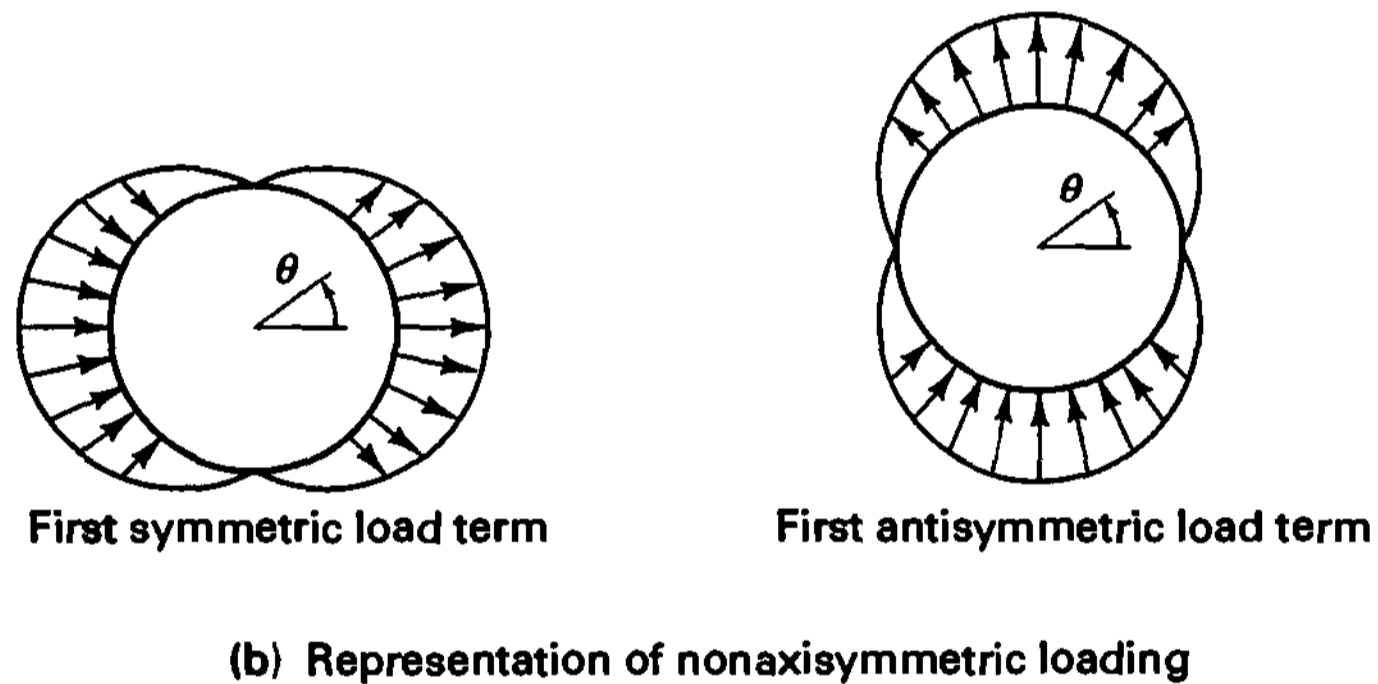
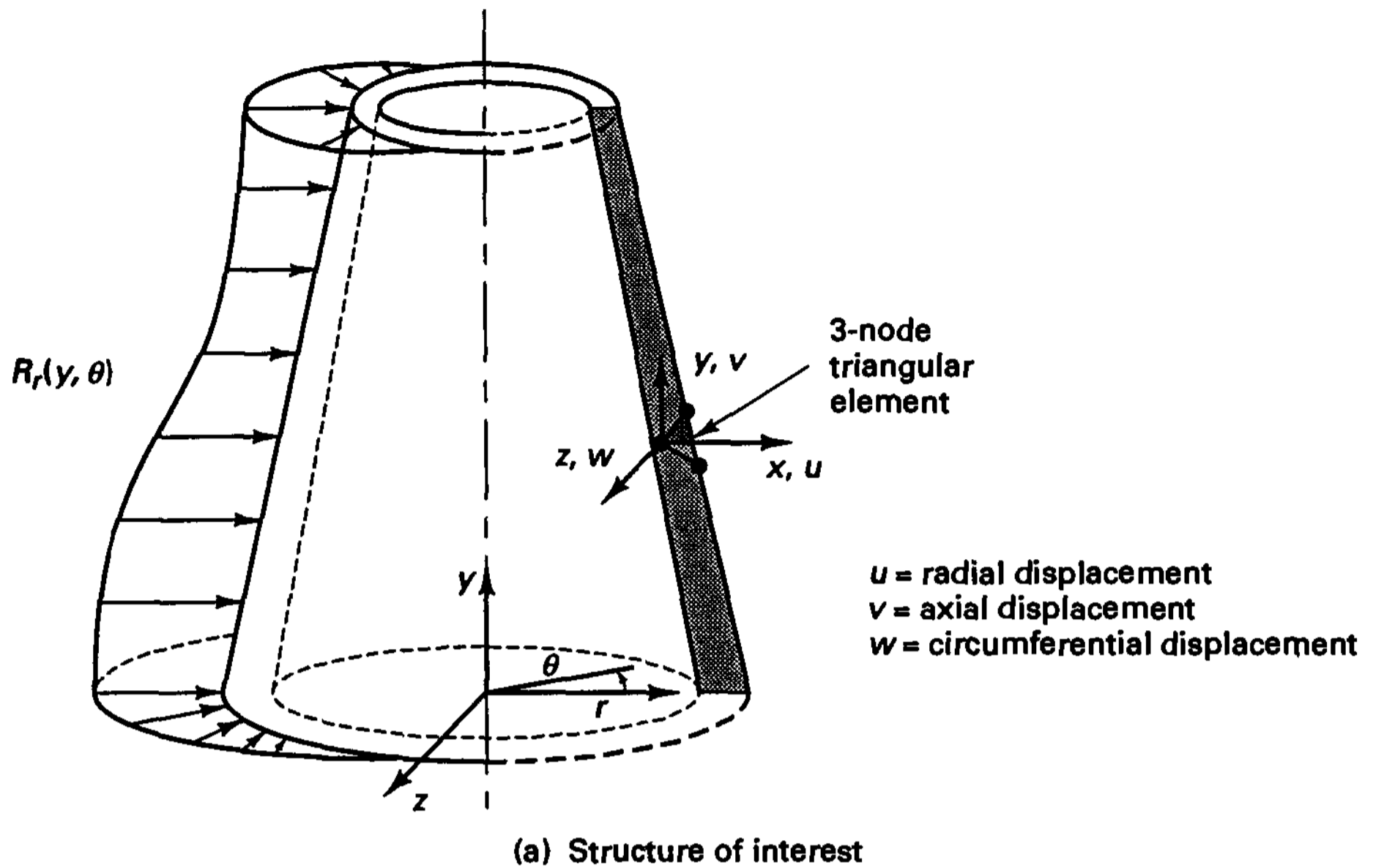


Figure E4.20 Axisymmetric structure subjected to nonaxisymmetric loading

where p_c and p_s are the total number of symmetric and antisymmetric load contributions about $\theta = 0$, respectively. Figure E4.20(b) illustrates the first terms in the expansion of (a).

The complete analysis can now be performed by superimposing the responses due to the symmetric and antisymmetric load contributions defined in (a). For example, considering the symmetric response, we use for an element

$$\begin{aligned}
 u(x, y, \theta) &= \sum_{p=1}^{p_c} \cos p\theta \mathbf{H}\hat{u}^p \\
 v(x, y, \theta) &= \sum_{p=1}^{p_c} \cos p\theta \mathbf{H}\hat{v}^p \\
 w(x, y, \theta) &= \sum_{p=1}^{p_c} \sin p\theta \mathbf{H}\hat{w}^p
 \end{aligned}
 \tag{b}$$

where for the triangular elements, referring to Example 4.17,

$$\mathbf{H} = [1 \quad x \quad y] \mathbf{A}_1^{-1} \quad (c)$$

and the $\hat{\mathbf{u}}^p$, $\hat{\mathbf{v}}^p$, and $\hat{\mathbf{w}}^p$ are the element unknown generalized nodal point displacements corresponding to mode p .

We should note that we superimpose in (b) the response measured in individual harmonic displacement distributions. Using (b), we can now establish the strain-displacement matrix of the element. Since we are dealing with a three-dimensional stress distribution, we use the expression for three-dimensional strain distributions in cylindrical coordinates:

$$\boldsymbol{\epsilon} = \begin{bmatrix} \frac{\partial u}{\partial r} \\ \frac{\partial v}{\partial y} \\ \frac{u}{r} + \frac{1}{r} \frac{\partial w}{\partial \theta} \\ \frac{\partial u}{\partial y} + \frac{\partial v}{\partial r} \\ \frac{\partial w}{\partial y} + \frac{1}{r} \frac{\partial v}{\partial \theta} \\ \frac{\partial w}{\partial r} + \frac{1}{r} \frac{\partial u}{\partial \theta} - \frac{w}{r} \end{bmatrix} \quad (d)$$

where
$$\boldsymbol{\epsilon}^T = [\epsilon_{rr} \quad \epsilon_{yy} \quad \epsilon_{\theta\theta} \quad \gamma_{ry} \quad \gamma_{y\theta} \quad \gamma_{\theta r}] \quad (e)$$

Substituting from (b) into (d) we obtain a strain-displacement matrix \mathbf{B}_p for each value of p , and the total strains can be thought of as the superposition of the strain distributions contained in each harmonic.

The unknown nodal point displacements can now be evaluated using the usual procedures. The equilibrium equations corresponding to the generalized nodal point displacements U_i^p , V_i^p , W_i^p , $i = 1, \dots, N$ (N is equal to the total number of nodes) and $p = 1, \dots, p_c$ are evaluated as given in (4.17) to (4.22), where we now have

$$\mathbf{U}^T = [\mathbf{U}^{1T} \quad \mathbf{U}^{2T} \quad \dots \quad \mathbf{U}^{p_c T}] \quad (f)$$

and

$$\mathbf{U}^{pT} = [U_1^p \quad V_1^p \quad W_1^p \quad \vdots \quad U_N^p \quad \dots \quad W_N^p] \quad (g)$$

In the calculations of \mathbf{K} and \mathbf{R}_S we note that because of the orthogonality properties

$$\int_0^{2\pi} \sin n\theta \sin m\theta d\theta = 0 \quad n \neq m$$

$$\int_0^{2\pi} \cos n\theta \cos m\theta d\theta = 0 \quad n \neq m$$

(h)

the stiffness matrices corresponding to the different harmonics are decoupled from each other. Hence, we have the following equilibrium equations for the structure:

$$\mathbf{K}^p \mathbf{U}^p = \mathbf{R}_S^p \quad p = 1, \dots, p_c \quad (i)$$

where \mathbf{K}^p and \mathbf{R}_S^p are the stiffness matrix and load vector corresponding to the p th harmonic.

Solution of the equations in (i) gives the generalized nodal point displacements of each element, and (b) then yields all element internal displacements.

In the above displacement solution we considered only the symmetric load contributions. But an analogous analysis can be performed for the antisymmetric load harmonics of (a) by simply replacing in (b) to (i) all sine and cosine terms by cosine and sine terms, respectively. The complete structural response is then obtained by superimposing the displacements corresponding to all harmonics.

Although we have considered only surface loading in the discussion, the analysis can be extended using the same approach to include body force loading and initial stresses.

Finally, we note that the computational effort required in the analysis is directly proportional to the number of load harmonics used. Hence, the solution procedure is very efficient if the loading can be represented using only a few harmonics (e.g., wind loading) but may be inefficient when many harmonics must be used to represent the loading (e.g., a concentrated force).

4.2.4 Lumping of Structure Properties and Loads

A physical interpretation of the finite element procedure of analysis as presented in the previous sections is that the structure properties—stiffness and mass—and the loads, internal and external, are lumped to the discrete nodes of the element assemblage using the virtual work principle. *Because the same interpolation functions are employed in the*

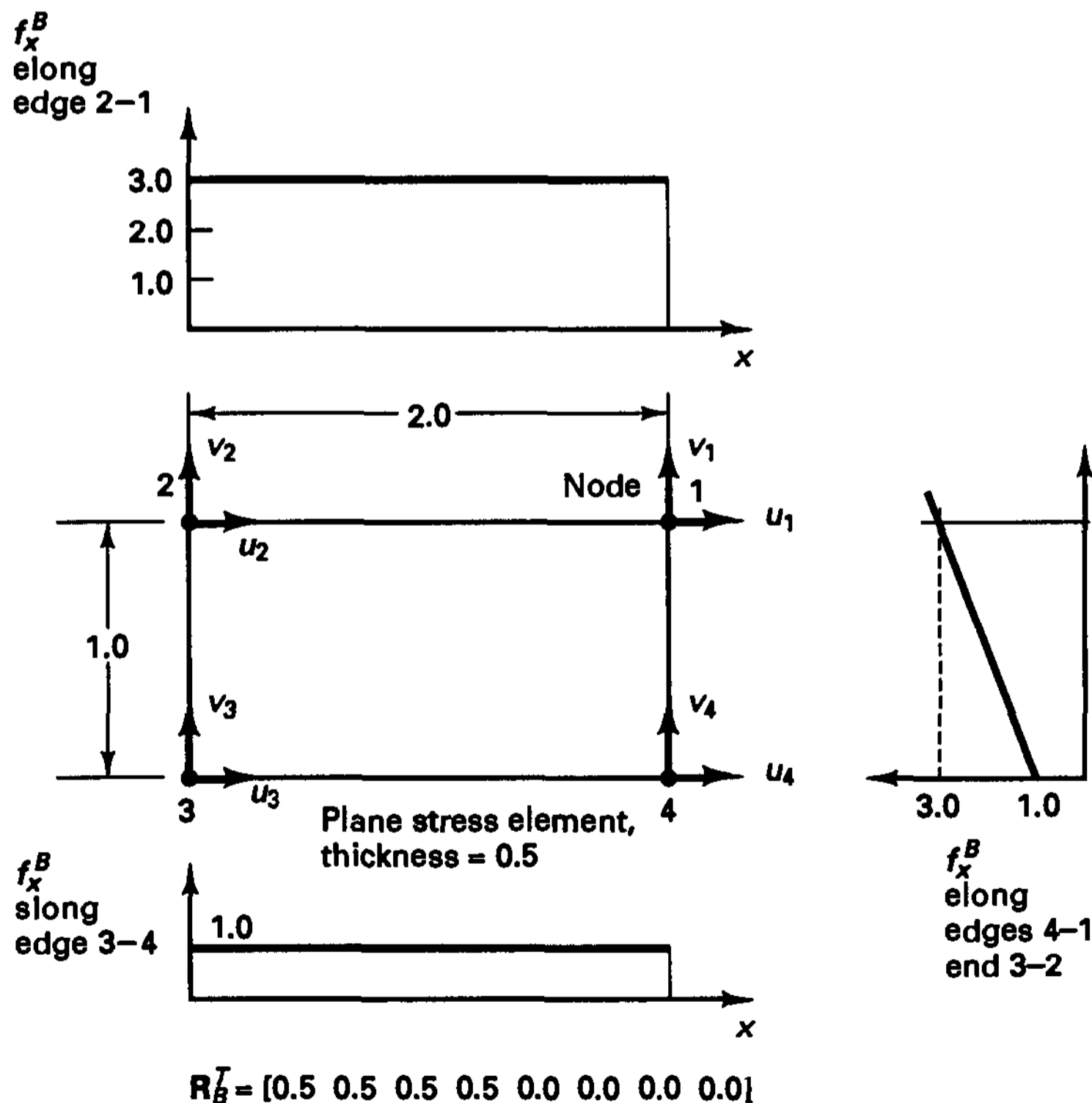


Figure 4.6 Body force distribution and corresponding lumped body force vector R_B of a rectangular element

calculation of the load vectors and the mass matrix as in the evaluation of the stiffness matrix, we say that “consistent” load vectors and a consistent mass matrix are evaluated. In this case, provided certain conditions are fulfilled (see Section 4.3.3), the finite element solution is a Ritz analysis.

It may now be recognized that instead of performing the integrations leading to the consistent load vector, we may evaluate an approximate load vector by simply adding to the actually applied concentrated nodal forces \mathbf{R}_C additional forces that are in some sense equivalent to the distributed loads on the elements. A somewhat obvious way of constructing approximate load vectors is to calculate the total body and surface forces corresponding to an element and to assign equal parts to the appropriate element nodal degrees of freedom. Consider as an example the rectangular plane stress element in Fig. 4.6 with the variation of the body force shown. The total body force is equal to 2.0, and hence we obtain the lumped body force vector given in the figure.

In considering the derivation of an element mass matrix, we recall that the inertia forces have been considered part of the body forces. Hence we may also establish an approximate mass matrix by lumping equal parts of the total element mass to the nodal points. Realizing that each nodal mass essentially corresponds to the mass of an element contributing volume around the node, we note that using this procedure of lumping mass, we assume in essence that the accelerations of the contributing volume to a node are constant and equal to the nodal values.

An important advantage of using a lumped mass matrix is that the matrix is diagonal, and, as will be seen later, the numerical operations for the solution of the dynamic equations of equilibrium are in some cases reduced very significantly.

EXAMPLE 4.21: Evaluate the lumped body force vector and the lumped mass matrix of the element assemblage in Fig. E4.5.

The lumped mass matrix is

$$\mathbf{M} = \rho \int_0^{100} (1) \begin{bmatrix} \frac{1}{2} & 0 & 0 \\ 0 & \frac{1}{2} & 0 \\ 0 & 0 & 0 \end{bmatrix} dx + \rho \int_0^{80} \left(1 + \frac{x}{40}\right)^2 \begin{bmatrix} 0 & 0 & 0 \\ 0 & \frac{1}{2} & 0 \\ 0 & 0 & \frac{1}{2} \end{bmatrix} dx$$

or

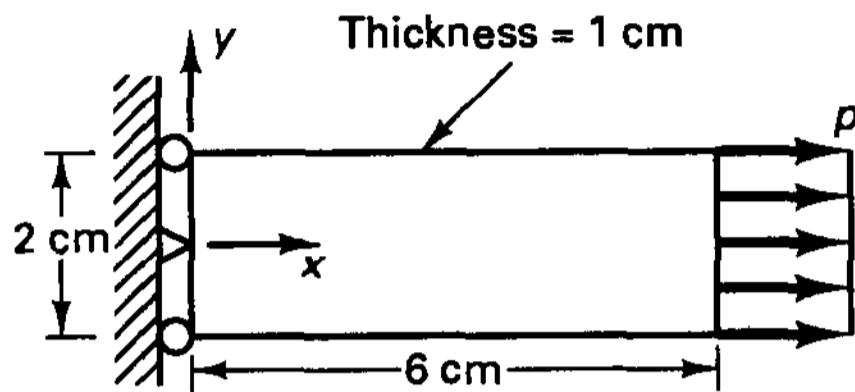
$$\mathbf{M} = \frac{\rho}{3} \begin{bmatrix} 150 & 0 & 0 \\ 0 & 670 & 0 \\ 0 & 0 & 520 \end{bmatrix}$$

Similarly, the lumped body force vector is

$$\begin{aligned} \mathbf{R}_B &= \left(\int_0^{100} (1) \begin{bmatrix} \frac{1}{2} \\ \frac{1}{2} \\ 0 \end{bmatrix} (1) dx + \int_0^{80} \left(1 + \frac{x}{40}\right)^2 \begin{bmatrix} 0 \\ \frac{1}{2} \\ \frac{1}{2} \end{bmatrix} \left(\frac{1}{10}\right) dx \right) f_2(t) \\ &= \frac{1}{3} \begin{bmatrix} 150 \\ 202 \\ 52 \end{bmatrix} f_2(t) \end{aligned}$$

It may be noted that, as required, the sums of the elements in \mathbf{M} and \mathbf{R}_B in both this example and in Example 4.5 are the same.

When using the load lumping procedure it should be recognized that the nodal point loads are, in general, calculated only approximately, and if a coarse finite element mesh is employed, the resulting solution may be very inaccurate. Indeed, in some cases when higher-order finite elements are used, surprising results are obtained. Figure 4.7 demonstrates such a case (see also Example 5.12).

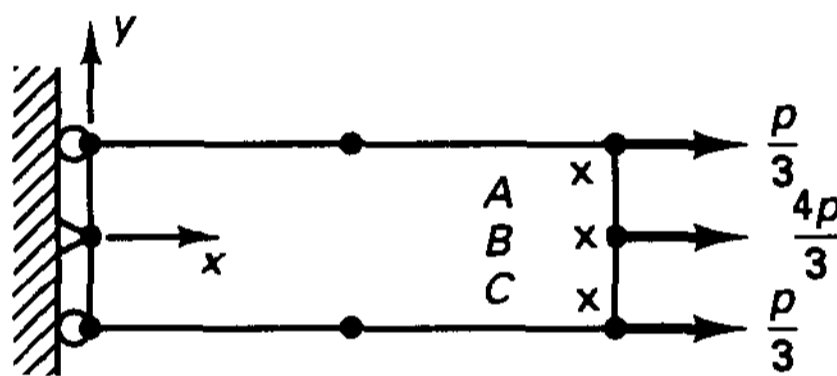


$$p = 300 \text{ N/cm}^2$$

$$E = 3 \times 10^7 \text{ N/cm}^2$$

$$\nu = 0.3$$

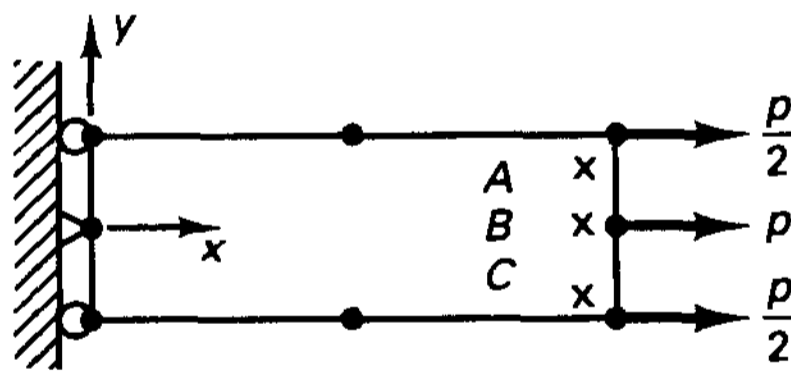
(a) Problem



Integration point	τ_{xx}	τ_{yy}	τ_{xy}
A	300.00	0.0	0.0
B	300.00	0.0	0.0
C	300.00	0.0	0.0

(b) Finite element model with consistent loading

(All stresses have units of N/cm²)



Integration point	τ_{xx}	τ_{yy}	τ_{xy}
A	301.41	-7.85	-24.72
B	295.74	-9.55	0.0
C	301.41	-7.85	24.72

(c) Finite element model with lumped loading

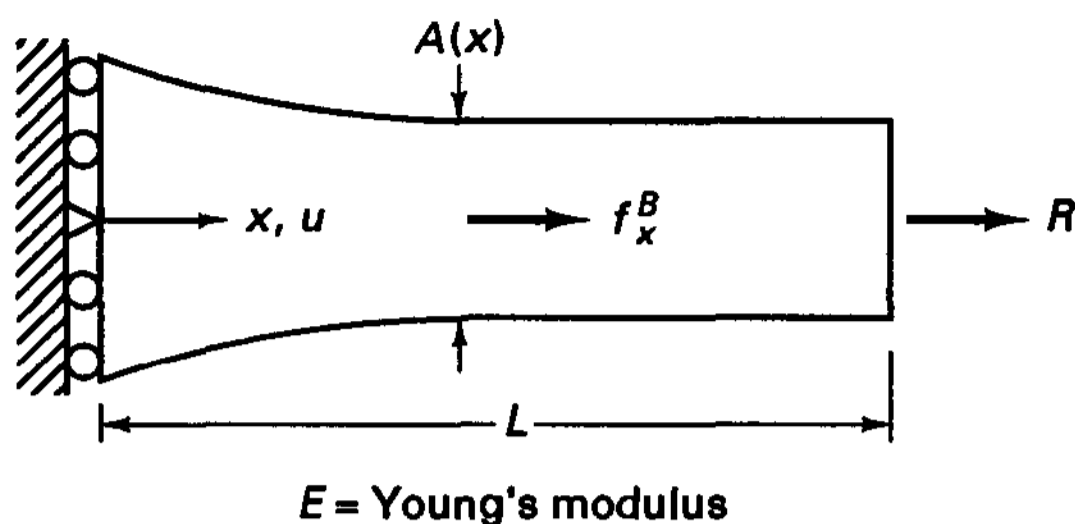
(All stresses have units of N/cm²)
(3 × 3 Gauss points are used, see Table 5.7)

Figure 4.7 Some sample analysis results with and without consistent loading

Considering dynamic analysis, the inertia effects can be thought of as body forces. Therefore, if a lumped mass matrix is employed, little might be gained by using a consistent load vector, whereas consistent nodal point loads should be used if a consistent mass matrix is employed in the analysis.

4.2.5 Exercises

- Use the procedure in Example 4.2 to formally derive the principle of virtual work for the one-dimensional bar shown.



The differential equations of equilibrium are

$$E \frac{\partial}{\partial x} \left(A \frac{\partial u}{\partial x} \right) + f_x^B = 0$$

$$EA \frac{\partial u}{\partial x} \Big|_{x=L} = R$$

4.2. Consider the structure shown.

- (a) Write down the principle of virtual displacements by specializing the general equation (4.7) to this case.
- (b) Use the principle of virtual work to check whether the exact solution is

$$\tau(x) = \left(\frac{72}{73} + \frac{24x}{73L} \right) \frac{F}{A_0}$$

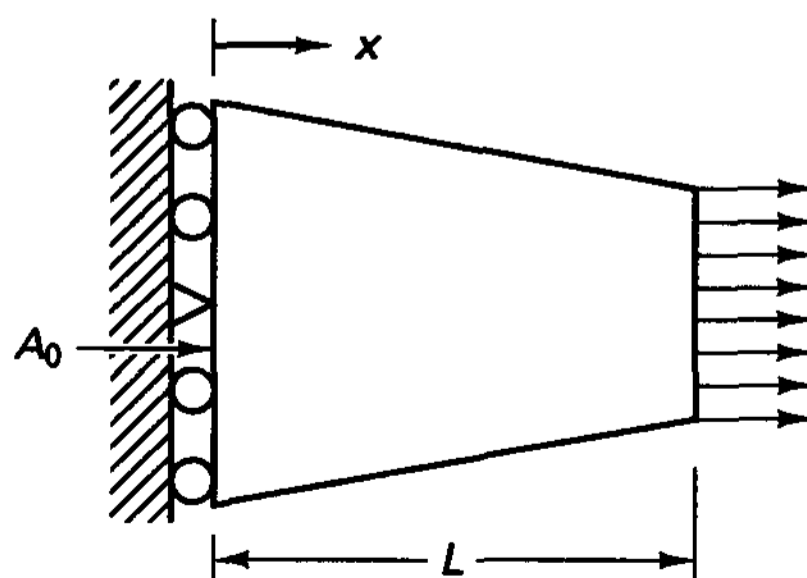
Use the following three virtual displacements: (i) $\bar{u}(x) = a_0x$, (ii) $\bar{u}(x) = a_0x^2$, (iii) $\bar{u}(x) = a_0x^3$.

- (c) Solve the governing differential equations of equilibrium,

$$E \frac{\partial}{\partial x} \left(A \frac{\partial u}{\partial x} \right) = 0$$

$$EA \frac{\partial u}{\partial x} \Big|_{x=L} = F$$

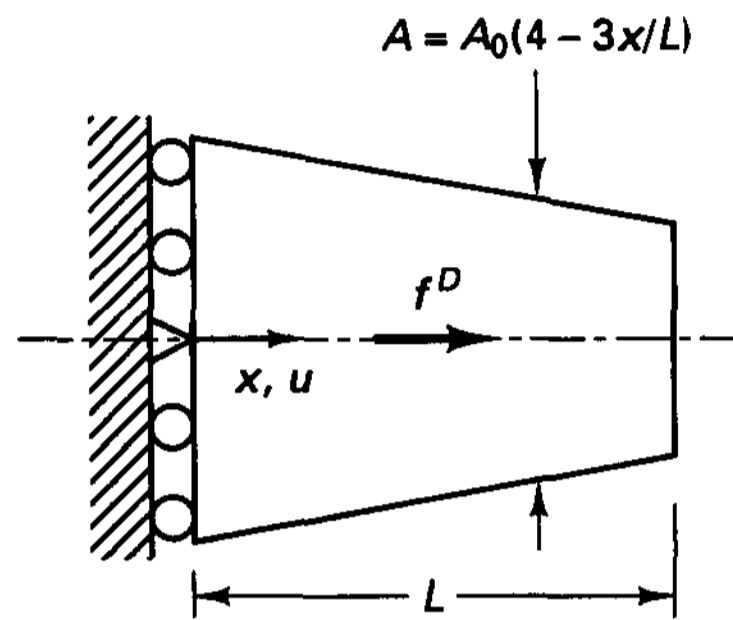
- (d) Use the three different virtual displacement patterns given in part (b), substitute into the principle of virtual work using the exact solution for the stress [from part (c)], and explicitly show that the principle holds.



$F = \text{total force exerted on right end}$
 $E = \text{Young's modulus}$
 $A(x) = A_0(1 - x/4L)$

4.3. Consider the bar shown.

- Solve for the exact displacement response of the structure.
- Show explicitly that the principle of virtual work is satisfied with the displacement patterns (i) $\bar{u} = ax$ and (ii) $\bar{u} = ax^2$.
- Identify a stress τ_{xx} for which the principle of virtual work is satisfied with pattern (ii) but not with pattern (i).



$f^D =$ constant force per unit length
Young's modulus E

4.4. For the two-dimensional body shown, use the principle of virtual work to show that the body forces are in equilibrium with the applied concentrated nodal loads.

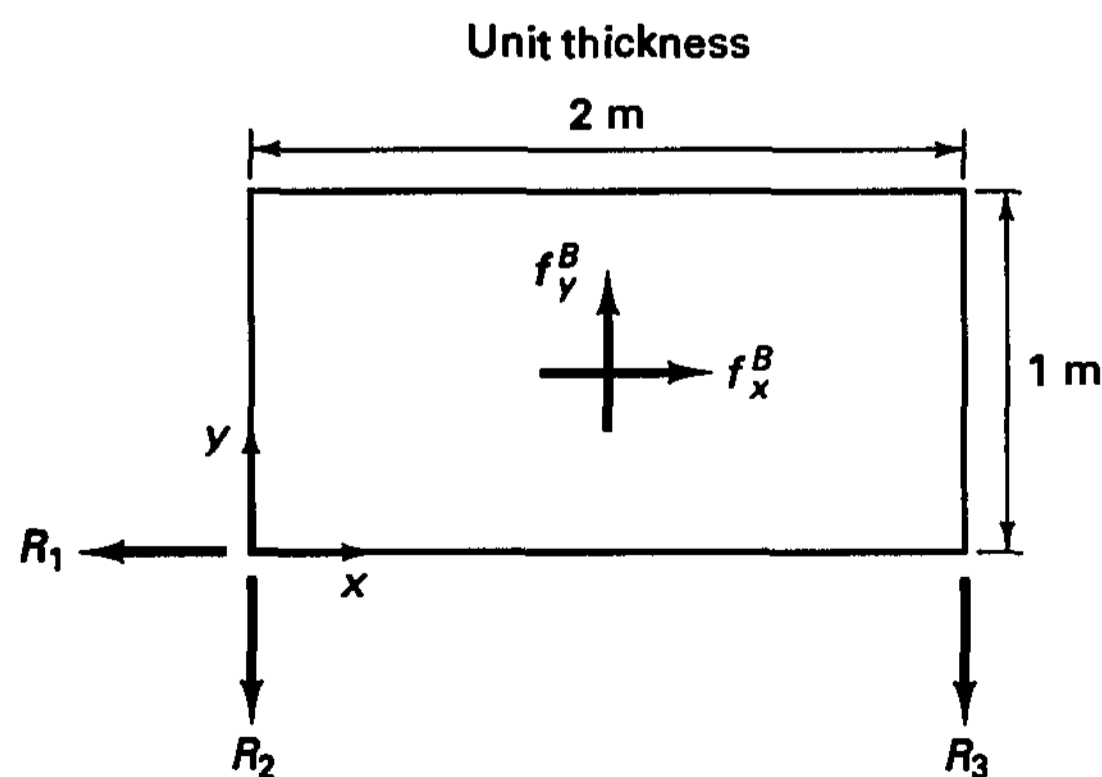
$$f_x^B = 10(1 + 2x) \text{ N/m}^3$$

$$f_y^B = 20(1 + y) \text{ N/m}^3$$

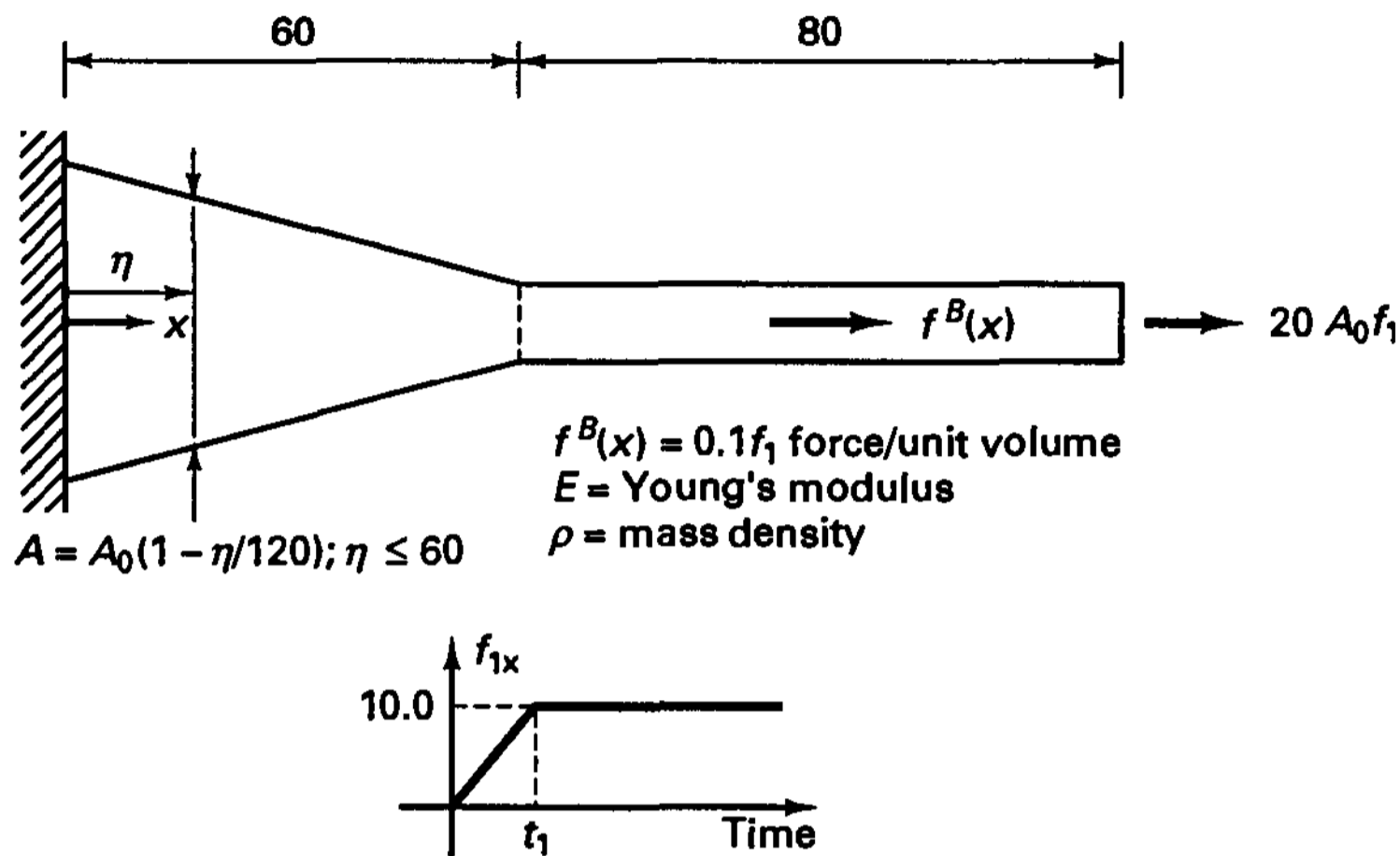
$$R_1 = 60 \text{ N}$$

$$R_2 = 45 \text{ N}$$

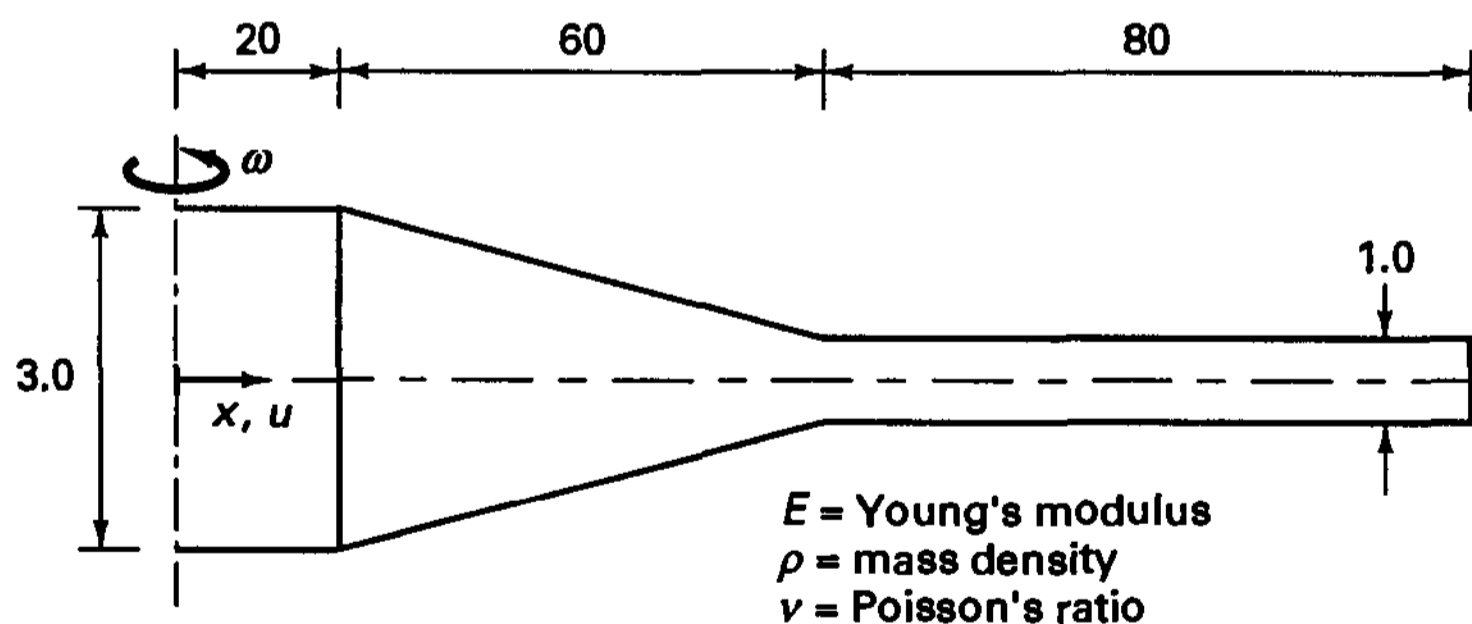
$$R_3 = 15 \text{ N}$$



- 4.5. Idealize the bar structure shown as an assemblage of 2 two-node bar elements.
 (a) Calculate the equilibrium equations $\mathbf{KU} = \mathbf{R}$.
 (b) Calculate the mass matrix of the element assemblage.



- 4.6. Consider the disk with a centerline hole of radius 20 shown spinning at a rotational velocity of ω radians/second.



Idealize the structure as an assemblage of 2 two-node elements and calculate the steady-state (pseudostatic) equilibrium equations. (Note that the strains are now $\partial u/\partial x$ and u/x , where u/x is the hoop strain.)

- 4.7. Consider Example 4.5 and the state at time $t = 2.0$ with $U_1(t) = 0$ at all times.
 (a) Use the finite element formulation given in the example to calculate the static nodal point displacements and the element stresses.
 (b) Calculate the reaction at the support.

- (c) Let the calculated finite element solution be u^{FE} . Calculate and plot the error r measured in satisfying the differential equation of equilibrium, i.e.,

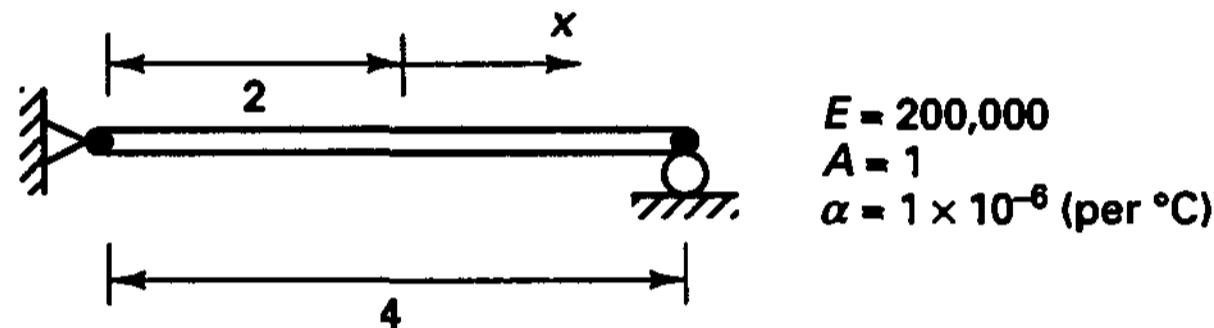
$$r = E \left[\frac{\partial}{\partial x} \left(A \frac{\partial u^{FE}}{\partial x} \right) \right] + f_x^B A$$

- (d) Calculate the strain energy of the structure as evaluated in the finite element solution and compare this strain energy with the exact strain energy of the mathematical model.

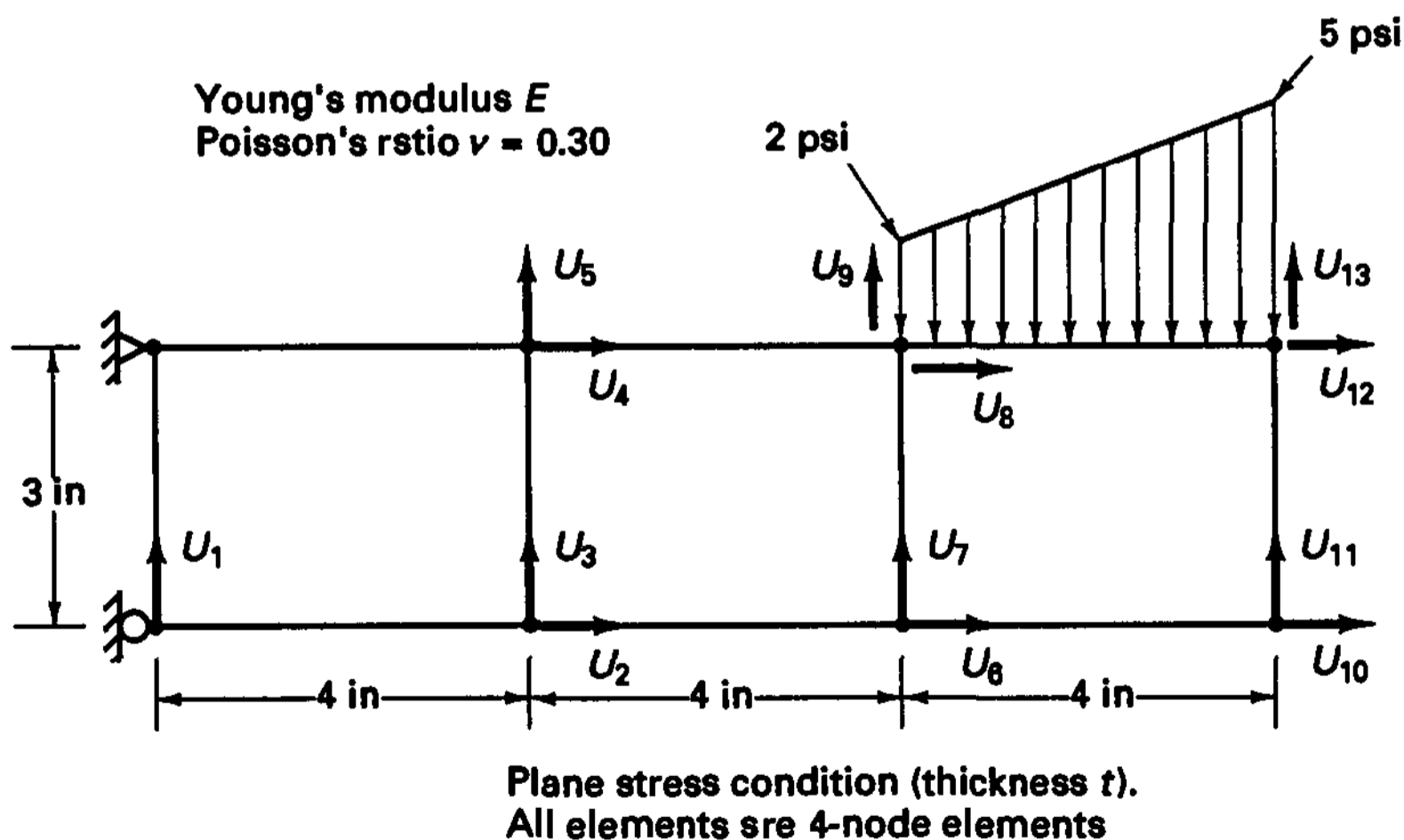
- 4.8. The two-node truss element shown, originally at a uniform temperature, 20°C, is subjected to a temperature variation

$$\theta = (10x + 20)^\circ\text{C}$$

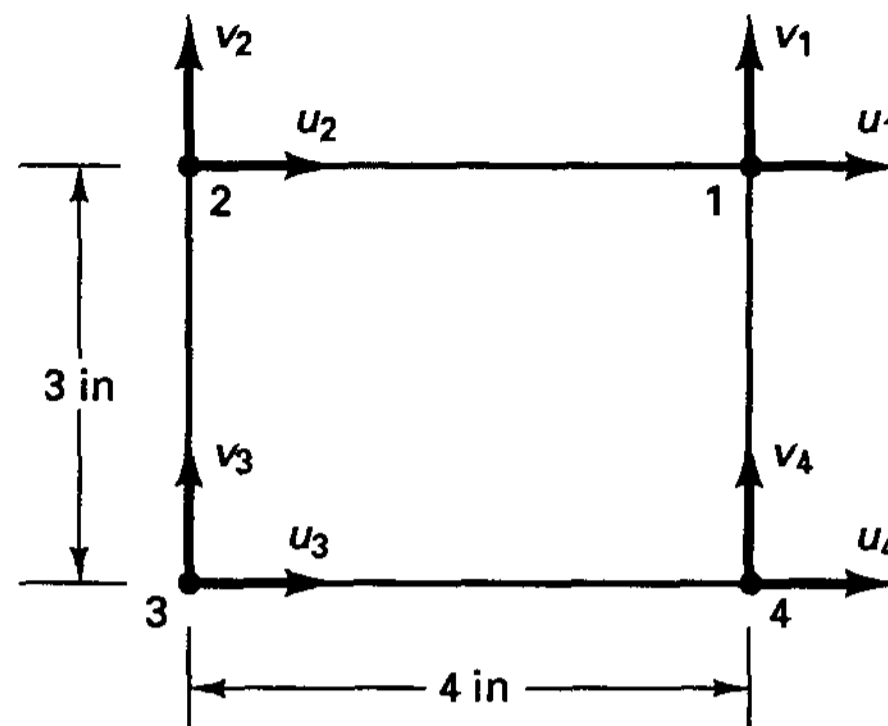
Calculate the resulting stress and nodal point displacement. Also obtain the analytical solution, assuming a continuum, and briefly discuss your results.



- 4.9. Consider the finite element analysis illustrated.

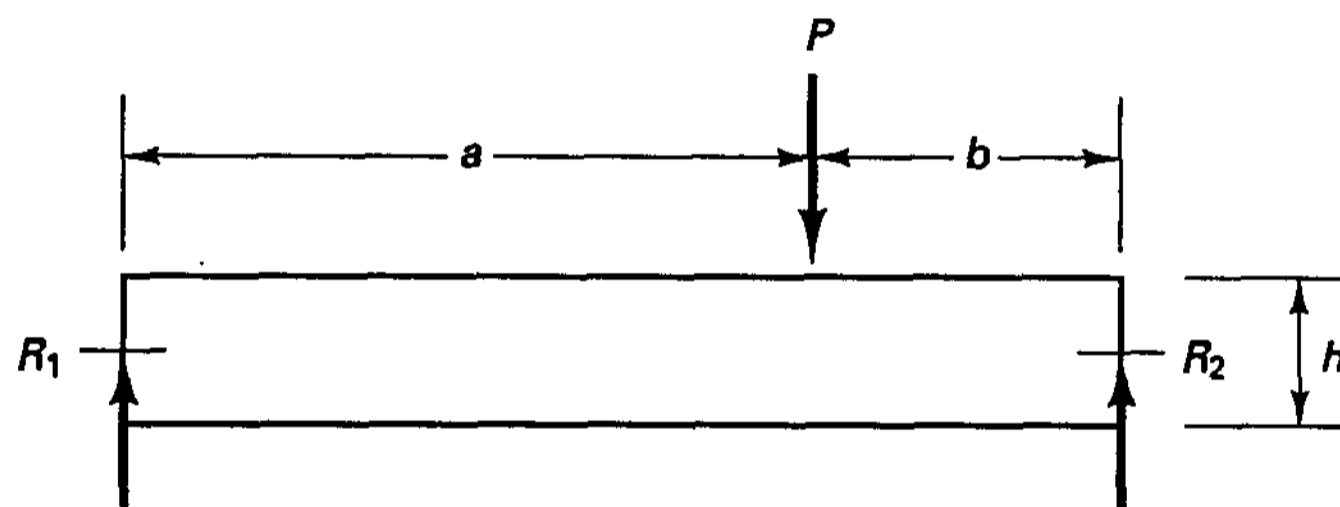


- (a) Begin by establishing the typical matrix \mathbf{B} of an element for the vector $\hat{\mathbf{u}}^T = [u_1 \ v_1 \ u_2 \ v_2 \ u_3 \ v_3 \ u_4 \ v_4]$.
- (b) Calculate the elements of the \mathbf{K} matrix, $K_{U_2 U_2}$, $K_{U_6 U_7}$, $K_{U_7 U_6}$, and $K_{U_5 U_{12}}$ of the structural assemblage.
- (c) Calculate the nodal load R_9 due to the linearly varying surface pressure distribution.

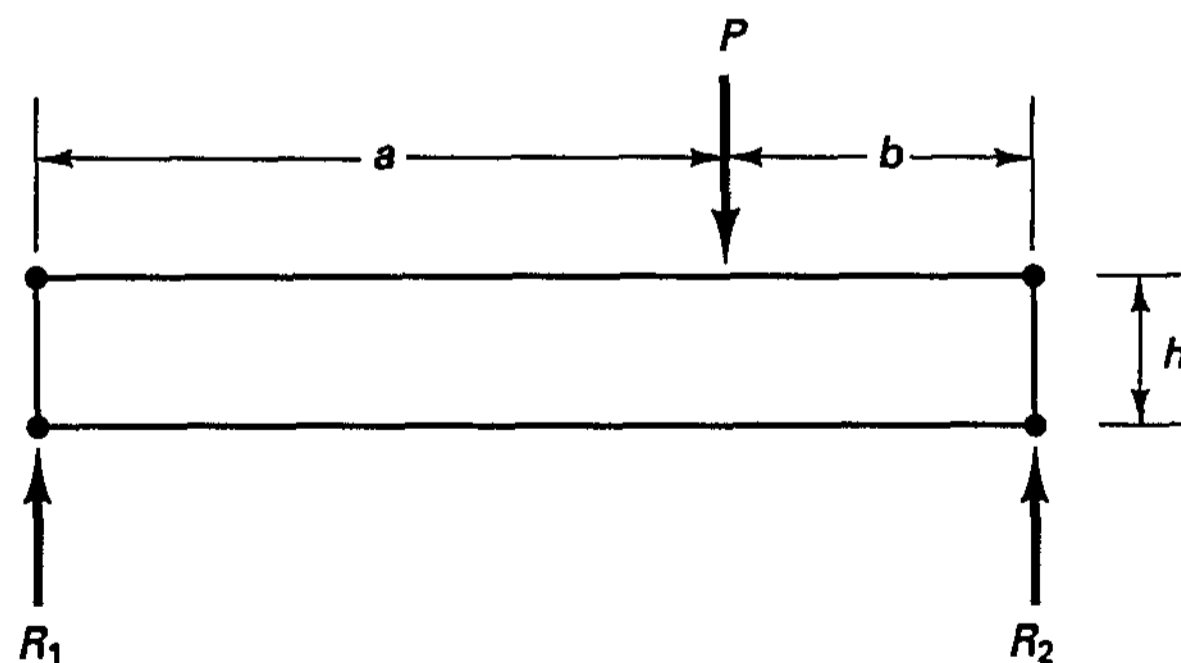


4.10. Consider the simply supported beam shown.

- (a) Assume that usual beam theory is employed and use the principle of virtual work to evaluate the reactions R_1 and R_2 .



- (b) Now assume that the beam is modeled by a four-node finite element. Show that to be able to evaluate R_1 and R_2 as in part (a) it is necessary that the finite element displacement functions can represent the rigid body mode displacements.



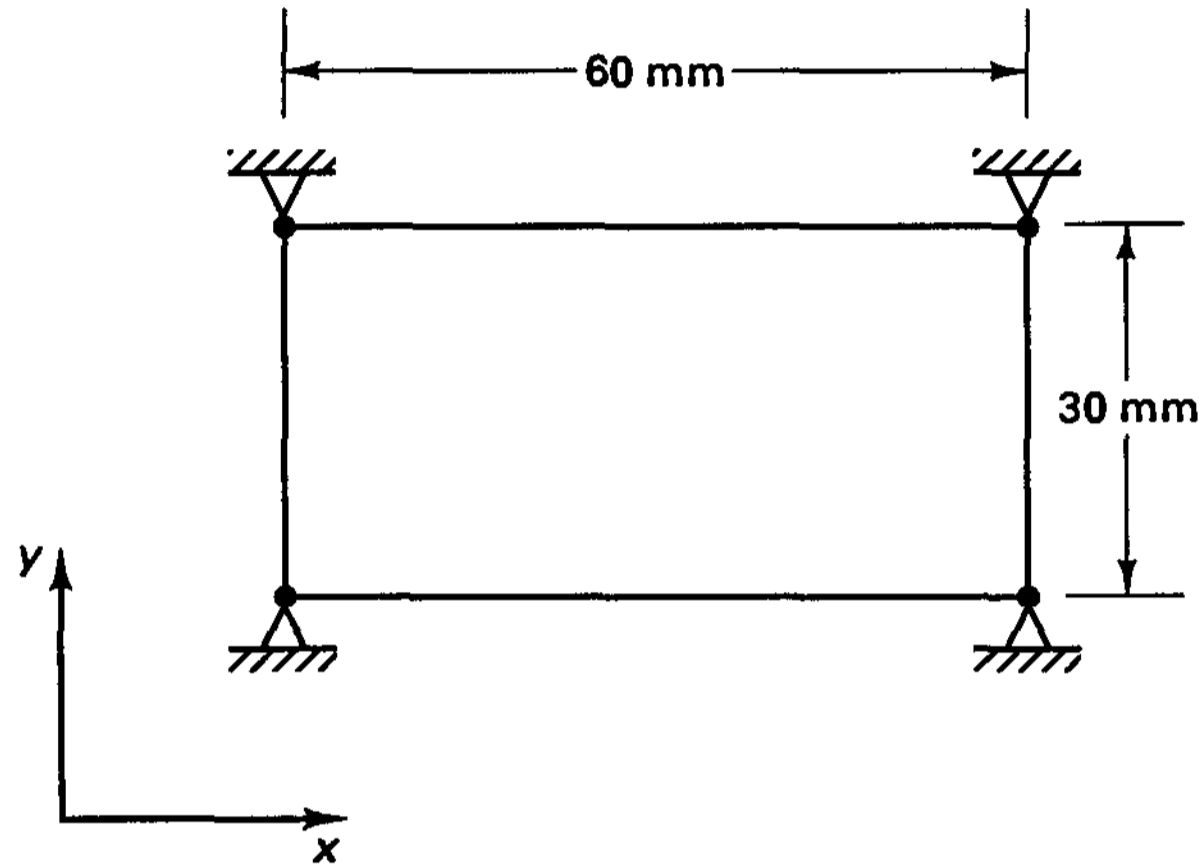
4.11. The four-node plane stress element shown carries the initial stresses

$$\tau'_{xx} = 0 \text{ MPa}$$

$$\tau'_{yy} = 10 \text{ MPa}$$

$$\tau'_{xy} = 20 \text{ MPa}$$

- (a) Calculate the corresponding nodal point forces \mathbf{R}_f .
- (b) Evaluate the nodal point forces \mathbf{R}_s equivalent to the surface tractions that correspond to the element stresses. Check your results using elementary statics and show that \mathbf{R}_s is equal to \mathbf{R}_f evaluated in part (a). Explain why this result makes sense.
- (c) Derive a general result: Assume that any stresses are given, and \mathbf{R}_f and \mathbf{R}_s are calculated. What conditions must the given stresses satisfy in order that $\mathbf{R}_f = \mathbf{R}_s$, where the surface tractions in \mathbf{R}_s are obtained from equation (b) in Example 4.2?



Young's modulus E
 Poisson's ratio ν
 Thickness = 0.5 mm

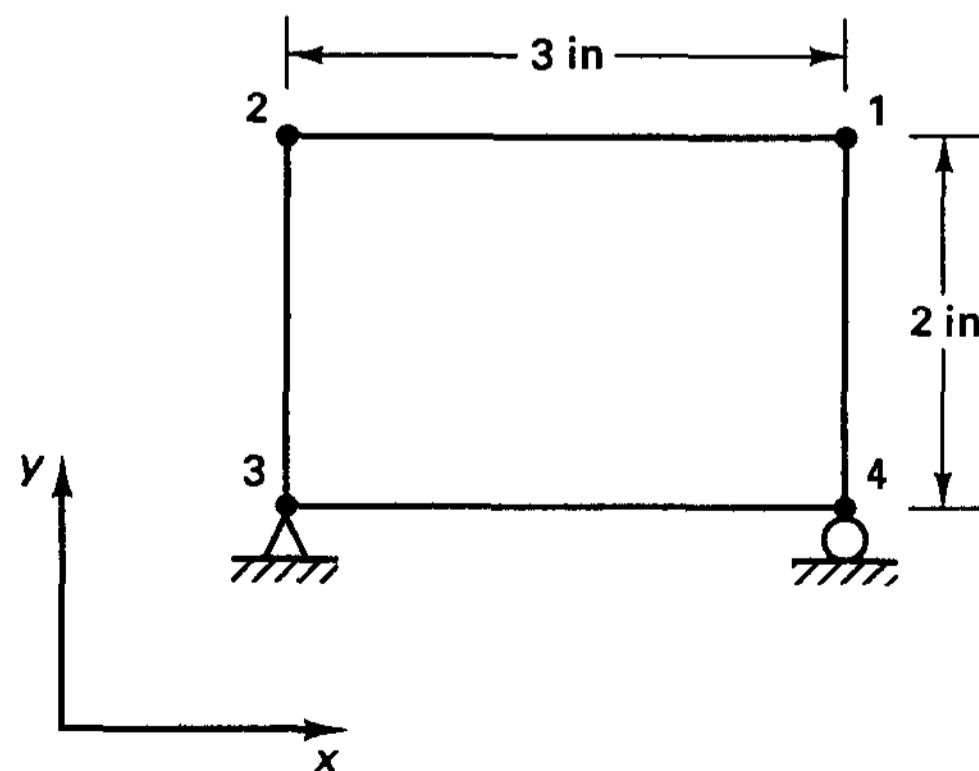
4.12. The four-node plane strain element shown is subjected to the constant stresses

$$\tau_{xx} = 20 \text{ psi}$$

$$\tau_{yy} = 10 \text{ psi}$$

$$\tau_{xy} = 10 \text{ psi}$$

Calculate the nodal point displacements of the element.



Young's modulus $E = 30 \times 10^6 \text{ psi}$
 Poisson's ratio $\nu = 0.30$

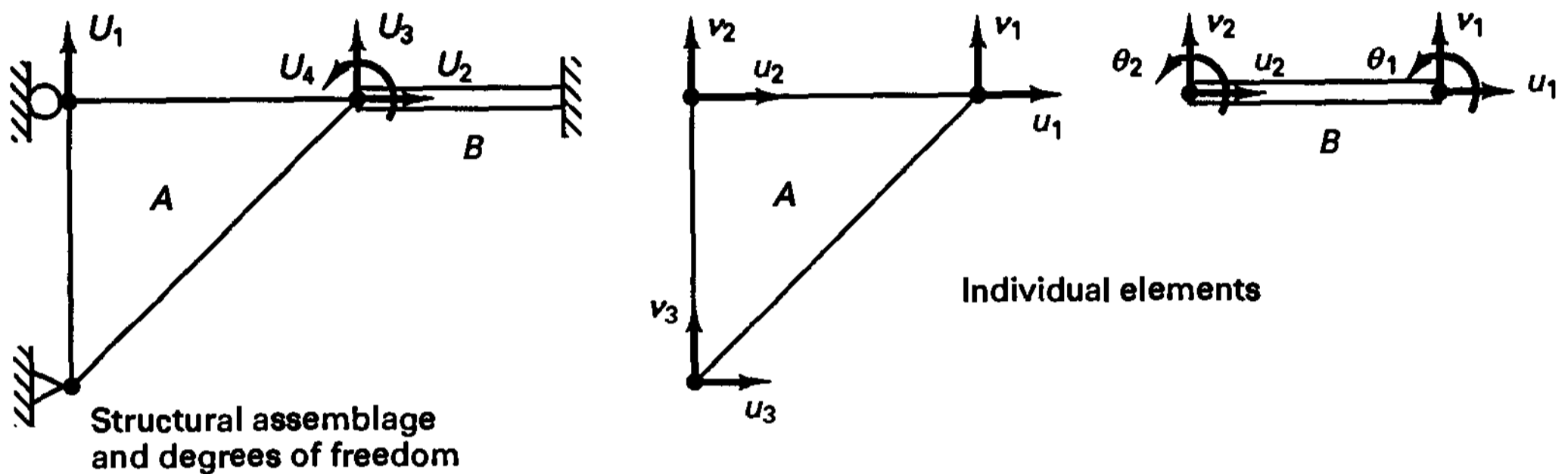
4.13. Consider element 2 in Fig. E4.9.

(a) Show explicitly that

$$\mathbf{F}^{(2)} = \int_{V^{(2)}} \mathbf{B}^{(2)T} \boldsymbol{\tau}^{(2)} dV^{(2)}$$

(b) Show that the element nodal point forces $\mathbf{F}^{(2)}$ are in equilibrium.

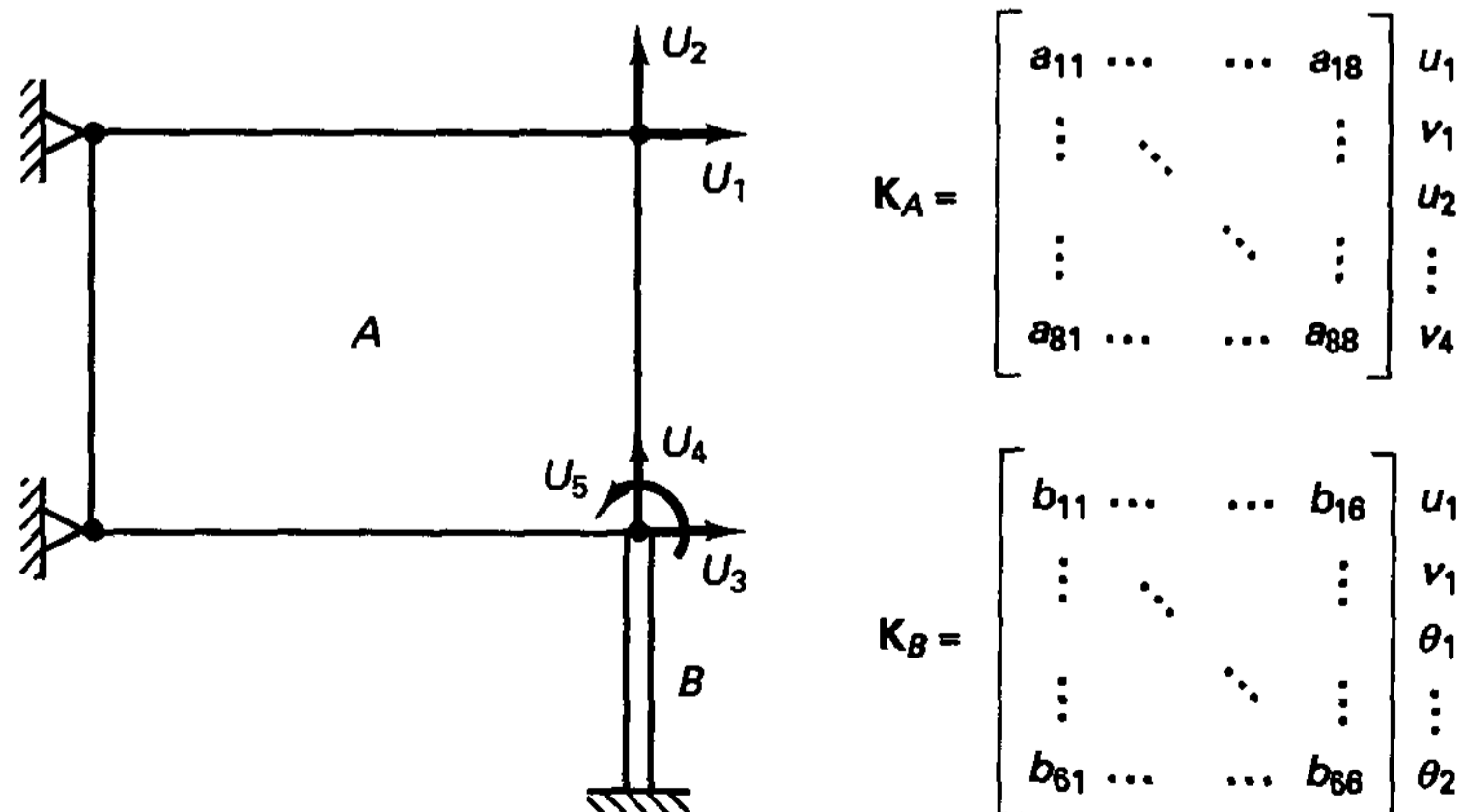
4.14. Assume that the element stiffness matrices \mathbf{K}_A and \mathbf{K}_B corresponding to the element displacements shown have been calculated. Assemble these element matrices directly into the global structure stiffness matrix with the displacement boundary conditions shown.



$$\mathbf{K}_A = \begin{bmatrix} a_{11} & a_{12} & a_{13} & a_{14} & a_{15} & a_{16} \\ a_{21} & a_{22} & a_{23} & a_{24} & a_{25} & a_{26} \\ a_{31} & a_{32} & a_{33} & a_{34} & a_{35} & a_{36} \\ a_{41} & a_{42} & a_{43} & a_{44} & a_{45} & a_{46} \\ a_{51} & a_{52} & a_{53} & a_{54} & a_{55} & a_{56} \\ a_{61} & a_{62} & a_{63} & a_{64} & a_{65} & a_{66} \end{bmatrix} \begin{matrix} u_1 \\ v_1 \\ u_2 \\ v_2 \\ u_3 \\ v_3 \end{matrix}$$

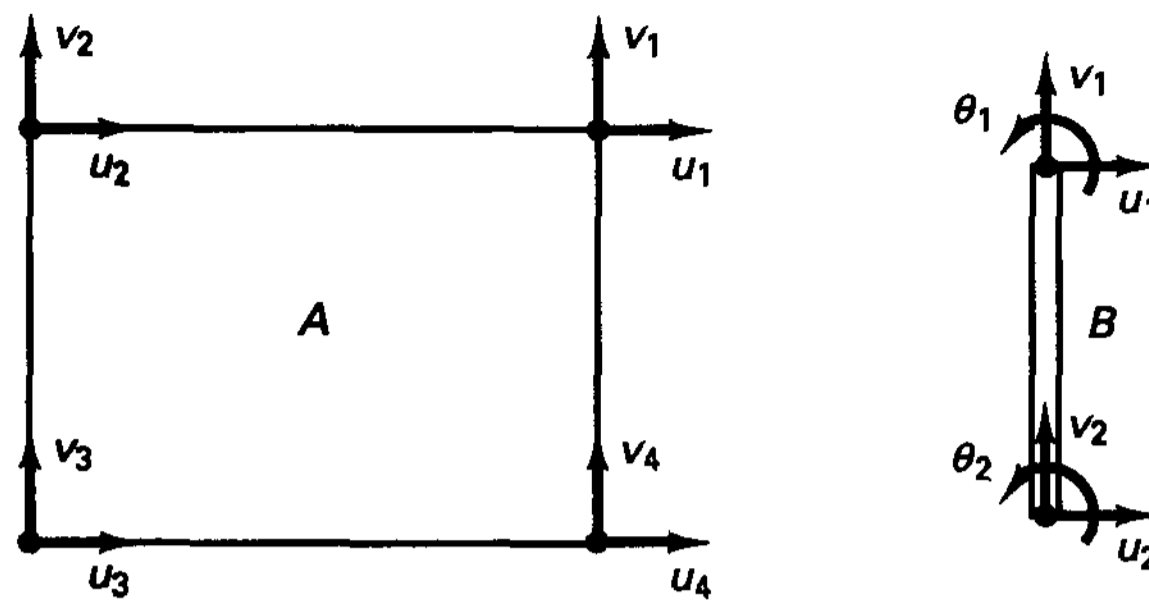
$$\mathbf{K}_B = \begin{bmatrix} b_{11} & b_{12} & b_{13} & b_{14} & b_{15} & b_{16} \\ b_{21} & b_{22} & b_{23} & b_{24} & b_{25} & b_{26} \\ b_{31} & b_{32} & b_{33} & b_{34} & b_{35} & b_{36} \\ b_{41} & b_{42} & b_{43} & b_{44} & b_{45} & b_{46} \\ b_{51} & b_{52} & b_{53} & b_{54} & b_{55} & b_{56} \\ b_{61} & b_{62} & b_{63} & b_{64} & b_{65} & b_{66} \end{bmatrix} \begin{matrix} u_1 \\ v_1 \\ \theta_1 \\ u_2 \\ v_2 \\ \theta_2 \end{matrix}$$

4.15. Assume that the element stiffness matrices \mathbf{K}_A and \mathbf{K}_B corresponding to the element displacements shown have been calculated. Assemble these element matrices directly into the global structure stiffness matrix with the displacement boundary conditions shown.

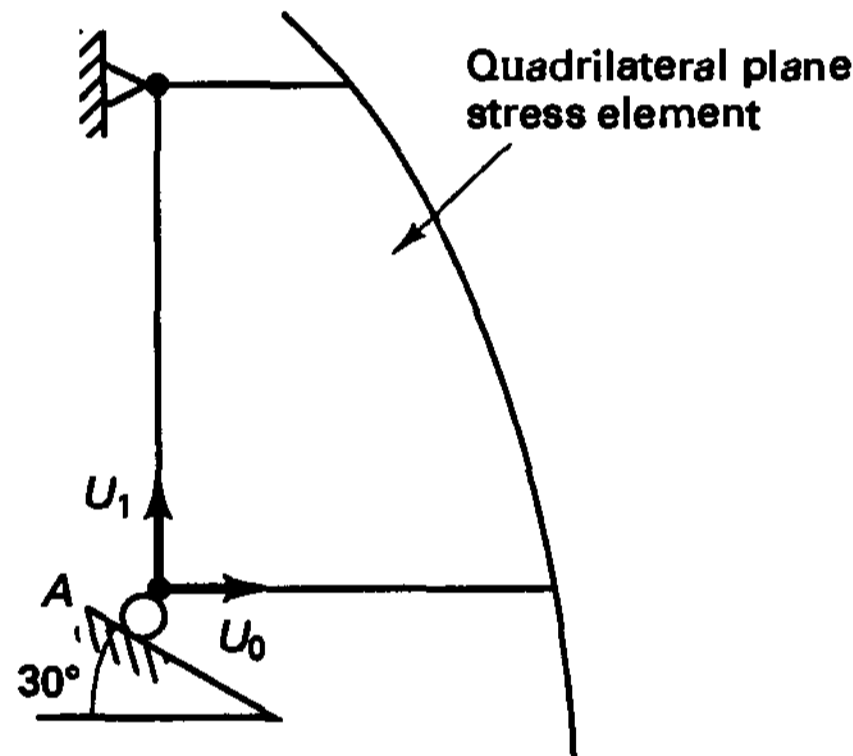


$$\mathbf{K}_A = \begin{bmatrix} a_{11} & \dots & \dots & a_{18} \\ \vdots & \ddots & & \vdots \\ \vdots & & \ddots & \vdots \\ a_{81} & \dots & \dots & a_{88} \end{bmatrix} \begin{matrix} u_1 \\ v_1 \\ u_2 \\ \vdots \\ v_4 \end{matrix}$$

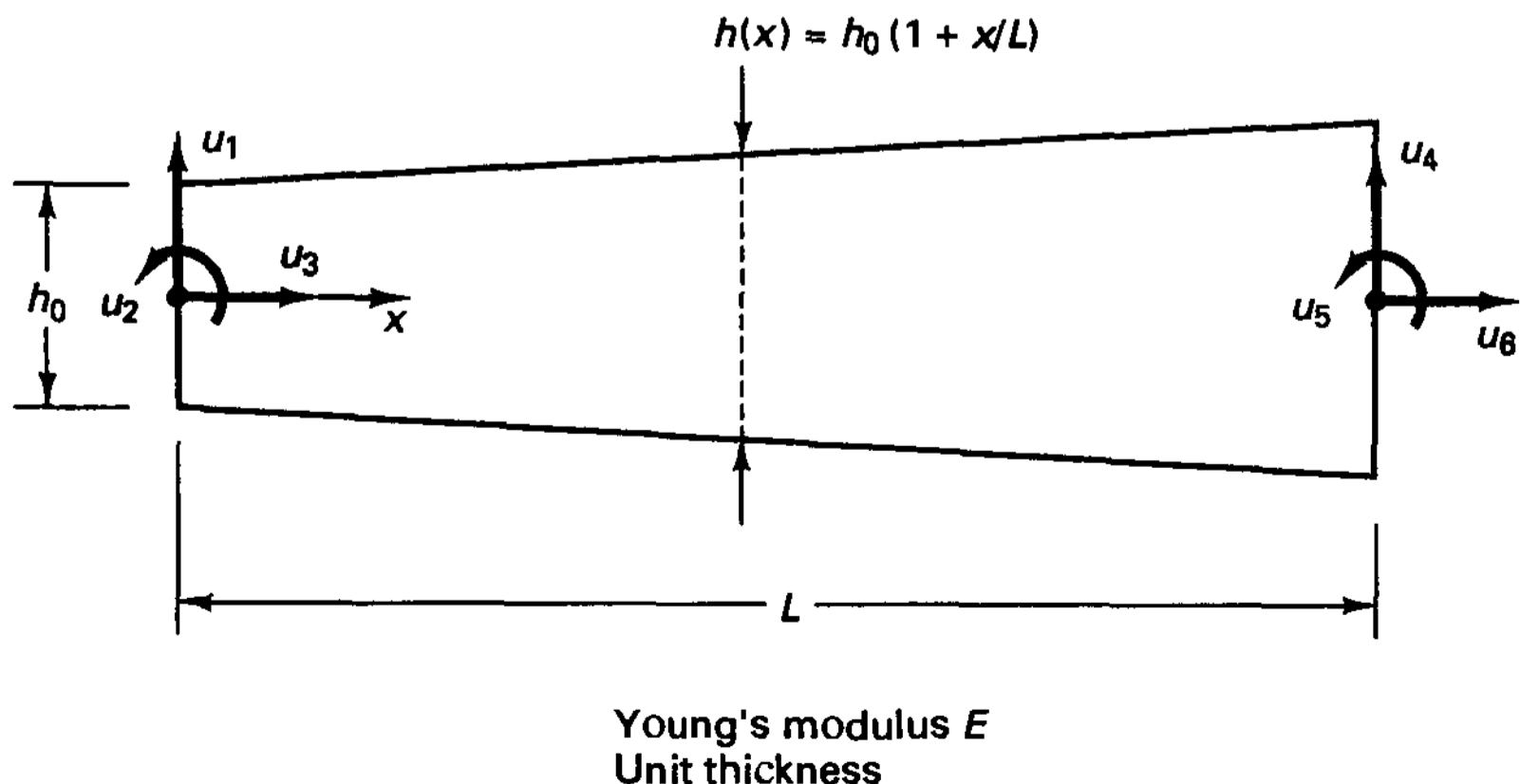
$$\mathbf{K}_B = \begin{bmatrix} b_{11} & \dots & \dots & b_{16} \\ \vdots & \ddots & & \vdots \\ \vdots & & \ddots & \vdots \\ b_{61} & \dots & \dots & b_{66} \end{bmatrix} \begin{matrix} u_1 \\ v_1 \\ \theta_1 \\ \vdots \\ \theta_2 \end{matrix}$$



- 4.16. Consider Example 4.11. Assume that at the support A, the roller allows a displacement only along a slope of 30 degrees to the horizontal direction. Determine the modifications necessary in the solution in Example 4.11 to obtain the structure matrix K for this situation.
- (a) Consider imposing the zero displacement condition exactly.
 - (b) Consider imposing the zero displacement condition using the penalty method.

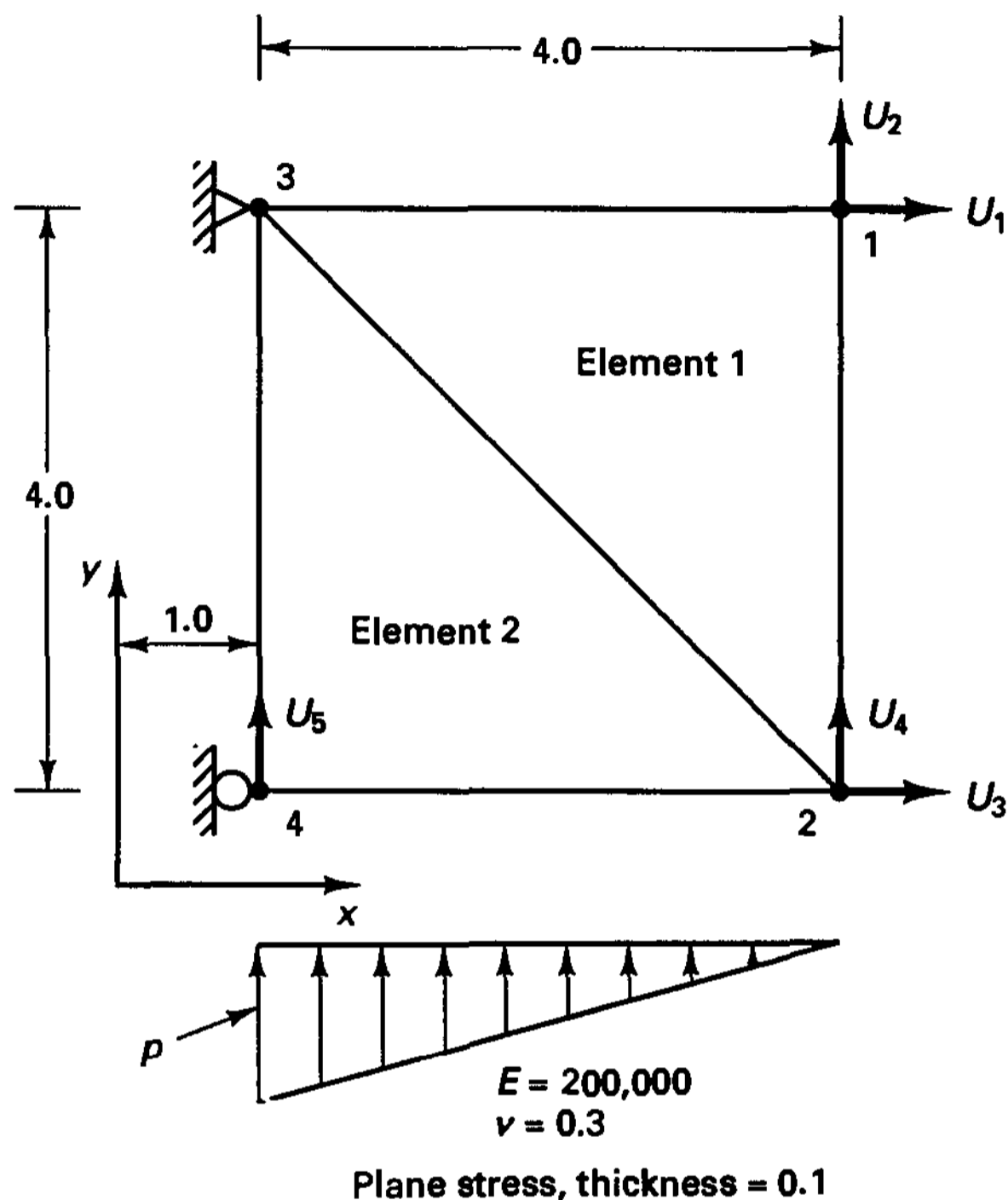


- 4.17. Consider the beam element shown. Evaluate the stiffness coefficients k_{11} and k_{12} .
- (a) Obtain the exact coefficients from the solution of the differential equation of equilibrium (using the mathematical model of Bernoulli beam theory).
 - (b) Obtain the coefficients using the principle of virtual work with the Hermitian beam functions (see Example 4.16).



4.18. Consider the two-element assemblage shown.

- (a) Evaluate the stiffness coefficients K_{11} , K_{14} for the finite element idealization.
- (b) Calculate the load vector of the element assemblage.

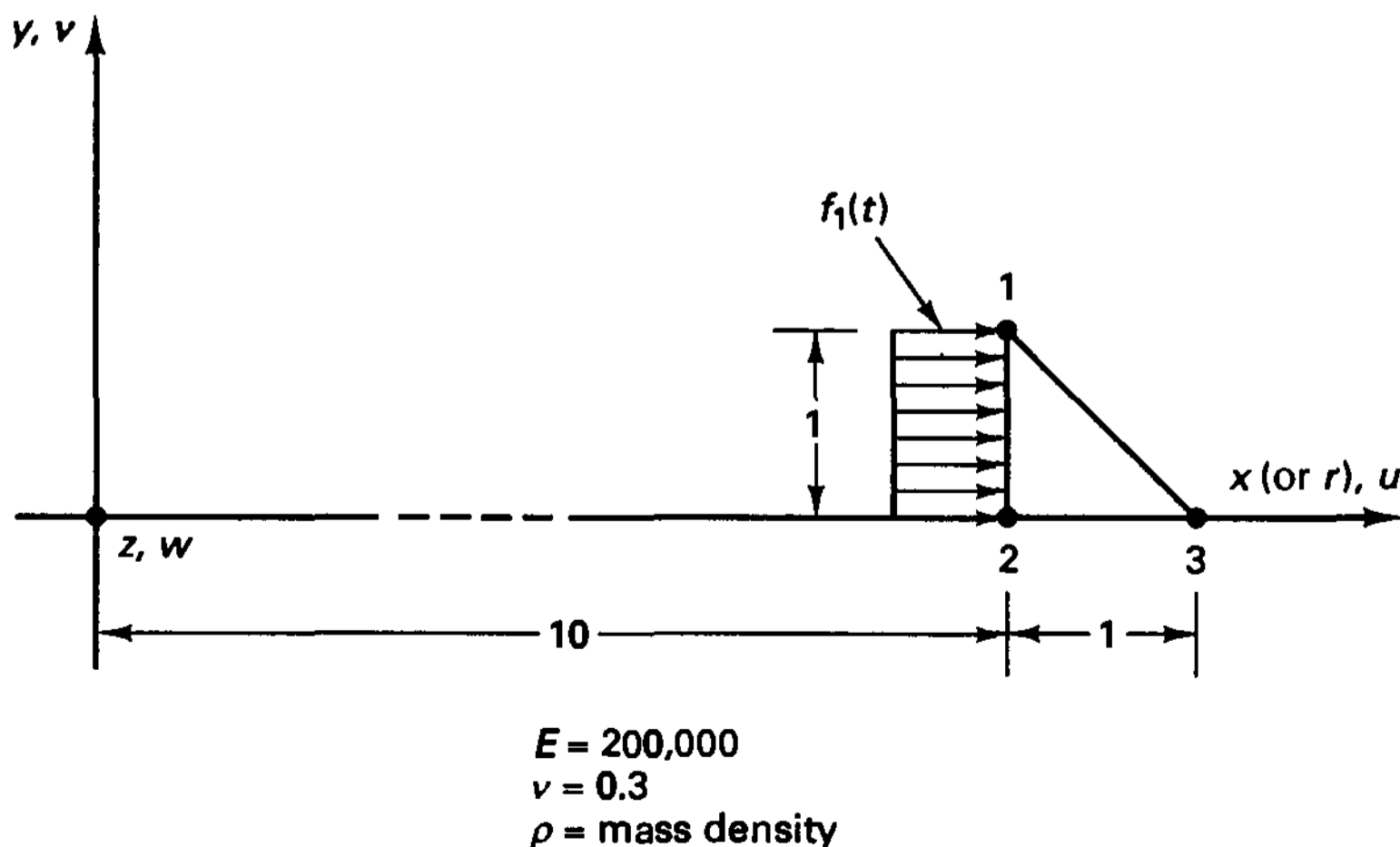


4.19. Consider the two-element assemblage in Exercise 4.18 but now assume axisymmetric conditions. The y -axis is the axis of revolution.

- (a) Evaluate the stiffness coefficients K_{11} , K_{14} for the finite element idealization.
- (b) Evaluate the corresponding load vector.

4.20. Consider Example 4.20 and let the loading on the structure be $R_r = f_1(t) \cos \theta$.

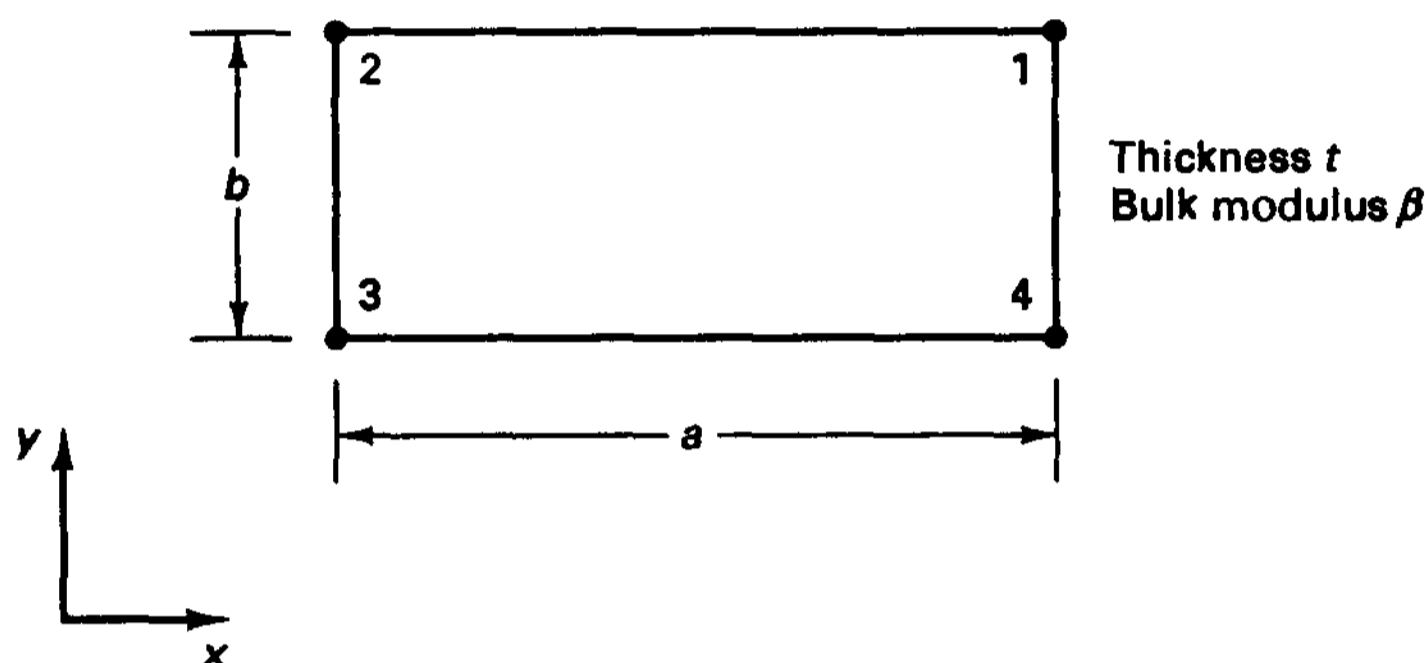
- (a) Establish the stiffness matrix, mass matrix, and load vector of the three-node element



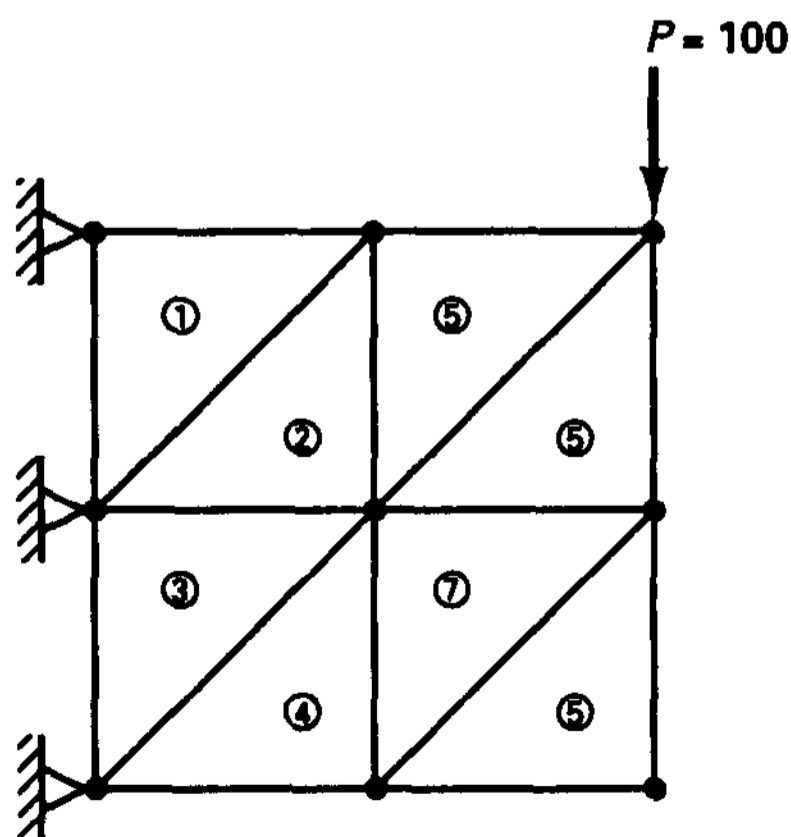
shown. Establish explicitly all matrices you need but do not perform any multiplications and integrations.

(b) Explain (by physical reasoning) that your assumptions on u , v , w make sense.

- 4.21. An inviscid fluid element (for acoustic motions) can be obtained by considering only volumetric strain energy (since inviscid fluids provide no resistance to shear). Formulate the finite element fluid stiffness matrix for the four-node plane element shown and write out all matrices required. Do not actually perform any integrations or matrix multiplications. *Hint:* Remember that $p = -\beta \Delta V/V$ and $\tau^T = [\tau_{xx} \ \tau_{yy} \ \tau_{xy} \ \tau_{zy}] = [-p \ -p \ 0 \ -p]$ and $\Delta V/V = \epsilon_{xx} + \epsilon_{yy}$.

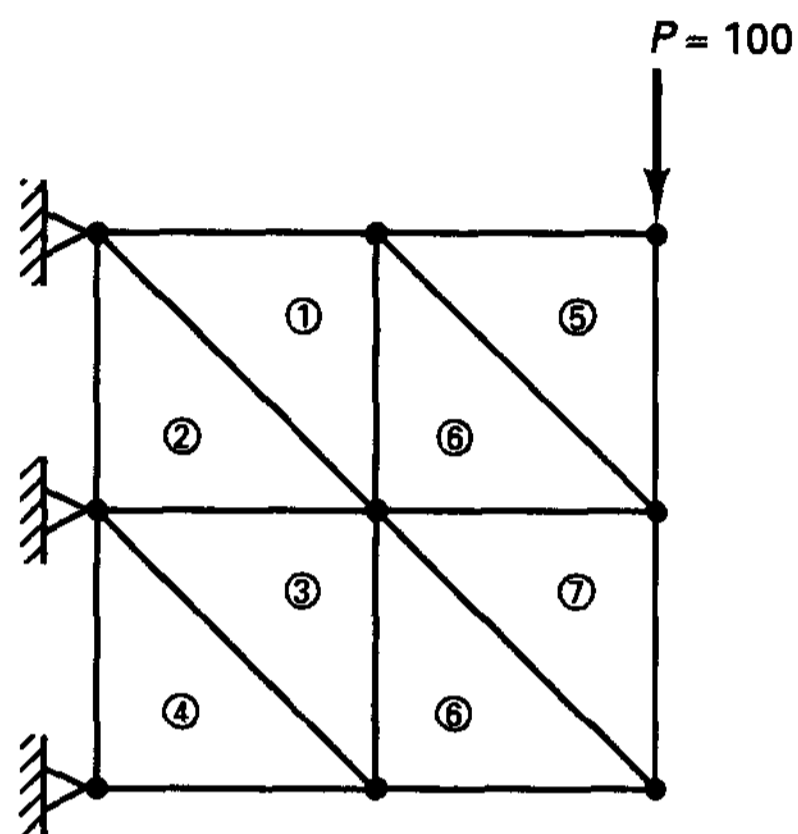


- 4.22. Consider the element assemblages in Exercises 4.18 and 4.19. For each case, evaluate a lumped mass matrix (using a uniform mass density ρ) and a lumped load vector.
- 4.23. Use a finite element program to solve the model shown of the problem in Example 4.6.
- Print out the element stresses and element nodal point forces and draw the “exploded element views” for the stresses and nodal point forces as in Example 4.9.
 - Show that the element nodal point forces of element 5 are in equilibrium and that the element nodal point forces of elements 5 and 6 equilibrate the applied load.
 - Print out the reactions and show that the element nodal point forces equilibrate these reactions.
 - Calculate the strain energy of the finite element model.



Eight constant-strain triangles

4.24. Use a finite element program to solve the model shown of the problem in Example 4.6. Print out the element stresses and reactions and calculate the strain energy of the model. Draw the “exploded element views” for the stresses and nodal point forces. Compare your results with those for Exercise 4.23 and discuss why we should not be surprised to have obtained different results (although the same kind and same number of elements are used in both idealizations).



Eight constant-strain triangles

4.3 CONVERGENCE OF ANALYSIS RESULTS

Since the finite element method is a numerical procedure for solving complex engineering problems, important considerations pertain to the accuracy of the analysis results and the convergence of the numerical solution. The objective in this section is to address these issues. We start by defining in Section 4.3.1 what we mean by convergence. Then we consider in a rather physical manner the criteria for monotonic convergence and relate these criteria to the conditions in a Ritz analysis (introduced in Section 3.3.3). Next, some important properties of the finite element solution are summarized (and proven) and the rate of convergence is discussed. Finally, we consider the calculation of stresses and the evaluation of error measures that indicate the magnitude of the error in stresses at the completion of an analysis.

We consider in this section displacement-based finite elements leading to monotonically convergent solutions. Formulations that lead to a nonmonotonic convergence are considered in Sections 4.4 and 4.5.

4.3.1 The Model Problem and a Definition of Convergence

Based on the preceding discussions, we can now say that, in general, a finite element analysis requires the idealization of an actual physical problem into a mathematical model and then the finite element solution of that model (see Section 1.2). Figure 4.8 summarizes these concepts. The distinction given in the figure is frequently not recognized in practical analysis because the differential equations of motion of the mathematical model are not dealt with, and indeed the equations may be unknown in the analysis of a complex problem,

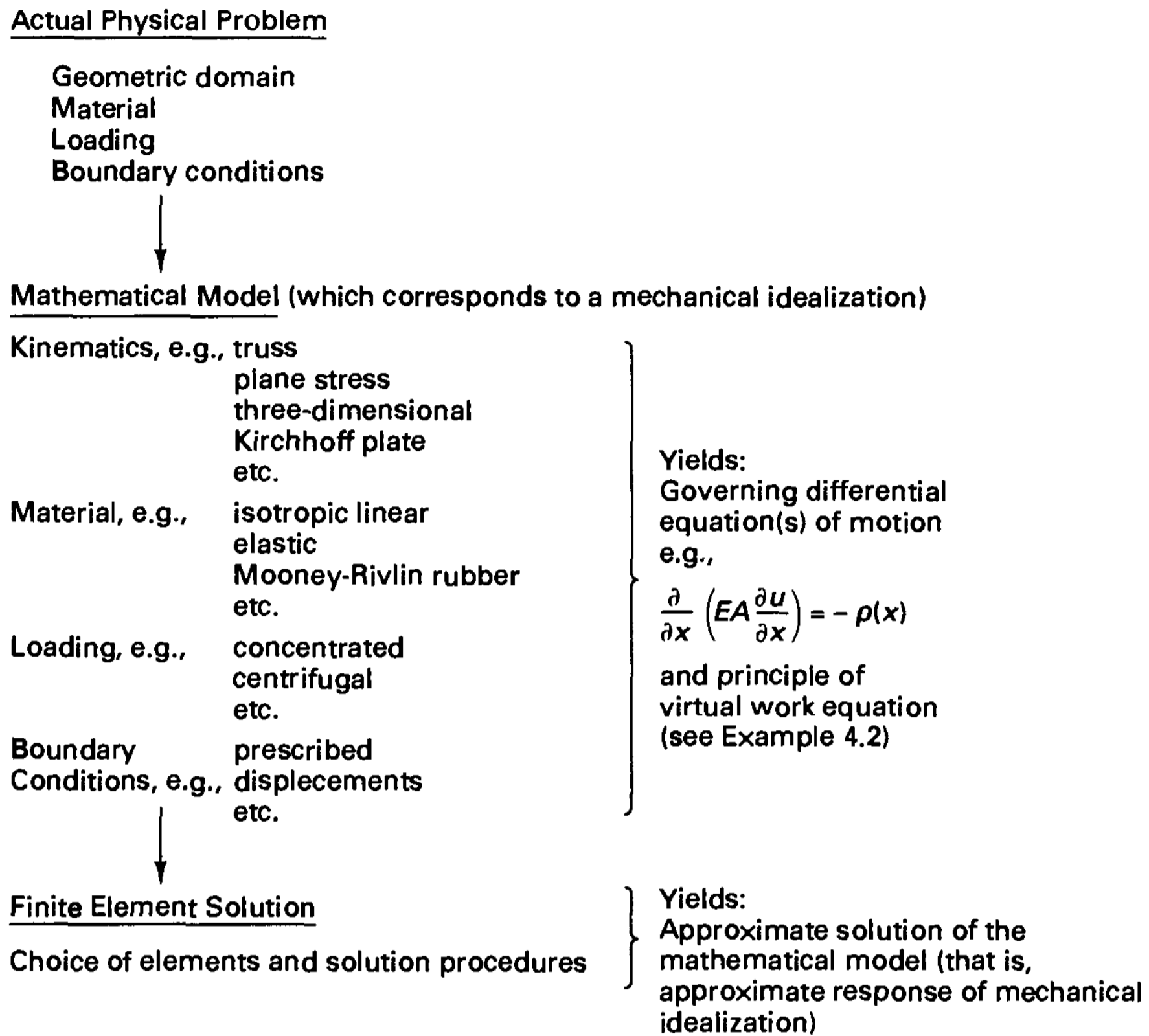


Figure 4.8 Finite element solution process

such as the response prediction of a three-dimensional shell. Instead, in a practical analysis, a finite element idealization of the physical problem is established directly. However, to study the convergence of the finite element solution as the number of elements increases, it is valuable to recognize that a mathematical model is actually implied in the finite element representation of the physical problem. That is, a proper finite element solution should converge (as the number of elements is increased) to the analytical (exact) solution of the differential equations that govern the response of the mathematical model. Furthermore, the convergence behavior displays all the characteristics of the finite element scheme because the differential equations of motion of the mathematical model express in a very precise and compact manner all basic conditions that the solution variables (stress, displacement, strain, and so on) must satisfy. If the differential equations of motion are not known, as in a complex shell analysis, and/or analytical solutions cannot be obtained, the convergence of the finite element solutions can be measured only on the fact that all basic kinematic, static, and constitutive conditions contained in the mathematical model must ultimately (at convergence) be satisfied. Therefore, in all discussions of the convergence of finite element solutions we imply that the convergence to the exact solution of a mathematical model is meant.

Here it is important to recognize that in linear elastic analysis there is a unique exact solution to the mathematical model. Hence if we have a solution that satisfies the governing

mathematical equations exactly, then this is *the* exact solution to the problem (see Section 4.3.4).

In considering the approximate finite element solution to the exact response of the mathematical model, we need to recognize that different sources of errors affect the finite element solution results. Table 4.4 summarizes various general sources of errors. Round-off errors are a result of the finite precision arithmetic of the computer used; solution errors in the constitutive modeling are due to the linearization and integration of the constitutive relations; solution errors in the calculation of the dynamic response arise in the numerical integration of the equations of motion or because only a few modes are used in a mode superposition analysis; and solution errors arise when an iterative solution is obtained because convergence is measured on increments in the solution variables that are small but not zero. In this section, we will discuss only the finite element discretization errors, which are due to interpolation of the solution variables. Thus, in essence, *we consider in this section a model problem in which the other solution errors referred to above do not arise: a linear elastic static problem with the geometry represented exactly with the exact calculation of the element matrices and solution of equations, i.e., also negligible round-off errors.* For ease of presentation, we assume that the prescribed displacements are zero. Nonzero displacement boundary conditions would be imposed as discussed in Section 4.2.2, and such boundary conditions do not change the properties of the finite element solution.

For this model problem, let us restate for purposes of our discussion the basic equation of the principle of virtual work governing the exact solution of the mathematical model

$$\int_V \bar{\epsilon}^T \tau \, dV = \int_{S_f} \bar{u}^{S_f T} f^{S_f} \, dS + \int_V \bar{u}^T f^B \, dV \tag{4.62}$$

TABLE 4.4 *Finite element solution errors*

Error	Error occurrence in	See section
Discretization	Use of finite element interpolations for geometry and solution variables	4.2.1 4.2.3, 5.3
Numerical integration in space	Evaluation of finite element matrices using numerical integration	5.5 6.8.4
Evaluation of constitutive relations	Use of nonlinear material models	6.6.3 6.6.4
Solution of dynamic equilibrium equations	Direct time integration, mode superposition	9.2–9.4
Solution of finite element equations by iteration	Gauss-Seidel, conjugate gradient, Newton-Raphson, quasi-Newton methods, eigensolutions	8.3, 8.4 9.5 10.4
Round-off	Setting up equations and their solution	8.2.6

We recall that for τ to be the exact solution of the mathematical model, (4.62) must hold for arbitrary virtual displacements $\bar{\mathbf{u}}$ (and corresponding virtual strains $\bar{\boldsymbol{\epsilon}}$), with $\bar{\mathbf{u}}$ zero at and corresponding to the prescribed displacements. A short notation for (4.62) is

Find the displacements \mathbf{u} (and corresponding stresses $\boldsymbol{\tau}$) such that $a(\mathbf{u}, \mathbf{v}) = (\mathbf{f}, \mathbf{v}) \quad \text{for all admissible } \mathbf{v}$	(4.63)
---	--------

Here $a(\cdot, \cdot)$ is a bilinear form and (\mathbf{f}, \cdot) is a linear form⁹—these forms depend on the mathematical model considered— \mathbf{u} is the exact displacement solution, \mathbf{v} is any admissible virtual displacement [“admissible” because the functions \mathbf{v} must be continuous and zero at and corresponding to actually prescribed displacements (see (4.7)], and \mathbf{f} represents the forcing functions (loads \mathbf{f}^S and \mathbf{f}^B). Note that the notation in (4.63) implies an integration process. The bilinear forms $a(\cdot, \cdot)$ that we consider in this section are symmetric in the sense that $a(\mathbf{u}, \mathbf{v}) = a(\mathbf{v}, \mathbf{u})$.

From (4.63) we have that the strain energy corresponding to the exact solution \mathbf{u} is $1/2 a(\mathbf{u}, \mathbf{u})$. We assume that the material properties and boundary conditions of our model problem are such that this strain energy is finite. This is not a serious restriction in practice but requires the proper choice of a mathematical model. In particular, the material properties must be physically realistic and the load distributions (externally applied or due to displacement constraints) must be sufficiently smooth. We have discussed the need of modeling the applied loads properly already in Section 1.2 and will comment further on it in Section 4.3.4.

Assume that the finite element solution is \mathbf{u}_h : this solution lies of course in the finite element space given by the displacement interpolation functions (h denoting here the size of the generic element and hence denoting a specific mesh). Then we define “convergence” to mean that

$a(\mathbf{u} - \mathbf{u}_h, \mathbf{u} - \mathbf{u}_h) \rightarrow 0 \quad \text{as } h \rightarrow 0$	(4.64)
--	--------

or, equivalently [see (4.90)], that

$$a(\mathbf{u}_h, \mathbf{u}_h) \rightarrow a(\mathbf{u}, \mathbf{u}) \quad \text{as } h \rightarrow 0$$

Physically, this statement means that the strain energy calculated by the finite element solution converges to the exact strain energy of the mathematical model as the finite element mesh is refined. Let us consider a simple example to show what we mean by the bilinear form $a(\cdot, \cdot)$.

⁹The bilinearity of $a(\cdot, \cdot)$ refers to the fact that for any constants γ_1 and γ_2 ,

$$a(\gamma_1 \mathbf{u}_1 + \gamma_2 \mathbf{u}_2, \mathbf{v}) = \gamma_1 a(\mathbf{u}_1, \mathbf{v}) + \gamma_2 a(\mathbf{u}_2, \mathbf{v})$$

$$a(\mathbf{u}, \gamma_1 \mathbf{v}_1 + \gamma_2 \mathbf{v}_2) = \gamma_1 a(\mathbf{u}, \mathbf{v}_1) + \gamma_2 a(\mathbf{u}, \mathbf{v}_2)$$

and the linearity of (\mathbf{f}, \cdot) refers to the fact that for any constants γ_1 and γ_2 ,

$$(\mathbf{f}, \gamma_1 \mathbf{v}_1 + \gamma_2 \mathbf{v}_2) = \gamma_1 (\mathbf{f}, \mathbf{v}_1) + \gamma_2 (\mathbf{f}, \mathbf{v}_2).$$

EXAMPLE 4.22: Assume that a simply supported prestressed membrane, with (constant) prestress tension T , subjected to transverse loading p is to be analyzed (see Fig. E4.22). Establish for this problem the form (4.63) of the principle of virtual work.

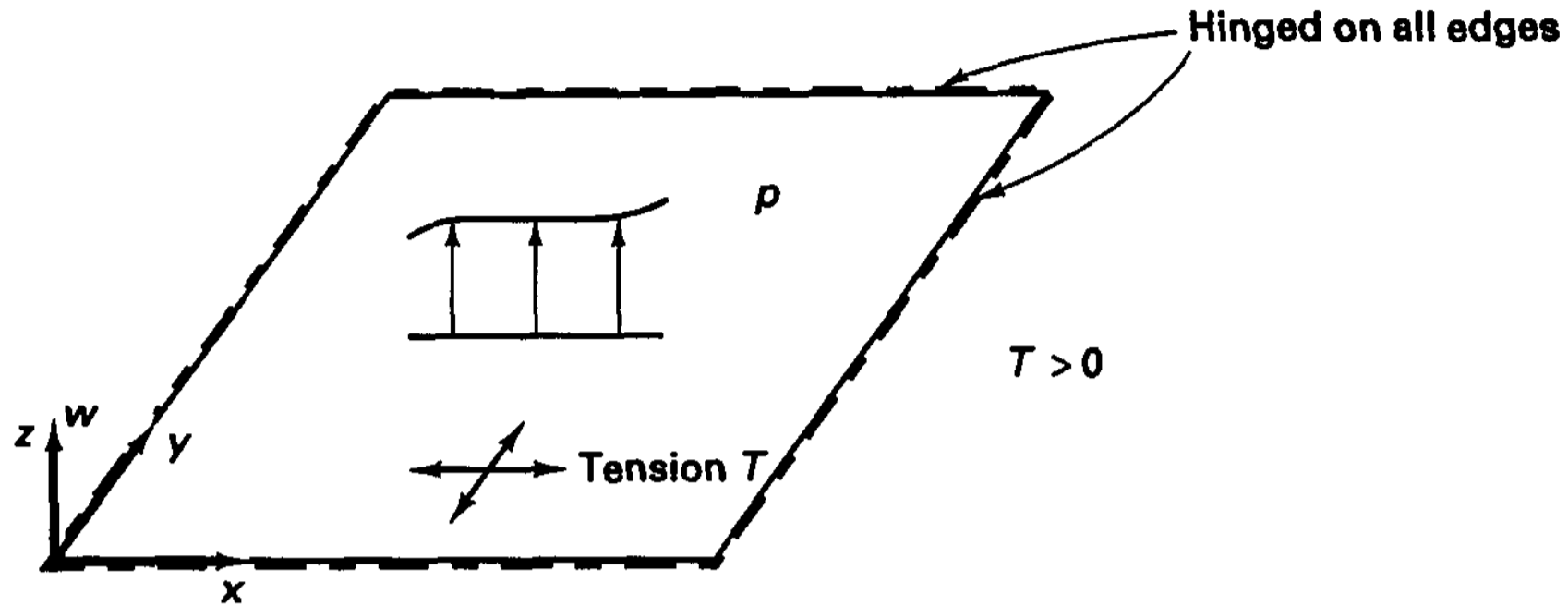


Figure E4.22 Prestressed membrane

The principle of virtual work gives for this problem

$$\int_A \begin{bmatrix} \frac{\partial \bar{w}}{\partial x} \\ \frac{\partial \bar{w}}{\partial y} \end{bmatrix}^T T \begin{bmatrix} \frac{\partial w}{\partial x} \\ \frac{\partial w}{\partial y} \end{bmatrix} dx dy = \int_A p \bar{w} dx dy$$

where $w(x, y)$ is the transverse displacement. The left-hand side of this equation gives the bilinear form $a(v, u)$, with $v = \bar{w}$, $u = w$, and the integration on the right-hand side gives (f, v) .

Depending on the specific (properly formulated) displacement-based finite elements used in the analysis of the model problem defined above, we may converge monotonically or nonmonotonically to the exact solution as the number of finite elements is increased. In the following discussion we consider the criteria for the monotonic convergence of solutions. Finite element analysis conditions that lead to nonmonotonic convergence are discussed in Section 4.4.

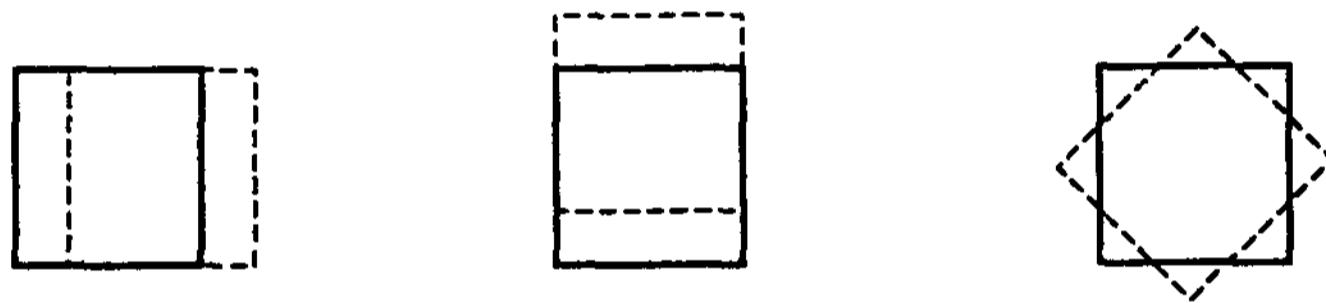
4.3.2 Criteria for Monotonic Convergence

For monotonic convergence, the elements must be complete and the elements and mesh must be compatible. If these conditions are fulfilled, the accuracy of the solution results will increase continuously as we continue to refine the finite element mesh. This mesh refinement should be performed by subdividing a previously used element into two or more elements; thus, the old mesh will be “embedded” in the new mesh. This means mathematically that the new space of finite element interpolation functions will contain the previously used space, and as the mesh is refined, the dimension of the finite element solution space will be continuously increased to contain ultimately the exact solution.

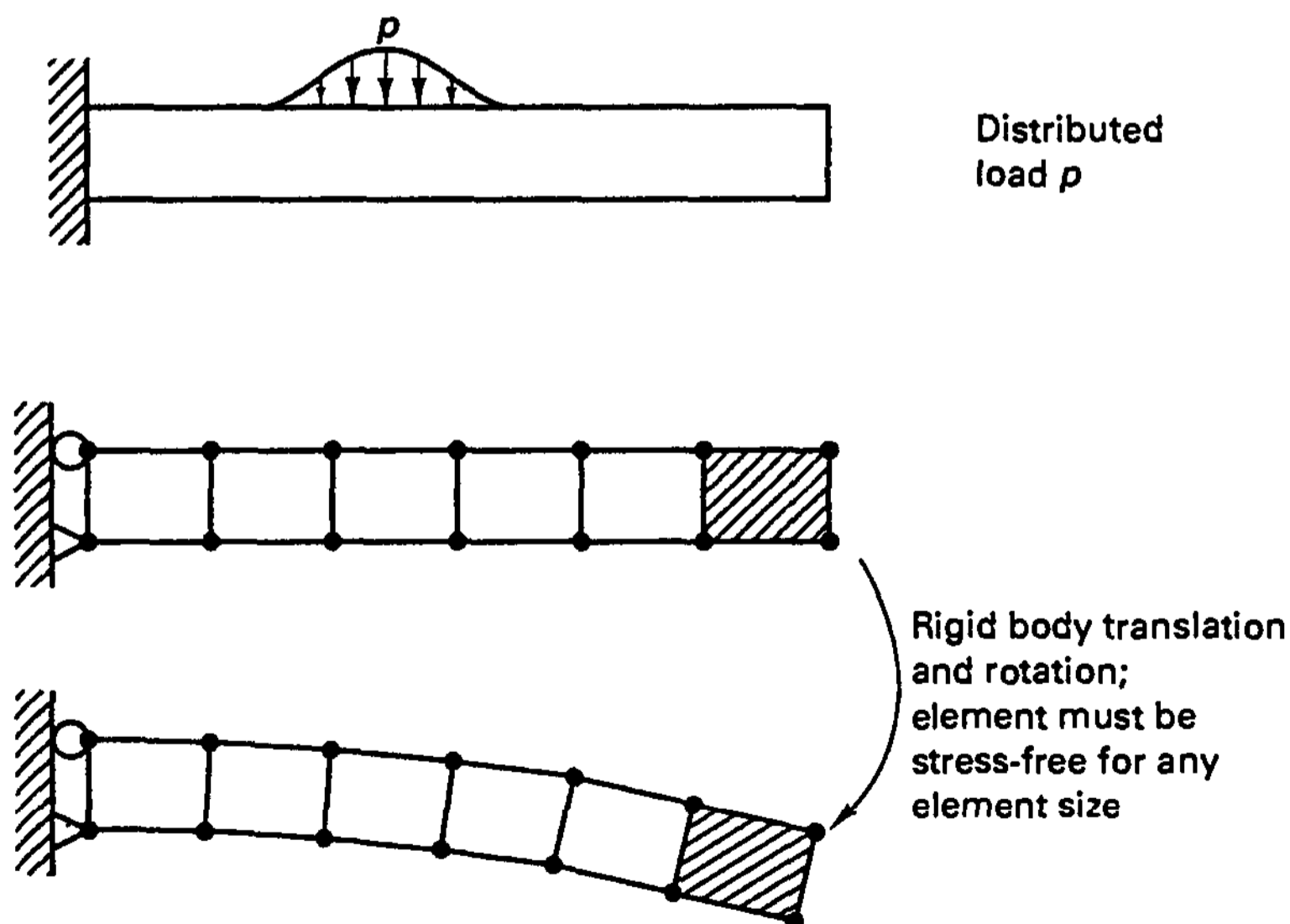
The requirement of completeness of an element means that the displacement functions of the element must be able to represent *the rigid body displacements* and the *constant strain states*.

The rigid body displacements are those displacement modes that the element must be able to undergo as a rigid body without stresses being developed in it. As an example, a two-dimensional plane stress element must be able to translate uniformly in either direction of its plane and to rotate without straining. The reason that the element must be able to undergo these displacements without developing stresses is illustrated in the analysis of the cantilever shown in Fig. 4.9: the element at the tip of the beam—for any element size—must translate and rotate stress-free because by simple statics the cantilever is not subjected to stresses beyond the point of load application.

The number of rigid body modes that an element must be able to undergo can usually be identified without difficulty by inspection, but it is instructive to note that the number of element rigid body modes is equal to the number of element degrees of freedom minus the number of element straining modes (or natural modes). As an example, a two-noded truss has one straining mode (constant strain state), and thus one, three, and five rigid body modes in one-, two-, and three-dimensional conditions, respectively. For more complex finite



(a) Rigid body modes of a plane stress element



(b) Analysis to illustrate the rigid body mode condition

Figure 4.9 Use of plane stress element in analysis of cantilever

elements the individual straining modes and rigid body modes are displayed effectively by representing the stiffness matrix in the basis of eigenvectors. Thus, solving the eigenproblem

$$\mathbf{K}\boldsymbol{\phi} = \lambda\boldsymbol{\phi} \quad (4.65)$$

we have (see Section 2.5)

$$\mathbf{K}\boldsymbol{\Phi} = \boldsymbol{\Phi}\boldsymbol{\Lambda} \quad (4.66)$$

where $\boldsymbol{\Phi}$ is a matrix storing the eigenvectors $\boldsymbol{\phi}_1, \dots, \boldsymbol{\phi}_n$ and $\boldsymbol{\Lambda}$ is a diagonal matrix storing the corresponding eigenvalues, $\boldsymbol{\Lambda} = \text{diag}(\lambda_i)$. Using the eigenvector orthonormality property we thus have

$$\boldsymbol{\Phi}^T \mathbf{K} \boldsymbol{\Phi} = \boldsymbol{\Lambda} \quad (4.67)$$

We may look at $\boldsymbol{\Lambda}$ as being the stiffness matrix of the element corresponding to the eigenvector displacement modes. The stiffness coefficients $\lambda_1, \dots, \lambda_n$ display directly how stiff the element is in the corresponding displacement mode. Thus, the transformation in (4.67) shows clearly whether the rigid body modes and what additional straining modes are present.¹⁰ As an example, the eight eigenvectors and corresponding eigenvalues of a four-node element are shown in Fig. 4.10.

The necessity for the constant strain states can be physically understood if we imagine that more and more elements are used in the assemblage to represent the structure. Then in the limit as each element approaches a very small size, the strain in each element approaches a constant value, and any complex variation of strain within the structure can be approximated. As an example, the plane stress element used in Fig. 4.9 must be able to represent two constant normal stress conditions and one constant shearing stress condition. Figure 4.10 shows that the element can represent these constant stress conditions and, in addition, contains two flexural straining modes.

The rigid body modes and constant strain states that an element can represent can also be directly identified by studying the element strain-displacement matrix (see Example 4.23).

The requirement of compatibility means that the displacements within the elements and across the element boundaries must be continuous. Physically, compatibility ensures that no gaps occur between elements when the assemblage is loaded. When only translational degrees of freedom are defined at the element nodes, only continuity in the displacements u , v , or w , whichever are applicable, must be preserved. However, when rotational degrees of freedom are also defined that are obtained by differentiation of the transverse displacement (such as in the formulation of the plate bending element in Example 4.18), it is also necessary to satisfy element continuity in the corresponding first displacement derivatives. This is a consequence of the kinematic assumption on the displacements over the depth of the plate bending element; that is, the continuity in the displacement w and the derivatives $\partial w/\partial x$ and/or $\partial w/\partial y$ along the respective element edges ensures continuity of displacements over the thickness of adjoining elements.

Compatibility is automatically ensured between truss and beam elements because they join only at the nodal points, and compatibility is relatively easy to maintain in

¹⁰Note also that since the finite element analysis overestimates the stiffness, as discussed in Section 4.3.4, the "smaller" the eigenvalues, the more effective the element.

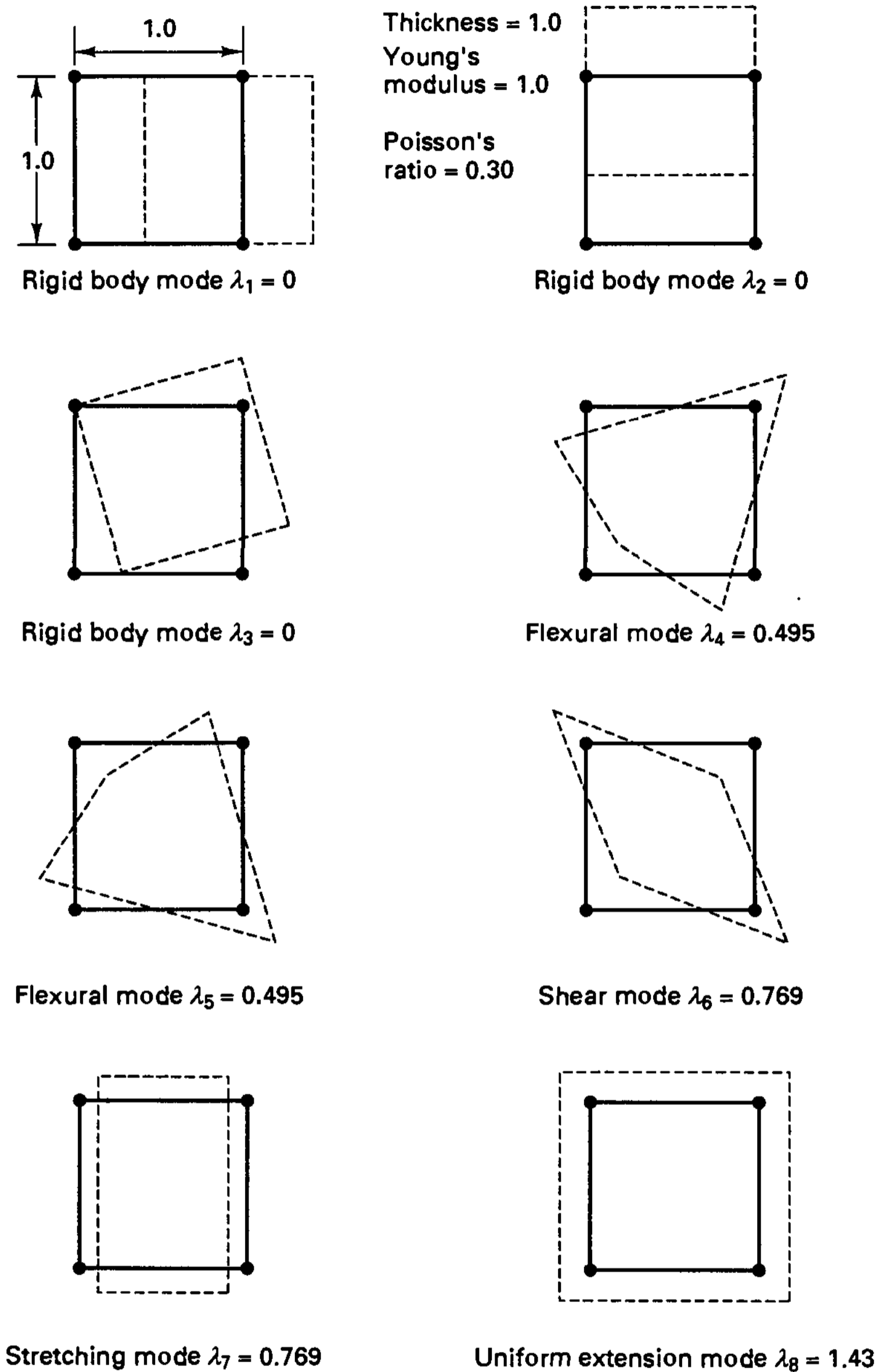


Figure 4.10 Eigenvectors and eigenvalues of four-node plane stress element

two-dimensional plane strain, plane stress, and axisymmetric analysis and in three-dimensional analysis, when only u , v , and w degrees of freedom are used as nodal point variables. However, the requirements of compatibility are difficult to satisfy in plate bending analysis, and particularly in thin shell analysis if the rotations are derived from the transverse displacements. For this reason, much emphasis has been directed toward the development of plate and shell elements, in which the displacements and rotations are

variables (see Section 5.4). With such elements the compatibility requirements are just as easy to fulfill as in the case of dealing only with translational degrees of freedom.

Whether a specific element is complete and compatible depends on the formulation used, and each formulation need be analyzed individually. Consider the following simple example.

EXAMPLE 4.23: Investigate if the plane stress element used in Example 4.6 is compatible and complete.

We have for the displacements of the element,

$$u(x, y) = \alpha_1 + \alpha_2x + \alpha_3y + \alpha_4xy$$

$$v(x, y) = \beta_1 + \beta_2x + \beta_3y + \beta_4xy$$

Observing that the displacements within an element are continuous, in order to show that the element is compatible, we need only investigate if interelement continuity is also preserved when an element assemblage is loaded. Consider two elements interconnected at two node points (Fig. E4.23) on which we impose two arbitrary displacements. It follows from the displacement assumptions that the points (i.e., the material particles) on the adjoining element edges displace linearly, and therefore continuity between the elements is preserved. Hence the element is compatible.

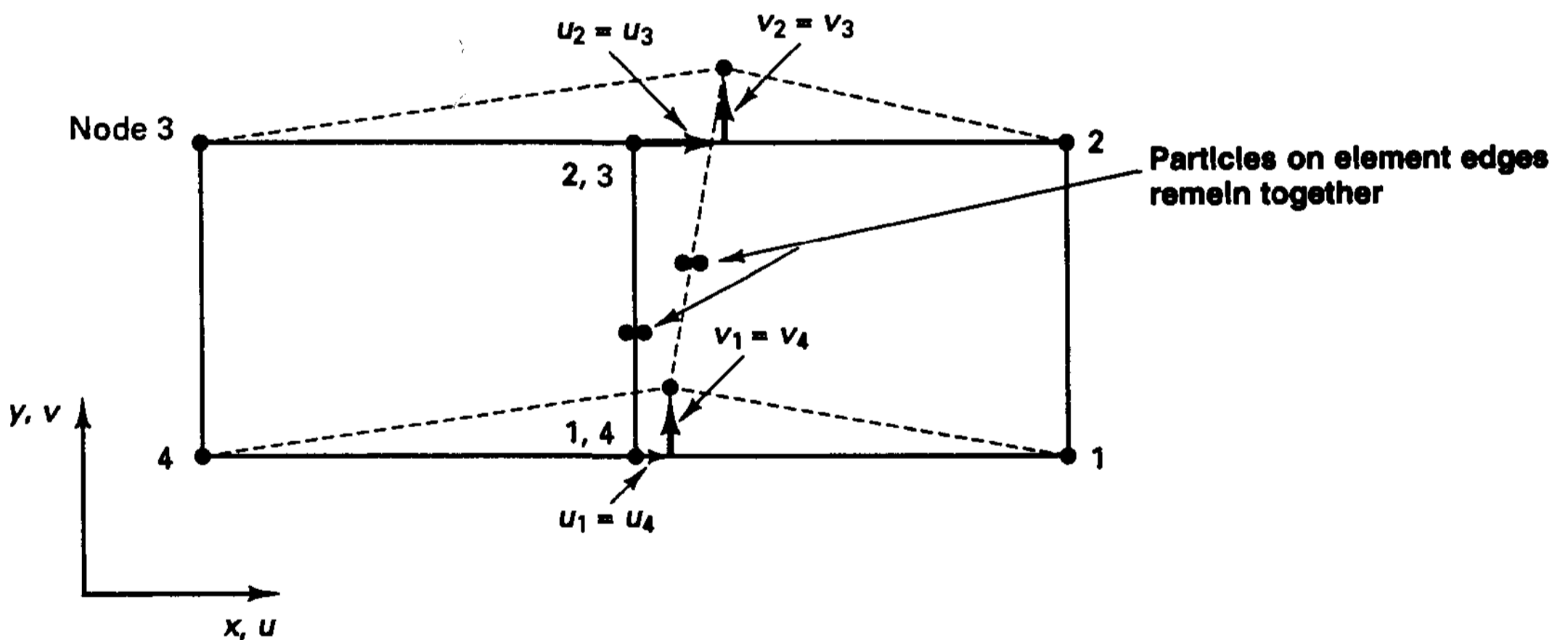


Figure E4.23 Compatibility of plane stress element

Considering completeness, the displacement functions show that a rigid body translation in the x direction is achieved if only α_1 is nonzero. Similarly, a rigid body displacement in the y direction is imposed by having only β_1 nonzero, and for a rigid body rotation α_3 and β_2 must be nonzero only with $\beta_2 = -\alpha_3$. The same conclusion can also be arrived at using the matrix E that relates the strains to the generalized coordinates (see Example 4.6). This matrix also shows that the constant strain states are possible. Therefore the element is complete.

4.3.3 The Monotonically Convergent Finite Element Solution: A Ritz Solution

We observed earlier that the application of the principle of virtual work is identical to using the stationarity condition of the total potential of the system (see Example 4.4). Considering also the discussion of the Ritz method in Section 3.3.3, we can conclude that monotonically convergent displacement-based finite element solutions are really only applications of this method. In the finite element analysis the Ritz functions are contained in the element displacement interpolation matrices $\mathbf{H}^{(m)}$, $m = 1, 2, \dots$, and the Ritz parameters are the unknown nodal point displacements stored in \mathbf{U} . As we discuss further below, the mathematical conditions on the displacement interpolation functions in the matrices $\mathbf{H}^{(m)}$, in order that the finite element solution be a Ritz analysis, are exactly those that we identified earlier using physical reasoning. The correspondence between the analysis methods is illustrated in Examples 3.22 and 4.5.

Considering the Ritz method of analysis with the finite element interpolations, we have

$$\Pi = \frac{1}{2} \mathbf{U}^T \mathbf{K} \mathbf{U} - \mathbf{U}^T \mathbf{R} \quad (4.68)$$

where Π is the total potential of the system. Invoking the stationarity of Π with respect to the Ritz parameters U_i stored in \mathbf{U} and recognizing that the matrix \mathbf{K} is symmetric, we obtain

$$\mathbf{K} \mathbf{U} = \mathbf{R} \quad (4.69)$$

The solution of (4.69) yields the Ritz parameters, and then the displacement solution in the domain considered is

$$\mathbf{u}^{(m)} = \mathbf{H}^{(m)} \mathbf{U}; \quad m = 1, 2, \dots \quad (4.70)$$

The relations in (4.68) to (4.70) represent a Ritz analysis provided the functions used satisfy certain conditions. We defined in Section 3.3.2 a C^{m-1} variational problem as one in which the variational indicator of the problem contains derivatives of order m and lower. We then noted that for convergence the Ritz functions must satisfy the essential (or geometric) boundary conditions of the problem involving derivatives up to order $(m - 1)$, but that the functions do not need to satisfy the natural (or force) boundary conditions involving derivatives of order m to $(2m - 1)$ because these conditions are implicitly contained in the variational indicator Π . Therefore, in order for a finite element solution to be a Ritz analysis, the essential boundary conditions must be completely satisfied by the finite element nodal point displacements and the displacement interpolations between the nodal points. However, in selecting the finite element displacement functions, no special attention need be given to the natural boundary conditions because these conditions are imposed with the load vector and are satisfied approximately in the Ritz solution. The accuracy with which the natural or force boundary conditions are satisfied depends on the specific Ritz functions employed, but this accuracy can always be increased by using a larger number of functions, i.e., a larger number of finite elements to model the problem.

In the classical Ritz analysis the Ritz functions extend over the complete domain considered, whereas in the finite element analysis the individual Ritz functions extend only over subdomains (finite elements) of the complete region. Hence, there must be a question as to what conditions must be fulfilled by the finite element interpolations with regard to

continuity requirements *between* adjacent subdomains. To answer this question we consider the integrations that must be performed to evaluate the coefficient matrix \mathbf{K} . We recognize that in considering a C^{m-1} problem we need continuity in at least the $(m - 1)$ st derivatives of the Ritz trial functions in order that we can perform the integrations across the element boundaries. However, this continuity requirement corresponds entirely to the element compatibility conditions that we discussed in Section 4.3.2. For example, in the analysis of fully three-dimensional problems only the displacements between elements must be continuous, whereas in the analysis of plate problems formulated using the Kirchhoff plate theory we also need continuity in the first derivatives of the displacement functions.

In summary, therefore, for a C^{m-1} problem [$C^{m-1} \equiv$ continuity on trial functions and their derivatives up to order $(m - 1)$], in the classical Ritz analysis the trial functions are selected to satisfy exactly all boundary conditions that involve derivatives up to order $(m - 1)$. The same holds in finite element analysis, but in addition, continuity in the trial functions and their derivatives up to order $(m - 1)$ must be satisfied between elements in order for the finite element solution to correspond to a Ritz analysis.

Although the classical Ritz analysis procedure and the displacement-based finite element method are theoretically identical, in practice, the finite element method has important advantages over a conventional Ritz analysis. One disadvantage of the conventional Ritz analysis is that the Ritz functions are defined over the whole region considered. For example, in the analysis of the cantilever in Example 3.24, the Ritz functions spanned from $x = 0$ to $x = L$. Therefore, in the conventional Ritz analysis, the matrix \mathbf{K} is a full matrix, and as pointed out in Section 8.2.3, the numerical operations required for solution of the resulting algebraic equations are considerable if many functions are used.

A particular difficulty in a conventional Ritz analysis is the selection of appropriate Ritz functions since the solution is a linear combination of these functions. In order to solve accurately for large displacement or stress gradients, many functions may be needed. However, these functions also unnecessarily extend over the regions in which the displacements and stresses vary rather slowly and where not many functions are needed.

Another difficulty arises in the conventional Ritz analysis when the total region of interest is made up of subregions with different kinds of strain distributions. As an example, consider a plate that is supported by edge beams and columns. In such a case, the Ritz functions used for one region (e.g., the plate) are not appropriate for the other regions (i.e., the edge beams and columns), and special displacement continuity conditions or boundary relations must be introduced.

The few reasons given already show that the conventional Ritz analysis is, in general, not particularly computer-oriented, except in some cases for the development of special-purpose programs. On the other hand, the finite element method has to a large extent removed the practical difficulties while retaining the advantageous properties of the conventional Ritz method. With regard to the difficulties mentioned above, the selection of Ritz functions is handled by using an adequate element library in the computer program. The use of relatively many functions in regions of high stress and displacement gradients is possible simply by using many elements, and the combination of domains with different kinds of strain distributions is possible by using different kinds of elements to idealize the domains. It is this generality of the finite element method, and the good mathematical foundation, that have made the finite element method the very widely used analysis tool in today's engineering environments.

4.3.4 Properties of the Finite Element Solution

Let us consider the general linear elasticity problem and its finite element solution and identify certain properties that are useful for an understanding of the finite element method. We shall use the notation summarized in Table 4.5.

The elasticity problem can be written as follows (see, for example, G. Strang and G. F. Fix [A], P. G. Ciarlet [A], or F. Brezzi and M. Fortin [A]).

$$\boxed{\begin{array}{l} \text{Find } \mathbf{u} \in V \text{ such that} \\ a(\mathbf{u}, \mathbf{v}) = (\mathbf{f}, \mathbf{v}) \quad \forall \mathbf{v} \in V \end{array}} \quad (4.71)$$

where the space V is defined as

$$\boxed{V = \left\{ \mathbf{v} \mid \mathbf{v} \in L^2(\text{Vol}); \frac{\partial v_i}{\partial x_j} \in L^2(\text{Vol}), i, j = 1, 2, 3; v_i|_{S_u} = 0, i = 1, 2, 3 \right\}} \quad (4.72)$$

Here $L^2(\text{Vol})$ is the space of square integrable functions in the volume, "Vol", of the body being considered,

$$\boxed{L^2(\text{Vol}) = \left\{ \mathbf{w} \mid \mathbf{w} \text{ is defined in Vol and } \int_{\text{Vol}} \left(\sum_{i=1}^3 (w_i)^2 \right) d\text{Vol} = \|\mathbf{w}\|_{L^2(\text{Vol})}^2 < +\infty \right\}} \quad (4.73)$$

TABLE 4.5 Notation used in discussion of the properties and convergence of finite element solutions

Symbol	Meaning
$a(., .)$	Bilinear form corresponding to model problem being considered (see Example 4.22)
\mathbf{f}	Load vector
\mathbf{u}	Exact displacement solution to mathematical model; an element of the space V
\mathbf{v}	Displacements; an element of the space V
\mathbf{u}_h	Finite element solution, an element of the space V_h
\mathbf{v}_h	Finite element displacements; an element of the space V_h
\forall	For all
\in	An element of
V, V_h	Spaces of functions [see (4.72) and (4.84)]
Vol	Volume of body considered
L^2	Space of a square integrable functions [see (4.73)]
\mathbf{e}_h	Error between exact and finite element solution, $\mathbf{e}_h = \mathbf{u} - \mathbf{u}_h$
\exists	There exists
\subset	Contained in
$\not\subset$	Contained in but not equal to
$\ \cdot\ _E$	Energy norm [see (4.74)]
inf	We take the infimum.
sup	We take the supremum.

Hence, (4.72) defines a space of functions corresponding to a general three-dimensional analysis. The functions in the space vanish on the boundary S_u , and the squares of the functions and of their first derivatives are integrable. Corresponding to V , we use the energy norm

$$\| \mathbf{v} \|_E^2 = a(\mathbf{v}, \mathbf{v}) \tag{4.74}$$

which actually corresponds to twice the strain energy stored in the body when the body is subjected to the displacement field \mathbf{v} .

We assume in our discussion that the structure considered in (4.71) is properly supported, corresponding to the zero displacement conditions on S_u , so that $\| \mathbf{v} \|_E^2$ is greater than zero for any \mathbf{v} different from zero.

In addition, we shall also use the Sobolev norms of order $m = 0$ and $m = 1$ defined as

$m = 0$:

$$\boxed{(\| \mathbf{v} \|_0)^2 = \int_{\text{Vol}} \left(\sum_{i=1}^3 (v_i)^2 \right) d\text{Vol}} \tag{4.75}$$

$m = 1$:

$$\boxed{(\| \mathbf{v} \|_1)^2 = (\| \mathbf{v} \|_0)^2 + \int_{\text{Vol}} \left[\sum_{i=1, j=1}^3 \left(\frac{\partial v_i}{\partial x_j} \right)^2 \right] d\text{Vol}} \tag{4.76}$$

For our elasticity problem the norm of order 1 is used,¹¹ and we have the following two important properties for our bilinear form a .

Continuity:

$$\boxed{\exists M > 0 \text{ such that } \forall \mathbf{v}_1, \mathbf{v}_2 \in V, \quad |a(\mathbf{v}_1, \mathbf{v}_2)| \leq M \| \mathbf{v}_1 \|_1 \| \mathbf{v}_2 \|_1} \tag{4.77}$$

Ellipticity:

$$\boxed{\exists \alpha > 0 \text{ such that } \forall \mathbf{v} \in V, \quad a(\mathbf{v}, \mathbf{v}) \geq \alpha \| \mathbf{v} \|_1^2} \tag{4.78}$$

where the constants α and M depend on the actual elasticity problem being considered, including the material constants used, but are independent of \mathbf{v} .

¹¹ In our discussion, we shall also use the Poincaré-Friedrichs inequality, namely, that for the analysis problems we consider, for any \mathbf{v} we have

$$\int_{\text{Vol}} \left(\sum_{i=1}^3 (v_i)^2 \right) d\text{Vol} \leq c \int_{\text{Vol}} \left(\sum_{i, j=1}^3 \left(\frac{\partial v_i}{\partial x_j} \right)^2 \right) d\text{Vol}$$

where c is a constant (see, for example, P. G. Ciarlet [A]).

The continuity property is satisfied because reasonable norms are used in (4.77), and the ellipticity property is satisfied because a properly supported (i.e., stable) structure is being considered (see P. G. Ciarlet [A] for a mathematical proof). Based on these properties we have

$$c_1 \| \mathbf{v} \|_1 \leq (a(\mathbf{v}, \mathbf{v}))^{1/2} \leq c_2 \| \mathbf{v} \|_1 \quad (4.79)$$

where c_1 and c_2 are constants independent of \mathbf{v} , and we therefore have that the energy norm is equivalent to the 1-norm (see Section 2.7). In mathematical analysis the Sobolev norms are commonly used to measure rates of convergence (see Section 4.3.5), but in practice the energy norm is frequently more easily evaluated [see (4.97)]. Because of (4.79), we can say that convergence can also be defined, instead of using (4.64), as

$$\| \mathbf{u} - \mathbf{u}_h \|_1 \rightarrow 0 \quad \text{as } h \rightarrow 0$$

and the energy norm in problem solutions will converge with the same order as the 1-norm. We examine the continuity and ellipticity of a bilinear form a in the following example.

EXAMPLE 4.24: Consider the problem in Example 4.22. Show that the bilinear form a satisfies the continuity and ellipticity conditions.

Continuity follows because¹²

$$\begin{aligned} a(w_1, w_2) &= \int_A T \left(\frac{\partial w_1}{\partial x} \frac{\partial w_2}{\partial x} + \frac{\partial w_1}{\partial y} \frac{\partial w_2}{\partial y} \right) dx dy \\ &\leq \int_A T \left[\left(\frac{\partial w_1}{\partial x} \right)^2 + \left(\frac{\partial w_1}{\partial y} \right)^2 \right]^{1/2} \left[\left(\frac{\partial w_2}{\partial x} \right)^2 + \left(\frac{\partial w_2}{\partial y} \right)^2 \right]^{1/2} dx dy \\ &\leq \left\{ \int_A T \left[\left(\frac{\partial w_1}{\partial x} \right)^2 + \left(\frac{\partial w_1}{\partial y} \right)^2 \right] dx dy \right\}^{1/2} \\ &\quad \times \left\{ \int_A T \left[\left(\frac{\partial w_2}{\partial x} \right)^2 + \left(\frac{\partial w_2}{\partial y} \right)^2 \right] dx dy \right\}^{1/2} \leq c \|w_1\|_1 \|w_2\|_1 \end{aligned}$$

Ellipticity requires that

$$\begin{aligned} a(w, w) &= \int_A T \left[\left(\frac{\partial w}{\partial x} \right)^2 + \left(\frac{\partial w}{\partial y} \right)^2 \right] dx dy \\ &\geq \alpha \int_A \left[w^2 + \left(\frac{\partial w}{\partial x} \right)^2 + \left(\frac{\partial w}{\partial y} \right)^2 \right] dx dy = \alpha \|w\|_1^2 \end{aligned} \quad (a)$$

However, the Poincaré-Friedrichs inequality,

$$\int_A w^2 dx dy \leq c \int_A \left[\left(\frac{\partial w}{\partial x} \right)^2 + \left(\frac{\partial w}{\partial y} \right)^2 \right] dx dy$$

where c is a constant, ensures that (a) is satisfied.

¹² Here we use the Schwarz inequality, which says that for vectors \mathbf{a} and \mathbf{b} , $|\mathbf{a} \cdot \mathbf{b}| \leq \| \mathbf{a} \|_2 \| \mathbf{b} \|_2$, where $\| \cdot \|_2$ is defined in (2.148).

The above statements on the elasticity problem encompass one important point already mentioned earlier: the exact solution to the problem must correspond to a finite strain energy, see (4.64) and (4.79). Therefore, for example,—strictly—we do not endeavor to solve general two- or three-dimensional elasticity problems with the mathematical idealization of point loads (the solution for a point load on a half space corresponds to infinite strain energy, see for instance S. Timoshenko and J. N. Goodier [A]). Instead, we represent the loads in the elasticity problem closer to how they actually act in nature, namely as smoothly distributed loads, which however can have high magnitudes and act over very small areas. Then the solution of the variational formulation in (4.71) is the same as the solution of the differential formulation. Of course, in our finite element analysis so long as the finite elements are much larger than the area of load application, we can replace the distributed load over the area with an equivalent point load, merely for efficiency of solution; see Section 1.2 and the example in Fig. 1.4.

An important observation is that the exact solution to our elasticity problem is unique. Namely, assume that \mathbf{u}_1 and \mathbf{u}_2 are two different solutions; then we would have

$$a(\mathbf{u}_1, \mathbf{v}) = (\mathbf{f}, \mathbf{v}) \quad \forall \mathbf{v} \in V \tag{4.80}$$

and
$$a(\mathbf{u}_2, \mathbf{v}) = (\mathbf{f}, \mathbf{v}) \quad \forall \mathbf{v} \in V \tag{4.81}$$

Subtracting, we obtain

$$a(\mathbf{u}_1 - \mathbf{u}_2, \mathbf{v}) = 0 \quad \forall \mathbf{v} \in V \tag{4.82}$$

and taking $\mathbf{v} = \mathbf{u}_1 - \mathbf{u}_2$, we have $a(\mathbf{u}_1 - \mathbf{u}_2, \mathbf{u}_1 - \mathbf{u}_2) = 0$. Using (4.79) with $\mathbf{v} = \mathbf{u}_1 - \mathbf{u}_2$, we obtain $\|\mathbf{u}_1 - \mathbf{u}_2\|_1 = 0$, which means $\mathbf{u}_1 \equiv \mathbf{u}_2$, and hence we have proven that our assumption of two different solutions is untenable.

Now let V_h be the space of finite element displacement functions (which correspond to the displacement interpolations contained in all element displacement interpolation matrices $\mathbf{H}^{(m)}$) and let \mathbf{v}_h be any element in that space (i.e., any displacement pattern that can be obtained by the displacement interpolations). Let \mathbf{u}_h be the finite element solution; hence \mathbf{u}_h is also an element in V_h and the specific element that we seek. Then the finite element solution of the problem in (4.71) can be written as

Find $\mathbf{u}_h \in V_h$ such that $a(\mathbf{u}_h, \mathbf{v}_h) = (\mathbf{f}, \mathbf{v}_h) \quad \forall \mathbf{v}_h \in V_h$	(4.83)
--	--------

The space V_h is defined as

$V_h = \left\{ \mathbf{v}_h \mid \mathbf{v}_h \in L^2(\text{Vol}); \frac{\partial (v_h)_i}{\partial x_j} \in L^2(\text{Vol}), i, j = 1, 2, 3; (v_h)_i _{S_u} = 0, i = 1, 2, 3 \right\}$	(4.84)
---	--------

and for the elements of this space we use the energy norm (4.74) and the Sobolev norm (4.76). Of course, $V_h \subset V$.

The relation in (4.83) is the principle of virtual work for the finite element discretization corresponding to V_h . With this solution space, the continuity and ellipticity conditions (4.77) and (4.78) are satisfied, using $\mathbf{v}_h \in V_h$, and a positive definite stiffness matrix is obtained for any V_h .

We should note that V_h corresponds to a given mesh, where h denotes the generic element size, and that in the discussion of convergence we of course consider a sequence of spaces V_h (a sequence of meshes with decreasing h). We illustrate in Figure 4.11 the elements of V_h for the discretization dealt with in Example 4.6.

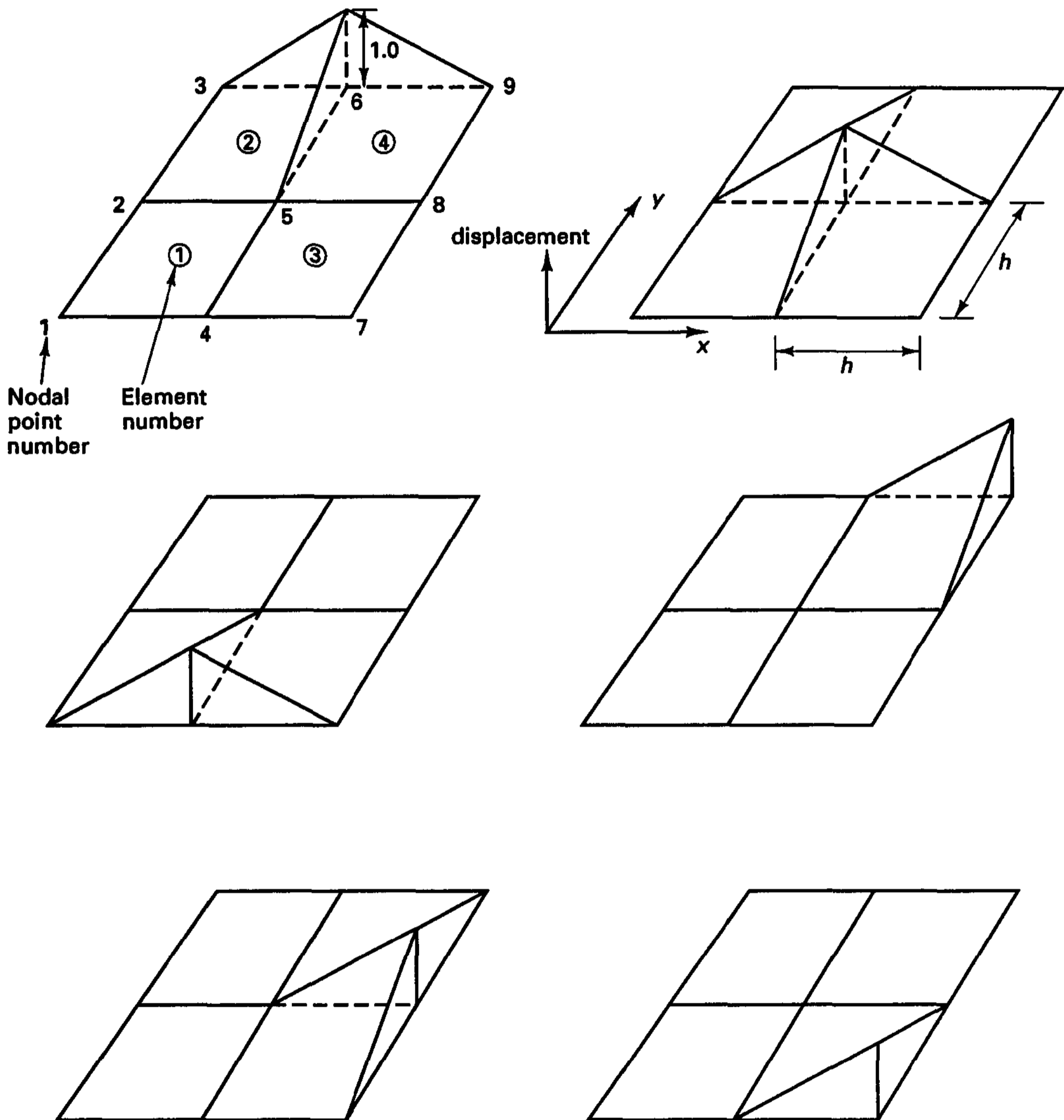


Figure 4.11 Aerial view of basis functions for space V_h used in analysis of cantilever plate of Example 4.6. The displacement functions are plotted upwards for ease of display, but each function shown is applicable to the u and v displacements. An element of V_h is any linear combination of the 12 displacement functions. Note that the functions correspond to the element displacement interpolation matrices $\mathbf{H}^{(m)}$, discussed in Example 4.6, and that the displacements at nodes 1, 2 and 3 are zero.

Considering the finite element solution \mathbf{u}_h and the exact solution \mathbf{u} to the problem, we have the following important properties.

Property 1. Let the error between the exact solution \mathbf{u} and the finite element solution \mathbf{u}_h be \mathbf{e}_h ,

$$\mathbf{e}_h = \mathbf{u} - \mathbf{u}_h \quad (4.85)$$

Then the first property is

$$\boxed{a(\mathbf{e}_h, \mathbf{v}_h) = 0 \quad \forall \mathbf{v}_h \in V_h} \quad (4.86)$$

The proof is obtained by realizing that the principle of virtual work gives

$$a(\mathbf{u}, \mathbf{v}_h) = (\mathbf{f}, \mathbf{v}_h) \quad \forall \mathbf{v}_h \in V_h \quad (4.87)$$

and

$$a(\mathbf{u}_h, \mathbf{v}_h) = (\mathbf{f}, \mathbf{v}_h) \quad \forall \mathbf{v}_h \in V_h \quad (4.88)$$

so that by subtraction we obtain (4.86). We may say that the error is “orthogonal in $a(\cdot, \cdot)$ ” to all \mathbf{v}_h in V_h . Clearly, as the space V_h increases, with the larger space always containing the smaller space, the solution accuracy will increase continuously. The next two properties are based on Property 1.

Property 2. The second property is

$$\boxed{a(\mathbf{u}_h, \mathbf{u}_h) \leq a(\mathbf{u}, \mathbf{u})} \quad (4.89)$$

We prove this property by considering

$$\begin{aligned} a(\mathbf{u}, \mathbf{u}) &= a(\mathbf{u}_h + \mathbf{e}_h, \mathbf{u}_h + \mathbf{e}_h) \\ &= a(\mathbf{u}_h, \mathbf{u}_h) + 2a(\mathbf{u}_h, \mathbf{e}_h) + a(\mathbf{e}_h, \mathbf{e}_h) \\ &= a(\mathbf{u}_h, \mathbf{u}_h) + a(\mathbf{e}_h, \mathbf{e}_h) \end{aligned} \quad (4.90)$$

where we have used (4.86) with $\mathbf{v}_h = \mathbf{u}_h$. The relation (4.89) follows because $a(\mathbf{e}_h, \mathbf{e}_h) > 0$ for any $\mathbf{e}_h \neq \mathbf{0}$ (since for the properly supported structure $\|\mathbf{v}\|_E > 0$ for any nonzero \mathbf{v}).

Hence, the strain energy corresponding to the finite element solution is always smaller than or equal to the strain energy corresponding to the exact solution.

Property 3. The third property is

$$\boxed{a(\mathbf{e}_h, \mathbf{e}_h) \leq a(\mathbf{u} - \mathbf{v}_h, \mathbf{u} - \mathbf{v}_h) \quad \forall \mathbf{v}_h \in V_h} \quad (4.91)$$

For the proof we use that for any \mathbf{w}_h in V_h , we have

$$a(\mathbf{e}_h + \mathbf{w}_h, \mathbf{e}_h + \mathbf{w}_h) = a(\mathbf{e}_h, \mathbf{e}_h) + a(\mathbf{w}_h, \mathbf{w}_h) \quad (4.92)$$

Hence,
$$a(\mathbf{e}_h, \mathbf{e}_h) \leq a(\mathbf{e}_h + \mathbf{w}_h, \mathbf{e}_h + \mathbf{w}_h) \quad (4.93)$$

Choosing $\mathbf{w}_h = \mathbf{u}_h - \mathbf{v}_h$ gives (4.91).

This third property says that the finite element solution \mathbf{u}_h is chosen from all the possible displacement patterns \mathbf{v}_h in V_h such that the strain energy corresponding to $\mathbf{u} - \mathbf{u}_h$ is the minimum. Hence, in that sense, the “energy distance” between \mathbf{u} and the elements in V_h is minimized by the solution \mathbf{u}_h in V_h .

Using (4.91) and the ellipticity and continuity of the bilinear form, we further obtain

$$\begin{aligned} \alpha \|\mathbf{u} - \mathbf{u}_h\|_1^2 &\leq a(\mathbf{u} - \mathbf{u}_h, \mathbf{u} - \mathbf{u}_h) \\ &= \inf_{\mathbf{v}_h \in V_h} a(\mathbf{u} - \mathbf{v}_h, \mathbf{u} - \mathbf{v}_h) \\ &\leq M \inf_{\mathbf{v}_h \in V_h} \|\mathbf{u} - \mathbf{v}_h\|_1 \|\mathbf{u} - \mathbf{v}_h\|_1 \end{aligned} \quad (4.94)$$

where “inf” denotes the infimum (see Table 4.5). If we let $d(\mathbf{u}, V_h) = \lim_{\mathbf{v}_h \in V_h} \|\mathbf{u} - \mathbf{v}_h\|_1$, we recognize that we have the *property*

$$\boxed{\|\mathbf{u} - \mathbf{u}_h\|_1 \leq c d(\mathbf{u}, V_h)} \quad (4.95)$$

where c is a constant, $c = \sqrt{M/\alpha}$, independent of h but dependent on the material properties.¹³ This result is referred to as Cea’s lemma (see, for example, P. G. Ciarlet [A]).

The above three properties give valuable insight into how the finite element solution is chosen from the displacement patterns possible within a given finite element mesh and what we can expect as the mesh is refined.

We note, in particular, that (4.95), which is based on Property 3, states that a sufficient condition for convergence with our sequence of finite element spaces is that for any $\mathbf{u} \in V$ we have $\lim_{h \rightarrow 0} \inf \|\mathbf{u} - \mathbf{v}_h\|_1 = 0$. Also, (4.95) can be used to measure the rate of convergence as the mesh is refined by introducing an upper bound on how $d(\mathbf{u}, V_h)$ changes with the mesh refinement (see Section 4.3.5).

Further, Properties 2 and 3 say that *at* the finite element solution the error in strain energy is minimized within the possible displacement patterns of a given mesh and that the strain energy corresponding to the finite element solution will approach the exact strain energy (from below) as increasingly finer meshes are used (with the displacement patterns of the finer mesh containing the displacement patterns of the previous coarser mesh).

We can also relate these statements to earlier observations that in a finite element solution the stationarity of the total potential is established (see Section 4.3.2). That is, for a *given* mesh and *any* nodal displacements \mathbf{U}_{any} , we have

$$\boxed{\Pi|_{\mathbf{U}_{\text{any}}} = \frac{1}{2} \mathbf{U}_{\text{any}}^T \mathbf{K} \mathbf{U}_{\text{any}} - \mathbf{U}_{\text{any}}^T \mathbf{R}} \quad (4.96)$$

¹³ There is a subtle point in considering the *property* (4.95) and the *condition* (4.156) discussed later; namely, while (4.95) is always valid for any values of bulk and shear moduli, the constant c becomes very large as the bulk modulus increases, and the *property* (4.95) is no longer useful. For this reason, when the bulk modulus κ is very large, we *need* the new *property* (4.156) in which the constant is independent of κ , and this leads to the inf-sup condition.

The finite element solution \mathbf{U} is obtained by invoking the stationarity of Π to obtain

$$\mathbf{KU} = \mathbf{R}$$

At the finite element displacement solution \mathbf{U} we have the total potential Π and strain energy \mathcal{U}

$$\boxed{\Pi = -\frac{1}{2}\mathbf{U}^T\mathbf{R}; \quad \mathcal{U} = \frac{1}{2}\mathbf{U}^T\mathbf{R}} \quad (4.97)$$

Therefore, to evaluate the strain energy corresponding to the finite element solution, we only need to perform a vector multiplication.

To show with this notation that within the given possible finite element displacements (i.e., within the space V_h) Π is minimized at the finite element solution \mathbf{U} , let us calculate Π at $\mathbf{U} + \boldsymbol{\epsilon}$, where $\boldsymbol{\epsilon}$ is any arbitrary vector,

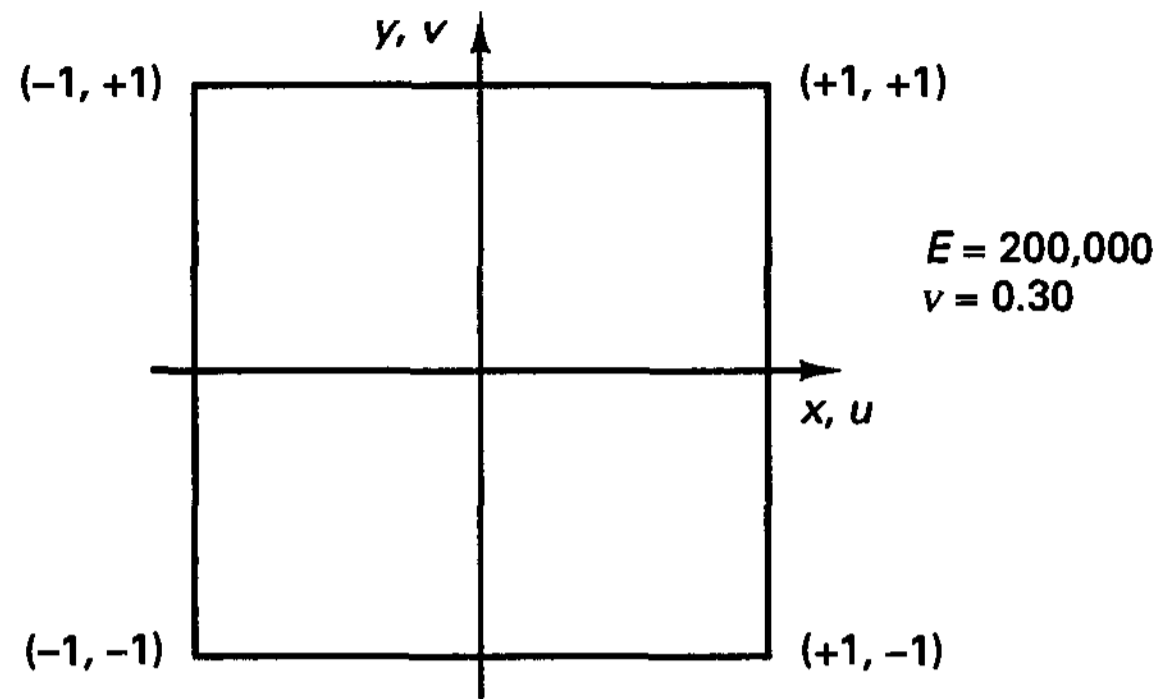
$$\begin{aligned} \Pi|_{\mathbf{U}+\boldsymbol{\epsilon}} &= \frac{1}{2}(\mathbf{U} + \boldsymbol{\epsilon})^T\mathbf{K}(\mathbf{U} + \boldsymbol{\epsilon}) - (\mathbf{U} + \boldsymbol{\epsilon})^T\mathbf{R} \\ &= \Pi|_{\mathbf{U}} + \boldsymbol{\epsilon}^T(\mathbf{KU} - \mathbf{R}) + \frac{1}{2}\boldsymbol{\epsilon}^T\mathbf{K}\boldsymbol{\epsilon} \\ &= \Pi|_{\mathbf{U}} + \frac{1}{2}\boldsymbol{\epsilon}^T\mathbf{K}\boldsymbol{\epsilon} \end{aligned} \quad (4.98)$$

where we used that $\mathbf{KU} = \mathbf{R}$ and the fact that \mathbf{K} is a symmetric matrix. However, since \mathbf{K} is positive definite, $\Pi|_{\mathbf{U}}$ is the minimum of Π for the given finite element mesh. As the mesh is refined, Π will decrease and according to (4.97) \mathcal{U} will correspondingly increase.

Considering (4.89), (4.91), and (4.97), we observe that in the finite element solution the displacements are (on the “whole”) underestimated and hence the stiffness of the mathematical model is (on the “whole”) overestimated. This overestimation of the stiffness is (physically) a result of the “internal displacement constraints” that are implicitly imposed on the solution as a result of the displacement assumptions. As the finite element discretization is refined, these “internal displacement constraints” are reduced, and convergence to the exact solution (and stiffness) of the mathematical model is obtained.

To exemplify the preceding discussion, Figure 4.12 shows the results obtained in the analysis of an ad hoc test problem for two-dimensional finite element discretizations. The problem is constructed so as to have no singularities. As we discuss in the next section, in this case the full (maximum) order of convergence is obtained with a given finite element in a sequence of uniform finite element meshes (in each mesh all elements are of equal square size).

Figure 4.12 shows the convergence in strain energy when a sequence of uniform meshes of nine-node elements is employed for the solutions. The meshes are constructed by starting with a 2×2 mesh of square elements of unit side length (for which $h = 1$), then subdividing each element into four equal square elements (for which $h = \frac{1}{2}$), to obtain the second mesh, and continuing this process. We clearly see that the error in the strain energy decreases with decreasing element size h , as we would expect according to (4.91). We compare the order of convergence seen in the finite element computations with a theoretically established value in the next section.



N elements per side, $N = 2, 4, 8, \dots$

(a) Square domain considered

$$\begin{aligned} u &= c_1 (1 - x^2) (1 - y^2) e^{ky} \cos kx \\ v &= c_1 (1 - x^2) (1 - y^2) e^{ky} \sin kx \\ c_1 &= \text{constant}; k = 5 \end{aligned}$$

(b) Exact in-plane displacements

Obtain the finite element solution for the body loads f_x^B and f_y^B , where

$$\begin{aligned} f_x^B &= - \left(\frac{\partial \tau_{xx}}{\partial x} + \frac{\partial \tau_{xy}}{\partial y} \right) \\ f_y^B &= - \left(\frac{\partial \tau_{yy}}{\partial y} + \frac{\partial \tau_{yx}}{\partial x} \right) \end{aligned}$$

and $\tau_{xx}, \tau_{yy}, \tau_{xy}$ are the stresses corresponding to the exact in-plane displacements given in (b).

(c) Test problem

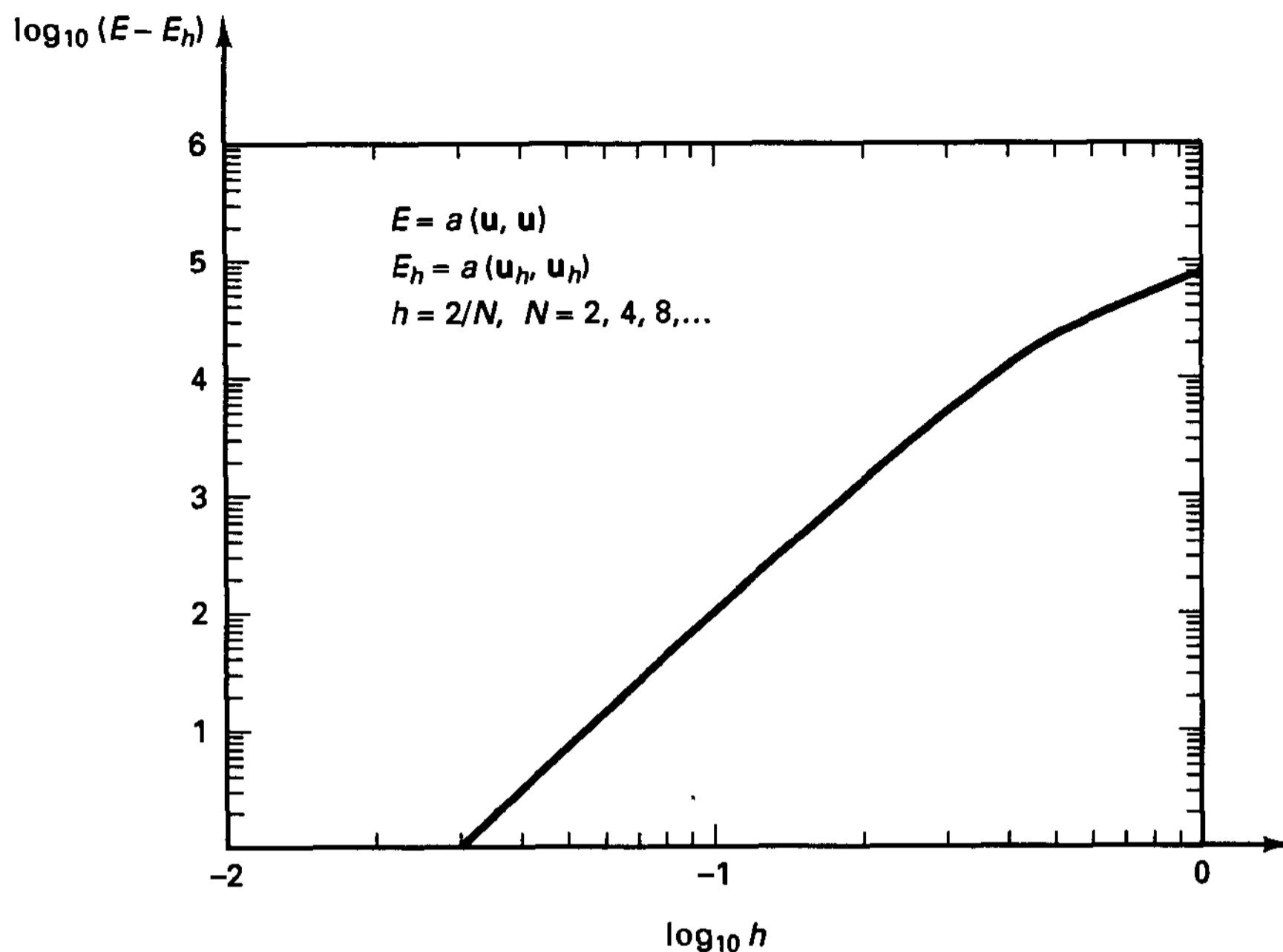
Figure 4.12 Ad-hoc test problem for plane stress (or plane strain, axisymmetric) elements. We use, for h small, $E - E_h = c h^\alpha$ and hence $\log(E - E_h) = \log c + \alpha \log h$ (see also (4.101)). The numerical solutions give $\alpha = 3.91$.

4.3.5 Rate of Convergence

In the previous sections we considered the conditions required for monotonic convergence of the finite element analysis results and discussed how in general convergence is reached, but we did not mention the rate at which convergence occurs.

As must be expected, the rate of convergence depends on the order of the polynomials used in the displacement assumptions. In this context the notion of *complete* polynomials is useful.

Figure 4.13 shows the polynomial terms that should be included to have complete polynomials in x and y for two-dimensional analysis. It is seen that all possible terms of the form $x^\alpha y^\beta$ are present, where $\alpha + \beta = k$ and k is the degree to which the polynomial is complete. For example, we may note that the element investigated in Example 4.6 uses a



(d) Solution for plane stress problem

Figure 4.12 (continued)

polynomial displacement that is complete to degree 1 only. Figure 4.13 also shows important notation for polynomial spaces. The spaces P_k correspond to the complete polynomials up to degree k . They can also be thought of as the basis functions of triangular elements: the functions in P_1 correspond to the functions of the linear displacement (constant strain) triangle (see Example 4.17); the functions in P_2 correspond to the functions of the parabolic displacement (linear strain) triangle (see Section 5.3.2); and so on.

In addition, Fig. 4.13 shows the polynomial spaces Q_k , $k = 1, 2, 3$, which correspond to the 4-node, 9-node, and 16-node elements, referred to as Lagrangian elements because the displacement functions of these elements are Lagrangian functions (see also Section 5.5.1).

In considering three-dimensional analysis of course a figure analogous to Fig. 4.13 could be drawn in which the variable z would be included.

Let us think about a sequence of uniform meshes idealizing the complete volume of the body being considered. A mesh of a sequence of uniform meshes consists of elements of equal size—square elements when the polynomial spaces Q_k are used. Hence, the parameter h can be taken to be a typical length of an element side. The sequence is obtained by taking a starting mesh of elements and subdividing each element with a natural pattern to obtain the next mesh, and then repeating this process. We did this in solving the ad hoc test problem in Fig. 4.12. However, considering an additional analysis problem, for example, the problem in Example 4.6, we would in Fig. 4.11 subdivide each four-node element into four equal new four-node elements to obtain the first refined mesh; then we would

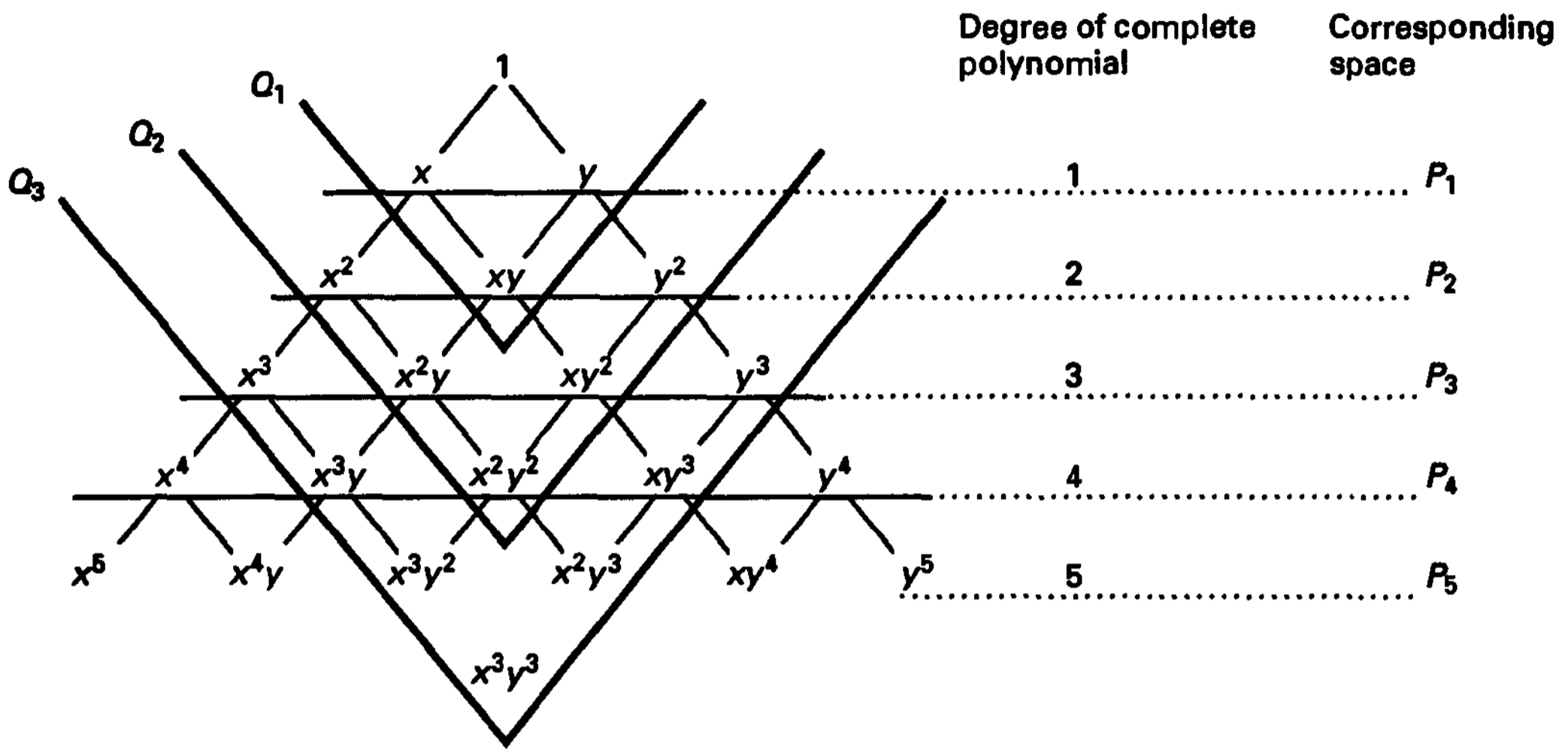


Figure 4.13 Polynomial terms in two-dimensional analysis, Pascal triangle

subdivide each element of the first refined mesh into four equal new four-node elements to obtain the second refined mesh; and so on. The continuation of this subdivision process would give the complete sequence of meshes.

To obtain an expression for the rate of convergence, we would ideally use a formula giving $d(\mathbf{u}, V_h)$ in (4.95) as a function of h . However, such a formula is difficult to obtain, and it is more convenient to use interpolation theory and work with an upper bound on $d(\mathbf{u}, V_h)$.

Let us assume that we employ elements with complete polynomials of degree k and that the exact solution \mathbf{u} to our elasticity problem is “smooth” in the sense that the solution satisfies the relation¹⁴

$$\begin{aligned} \|\mathbf{u}\|_{k+1} = & \left\{ \int_{\text{Vol}} \left[\sum_{i=1}^3 (u_i)^2 + \sum_{i=1}^3 \sum_{j=1}^3 \left(\frac{\partial u_i}{\partial x_j} \right)^2 \right. \right. \\ & \left. \left. + \sum_{n=2}^{k+1} \sum_{i=1}^3 \sum_{r+s+t=n} \left(\frac{\partial^n u_i}{\partial x_1^r \partial x_2^s \partial x_3^t} \right)^2 \right] d\text{Vol} \right\}^{1/2} < \infty \end{aligned} \tag{4.99}$$

where of course $k \geq 1$.

Therefore, we assume that all derivatives of the exact solution up to order $(k + 1)$ in (4.99) can be calculated.

A basic result of interpolation theory is that there exists an interpolation function $\mathbf{u}_I \in V_h$ such that

$$\|\mathbf{u} - \mathbf{u}_I\|_1 \leq \hat{c} h^k \|\mathbf{u}\|_{k+1} \tag{4.100}$$

where h is the mesh size parameter indicating the “size” of the elements and \hat{c} is a constant independent of h . Typically, h is taken to be the length of the side of a generic element or the diameter of a circle encompassing that element. Note that \mathbf{u}_I is not the finite element solution in V_h but merely an element in V_h that geometrically corresponds to a function

¹⁴ We then have \mathbf{u} is an element of the Hilbert space H^{k+1} .

close to \mathbf{u} . Frequently, as here, we let \mathbf{u}_I , at the finite element nodes, take the value of the exact solution \mathbf{u} .

Using (4.100) and Property 3 discussed in Section 4.3.4 [see (4.91)], we can now show that the rate of convergence of the finite element solution \mathbf{u}_h to the exact theory of elasticity solution \mathbf{u} is given by the error estimate

$$\boxed{\|\mathbf{u} - \mathbf{u}_h\|_1 \leq c h^k \|\mathbf{u}\|_{k+1}} \quad (4.101)$$

where c is a constant independent of h but dependent on the material properties. Namely, using (4.95) and (4.100), we have

$$\begin{aligned} \|\mathbf{u} - \mathbf{u}_h\|_1 &\leq c d(\mathbf{u}, V_h) \\ &\leq c \|\mathbf{u} - \mathbf{u}_I\|_1 \\ &\leq c \hat{c} h^k \|\mathbf{u}\|_{k+1} \end{aligned} \quad (4.101a)$$

which gives (4.101) with a new constant c . For (4.101), we say that the *rate of convergence* is given by the complete right-hand-side expression, and we say that the *order of convergence* is k or, equivalently, that we have $o(h^k)$ convergence.

Another way to look at the derivation of (4.101)—which is of course closely related to the previous derivation—is to use (4.79) and (4.91). Then we have

$$\begin{aligned} \|\mathbf{u} - \mathbf{u}_h\|_1 &\leq \frac{1}{c_1} [a(\mathbf{u} - \mathbf{u}_h, \mathbf{u} - \mathbf{u}_h)]^{1/2} \\ &\leq \frac{1}{c_1} [a(\mathbf{u} - \mathbf{u}_I, \mathbf{u} - \mathbf{u}_I)]^{1/2} \\ &\leq \frac{c_2}{c_1} \|\mathbf{u} - \mathbf{u}_I\|_1 \\ &\leq c h^k \|\mathbf{u}\|_{k+1} \end{aligned} \quad (4.101b)$$

Hence, we see directly that to obtain the rate of convergence, we really only expressed the distance $d(\mathbf{u}, V_h)$ in terms of an upper bound given by (4.100).

In practice, we frequently simply write (4.101) as

$$\boxed{\|\mathbf{u} - \mathbf{u}_h\|_1 \leq c h^k} \quad (4.102)$$

and we now recognize that the constant c used here is independent of h but depends on the solution *and* the material properties [because c in (4.101a) and c_2, c_1 in (4.101b) depend on the material properties]. This dependence on the material properties is detrimental when (almost) incompressible material conditions are considered because the constant then becomes very large and the order of convergence k results in good accuracy only at very small (impractical) values of h . For this reason we need in that case the property (4.95) with the constant independent of the material properties, and this requirement leads to the condition (4.156) (see Section 4.5).

The constant c also depends on the kind of element used. While we have assumed that the element is based on a complete polynomial of order k , different kinds of elements within that class in general display a different constant c for the same analysis problem (e.g., triangular and quadrilateral elements). Hence, the actual magnitude of the error may be considerably different for a given h , while the order with which the error decreases as the mesh is refined is the same. Clearly, the magnitude of the constant c can be crucial in practical analysis because it largely determines how small h actually has to be in order to reach an acceptable error.

These derivations of course represent theoretical results, and we may question in how far these results are applicable in practice. Experience shows that the theoretical results indeed closely represent the actual convergence behavior of the finite element discretizations being considered. Indeed, to measure the order of convergence, we may simply consider the equal sign in (4.102) to obtain

$$\log (\|\mathbf{u} - \mathbf{u}_h\|_1) = \log c + k \log h \quad (4.103)$$

Then, if we plot from our computed results the graph of $\log (\|\mathbf{u} - \mathbf{u}_h\|_1)$ versus $\log h$, we find that the resulting curve indeed has the approximate slope k when h is sufficiently small.

Evaluating the Sobolev norm may require considerable effort, and in practice, we may use the equivalence of the energy norm with the 1-norm. Namely, because of (4.79), we see that (4.101) also holds for the energy norm on the left side, and this norm can frequently be evaluated more easily [see (4.97)]. Figure 4.12 shows an application. Note that the error in strain energy can be evaluated simply by subtracting the current strain energy from the strain energy of the limit solution (or, if known, the exact solution) [see (4.90)]. In the solution in Fig. 4.12 we obtained an order of convergence (of the numerical results) of 3.91, which compares very well with the theoretical value of 4 (here $k = 2$ and the strain energy is the energy norm squared). Further results of convergence for this ad hoc problem are given in Fig. 5.39 (where distorted elements with numerically integrated stiffness matrices are considered).

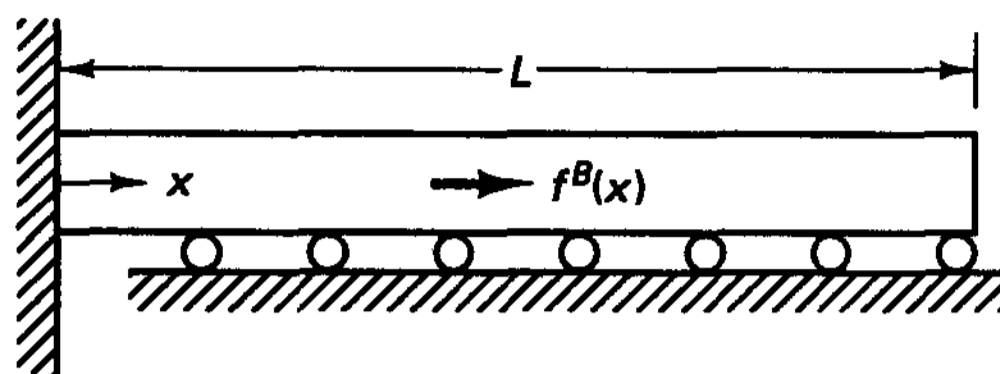
The relation in (4.101) gives, in essence, an error estimate for the displacement gradient, hence for the strains and stresses, because the primary contribution in the 1-norm will be due to the error in the derivatives of the displacements. We will primarily use (4.101) and (4.102) but also note that the error in the displacements is given by

$$\|\mathbf{u} - \mathbf{u}_h\|_0 \leq c h^{k+1} \|\mathbf{u}\|_{k+1} \quad (4.104)$$

Hence, the order of convergence for the displacements is one order higher than for the strains.

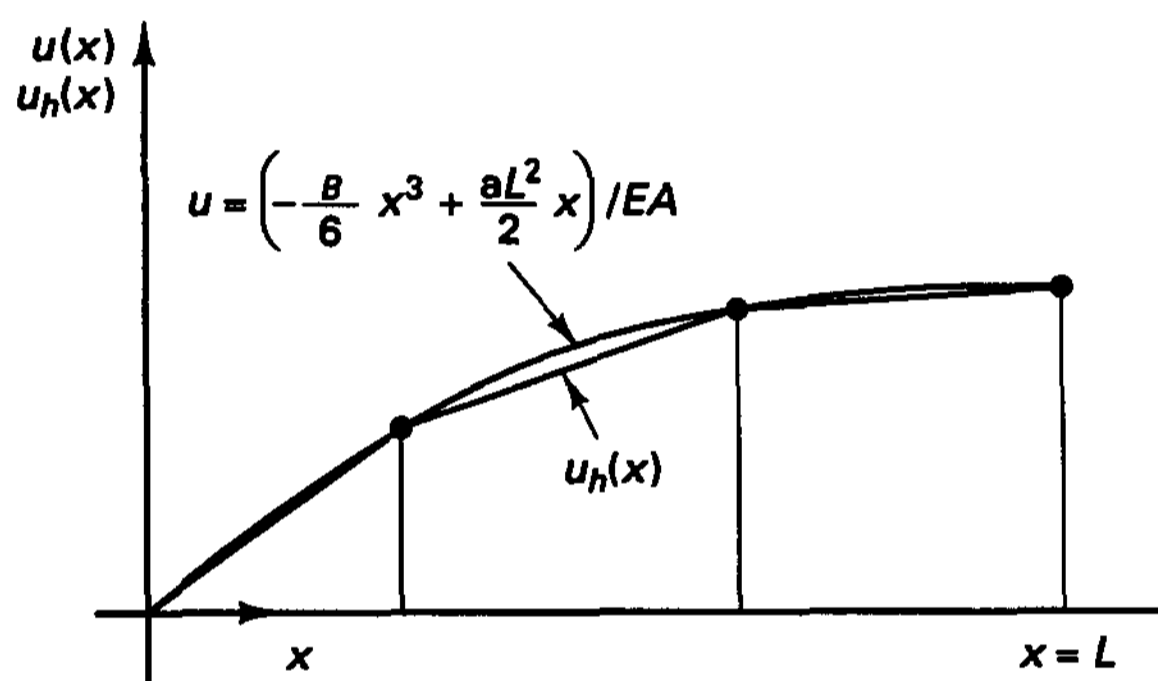
These results are intuitively reasonable. Namely, let us think in terms of a Taylor series analysis. Then, since a finite element of "dimension h " with a complete displacement expansion of order k can represent displacement variations up to that order exactly, the local error in representing arbitrary displacements with a uniform mesh should be $o(h^{k+1})$. Also, for a C^{m-1} problem the stresses are calculated by differentiating the displacements m times, and therefore the error in the stresses is $o(h^{k+1-m})$. For the theory of elasticity problem considered above, $m = 1$, and hence the relations in (4.101) and (4.104) are what we might expect.

EXAMPLE 4.25: Consider the problem shown in Figure E4.25. Estimate the error of the finite element solution if linear two-node finite elements are used.



Constant cross-sectional area A
Young's modulus E

(s) Bar subjected to load per unit length $f^B(x) = ax$



(b) Solutions (for finite element solution three elements are used)

Figure E4.25 Analysis of bar

The finite element problem in this case is to calculate $u_h \in V_h$ such that

$$(EA u'_h, v'_h) = (f^B, v_h) \quad \forall v_h \in V_h$$

with
$$V_h = \left\{ v_h \mid v_h \in L^2(\text{Vol}), \frac{\partial v_h}{\partial x} \in L^2(\text{Vol}), v_h|_{x=0} = 0 \right\}$$

To estimate the error we use (4.91) and can directly say for this simple problem

$$\int_0^L (u' - u'_h)^2 dx \leq \int_0^L (u' - u'_I)^2 dx \tag{a}$$

where u is the exact solution, u_h is the finite element solution, and u_I is the interpolant, meaning that u_I is considered to be equal to u at the nodal points. Hence, our aim is now to obtain an upper bound on $\int_0^L (u' - u'_I)^2 dx$.

Consider an arbitrary element with end points x_i and x_{i+1} in the mesh. Then we can say that for the exact solution $u(x)$ and $x_i \leq x \leq x_{i+1}$,

$$u'(x) = u'|_{x_c} + (x - x_c)u''|_{x=\bar{x}}$$

where $x = x_c$ denotes a chosen point in the element and \bar{x} is also a point in the element. Let us choose an x_c where $u'|_{x_c} = u'_I$, which can always be done because

$$u_I(x_i) = u(x_i), u_I(x_{i+1}) = u(x_{i+1})$$

Then we have for the element

$$|u'(x) - u'_I| \leq h \left(\max_{0 \leq x \leq L} |u''| \right) \quad (b)$$

where we have introduced the largest absolute value of the second derivative of the exact solution to obtain an upper bound.

With (b) we have

$$\int_0^L (u' - u'_I)^2 dx \leq Lh^2 \left(\max_{0 \leq x \leq L} |u''| \right)^2$$

and hence

$$\left(\int_0^L (u' - u'_I)^2 dx \right)^{1/2} \leq ch \quad (c)$$

where the constant c depends on A , E , L , and f^B but is independent of h .

We should recognize that this analysis is quite general but assumes that the exact solution is smooth so that its second derivative can be calculated (in this example given by $-f^B/EA$). Of course the result in (c) is just the error estimate (4.102).

An interesting additional result is that the nodal point displacements of the finite element solution are for two reasons the exact displacements. First, the exact solution at the nodes due to the distributed loading is the same as that due to the equivalent concentrated loading (the "equivalent" loading calculated by the principle of virtual work). Second, the finite element space V_h contains the exact solution corresponding to the equivalent concentrated loading. Of course, this nice result is a special property of the solution of one-dimensional problems and does not exist in general two- or three-dimensional analysis.

In the above convergence study it is assumed that uniform discretizations are used (that, for example, in two-dimensional analysis the elements are square and of equal size) and that the exact solution is smooth. Also, implicitly, the degree of the element polynomial displacement expansions is not varied. In practice, these conditions are generally not encountered, and we need to ask what the consequences might be.

If the solution is not smooth—for example, because of sudden changes in the geometry, in loads, or in material properties or thicknesses—and the uniform mesh subdivision is used, the order of convergence decreases; hence, the exponent of h in (4.102) is not k but a smaller value dependent on the degree of "loss of smoothness."

In practice of course graded meshes are used in such analyses, with small elements in the areas of high stress variation and larger elements away from these regions. The order of convergence of the solutions is then still given by (4.101) but rewritten as

$$\| \mathbf{u} - \mathbf{u}_h \|_1^2 \leq c \sum_m h_m^{2k} \| \mathbf{u} \|_{k+1,m}^2 \quad (4.101c)$$

where m denotes an individual element and h_m is a measure of the size of the element. Hence the total error is now estimated by summing the local contributions in (4.101) from each element. A good grading of elements means that the error density in each element is about the same.

In practice when mesh grading is employed, geometrically distorted elements are invariably used. Hence, for example, general quadrilateral elements are very frequently encountered in two-dimensional analyses. We discuss elements of general geometric shapes in Chapter 5 and point out in Section 5.3.3 that the same orders of convergence are applicable to these elements so long as the magnitude of the geometric distortions is reasonable.

In the above sequence of meshes the same kind of elements are used and the element sizes are uniformly decreased. This approach is referred to as the h -method of analysis. Alternatively, an initial mesh of relatively large and low-order elements may be chosen, and then the polynomial displacement expansions in the elements may be successively increased. For example, a mesh of elements with a bilinear displacement assumption may be used (here $k = 1$), and then the degree of the polynomial expansion is increased to order 2, 3, . . . p , where p may be 10 or even higher. This approach is referred to as the p -method of analysis. To achieve this increase in element polynomial order efficiently, special interpolation functions have been proposed that allow the calculation of the element stiffness matrix corresponding to a higher interpolation by using the previously calculated stiffness matrix and simply amending this matrix, and that have valuable orthogonality properties (see B. Szabó and I. Babuška [A]). However, unfortunately, these functions lack the internal element displacement variations which are important when elements are geometrically distorted (see K. Kato, N. S. Lee, and K. J. Bathe [A] and Section 5.3.3). We demonstrate the use of these functions in the following example.

EXAMPLE 4.26: Consider the one-dimensional bar element shown in Fig. E4.26. Let (\mathbf{K}_p) be the stiffness matrix corresponding to the order of displacement interpolation p , where $p = 1, 2, 3, \dots$, and let the interpolation functions corresponding to $p = 1$ be

$$h_1 = \frac{1}{2}(1 - x); \quad h_2 = \frac{1}{2}(1 + x) \tag{a}$$

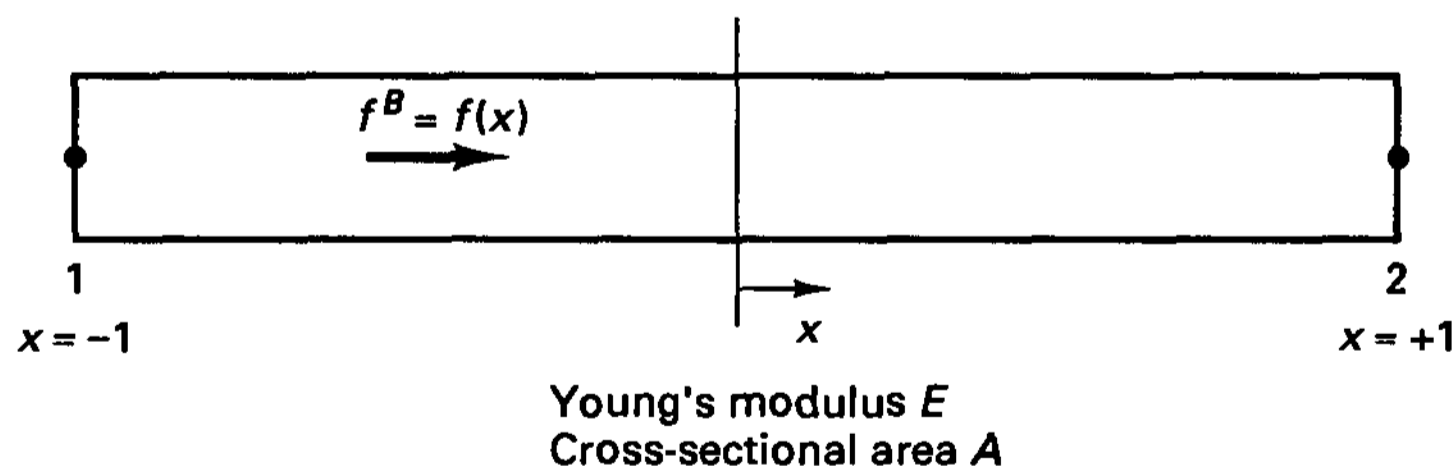


Figure E4.26 Bar element subjected to varying body force

For the higher-order interpolations use

$$h_i(x) = \phi_{i-1}(x) \quad i = 3, 4, \dots \tag{b}$$

where

$$\phi_j = \frac{1}{[2(2j - 1)]^{1/2}} [P_j(x) - P_{j-2}(x)] \tag{c}$$

and the P_j are the Legendre polynomials (see, for example, E. Kreyszig [A]),

$$P_0 = 1$$

$$P_1 = x$$

$$P_2 = \frac{1}{2}(3x^2 - 1)$$

$$P_3 = \frac{1}{2}(5x^3 - 3x)$$

$$P_4 = \frac{1}{8}(35x^4 - 30x^2 + 3)$$

$$\vdots$$

$$(n + 1)P_{n+1} = (2n + 1)xP_n - nP_{n-1}$$

Calculate the stiffness matrix $(\mathbf{K})_p$ and corresponding load vector of the element for $p \geq 1$.

Let us first note that these interpolation functions fulfill the requirements of monotonic convergence: the displacement continuity between elements is enforced, and the functions are complete (they can represent the rigid body mode and the constant strain state). This follows because the functions in (a) fulfill these requirements and the functions in (b) merely add higher-order displacement variations within the element with $h_i = 0$ at $x = \pm 1$, $i \geq 3$.

The stiffness matrix and load vector of the element are obtained using (4.19) and (4.20). Hence, typical elements of the stiffness matrix and load vector are

$$K_{ij} = \int_{-1}^{+1} AE \frac{dh_i}{dx} \frac{dh_j}{dx} dx \quad (d)$$

$$R_i^B = \int_{-1}^{+1} f(x)h_i dx$$

The evaluation of (d) gives

$$(\mathbf{K})_p = \frac{AE}{2} \begin{bmatrix} 1 & -1 & & & & \\ -1 & 1 & & & & \\ & & 2 & & & \\ & & & \ddots & & \\ & & & & 2 & \\ & & & & & \ddots & \\ & & & & & & 2 \end{bmatrix} (p+1) \times (p+1) \quad (e)$$

where we note that, in essence, the usual 2×2 stiffness matrix corresponding to the interpolation functions (a) has been amended by diagonal entries corresponding to the internal element displacement modes (b). In this specific case, each such entry is uncoupled from all other entries because of the orthogonality properties of the Legendre functions. Hence, as the order of the element is increased, additional diagonal entries are simply computed and all other stiffness coefficients are unchanged.

This structure of the matrix $(\mathbf{K})_p$ makes the solution of the governing equations of an element assemblage simple, and the conditioning of the coefficient matrix is always good irrespective of how high an order of element matrices is used. Note also that if the finite element solution is known for elements with a given order of interpolation, then the solution for an increased order of interpolation within the elements is obtained simply by calculating and adding the additional displacements due to the additional internal element modes.

Since the sets of displacement functions corresponding to the matrix $(\mathbf{K})_{p+1}$ contain the sets of functions corresponding to the matrix $(\mathbf{K})_p$, we refer to the displacement functions and the stiffness matrices as hierarchical functions and matrices. This hierarchical property is generally available when the interpolation order is increased (see Exercise 4.29 and Section 5.2).

The concept given in Example 4.26 is also used to establish the displacement functions for higher-order two- and three-dimensional elements. For example, in the two-dimensional case, the basic functions are h_i , $i = 1, 2, 3, 4$, used in Example 4.6, and the additional functions are due to side modes and internal modes (see Exercises 4.30 and 4.31).

We noted that in the analysis of a bar structure idealized by elements of the kind discussed in Example 4.26, the coupling between elements is due only to the nodal point displacements with the functions h_1 and h_2 , and this leads to the very efficient solution. However, in the two- and three-dimensional cases this computational efficiency is not present because the element side modes couple the displacements of adjacent elements and the governing equations of the finite element assemblage have, in fact, a large bandwidth (see Section 8.2.3).

A very high rate of convergence in the solution of general stress conditions can be obtained if we increase the number of elements and at the same time increase the order of displacement variations in the elements. This approach of mesh/element refinement is referred to as the h/p method and can yield an exponential rate of convergence of the form (see B. Szabó and I. Babuška [A])

$$\| \mathbf{u} - \mathbf{u}_h \|_1 \leq \frac{c}{\exp [\beta(N)^\gamma]} \quad (4.105)$$

where c , β , and γ are positive constants and N is the number of nodes in the mesh. If for comparison with (4.105) we write (4.101) in the same form, we obtain for the h method the algebraic rate of convergence

$$\| \mathbf{u} - \mathbf{u}_h \|_1 \leq \frac{c}{(N)^{k/d}}$$

where $d = 1, 2, 3$, respectively, in one-, two-, and three-dimensional problems. The effectiveness of the h/p method lies in that it combines the two attractive properties of the h and p methods: using the p method, an exponential rate of convergence is obtained when the exact solution is smooth, and using the h method, the optimal rate of convergence is maintained by proper mesh grading independent of the smoothness of the exact solution.

While the rate of convergence can be very high in the h/p solution approach, of course, whether the solution procedure is effective depends on the total computational effort expended to reach a specified error (which also depends on the constant c).

A key feature of a finite element solution using the h , p , or h/p methods must therefore be the “proper” mesh grading. The above expressions indicate a priori how convergence to the exact solution will be obtained as the density of elements and the order of interpolations are increased, but the meshes used in the successive solutions must be properly graded. By this we mean that the local error density in each element should be about constant. We discuss the evaluation of errors in the next section.

We also assumed in the above discussion on convergence—considering the linear static model problem—that the finite element matrices are calculated exactly and that the governing equilibrium equations are solved without error. In practice, numerical integration is employed in the evaluation of the element matrices (see Section 5.5), and finite precision arithmetic is used to solve the governing equilibrium equations (see Section 8.2.6); hence some error will clearly be introduced in the solution steps. However, the numerical integration errors will not reduce the order of convergence, provided a reliable integration scheme

of high enough order is used (see Section 5.5.5), and the errors in the solution of equations are normally small unless a very ill-conditioned set of equations is solved (see Section 8.2.6).

4.3.6 Calculation of Stresses and the Assessment of Error

We discussed above that for monotonic convergence to the exact results (“exact” within the mechanical, i.e., mathematical, assumptions made) the elements must be complete and compatible. Using compatible (or conforming) elements means that in the finite element representation of a C^{m-1} variational problem, the displacements and their $(m - 1)$ st derivatives are continuous across the element boundaries. Hence, for example, in a plane stress analysis the u and v displacements are continuous, and in the analysis of a plate bending problem using the transverse displacement w as the only unknown variable, this displacement w and its derivatives, $\partial w/\partial x$ and $\partial w/\partial y$, are continuous. However, this continuity does not mean that the element stresses are continuous across element boundaries.

The element stresses are calculated using derivatives of the displacements [see (4.11) and (4.12)], and the stresses obtained at an element edge (or face) when calculated in adjacent elements may differ substantially if a coarse finite element mesh is used. The stress differences at the element boundaries decrease as the finite element mesh is refined, and the rate at which this decrease occurs is of course determined by the order of the elements in the discretization.

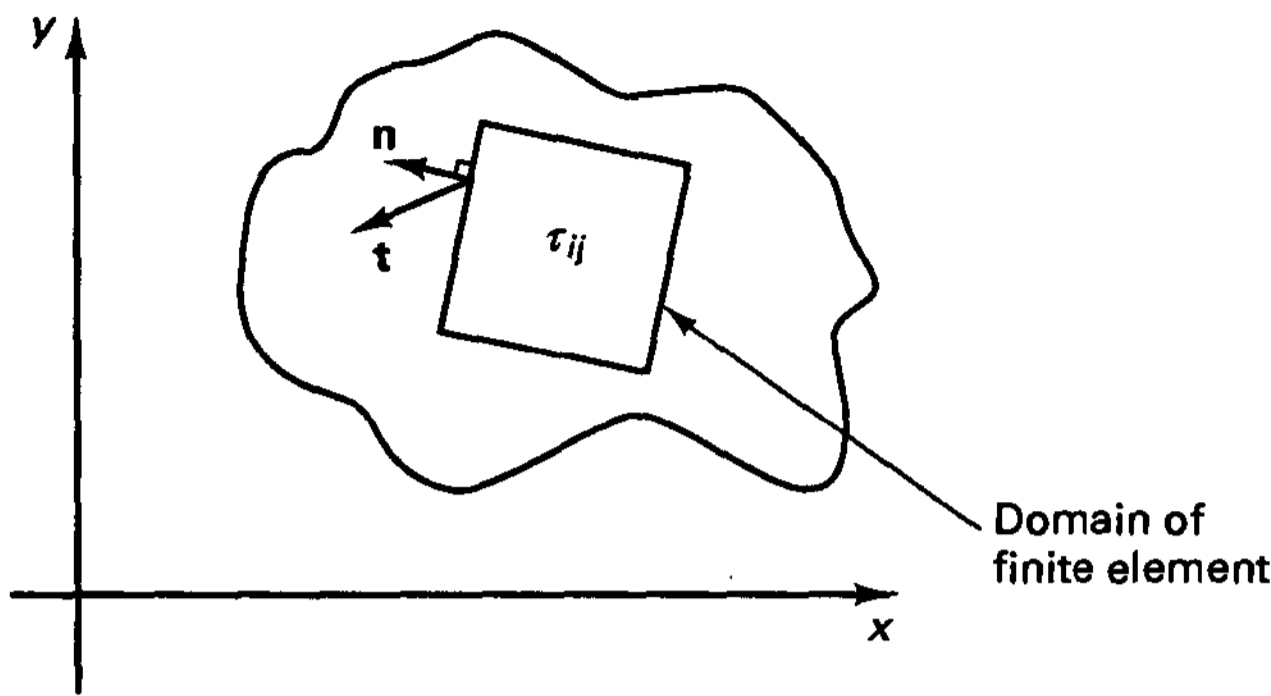
For the same mathematical reason that the element stresses are, in general, not continuous across element boundaries, the element stresses at the surface of the structure that is modeled are, in general, not in equilibrium with the externally applied tractions. However, as for the stress jumps between elements, the difference between the externally applied tractions and the element stresses decreases as the number of elements used to model the structure increases.

The stress jumps across element boundaries and stress imbalances at the boundary of the body are of course a consequence of the fact that stress equilibrium is not accurately satisfied at the differential level unless a very fine finite element discretization is used: we recall the derivation of the principle of virtual work in Example 4.2. The development in this example shows that the differential equations of equilibrium are fulfilled only if the virtual work equation is satisfied for *any* arbitrary virtual displacements that are zero on the surface of the displacement boundary conditions. In the finite element analysis, the number of “real” and virtual displacement patterns is equal to the number of nodal degrees of freedom, and hence only an approximate solution in terms of satisfying the stress equilibrium at the differential level is obtained (while the compatibility and constitutive conditions are satisfied exactly). The error in the solution can therefore be measured by substituting the finite element solution for the stresses τ_{ij}^h into the basic equations of equilibrium to find that for each geometric domain represented by a finite element,

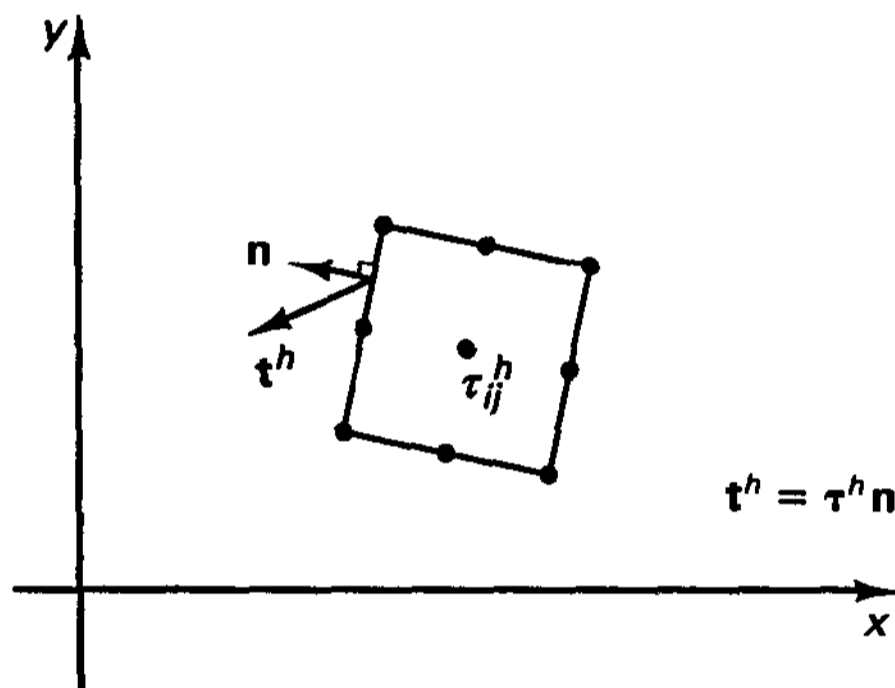
$$\tau_{ij,j}^h + f_i^B \neq 0 \quad (4.106)$$

$$\tau_{ij}^h n_j - t_i \neq 0 \quad (4.107)$$

where n_j represents the direction cosines of the normal to the element domain boundary and the t_i are the components of the exact traction vector along that boundary (see Fig. 4.14). Of course, this traction vector of the exact solution is not known, and that the left-hand side of (4.107) is not zero simply shows that we must expect stress jumps between elements.



(e) Exact solution to mathematical model



(b) Finite element solution

Figure 4.14 Finite element representing subdomain of continuum

It can be proven that for low-order elements the imbalance in (4.107) is larger than the imbalance in (4.106), and that for high-order elements the imbalance in (4.106) becomes predominant. In practice, (4.107) can be used to obtain an indication of the accuracy of the stress solution and is easily applied by using the isobands of stresses as proposed by T. Sussman and K. J. Bathe [A]. These isobands are constructed using the calculated stresses without stress smoothing as follows:

Choose a stress measure; typically, pressure or the effective (von Mises) stress is chosen, but of course any stress component may be selected.

Divide the entire range over which the stress measure varies into stress intervals, assign each interval a color (or use black and white shading or simply alternate black and white intervals).

A point in the mesh is given the color of the interval corresponding to the value of the stress measure at that point.

If all stresses are continuous across the element boundaries, then this procedure will yield unbroken isobands of stresses. However, in practice, stress discontinuities arise across the element boundaries, resulting in “breaks” in the bands. The magnitude of the intervals of the stress bands together with the severity of the breaks in the bands indicate directly the magnitude of stress discontinuities (see Fig. 4.15). Hence, the isobands represent an

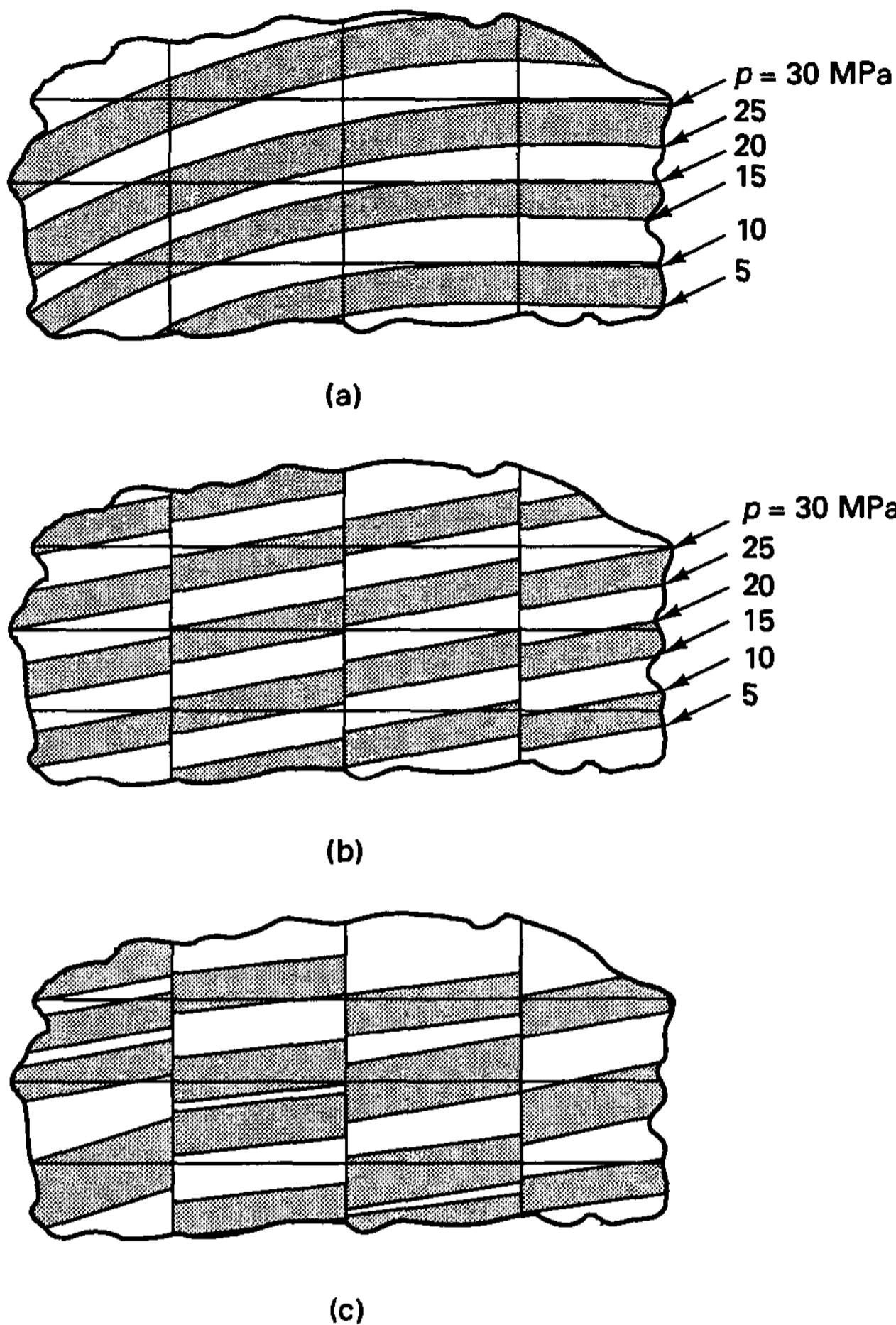


Figure 4.15 Schematic of estimating stress discontinuities using pressure bands, width of bands = 5 MPa; black and white intervals are used; (a) negligible discontinuities, $\Delta p \ll 5$ MPa; (b) visible discontinuities but bands still distinguishable, $\Delta p \approx 2$ MPa; (c) visible discontinuities, bands not distinguishable, $\Delta p > 5$ MPa.

“eyeball norm” for the accuracy of the stress prediction τ_{ij}^h achieved with a given finite element mesh.

In linear analysis, the finite element stress values can be calculated using the relation $\tau^h = \mathbf{CB}\hat{\mathbf{u}}$ at any point in the element; however, this evaluation is relatively expensive and hardly possible in general nonlinear analysis (including material nonlinear effects). An adequate approach is to use the integration point values to bilinearly interpolate over the corresponding domain of the element. Figure 4.16 illustrates an example in two-dimensional analysis.

An alternative procedure for obtaining an approximation to the error in the calculated stresses τ_{ij}^h is to first find some improved values $(\tau_{ij}^h)_{\text{impr.}}$ and then evaluate and display

$$\Delta\tau_{ij} = \tau_{ij}^h - (\tau_{ij}^h)_{\text{impr.}} \quad (4.108)$$

The display can again be achieved effectively using the isoband procedure discussed above.

Improved values might be found by simply averaging the stress values obtained at the nodes using the procedure indicated in Fig. 4.16 or by using a least squares fit over the integration point values of the elements (see E. Hinton and J. S. Campbell [A]). The least squares procedure might be applied over patches of adjacent elements or even globally over

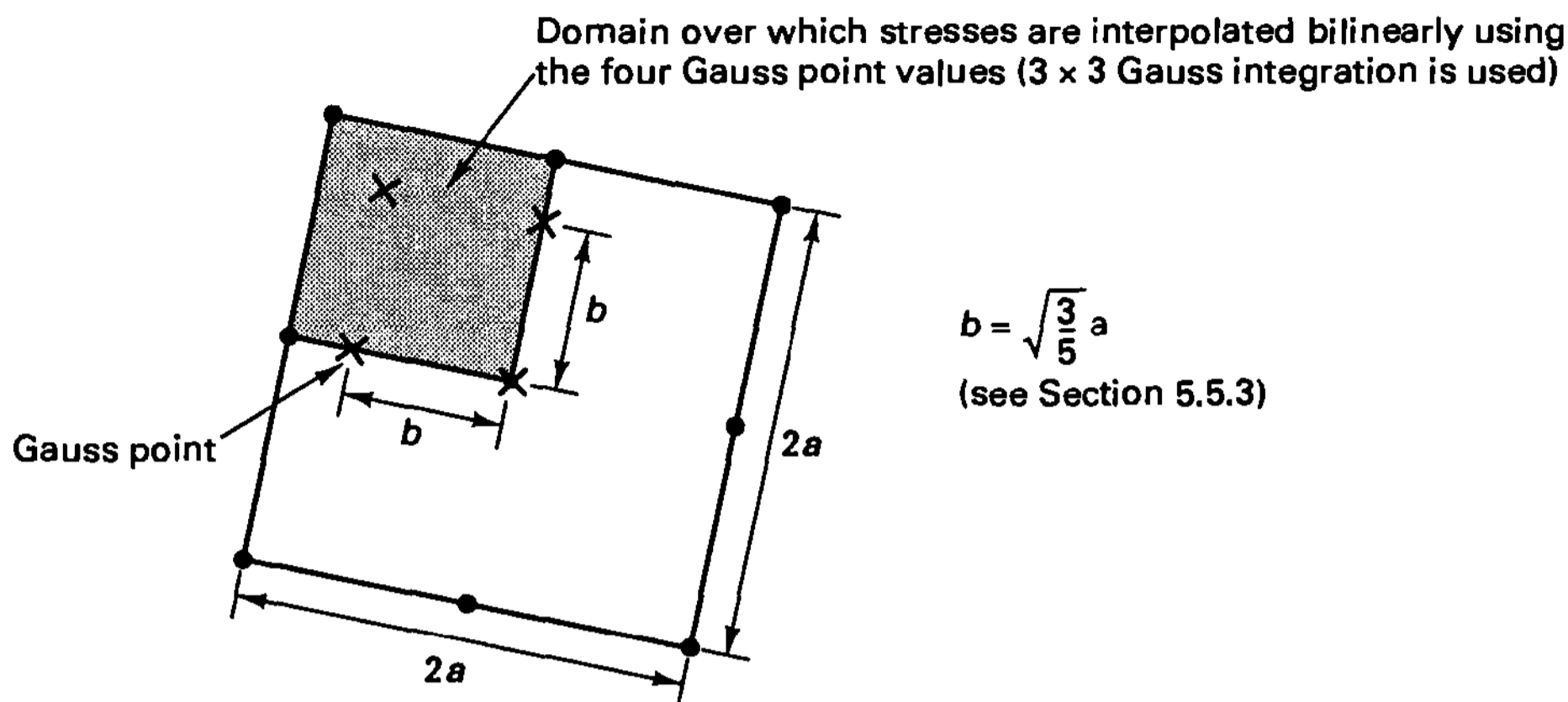


Figure 4.16 Interpolation of stresses from Gauss point stresses

a whole mesh. However, if the domain over which the least squares fit is applied involves many stress points, the solution will be expensive and, in addition, a large error in one part of the domain may affect rather strongly the least squares prediction in the other parts. Another consideration is that when using the direct stress evaluation in (4.12), the stresses are frequently more accurate at the numerical integration points used to evaluate the element matrices (see Section 5.5) than at the nodal points. Hence, for a least squares fit, it can be of value to use functions of order higher than that of the stress variations obtained from the assumed displacement functions because in this way improved values can be expected.

We demonstrate the nodal point and least squares stress averaging in the following example.

EXAMPLE 4.27: Consider the mesh of nine-node elements shown in Fig. E4.27. Propose reasonable schemes for improving the stress results by nodal point averaging and least squares fitting.

Let τ be a typical stress component. One simple and frequently effective way of improving the stress results is to bilinearly extrapolate the calculated stress components from the integration points of each element to node i . In this way, for the situation and node i in Fig. E4.27, four values for each stress component are obtained. The mean value, say $(\tau^h)_{\text{mean}}^i$, of these four values is then taken as the value at nodal point i . After performing similar calculations for each nodal point, the improved value of the stress component over a typical element is

$$(\tau^h)_{\text{impr.}} = \sum_{i=1}^9 h_i (\tau^h)_{\text{mean}}^i \tag{a}$$

where the h_i are the displacement interpolation functions because the averaged nodal values are deemed to be more accurate than the values obtained simply from the derivatives of the displacements (which would imply that an interpolation of one order lower is more appropriate).

The key step in this scheme is the calculation of $(\tau^h)_{\text{mean}}^i$. Such an improved value can also be extracted by using a procedure based on least squares.

Consider the eight nodes closest to node i , plus node i , and the values of the stress component of interest at the 16 integration points closest to node i (shown in Fig. E4.27). Let $(\tau^h)_{\text{integr.}}^j$ be the known values of the stress component at the integration points, $j = 1, \dots, 16$, and let $(\tau^h)_{\text{nodes}}^k$ be the unknown values at the nine nodes (of the domain corresponding to the

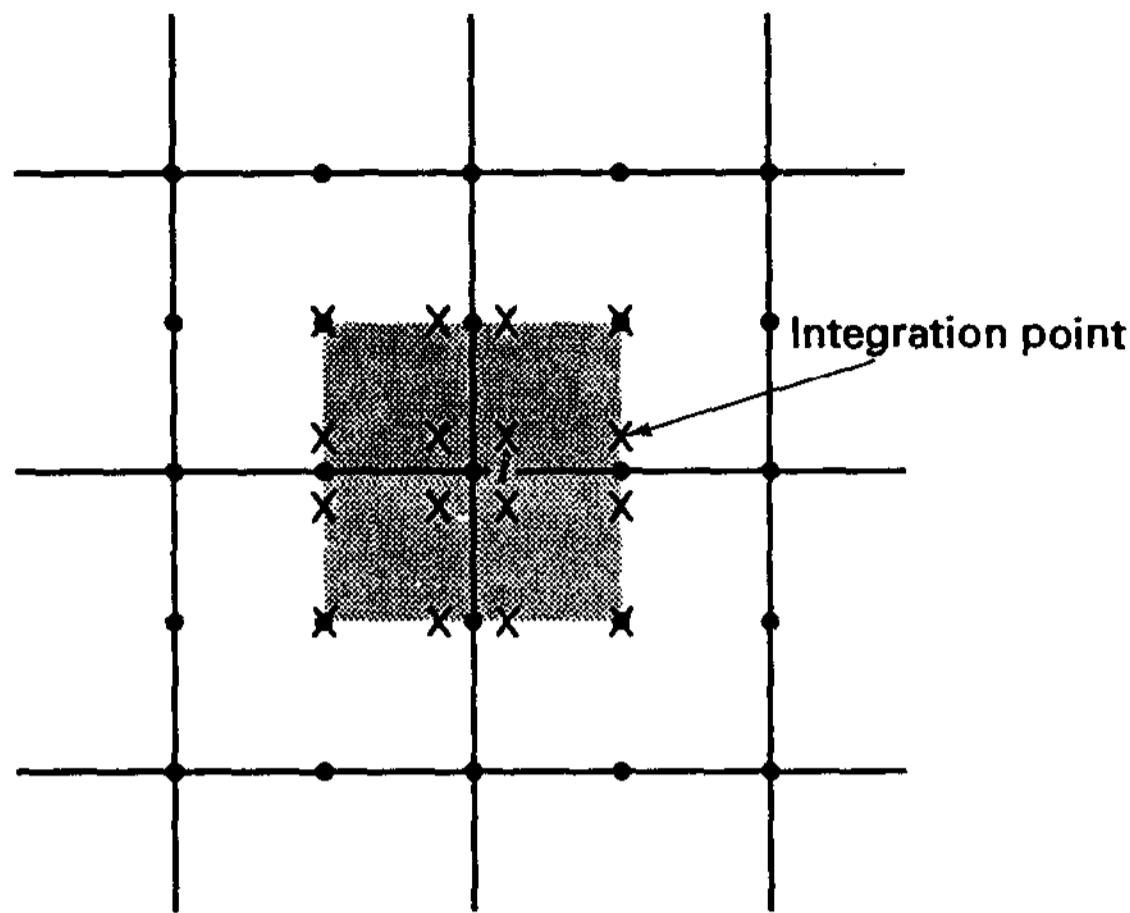


Figure E4.27 Mesh of nine-node elements. Integration points near node i are also shown.

integration points). We can use the least squares procedure (see Section 3.3.3) to calculate the values $(\tau^h)^k_{nodes}$ by minimizing the errors between the given integration point values and the values calculated at the same points by interpolation from the nodal point values $(\tau^h)^k_{nodes}$,

$$\frac{\partial}{\partial (\tau^h)^k_{nodes}} \left[\sum_{j=1}^{16} ((\tau^h)^j_{integr.} - (\hat{\tau}^h)^j_{integr.})^2 \right] = 0 \tag{b}$$

$$k = 1, \dots, 9$$

where

$$(\hat{\tau}^h)^j_{integr.} = \sum_{k=1}^9 h_k \Big|_{\substack{\text{at integr.} \\ \text{point } j}} (\tau^h)^k_{nodes} \tag{c}$$

Note that in (c) we evaluate the interpolation functions at the 16 integration stations shown in Fig. E4.27. The relations in (b) and (c) give nine equations for the values $(\tau^h)^k_{nodes}$, $k = 1, \dots, 9$. We solve for these values but accept only the value at node i as the improved stress value, which is now our value for $(\tau^h)^i_{mean}$ in (a). The same basic procedure is used for all nodes to arrive at nodal “mean” values, so that (a) can be used for all elements.

A least squares procedure clearly involves more computations, and in many cases the simpler scheme of merely extrapolating the Gauss values and averaging at the nodes as described above is adequate.

Of course, we presented in Fig. E4.27 a situation of four equal square elements. In practice, the elements are generally distorted and fewer or more elements may couple into the node i . Also, element non-corner nodes and special mesh topologies at boundaries need to be considered.

We emphasize that the calculation of an error measure and its display is a most important aspect of a finite element solution. The quality of the finite element stress solution τ^h_{ij} should be known. Once the error is acceptably small, values of stresses that have been smoothed, for example, by nodal point or least squares averaging, can be used with confidence.

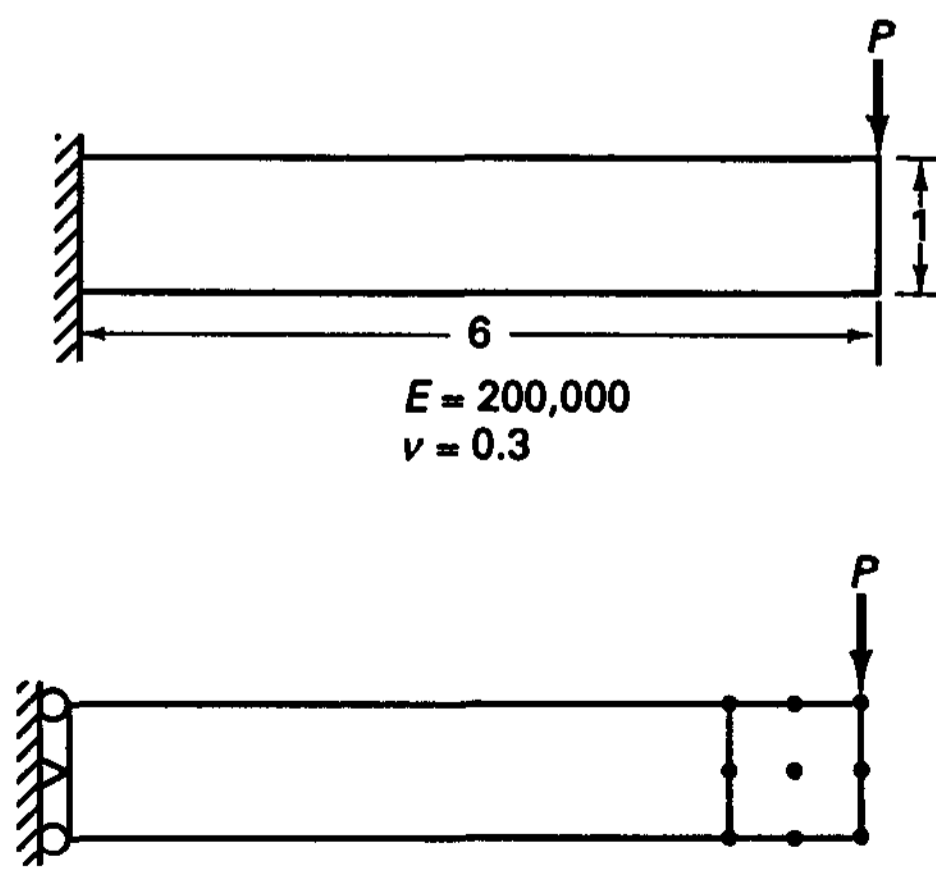
These error measures are based on the discontinuities of stresses between elements. However, for high-order elements (of order 4 and higher), such discontinuities can be small and yet the solution is not accurate because the differential equations of equilibrium of stresses within the elements are not satisfied to sufficient accuracy. In this case the error measure should also include the element internal stress imbalance (4.106).

Once an error measure for the stresses has been calculated in a finite element solution and the errors are deemed to be too large, a procedure needs to be used to establish a new mesh (with a refined discretization in certain areas, derefinement in other areas, and possibly new element interpolation orders). This process of new mesh selection can be automatized to a large degree and is important for the widespread use of finite element analysis in CAD (see Section 1.3).

4.3.7 Exercises

- 4.25. Calculate the eight smallest eigenvalues of the four-node shell element stiffness matrix available in a finite element program and interpret each eigenvalue and corresponding eigenvector. (*Hint:* The eigenvalues of the element stiffness matrix can be obtained by carrying out a frequency solution with a mass matrix corresponding to unit masses for each degree of freedom.)
- 4.26. Show that the strain energy corresponding to the displacement error \mathbf{e}_h , where $\mathbf{e}_h = \mathbf{u} - \mathbf{u}_h$, is equal to the difference in the strain energies, corresponding to the exact displacement solution \mathbf{u} and the finite element solution \mathbf{u}_h .
- 4.27. Consider the analysis problem in Example 4.6. Use a finite element program to perform the convergence study shown in Fig. 4.12 with the nine-node and four-node (Lagrangian) elements. That is, measure the rate of convergence in the energy norm and compare this rate with the theoretical results given in Section 4.3.5. Use $N = 2, 4, 8, 16, 32$; consider $N = 32$ to be the limit solution, and use uniform and graded meshes.
- 4.28. Perform an analysis of the cantilever problem shown using a finite element program. Use a two-dimensional plane stress element idealization to solve for the static response.
 - (a) Use meshes of four-node elements.
 - (b) Use meshes of nine-node elements.

In each case construct a sequence of meshes and identify the rate of convergence of strain energy.



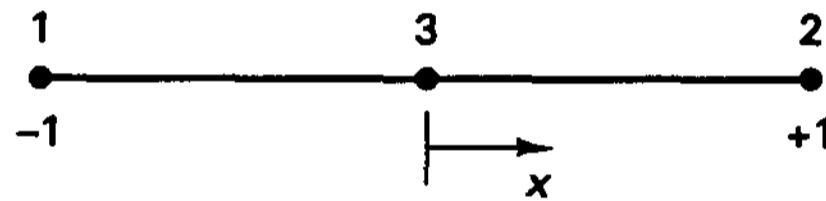
Also, compare your finite element solutions with the solutions using Bernoulli-Euler and Timoshenko beam theories (see S. H. Crandall, N. C. Dahl, and T. J. Lardner [A] and Section 5.4.1).

- 4.29. Consider the three-node bar element shown. Construct and plot the displacement functions of the element for the following two cases:

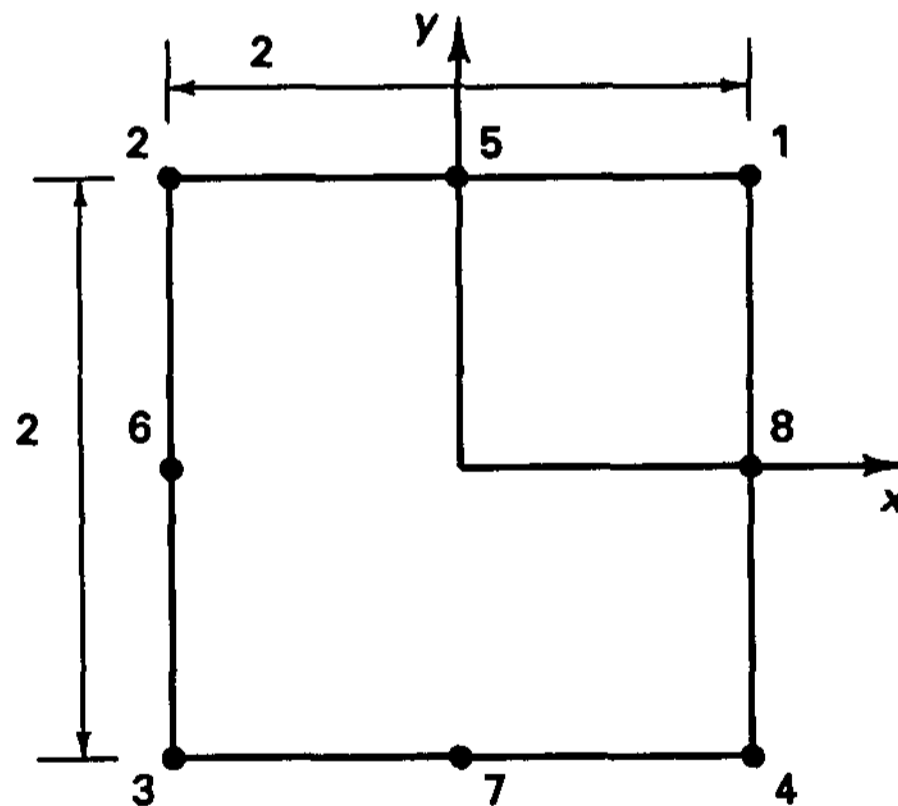
for case 1: $h_i = 1$ at node $i, i = 1, 2, 3$
 $= 0$ at node $j \neq i$

for case 2: $h_i = 1$ at node $i, i = 1, 2$
 $= 0$ at node $j \neq i, j = 1, 2$
 $h_3 = 1$ at node 3
 $h_3 = 0$ at node 1, 2

We note that the functions for case 1 and case 2 contain the same displacement variations, and hence correspond to the same displacement space. Also, the sets of functions are hierarchical because the three-node element contains the functions of the two-node element.



- 4.30. Consider the eight-node element shown. Identify the terms of the Pascal triangle present in the element interpolations.



$$h_1 = \frac{1}{4}(1+x)(1+y), h_2 = \frac{1}{4}(1-x)(1+y)$$

$$h_3 = \frac{1}{4}(1-x)(1-y), h_4 = \frac{1}{4}(1+x)(1-y)$$

$$h_5 = \frac{1}{2}(1+y)\phi_2(x), h_6 = \frac{1}{2}(1-x)\phi_2(y)$$

$$h_7 = \frac{1}{2}(1-y)\phi_2(x), h_8 = \frac{1}{2}(1+x)\phi_2(y)$$

where ϕ_2 is defined in Example 4.26.

4.31. A p -element of order $p = 4$ is obtained by using the following displacement functions.

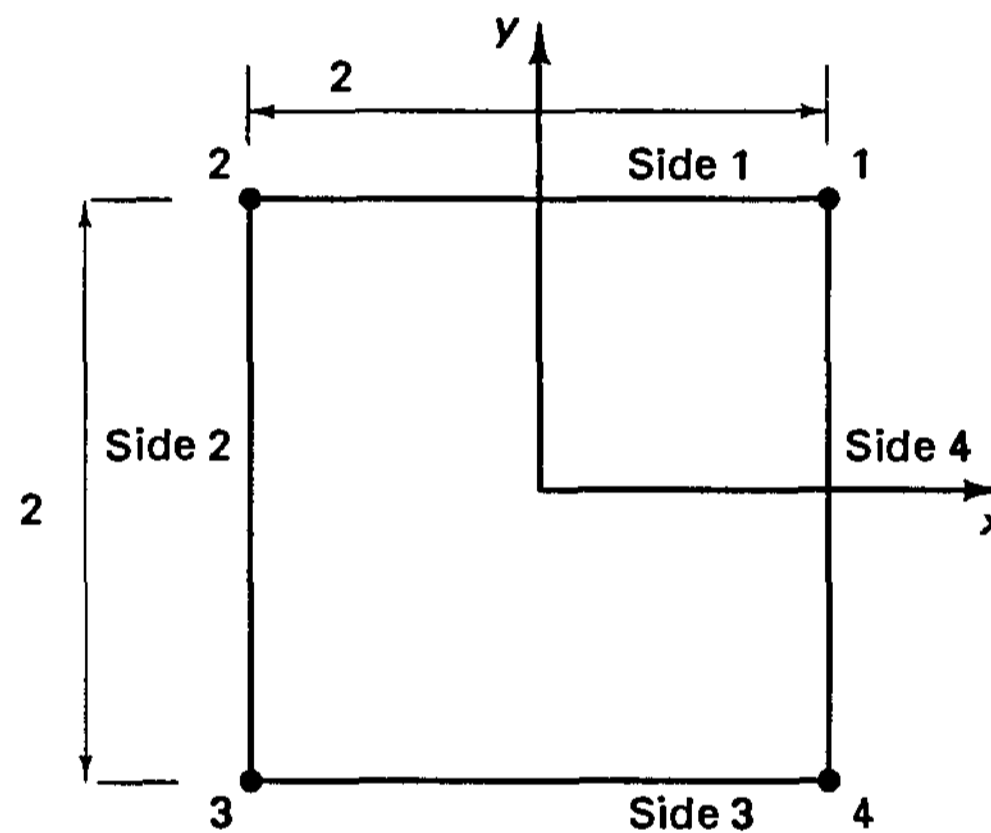
$h_i, i = 1, 2, 3, 4$, as for the basic four-node element (with corner nodes only; see Example 4.6).
 $h_i, i = 5, \dots, 16$ to represent side modes.

- side 1: $h_i^{(1)} = \frac{1}{2}(1 + y)\phi_j(x); \quad i = 5, 9, 13; j = 2, 3, 4$
- side 2: $h_i^{(2)} = \frac{1}{2}(1 - x)\phi_j(y); \quad i = 6, 10, 14; j = 2, 3, 4$
- side 3: $h_i^{(3)} = \frac{1}{2}(1 - y)\phi_j(x); \quad i = 7, 11, 15; j = 2, 3, 4$
- side 4: $h_i^{(4)} = \frac{1}{2}(1 + x)\phi_j(y); \quad i = 8, 12, 16; j = 2, 3, 4$

where ϕ_2, ϕ_3 , and ϕ_4 have been defined in Example 4.26. h_{17} to represent an internal mode

$$h_{17} = (1 - x^2)(1 - y^2)$$

Identify the terms of the Pascal triangle present in the element interpolations.



4.32. Consider the analysis problem in Example 4.6. Use a finite element program to solve the problem with the meshes of nine-node elements in Exercise 4.27 and plot isobands of the von Mises stress and the pressure (without using stress smoothing). Hence, the isobands will display stress discontinuities between elements. Show how the bands converge to continuous stress bands over the cantilever plate.

4.4 INCOMPATIBLE AND MIXED FINITE ELEMENT MODELS

In the previous sections we considered the displacement-based finite element method, and the conditions imposed so far on the assumed displacement (or field) functions were completeness and compatibility. If these conditions are satisfied, the calculated solution converges in the strain energy monotonically (i.e., one-sided) to the exact solution. The completeness condition can, in general, be satisfied with relative ease. The compatibility condition can also be satisfied without major difficulties in C^0 problems, for example, in

plane stress and plane strain problems or in the analysis of three-dimensional solids such as dams. Yet, in the analysis of shell problems, and in complex analyses in which completely different finite elements must be used to idealize different regions of the structure, compatibility may be quite impossible to maintain. However, although the compatibility requirements are violated, experience shows that good results are frequently obtained.

Also, in the search for finite elements it was realized that for shell analysis and the analysis of incompressible media, the pure displacement-based method is not efficient. The difficulties in developing compatible displacement-based finite elements for these problems that are computationally effective, and the realization that by using variational approaches many more finite element discretizations can be developed, led to large research efforts. In these activities various classes of new types of elements have been proposed, and the amount of information available on these elements is voluminous. We shall not present the various formulations in detail but only briefly outline some of the major ideas that have been used and then concentrate upon a formulation for a large class of problems—the analysis of almost incompressible media. The analysis of plate and shell structures using many of the concepts outlined below is then further addressed in Chapter 5.

4.4.1 Incompatible Displacement-Based Models

In practice, a frequently made observation is that satisfactory finite element analysis results have been obtained although some continuity requirements between displacement-based elements in the mesh employed were violated. In some instances the nodal point layout was such that interelement continuity was not preserved, and in other cases elements were used that contained interelement incompatibilities (see Example 4.28). The final result was the same in either case, namely, that the displacements or their derivatives between elements were not continuous to the degree necessary to satisfy all compatibility conditions discussed in Section 4.3.2.

Since in finite element analysis using incompatible (nonconforming) elements the requirements presented in Section 4.3.2 are not satisfied, the calculated total potential energy is not necessarily an upper bound to the exact total potential energy of the system, and consequently, monotonic convergence is not ensured. However, having relaxed the objective of monotonic convergence in the analysis, we still need to establish conditions that will ensure at least a nonmonotonic convergence.

Referring to Section 4.3, the element completeness condition must always be satisfied, and it may be noted that this condition is not affected by the size of the finite element. We recall that an element is complete if it can represent the physical rigid body modes (but the element matrix has no spurious zero eigenvalues) and the constant strain states.

However, the compatibility condition can be relaxed somewhat at the expense of not obtaining a monotonically convergent solution, provided that when relaxing this requirement, the essential ingredients of the completeness condition are not lost. We recall that as the finite element mesh is refined (i.e., the size of the elements gets smaller), each element should approach a constant strain condition. Therefore, the second condition on convergence of an assemblage of incompatible finite elements, where the elements may again be of any size, is that the elements together can represent constant strain conditions. We should

note that *this is not a condition on a single individual element but on an assemblage of elements*. That is, although an individual element is able to represent all constant strain states, when the element is used in an assemblage, the incompatibilities between elements may prohibit constant strain states from being represented. We may call this condition the *completeness condition on an element assemblage*.

As a test to investigate whether an assemblage of nonconforming elements is complete, the *patch test* has been proposed (see B. M. Irons and A. Razzaque [A]). In this test a specific element is considered and a patch of elements is subjected to the minimum displacement boundary conditions to eliminate all rigid body modes and to the boundary nodal point forces that by an analysis should result in constant stress conditions. If for *any* patch of elements the element stresses actually represent the constant stress conditions and all nodal point displacements are correctly predicted, we say that the element passes the patch test. Since a patch may also consist of only a single element, this test ensures that the element itself is complete and that the completeness condition is also satisfied by any element assemblage.

The number of constant stress states in a patch test depends of course on the actual number of constant stress states that pertain to the mathematical model; for example, in plane stress analysis three constant stress states must be considered in the patch test, whereas in a fully three-dimensional analysis six constant stress states should be possible.

Fig. 4.17 shows a typical patch of elements used in numerical investigations for various problems. Here of course only one mesh with distorted elements is considered, whereas in fact any patch of distorted elements should be analyzed. This, however, requires an analytical solution. If in practice the element is complete and the specific analyses shown here produce the correct results, then it is quite likely that the element passes the **patch test**.

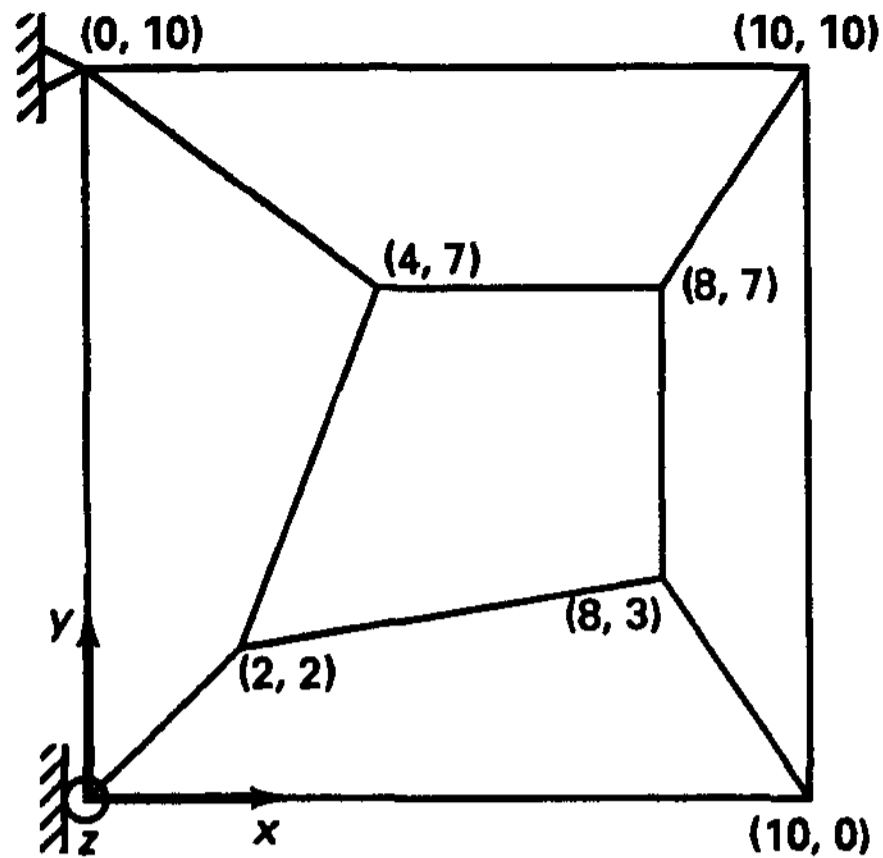
When considering displacement-based elements with incompatibilities, if ~~the~~ **the patch test** is passed, convergence is ensured (although convergence may not be ~~monotonic~~ **monotonic** and convergence may be slow).

The patch test is used to assess incompatible finite element meshes, and we may note that when properly formulated displacement-based elements are used in compatible meshes, the patch test is automatically passed.

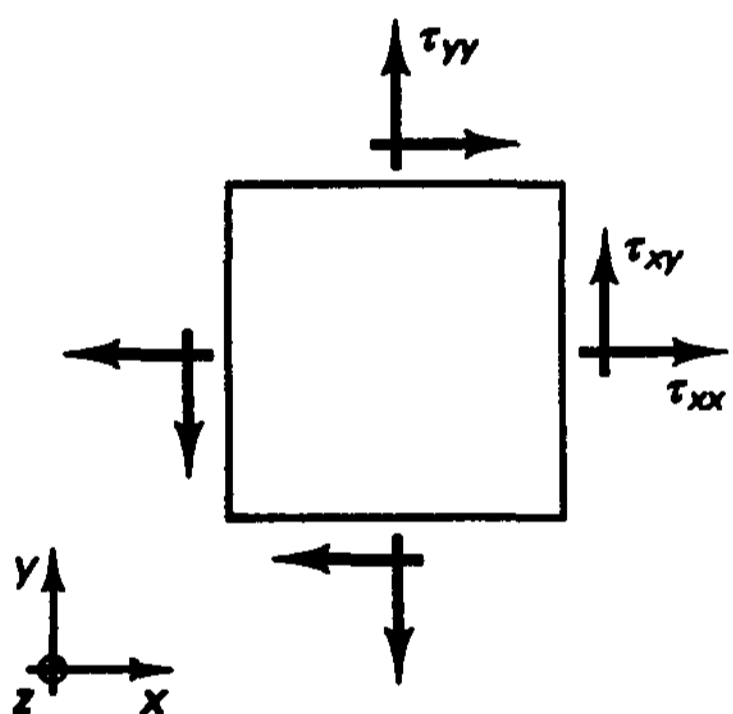
Figure 4.18(a) shows a patch of eight-node elements (which are discussed in detail in Section 5.2). The tractions corresponding to the plane stress patch test are also shown. The elements form a compatible mesh, and hence the patch test is passed.

However, if we next assign to nodes 1 to 8 individual degrees of freedom for the adjacent elements [e.g., at node 2 we assign two u and v degrees of freedom each for elements 1 and 2] such that the displacements are not tied together at these nodes (and therefore displacement incompatibilities exist along the edges), the patch test is not passed. Figure 4.18(b) gives some results of the solution.

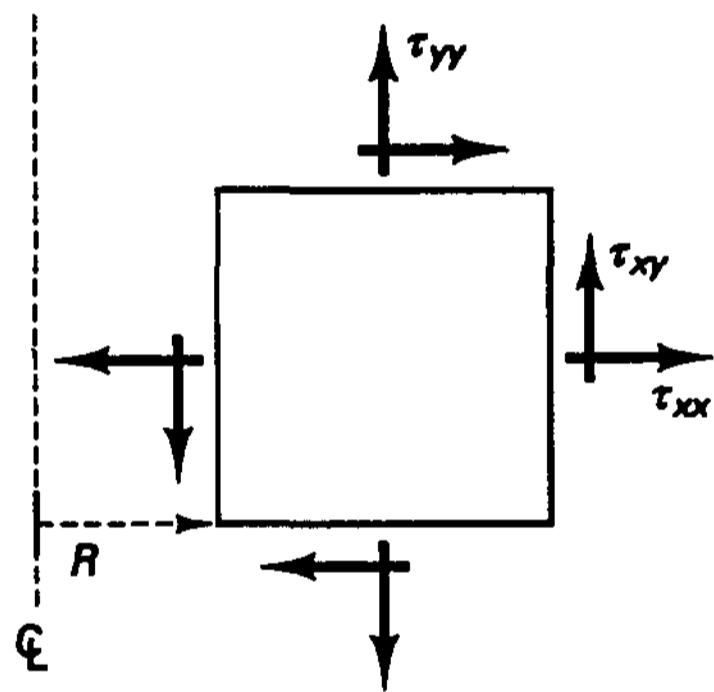
The example in Fig. 4.18(b) uses, in essence, an element that was proposed by E. L. Wilson, R. L. Taylor, W. P. Doherty, and J. Ghaboussi [A]. Since the degrees of freedom of the midside nodes of an element are not connected to the adjacent elements, they can be statically condensed out at the element level (see Section 8.2.4) and a four-node element is obtained. However, as indicated in Fig. 4.18(b), this element does not pass the patch test. In the following example, we consider the element in more detail, first as a square element



(a) Patch of elements, two-dimensional elements, plate bending elements, or side view of three-dimensional elements. Each quadrilateral domain represents an element; for triangular and tetrahedral elements, each quadrilateral domain is further subdivided



Plane stress and plane strain: $\tau_{xx}, \tau_{yy}, \tau_{xy}$ constant; In three-dimensional analysis the additional three stress conditions $\tau_{zz}, \tau_{zx}, \tau_{yz}$ constant are tested



Axisymmetric; here perform the test with $R \rightarrow \infty$

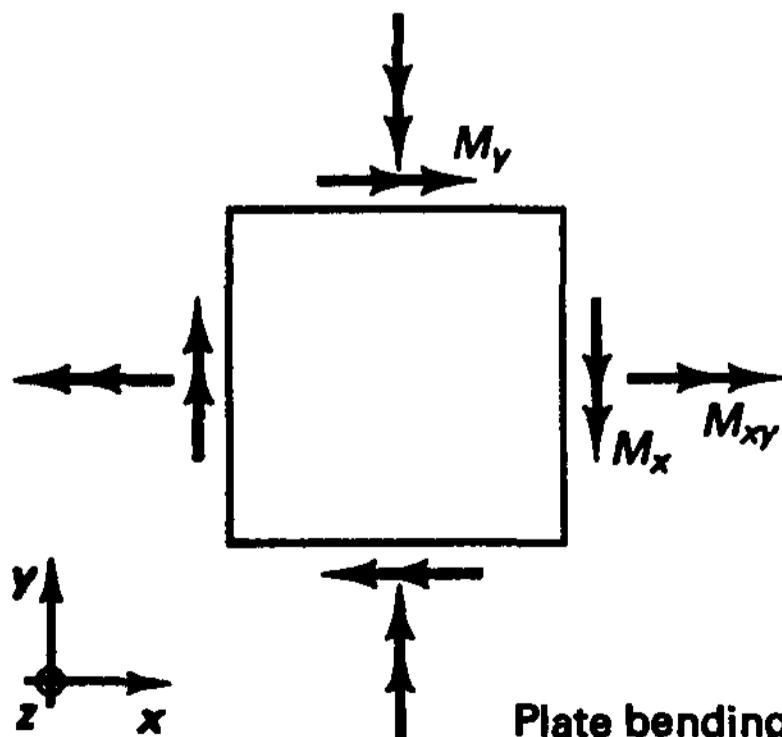
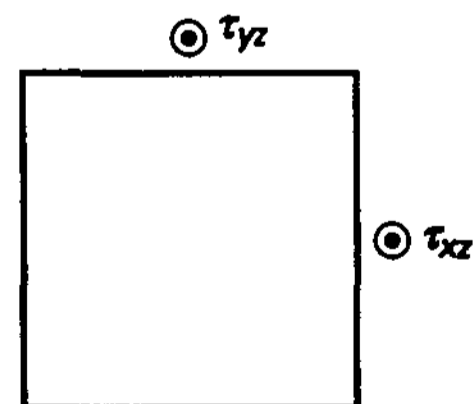


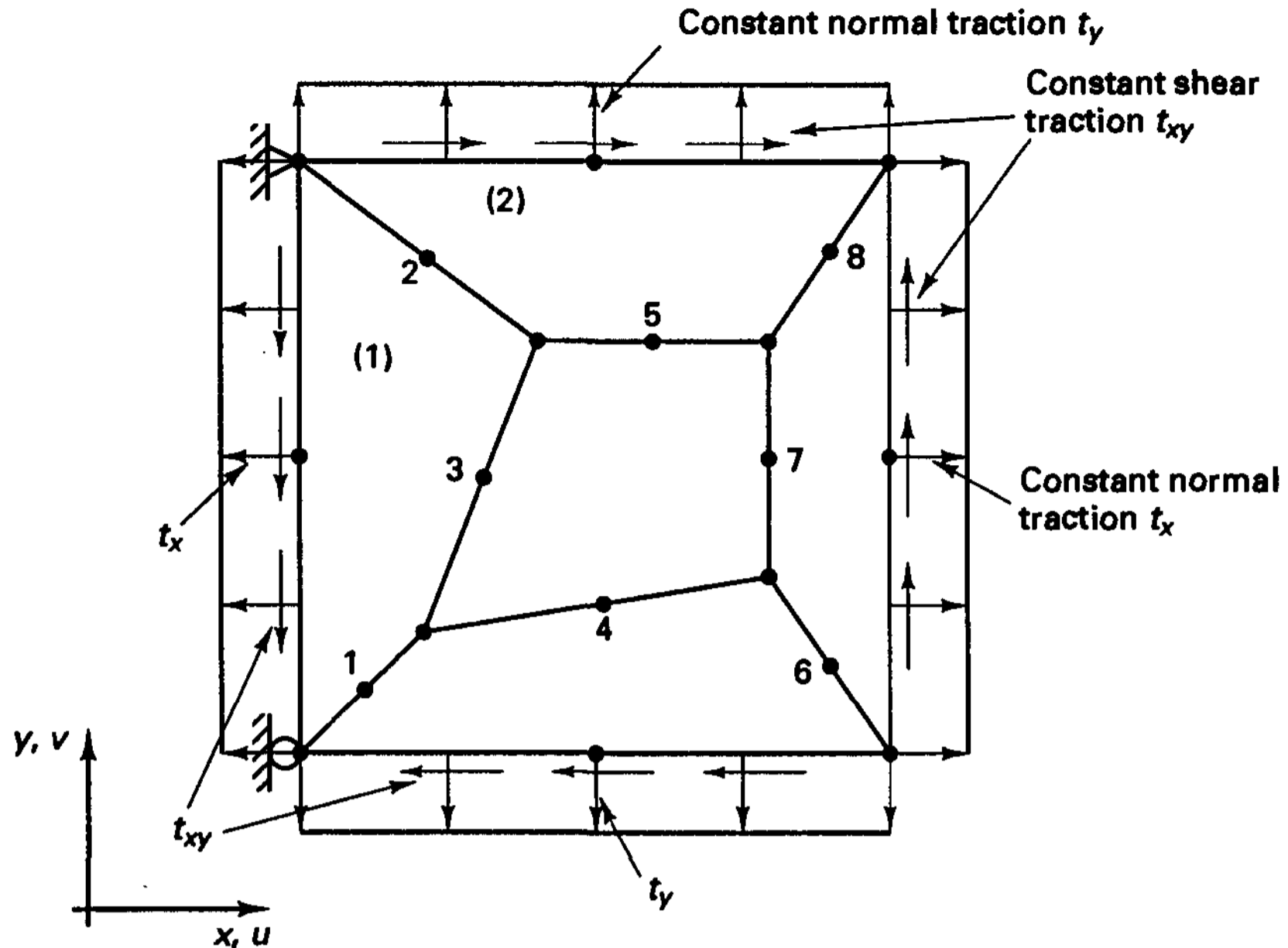
Plate bending (see Section 5.4.2)



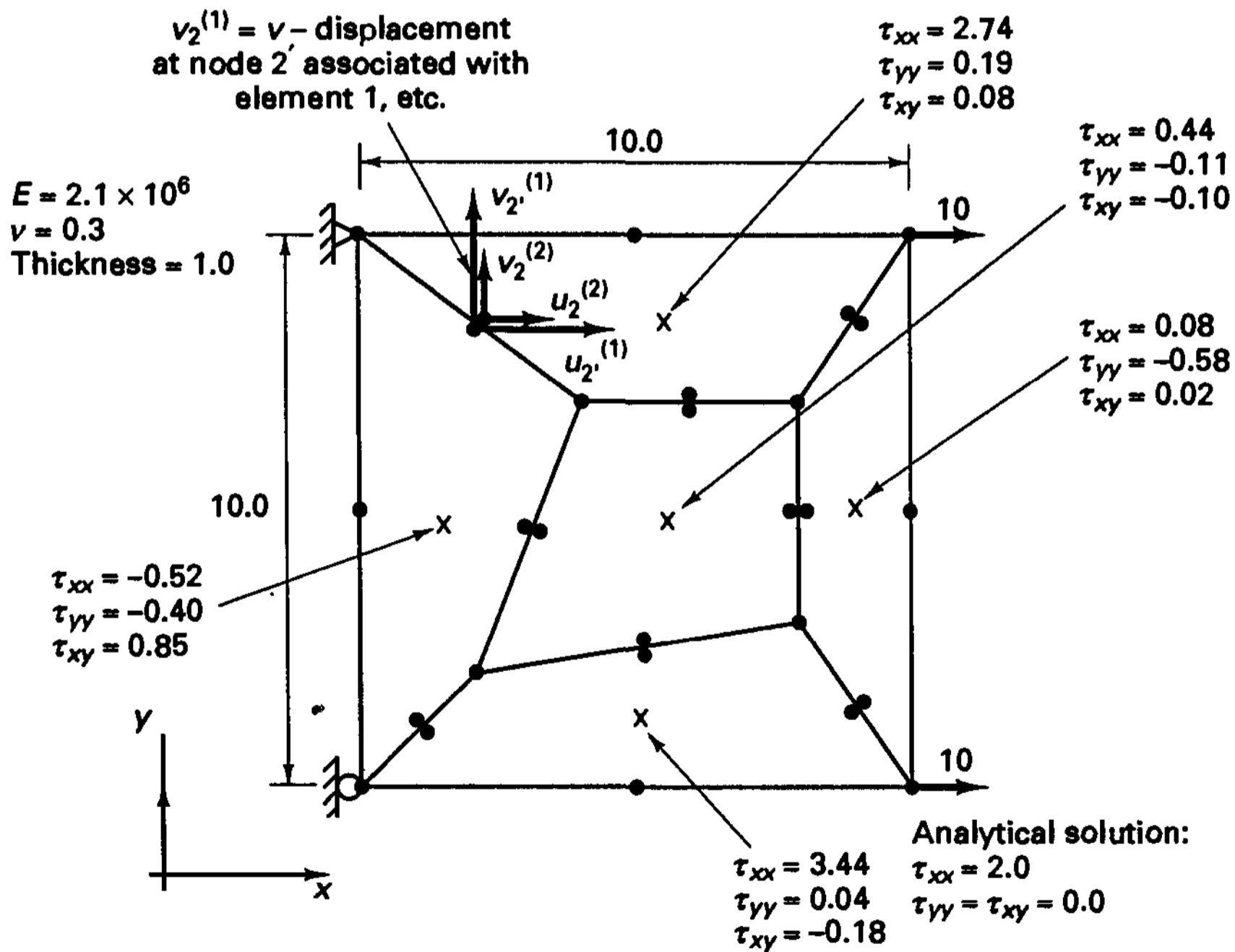
(This test also produces bending)

(b) Stress conditions to be tested

Figure 4.17 Patch tests



(a) Patch test of compatible mesh of 8-noda elements (discussed in Section 5.3.1). The patch test is passed; that is, all calculated element stresses are equal to the applied tractions



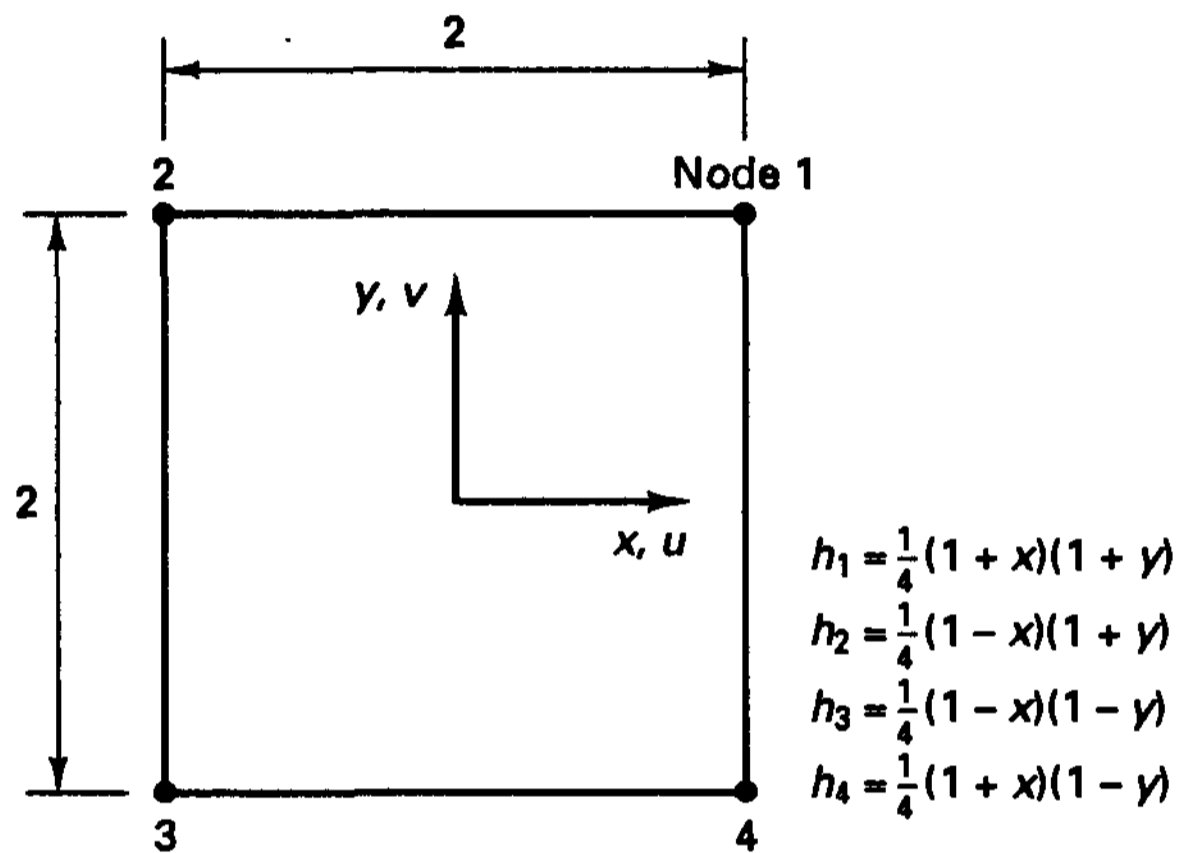
(b) Patch test of incompatible mesh of 8-node elements. All element midside nodes are now element individual nodes with degrees of freedom not coupled to the adjacent element. Hence, two nodes are located where in Fig. 4.18(a) only one node was located. Patch test results are shown at center of elements for external traction applied in the x-direction. (Note that only the corner nodes of the complete patch are subjected to externally applied loads)

Figure 4.18 Patch test results using the patch and element geometries of Fig. 4.17

and then as a general quadrilateral element. We also present a remedy to correct the element so that it will always pass the patch test (see E. L. Wilson and A. Ibrahimbegovic [A]).

EXAMPLE 4.28: Consider the four-node square element with incompatible modes in Fig. E4.28(a) and determine whether the patch test is passed. Then consider the general quadrilateral element in Fig. E4.28(b) and repeat the investigation.

We notice that the square element is really a special case of the general quadrilateral element. In fact, the quadrilateral element is formulated using the square element as a basis and using the natural coordinates (r, s) in the interpolations as discussed in Section 5.2.



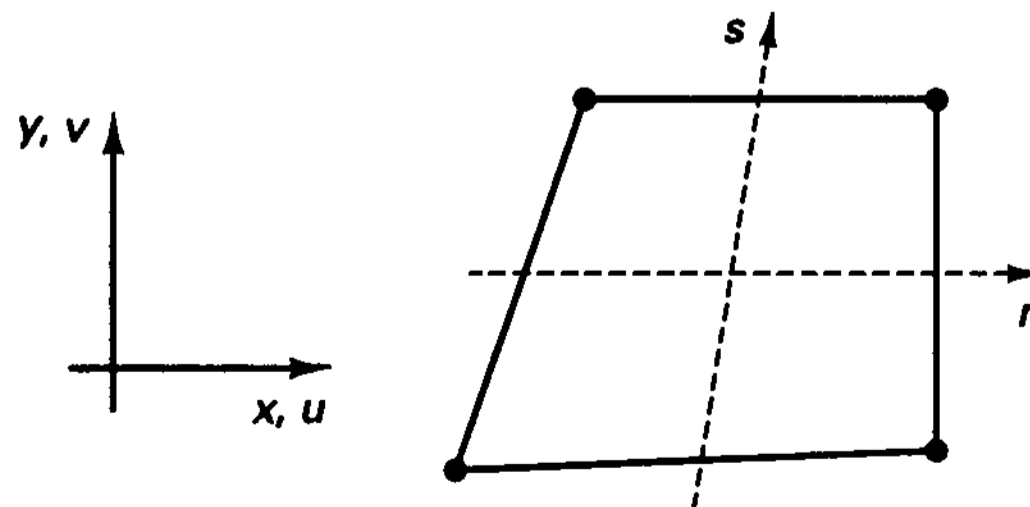
Displacement interpolation functions

$$u = \sum_{i=1}^4 h_i u_i + \alpha_1 \phi_1 + \alpha_2 \phi_2$$

$$v = \sum_{i=1}^4 h_i v_i + \alpha_3 \phi_1 + \alpha_4 \phi_2$$

$$\phi_1 = (1 - x^2); \phi_2 = (1 - y^2)$$

(a) Square element



(b) General quadrilateral element (here h_i and ϕ_i are used with r, s coordinates; see Section 5.2)

Figure E4.28 Four-node plane stress element with incompatible modes, constant thickness

For this element formulation we can analytically investigate whether, or under which conditions, the patch test is passed. First, we recall that the patch test is passed for the four-node compatible element (i.e., when the ϕ_1, ϕ_2 displacement interpolations are not used).

Next, let us consider that the element is placed in a condition of constant stresses τ^c . Then the requirement for passing the patch test is that, in these constant stress conditions, the element should behave in the same way as the four-node compatible element.

The formal mathematical condition can be derived by considering the stiffness matrix of the element with incompatible modes.

Let

$$\hat{\mathbf{u}}^* = \begin{bmatrix} \hat{\mathbf{u}} \\ \boldsymbol{\alpha} \end{bmatrix}$$

with $\hat{\mathbf{u}}^T = [u_1 \dots u_4 : v_1 \dots v_4]$

and $\boldsymbol{\alpha}^T = [\alpha_1 \dots \alpha_4]$

Then $\boldsymbol{\epsilon} = [\mathbf{B} : \mathbf{B}_{IC}] \begin{bmatrix} \hat{\mathbf{u}} \\ \boldsymbol{\alpha} \end{bmatrix}$

where \mathbf{B} is the usual strain-displacement matrix of the four-node element and \mathbf{B}_{IC} is the contribution due to the incompatible modes.

Hence, with our usual notation, we have

$$\begin{bmatrix} \int_V \mathbf{B}^T \mathbf{C} \mathbf{B} dV & \int_V \mathbf{B}^T \mathbf{C} \mathbf{B}_{IC} dV \\ \int_V \mathbf{B}_{IC}^T \mathbf{C} \mathbf{B} dV & \int_V \mathbf{B}_{IC}^T \mathbf{C} \mathbf{B}_{IC} dV \end{bmatrix} \begin{bmatrix} \hat{\mathbf{u}} \\ \boldsymbol{\alpha} \end{bmatrix} = \begin{bmatrix} \mathbf{R} \\ \mathbf{0} \end{bmatrix} \quad (a)$$

In practice, the incompatible displacement parameters $\boldsymbol{\alpha}$ would now be statically condensed out to obtain the element stiffness matrix corresponding to only the $\hat{\mathbf{u}}$ degrees of freedom.

If the nodal point displacements are the physically correct values $\hat{\mathbf{u}}^c$ for the constant stresses τ^c , we have

$$\int_V \mathbf{B}_{IC}^T \mathbf{C} \mathbf{B} dV \hat{\mathbf{u}}^c = \int_V \mathbf{B}_{IC}^T \tau^c dV \quad (b)$$

To now force the element to behave under constant stress conditions in the same way as the four-node compatible element, we require that (since the entries τ^c are independent of each other)

$$\int_V \mathbf{B}_{IC}^T dV = \mathbf{0} \quad (c)$$

Namely, when (c) is satisfied, we find from (a):

If the nodal point forces of the element are those of the compatible four-node element, the solution is $\hat{\mathbf{u}} = \hat{\mathbf{u}}^c$ and $\boldsymbol{\alpha} = \mathbf{0}$. Also, of course, if we set $\hat{\mathbf{u}} = \hat{\mathbf{u}}^c$ and $\boldsymbol{\alpha} = \mathbf{0}$, we obtain from (a) the nodal point forces of the compatible four-node element and no forces corresponding to the incompatible modes.

Hence, under constant stress conditions the element behaves as if the incompatible modes were not present.

We can now easily check that the condition in (c) is satisfied for the square element:

$$\int_V \begin{bmatrix} -2x & 0 & 0 & 0 \\ 0 & 0 & 0 & -2y \\ 0 & -2y & -2x & 0 \end{bmatrix} dV = \mathbf{0}$$

However, we can also check that the condition is not satisfied for the general quadrilateral element (here the Jacobian transformation of Section 5.2 is used to evaluate \mathbf{B}_{IC}). In order to satisfy (c) we therefore modify the \mathbf{B}_{IC} matrix by a correction \mathbf{B}_{IC}^C and use

$$\mathbf{B}_{IC}^{new} = \mathbf{B}_{IC} + \mathbf{B}_{IC}^C$$

The condition (c) on \mathbf{B}_{IC}^{new} gives

$$\mathbf{B}_{IC}^C = -\frac{1}{V} \int_V \mathbf{B}_{IC} dV$$

The element stiffness matrix is then obtained by using \mathbf{B}_{IC}^{new} in (a) instead of \mathbf{B}_{IC} . In practice, the element stiffness matrix is evaluated by numerical integration (see Chapter 5), and \mathbf{B}_{IC}^C is calculated by numerical integration prior to the evaluation of (a).

With the above patch test we test only for the constant stress conditions. Any patch of elements with incompatibilities must be able to represent these conditions if convergence is to be ensured.

In essence, this patch test is a boundary value problem in which the external forces are prescribed (the forces \mathbf{f}^B are zero and the tractions \mathbf{f}^S are constant) and the deformations and internal stresses are calculated (the rigid body modes are merely suppressed to render the solution possible). If the deformations and constant stresses are correctly predicted, the patch test is passed, and (because at least constant stresses can be correctly predicted) convergence in stresses will be at least $o(h)$.

This interpretation of the patch test suggests that we may in an analogous manner also test for the order of convergence of a discretization. Namely, using the same concept, we may instead apply the external forces that correspond to higher-order variations of internal stresses and test whether these stresses are correctly predicted. For example, in order to test whether a discretization will give a quadratic order of stress convergence, that is, whether the stresses converge $o(h^2)$, a linear stress variation needs to be correctly represented. We infer from the basic differential equations of equilibrium that the corresponding patch test is to apply a constant value of internal forces and the corresponding boundary tractions. While numerical results are again of interest and are valuable as in the test for constant stress conditions, only analytical results can ensure that for all geometric element distortions in the patch the correct stresses and deformations are obtained (see Section 5.3.3 for further discussion and results).

Of course, in practice, when testing element formulations, this formal procedure of evaluating the order of convergence frequently is not followed, and instead a sequence of simple test problems is used to identify the predictive capability of an element.

4.4.2 Mixed Formulations

To formulate the displacement-based finite elements we have used the principle of virtual displacements, which is equivalent to invoking the stationarity of the total potential energy Π (see Example 4.4). The essential theory used can be summarized briefly as follows.

1. We use¹⁵

$$\begin{aligned} \Pi(\mathbf{u}) &= \frac{1}{2} \int_V \boldsymbol{\epsilon}^T \mathbf{C} \boldsymbol{\epsilon} dV - \int_V \mathbf{u}^T \mathbf{f}^B dV - \int_{S_f} \mathbf{u}^{S_f T} \mathbf{f}^{S_f} dS \\ &= \text{stationary} \end{aligned} \tag{4.109}$$

with the conditions $\boldsymbol{\epsilon} = \boldsymbol{\partial}_\epsilon \mathbf{u}$ (4.110)

$$\mathbf{u}^{S_u} - \mathbf{u}_p = \mathbf{0} \tag{4.111}$$

where $\boldsymbol{\partial}_\epsilon$ represents the differential operator on \mathbf{u} to obtain the strain components, the vector \mathbf{u}_p contains the prescribed displacements, and the vector \mathbf{u}^{S_u} lists the corresponding displacement components of \mathbf{u} .

If the strain components are ordered as in (4.3), we have

$$\mathbf{u} = \begin{bmatrix} u(x, y, z) \\ v(x, y, z) \\ w(x, y, z) \end{bmatrix}; \quad \boldsymbol{\partial}_\epsilon = \begin{bmatrix} \frac{\partial}{\partial x} & 0 & 0 \\ 0 & \frac{\partial}{\partial y} & 0 \\ 0 & 0 & \frac{\partial}{\partial z} \\ \frac{\partial}{\partial y} & \frac{\partial}{\partial x} & 0 \\ 0 & \frac{\partial}{\partial z} & \frac{\partial}{\partial y} \\ \frac{\partial}{\partial z} & 0 & \frac{\partial}{\partial x} \end{bmatrix}$$

2. The equilibrium equations are obtained by invoking the stationarity of Π (with respect to the displacements which appear in the strains),

$$\int_V \delta \boldsymbol{\epsilon}^T \mathbf{C} \boldsymbol{\epsilon} dV = \int_V \delta \mathbf{u}^T \mathbf{f}^B dV + \int_{S_f} \delta \mathbf{u}^{S_f T} \mathbf{f}^{S_f} dS \tag{4.112}$$

The variations on \mathbf{u} must be zero at and corresponding to the prescribed displacements on the surface area S_u . We recall that to obtain from (4.112) the differential equations of equilibrium and the stress (natural) boundary conditions we substitute $\mathbf{C} \boldsymbol{\epsilon} = \boldsymbol{\tau}$ and reverse the process of transformation employed in Example 4.2 (see Sections 3.3.2 and 3.3.4). Therefore, the stress-strain relationship, the strain-displacement conditions [in (4.110)], and the displacement boundary conditions [in (4.111)] are directly fulfilled, and the condition of differential equilibrium (in the interior and on the boundary) is a consequence of the stationarity condition of Π .

3. In the displacement-based-finite element solution the stress-strain relationship, the strain-displacement conditions [in (4.110)], and the displacement boundary conditions [in (4.111)] are satisfied exactly, but the differential equations of equilibrium in the interior and the stress (natural) boundary conditions are satisfied only in the limit as the number of elements increases.

¹⁵ In this section, as in equation (4.7), we use the notation \mathbf{f}^{S_f} instead of the usual \mathbf{f}^S to explicitly denote that these are tractions applied to S_f . Similarly, we have in this section also the tractions \mathbf{f}^{S_u} and the surface displacements \mathbf{u}^{S_f} and \mathbf{u}^{S_u} . For definitions of these quantities, see Section 4.2.1.

The important point to note concerning the use of (4.109) to (4.112) for a finite element solution is that the only solution variables are the displacements which must satisfy the displacement boundary conditions in (4.111) and appropriate interelement conditions. Once we have calculated the displacements, other variables of interest such as strains and stresses can be directly obtained.

In practice, the displacement-based finite element formulation is used most frequently; however, other techniques have also been employed successfully and in some cases are much more effective (see Section 4.4.3).

Some very general finite element formulations are obtained by using variational principles that can be regarded as extensions of the principle of stationarity of total potential. These extended variational principles use not only the displacements but also the strains and/or stresses as primary variables. In the finite element solutions, the unknown variables are therefore then also displacements and strains and/or stresses. These finite element formulations are referred to as *mixed finite element formulations*.

Various extended variational principles can be used as the basis of a finite element formulation, and the use of many different finite element interpolations can be pursued. While a large number of mixed finite element formulations has consequently been proposed (see, for example, H. Kardestuncer and D. H. Norrie (eds.) [A] and F. Brezzi and M. Fortin [A]), our objective here is only to present briefly some of the basic ideas, which we shall then use to formulate some efficient solution schemes (see Sections 4.4.3 and 5.4).

To arrive at a very general and powerful variational principle we rewrite (4.109) in the form

$$\begin{aligned}\Pi^* &= \Pi - \int_V \boldsymbol{\lambda}_\epsilon^T (\boldsymbol{\epsilon} - \boldsymbol{\partial}_\epsilon \mathbf{u}) dV - \int_{S_u} \boldsymbol{\lambda}_u^T (\mathbf{u}^{S_u} - \mathbf{u}_p) dS \\ &= \text{stationary}\end{aligned}\quad (4.113)$$

where $\boldsymbol{\lambda}_\epsilon$ and $\boldsymbol{\lambda}_u$ are Lagrange multipliers and S_u is the surface on which displacements are prescribed. The Lagrange multipliers are used here to enforce the conditions (4.110) and (4.111) (see Section 3.4). The variables in (4.113) are \mathbf{u} , $\boldsymbol{\epsilon}$, $\boldsymbol{\lambda}_\epsilon$, and $\boldsymbol{\lambda}_u$. By invoking $\delta \Pi^* = 0$ the Lagrange multipliers $\boldsymbol{\lambda}_\epsilon$ and $\boldsymbol{\lambda}_u$ are identified, respectively, as the stresses $\boldsymbol{\tau}$ and tractions over S_u , \mathbf{f}^{S_u} , so that the variational indicator in (4.113) can be written as

$$\Pi_{\text{HW}} = \Pi - \int_V \boldsymbol{\tau}^T (\boldsymbol{\epsilon} - \boldsymbol{\partial}_\epsilon \mathbf{u}) dV - \int_{S_u} \mathbf{f}^{S_u T} (\mathbf{u}^{S_u} - \mathbf{u}_p) dS \quad (4.114)$$

This functional is referred to as the Hu-Washizu functional (see H. C. Hu [A] and K. Washizu [A, B]). The independent variables in this functional are the displacements \mathbf{u} , strains $\boldsymbol{\epsilon}$, stresses $\boldsymbol{\tau}$, and surface tractions \mathbf{f}^{S_u} . The functional can be used to derive a number of other functionals, such as the Hellinger-Reissner functionals (see E. Hellinger [A] and E. Reissner [A], Examples 4.30 and 4.31, and Exercise 4.36) and the minimum complementary energy functional, and can be regarded as the foundation of many finite element methods (see H. Kardestuncer and D. H. Norrie (eds.) [A], T. H. H. Pian and P. Tong [A], and W. Wunderlich [A]).

Invoking the stationarity of Π_{HW} with respect to \mathbf{u} , $\boldsymbol{\epsilon}$, $\boldsymbol{\tau}$, and \mathbf{f}^{S_u} , we obtain

$$\int_V \delta \boldsymbol{\epsilon}^T \mathbf{C} \boldsymbol{\epsilon} dV - \int_V \delta \mathbf{u}^T \mathbf{f}^B dV - \int_{S_f} \delta \mathbf{u}^{S_f T} \mathbf{f}^{S_f} dS - \int_V \delta \boldsymbol{\tau}^T (\boldsymbol{\epsilon} - \boldsymbol{\partial}_\epsilon \mathbf{u}) dV$$

$$- \int_V \boldsymbol{\tau}^T (\delta \boldsymbol{\epsilon} - \boldsymbol{\partial}_\epsilon \delta \mathbf{u}) dV - \int_{S_u} \delta \mathbf{f}^{S_u T} (\mathbf{u}^{S_u} - \mathbf{u}_p) dS - \int_{S_u} \mathbf{f}^{S_u T} \delta \mathbf{u}^{S_u} dS = 0 \quad (4.115)$$

where S_f is the surface on which known tractions are prescribed.

The above discussion shows that the Hu-Washizu variational formulation may be regarded as a generalization of the principle of virtual displacements, in which the displacement boundary conditions and strain compatibility conditions have been relaxed but then imposed by Lagrange multipliers, and variations are performed on all unknown displacements, strains, stresses, and unknown surface tractions. That this principle is indeed a valid and most general description of the static and kinematic conditions of the body under consideration follows because (4.115) yields, since (4.115) must hold for the individual variations used, the following.

For the volume of the body:

The stress-strain condition,

$$\boldsymbol{\tau} = \mathbf{C} \boldsymbol{\epsilon} \quad (4.116)$$

The compatibility condition,

$$\boldsymbol{\epsilon} = \boldsymbol{\partial}_\epsilon \mathbf{u} \quad (4.117)$$

The equilibrium conditions,

$$\begin{aligned} \frac{\partial \tau_{xx}}{\partial x} + \frac{\partial \tau_{xy}}{\partial y} + \frac{\partial \tau_{xz}}{\partial z} + f_x^B &= 0 \\ \frac{\partial \tau_{yx}}{\partial x} + \frac{\partial \tau_{yy}}{\partial y} + \frac{\partial \tau_{yz}}{\partial z} + f_y^B &= 0 \\ \frac{\partial \tau_{zx}}{\partial x} + \frac{\partial \tau_{zy}}{\partial y} + \frac{\partial \tau_{zz}}{\partial z} + f_z^B &= 0 \end{aligned} \quad (4.118)$$

For the surface of the body:

The applied tractions are equilibrated by the stresses,

$$\mathbf{f}^{S_f} = \bar{\boldsymbol{\tau}} \mathbf{n} \quad \text{on } S_f \quad (4.119)$$

The reactions are equilibrated by the stresses,

$$\mathbf{f}^{S_u} = \bar{\boldsymbol{\tau}} \mathbf{n} \quad \text{on } S_u \quad (4.120)$$

where \mathbf{n} represents the unit normal vector to the surface and $\bar{\boldsymbol{\tau}}$ contains in matrix form the components of the vector $\boldsymbol{\tau}$.

The displacements on S_u are equal to the prescribed displacements,

$$\mathbf{u}^{S_u} = \mathbf{u}_p \quad \text{on } S_u \quad (4.121)$$

The variational formulation in (4.115) represents a very general continuum mechanics formulation of the problems in elasticity.

Considering now the possibilities for finite element solution procedures, the Hu-Washizu variational principle and principles derived therefrom can be directly employed to derive various finite element discretizations. In these finite element solution procedures the applicable continuity requirements of the finite element variables between elements and on the boundaries need to be satisfied either directly or to be imposed by Lagrange multipliers. It now becomes apparent that with this added flexibility in formulating finite element methods a large number of different finite element discretizations can be devised, depending on which variational principle is used as the basis of the formulation, which finite element interpolations are employed, and how the continuity requirements are enforced. The various different discretization procedures have been classified as hybrid and mixed finite element formulations (see H. Kardestuncer and D. H. Norrie (eds.) [A] and T. H. H. Pian and P. Tong [A]).

We demonstrate the use of the Hu-Washizu principle in the following examples.

EXAMPLE 4.29: Consider the three-node truss element shown in Fig. E4.29. Assume a parabolic variation for the displacement and a linear variation in strain and stress. Also, let the stress and strain variables correspond to internal element degrees of freedom so that only the displacements at nodes 1 and 2 connect to the adjacent elements. Use the Hu-Washizu variational principle to calculate the element stiffness matrix.

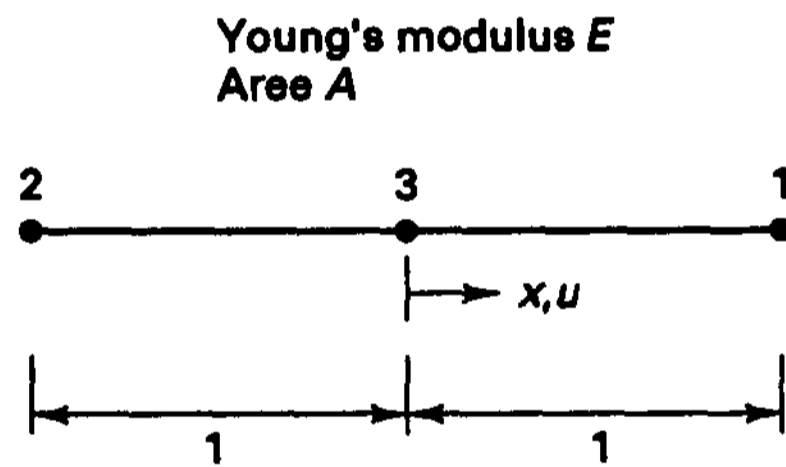


Figure E4.29 Three-node truss element

We can start directly with (4.115) to obtain

$$\underbrace{\int_V \delta \epsilon^T (C \epsilon - \tau) dV}_{\textcircled{1}} - \underbrace{\int_V \delta \tau^T (\epsilon - \partial_\epsilon u) dV}_{\textcircled{2}} + \underbrace{\int_V (\partial_\epsilon \delta u)^T \tau dV}_{\textcircled{3}} - \int_V \delta u^T f^B dV + \text{boundary terms} = 0 \tag{a}$$

where $\epsilon = \epsilon_{xx}; \quad \partial_\epsilon = \frac{\partial}{\partial x}; \quad \tau = \tau_{xx}; \quad C = E; \quad f^B = f_x^B$

and the boundary terms correspond to expressions for S_f and S_u and are not needed to evaluate the element stiffness matrix.

We now use the following interpolations:

$$u = \mathbf{H} \hat{\mathbf{u}}; \quad \mathbf{H} = \begin{bmatrix} \frac{(1+x)x}{2} & -\frac{(1-x)x}{2} & 1-x^2 \end{bmatrix}$$

$$\hat{\mathbf{u}}^T = [u_1 \quad u_2 \quad u_3]$$

$$\begin{aligned} \tau &= \mathbf{E}\hat{\tau}; & \mathbf{E} &= \begin{bmatrix} \frac{1+x}{2} & \frac{1-x}{2} \end{bmatrix} \\ \epsilon &= \mathbf{E}\hat{\epsilon} \\ \hat{\tau}^T &= [\tau_1 \quad \tau_2]; & \hat{\epsilon}^T &= [\epsilon_1 \quad \epsilon_2] \end{aligned}$$

Substituting the interpolations into (a), we obtain corresponding to term 1:

$$\delta \hat{\epsilon}^T \left[\left(\int_V \mathbf{E}^T \mathbf{C} \mathbf{E} dV \right) \hat{\epsilon} - \left(\int_V \mathbf{E}^T \mathbf{E} dV \right) \hat{\tau} \right]$$

corresponding to term 2:

$$\delta \hat{\tau}^T \left[- \left(\int_V \mathbf{E}^T \mathbf{E} dV \right) \hat{\epsilon} + \left(\int_V \mathbf{E}^T \mathbf{B} dV \right) \hat{\mathbf{u}} \right]$$

corresponding to term 3:

$$\delta \hat{\mathbf{u}}^T \left(\int_V \mathbf{B}^T \mathbf{E} dV \right) \hat{\tau}$$

where

$$\mathbf{B} = \left[\left(\frac{1}{2} + x \right) \quad \left(-\frac{1}{2} + x \right) \quad -2x \right]$$

Hence, we obtain

$$\begin{bmatrix} \mathbf{0} & \mathbf{0} & \mathbf{K}_{u\tau} \\ \mathbf{0} & \mathbf{K}_{\epsilon\epsilon} & \mathbf{K}_{\epsilon\tau} \\ \mathbf{K}_{u\tau}^T & \mathbf{K}_{\epsilon\tau}^T & \mathbf{0} \end{bmatrix} \begin{bmatrix} \hat{\mathbf{u}} \\ \hat{\epsilon} \\ \hat{\tau} \end{bmatrix} = \dots \tag{b}$$

where

$$\mathbf{K}_{\epsilon\epsilon} = \int_V \mathbf{E}^T \mathbf{C} \mathbf{E} dV$$

$$\mathbf{K}_{u\tau} = \int_V \mathbf{B}^T \mathbf{E} dV$$

and

$$\mathbf{K}_{\epsilon\tau} = - \int_V \mathbf{E}^T \mathbf{E} dV$$

If we now substitute the expressions for \mathbf{B} and \mathbf{E} and eliminate the ϵ_i and τ_i degrees of freedom (because they are assumed to pertain only to this element, thus allowing jumps in stresses and strains between adjacent elements), we obtain from (b)

$$\frac{EA}{6} \begin{bmatrix} 7 & 1 & -8 \\ 1 & 7 & -8 \\ -8 & -8 & 16 \end{bmatrix} \begin{bmatrix} u_1 \\ u_2 \\ u_3 \end{bmatrix} = \dots$$

This stiffness matrix is identical to the matrix of a three-node displacement-based truss element—as should be expected using a linear strain and parabolic displacement assumption.

However, we should note that if the element stress and strain variables are not eliminated on the element level and instead are used to impose continuity in stress and strain between elements, then clearly with the element stiffness matrix in (b) the stiffness matrix of the complete element assemblage is not positive definite.

This derivation could of course be extended to obtain the stiffness matrices of truss elements with various displacement, stress, and strain assumptions. However, a useful element is obtained only if the interpolations are “judiciously” chosen and actually fulfill specific requirements (see Section 4.5).

EXAMPLE 4.30: Consider the two-node beam element shown in Fig. E4.30. Assume linear variations in the transverse displacement w and section rotation θ and a constant element transverse shear strain γ . Establish the finite element equations.

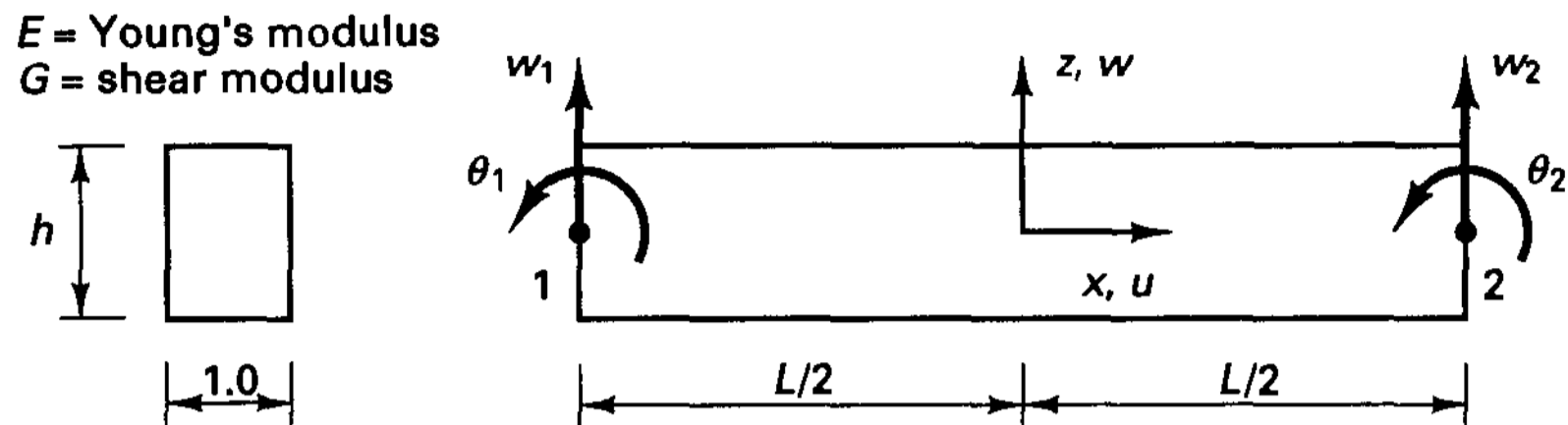


Figure E4.30 Two-node beam element

We assume that the stresses are given by the strains, and so we can substitute $\boldsymbol{\tau} = \mathbf{C}\boldsymbol{\epsilon}$ into (4.114) and obtain

$$\Pi_{\text{HR}}^* = \int_V \left(-\frac{1}{2} \boldsymbol{\epsilon}^T \mathbf{C} \boldsymbol{\epsilon} + \boldsymbol{\epsilon}^T \mathbf{C} \boldsymbol{\partial}_\epsilon \mathbf{u} - \mathbf{u}^T \mathbf{f}^B \right) dV + \text{boundary terms} \quad (\text{a})$$

This variational indicator is also a Hellinger-Reissner functional, but comparing (a) with the functional in Exercise 4.36, we note that here strains and displacements are the independent variables (instead of the stresses and displacements in Exercise 4.36).

In our beam formulation the variables are u , w , and γ_{xz}^{AS} (the superscript AS denotes the assumed constant value). Hence, the bending strain ϵ_{xx} is calculated from the displacement, and we can specialize (a) further:

$$\tilde{\Pi}_{\text{HR}}^* = \int_V \left(\frac{1}{2} \epsilon_{xx} E \epsilon_{xx} - \frac{1}{2} \gamma_{xz}^{\text{AS}} G \gamma_{xz}^{\text{AS}} + \gamma_{xz}^{\text{AS}} G \gamma_{xz} - \mathbf{u}^T \mathbf{f}^B \right) dV + \text{boundary terms}$$

where $\mathbf{u} = \begin{bmatrix} u \\ w \end{bmatrix}$; $\epsilon_{xx} = \frac{\partial u}{\partial x}$; $\gamma_{xz} = \frac{\partial w}{\partial x} + \frac{\partial u}{\partial z}$

Now invoking $\delta \tilde{\Pi}_{\text{HR}}^* = 0$, we obtain corresponding to $\delta \mathbf{u}$, (not including boundary terms)

$$\int_V (\delta \epsilon_{xx} E \epsilon_{xx} + \delta \gamma_{xz} G \gamma_{xz}^{\text{AS}}) dV = \int_V \delta \mathbf{u}^T \mathbf{f}^B dV \quad (\text{b})$$

and corresponding to $\delta \gamma_{xz}^{\text{AS}}$,

$$\int_V \delta \gamma_{xz}^{\text{AS}} G (\gamma_{xz} - \gamma_{xz}^{\text{AS}}) dV = 0 \quad (\text{c})$$

Let

$$\hat{\mathbf{u}} = \begin{bmatrix} w_1 \\ \theta_1 \\ w_2 \\ \theta_2 \end{bmatrix}; \quad \hat{\boldsymbol{\epsilon}} = [\gamma^{\text{AS}}]$$

Then we can write

$$\begin{aligned} \mathbf{u} &= \mathbf{H} \hat{\mathbf{u}}; & \epsilon_{xx} &= \mathbf{B}_b \hat{\mathbf{u}} \\ \gamma_{xz} &= \mathbf{B}_s \hat{\mathbf{u}}; & \gamma_{xz}^{\text{AS}} &= \mathbf{B}_s^{\text{AS}} \hat{\boldsymbol{\epsilon}} \end{aligned}$$

Substituting into (b) and (c), we obtain

$$\begin{bmatrix} \mathbf{K}_{uu} & \mathbf{K}_{ue} \\ \mathbf{K}_{ue}^T & \mathbf{K}_{ee} \end{bmatrix} \begin{bmatrix} \hat{\mathbf{u}} \\ \hat{\mathbf{e}} \end{bmatrix} = \begin{bmatrix} \mathbf{R}_B \\ \mathbf{0} \end{bmatrix} \tag{d}$$

where

$$\mathbf{K}_{uu} = \int_V \mathbf{B}_b^T E \mathbf{B}_b dV; \quad \mathbf{K}_{ue} = \int_V \mathbf{B}_s^T G \mathbf{B}_s^{AS} dV$$

$$\mathbf{K}_{ee} = - \int_V (\mathbf{B}_s^{AS})^T G \mathbf{B}_s^{AS} dV; \quad \mathbf{R}_B = \int_V \mathbf{H}^T \mathbf{f}^B dV$$

We can now use static condensation on $\hat{\mathbf{e}}$ to obtain the final element stiffness matrix:

$$\mathbf{K} = \mathbf{K}_{uu} - \mathbf{K}_{ue} \mathbf{K}_{ee}^{-1} \mathbf{K}_{ue}^T$$

In our case, we have

$$\mathbf{H} = \begin{bmatrix} 0 & -\frac{z}{L} \left(\frac{L}{2} - x \right) & 0 & -\frac{z}{L} \left(\frac{L}{2} + x \right) \\ \frac{1}{L} \left(\frac{L}{2} - x \right) & 0 & \frac{1}{L} \left(\frac{L}{2} + x \right) & 0 \end{bmatrix}$$

$$\mathbf{B}_b = \begin{bmatrix} 0 & \frac{z}{L} & 0 & -\frac{z}{L} \end{bmatrix}$$

$$\mathbf{B}_s = \begin{bmatrix} -\frac{1}{L} & -\frac{1}{L} \left(\frac{L}{2} - x \right) & \frac{1}{L} & -\frac{1}{L} \left(\frac{L}{2} + x \right) \end{bmatrix}$$

$$\mathbf{B}_s^{AS} = [1]$$

so that

$$\mathbf{K} = \begin{bmatrix} \frac{Gh}{L} & \frac{Gh}{2} & \frac{-Gh}{L} & \frac{Gh}{2} \\ \frac{Gh}{2} & \left(\frac{GhL}{4} \right) + \frac{Eh^3}{12L} & \frac{-Gh}{2} & \left(\frac{GhL}{4} \right) - \frac{Eh^3}{12L} \\ \frac{-Gh}{L} & \frac{-Gh}{2} & \frac{Gh}{L} & \frac{-Gh}{2} \\ \frac{Gh}{2} & \left(\frac{GhL}{4} \right) - \frac{Eh^3}{12L} & \frac{-Gh}{2} & \left(\frac{GhL}{4} \right) + \frac{Eh^3}{12L} \end{bmatrix} \tag{e}$$

It is interesting to note that a pure displacement formulation would give a very similar stiffness matrix. The only difference is that the circled terms would be $GhL/3$ on the diagonal and $GhL/6$ in the off-diagonal locations. However, the element predictive capability of the pure displacement-based formulation is drastically different, displaying a behavior that is much too stiff when the element is thin (we discuss this phenomenon in Sections 4.5.7 and 5.4.1).

Note that if we assume a displacement vector corresponding to section rotations only,

$$\hat{\mathbf{u}} = [0 \quad \alpha \quad 0 \quad -\alpha]$$

then using (e) the element displays bending stiffness only, whereas the pure displacement-based element shows an erroneous shear contribution.

Let us finally note that the stiffness matrix in (e) corresponds to the matrix obtained in the mixed interpolation approach discussed in detail in Section 5.4.1. Namely, if we use the last equation in (d), which corresponds to the equation (c), we obtain

$$\gamma_{xz}^{AS} = \frac{w_2 - w_1}{L} - \frac{\theta_1 + \theta_2}{2}$$

which shows that the assumed shear strain value is equal to the shear strain value at the midpoint of the beam calculated from the nodal point displacements.

As pointed out above, the Hu-Washizu principle provides the basis for the derivation of various variational principles, and many different mixed finite element discretizations can be designed. However, whether a specific finite element discretization is effective for practical analysis depends on a number of factors, particularly on whether the method is general for a certain class of applications, whether the method is stable with a sufficiently high rate of convergence, how efficient the method is computationally, and how the method compares to alternative schemes. While mixed finite element discretizations can offer some advantages in certain analyses, compared to the standard displacement-based discretization, there are two large areas in which the use of mixed elements is much more efficient than the use of pure displacement-based elements. These two areas are the analysis of almost incompressible media and the analysis of plate and shell structures (see the following sections and Section 5.4).

4.4.3 Mixed Interpolation—Displacement/Pressure Formulations for Incompressible Analysis

The displacement-based finite element procedure described in Section 4.2 is very widely used because of its simplicity and general effectiveness. However, there are two problem areas in which the pure displacement-based finite elements are not sufficiently effective, namely, the analysis of incompressible (or almost incompressible) media and the analysis of plates and shells. In each of these cases, a mixed interpolation approach—which can be thought of as a special use of the Hu-Washizu variational principle (see Example 4.30)—is far more efficient.

We discuss the mixed interpolation for beam, plate, and shell analyses in Section 5.4, and we address here the analysis of incompressible media.

Although we are dealing with the solution of incompressible solid media, the same basic observations are also directly applicable to the analysis of incompressible fluids (see Section 7.4). For example, the elements summarized in Tables 4.6 and 4.7 (later in this section) are also used effectively in fluid flow solutions.

The Basic Differential Equations for Incompressible Analysis

In the analysis of solids, it is frequently necessary to consider that the material is almost incompressible. For example, some rubberlike materials, and materials in inelastic conditions, may exhibit an almost incompressible response. Indeed, the compressibility effects may be so small that they could be neglected, in which case the material would be idealized as totally incompressible.

A basic observation in the analysis of almost incompressible media is that the pressure is difficult to predict accurately. Depending on how close the material is to being incompressible, the displacement-based finite element method may still provide accurate solutions, but the number of elements required to obtain a given solution accuracy is usually far greater than the number of elements required in a comparable analysis involving a compressible material.

To identify the basic difficulty in more detail, let us again consider the three-dimensional body in Fig. 4.1. The material of the body is isotropic and is described by Young's modulus E and Poisson's ratio ν .

Using indicial notation, the governing differential equations for this body are (see Example 4.2)

$$\tau_{ij,j} + f_i^B = 0 \quad \text{throughout the volume } V \text{ of the body} \quad (4.122)$$

$$\tau_{ij}n_j = f_i^{S_f} \quad \text{on } S_f \quad (4.123)$$

$$u_i = u_i^{S_u} \quad \text{on } S_u \quad (4.124)$$

If the body is made of an almost incompressible material, we anticipate that the volumetric strains will be small in comparison to the deviatoric strains, and therefore we use the constitutive relations in the form (see Exercise 4.39)

$$\tau_{ij} = \kappa \epsilon_v \delta_{ij} + 2G \epsilon'_{ij} \quad (4.125)$$

where κ is the bulk modulus,

$$\kappa = \frac{E}{3(1 - 2\nu)} \quad (4.126)$$

ϵ_v is the volumetric strain,

$$\begin{aligned} \epsilon_v &= \epsilon_{kk} \\ &= \frac{\Delta V}{V} \quad (= \epsilon_{xx} + \epsilon_{yy} + \epsilon_{zz} \text{ in Cartesian coordinates}) \end{aligned} \quad (4.127)$$

δ_{ij} is the Kronecker delta,

$$\delta_{ij} \begin{cases} = 1; & i = j \\ = 0; & i \neq j \end{cases} \quad (4.128)$$

ϵ'_{ij} are the deviatoric strain components,

$$\epsilon'_{ij} = \epsilon_{ij} - \frac{\epsilon_v}{3} \delta_{ij} \quad (4.129)$$

and G is the shear modulus,

$$G = \frac{E}{2(1 + \nu)} \quad (4.130)$$

We also have for the pressure in the body,

$$p = -\kappa \epsilon_v \quad (4.131)$$

where
$$p = -\frac{\tau_{kk}}{3} \left(= -\frac{\tau_{xx} + \tau_{yy} + \tau_{zz}}{3} \text{ in Cartesian coordinates} \right) \quad (4.132)$$

Now let us gradually increase κ (by increasing the Poisson ratio ν to approach 0.5). Then, as κ increases, the volumetric strain ϵ_v decreases and becomes very small.

In fact, in total incompressibility ν is exactly equal to 0.5, the bulk modulus is infinite, the volumetric strain is zero, and the pressure is of course finite (and of the order of the applied boundary tractions). The stress components are then expressed as [see (4.125) and (4.131)]

$$\tau_{ij} = -p\delta_{ij} + 2G\epsilon'_{ij} \quad (4.133)$$

and the solution of the governing differential equations (4.122) to (4.124) now involves using the displacements *and* the pressure as unknown variables.

In addition, special attention need also be given to the boundary conditions in (4.123) and (4.124) when material incompressibility is being considered and the displacements are prescribed on the complete surface of the body, i.e., when we have the special case $S_u = S$, $S_f = 0$. If the material is totally incompressible, a *first condition* is that the prescribed displacements u_i^s must be compatible with the zero volumetric strain throughout the body. This physical observation is expressed as

$$\epsilon_{ii} = 0 \quad \text{throughout } V \quad (4.134)$$

hence,
$$\int_V \epsilon_{ii} dV = \int_S \mathbf{u}^s \cdot \mathbf{n} dS = 0 \quad (4.135)$$

where we used the divergence theorem and \mathbf{n} is the unit normal vector on the surface of the body. Hence, the displacements prescribed normal to the body surface must be such that the volume of the body is preserved. This condition will of course be automatically satisfied if the prescribed surface displacements are zero (the particles on the surface of the body are not displaced).

Assuming that the volumetric strain/boundary displacement compatibility is satisfied, for the case $S_u = S$, the *second condition* is that the pressure must be prescribed at some point in the body. Otherwise, the pressure is not unique because an arbitrary constant pressure does not cause any deformations. Only when both these conditions are fulfilled is the problem well posed for solution.

Of course, the condition of prescribed displacements on the complete surface of the body is a somewhat special case in the analysis of solids, but we encounter an analogous situation frequently in fluid mechanics. Here the velocities may be prescribed on the complete boundary of the fluid domain (see Chapter 7).

Although we considered here a totally incompressible medium, it is clear that these considerations are also important when the material is only almost incompressible—a violation of the conditions discussed will lead to an ill-posed problem statement.

Of course, these observations also pertain to the use of the principle of virtual work. Let us consider the simple example shown in Fig. 4.19. Since only volumetric strain energy is present, the principle of virtual work gives for this case,

$$\int_V \bar{\epsilon}_v \kappa \epsilon_v dV = - \int_{S_f} \bar{v}^s p^* dS \quad (4.136)$$

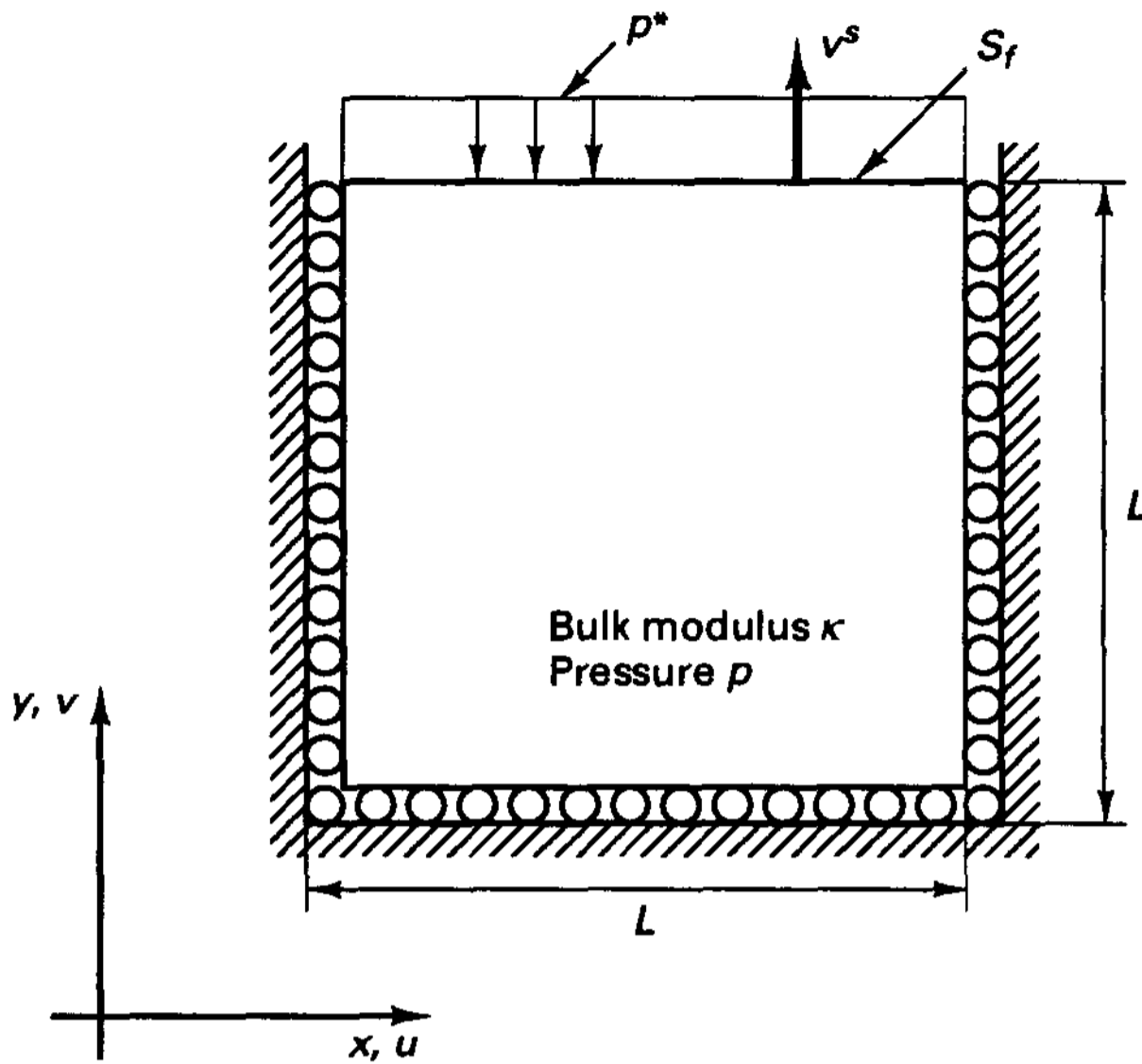


Figure 4.19 Block of material in plane strain condition, subjected to uniform surface pressure p^*

If the bulk modulus κ is finite, we obtain directly from (4.136),

$$v^s = -\frac{p^*L}{\kappa} \tag{4.137}$$

and

$$p = p^* \tag{4.138}$$

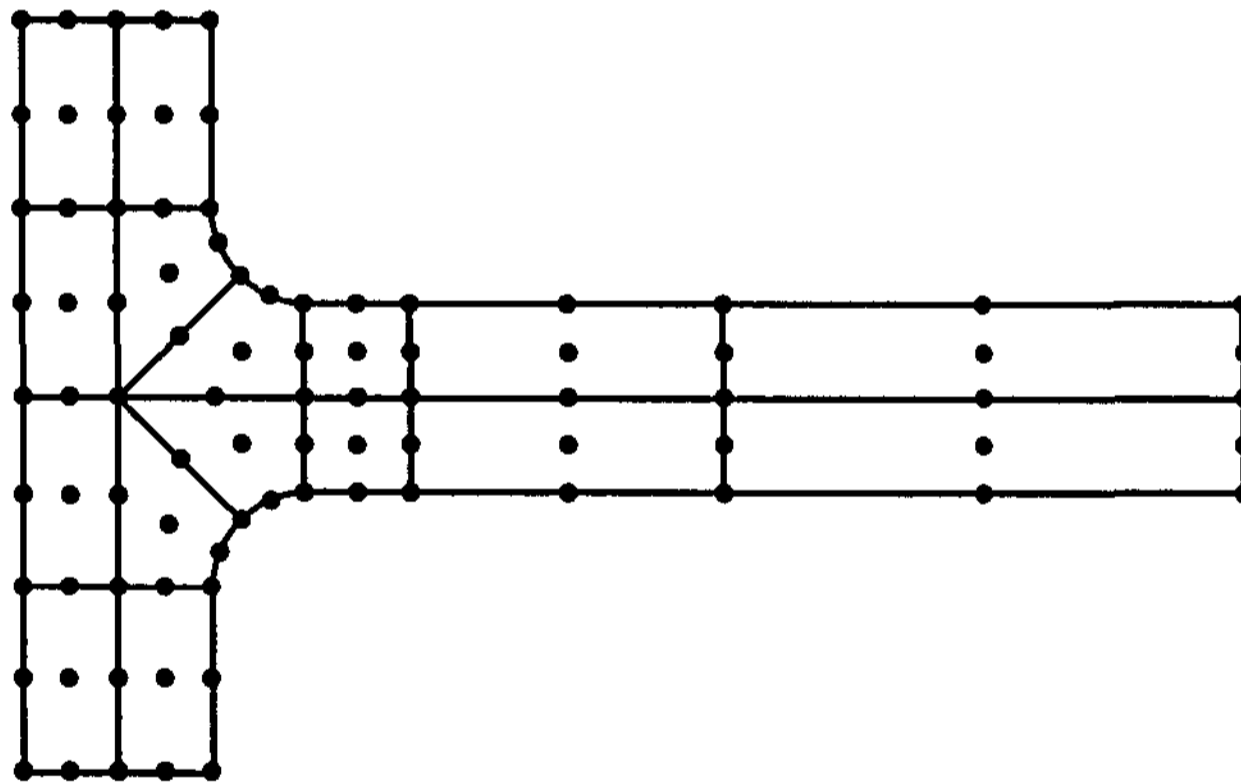
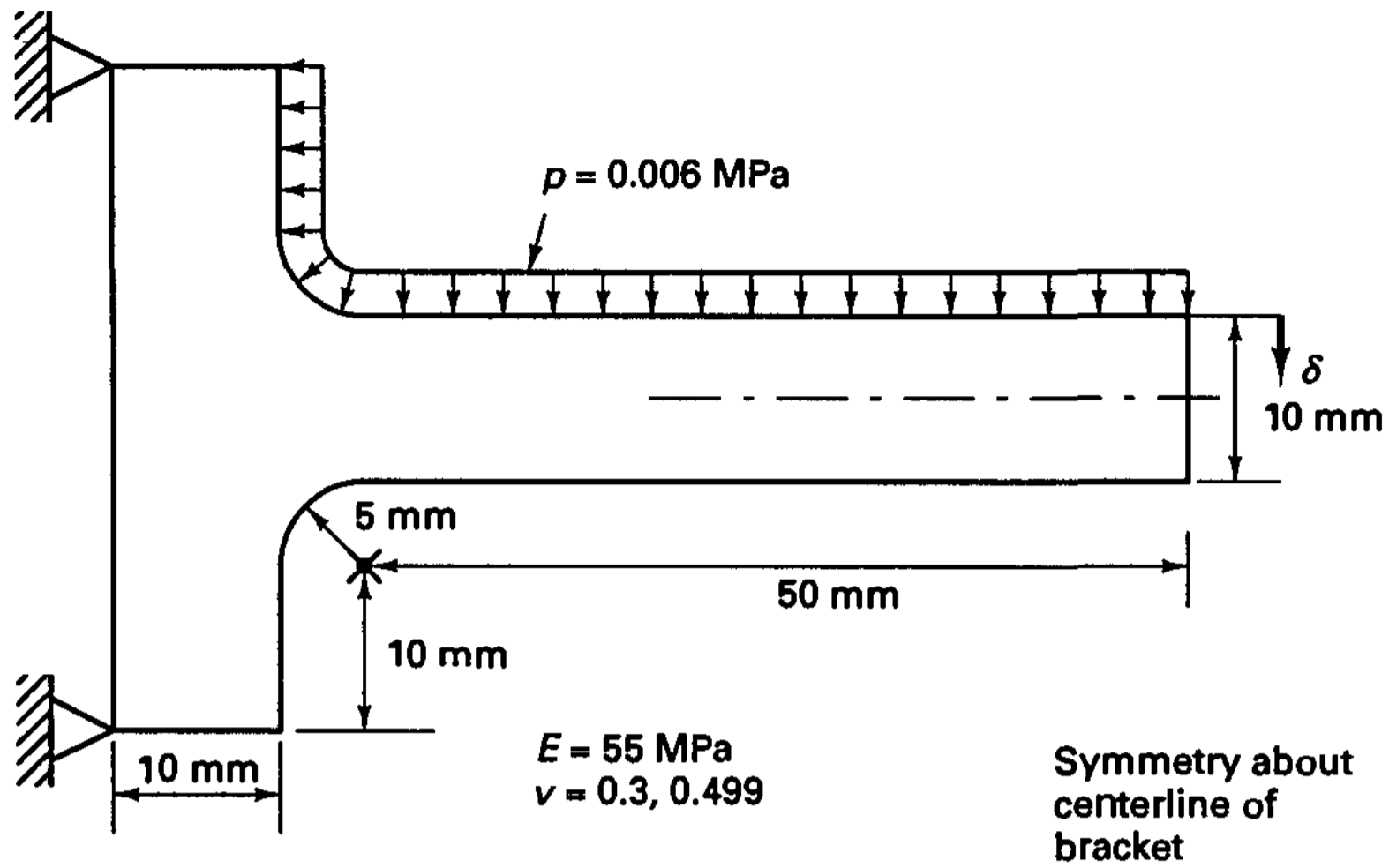
However, if κ is infinite, we need to use instead of (4.136) the following form of the principle of virtual work, with the pressure p unknown,

$$\int_V \bar{\epsilon}_v(-p) dV = -\int_{S_f} \bar{v}^s p^* dS \tag{4.139}$$

and we again obtain $p = p^*$. Of course, the solution of (4.139) does not use the constitutive relation but only the equilibrium condition.

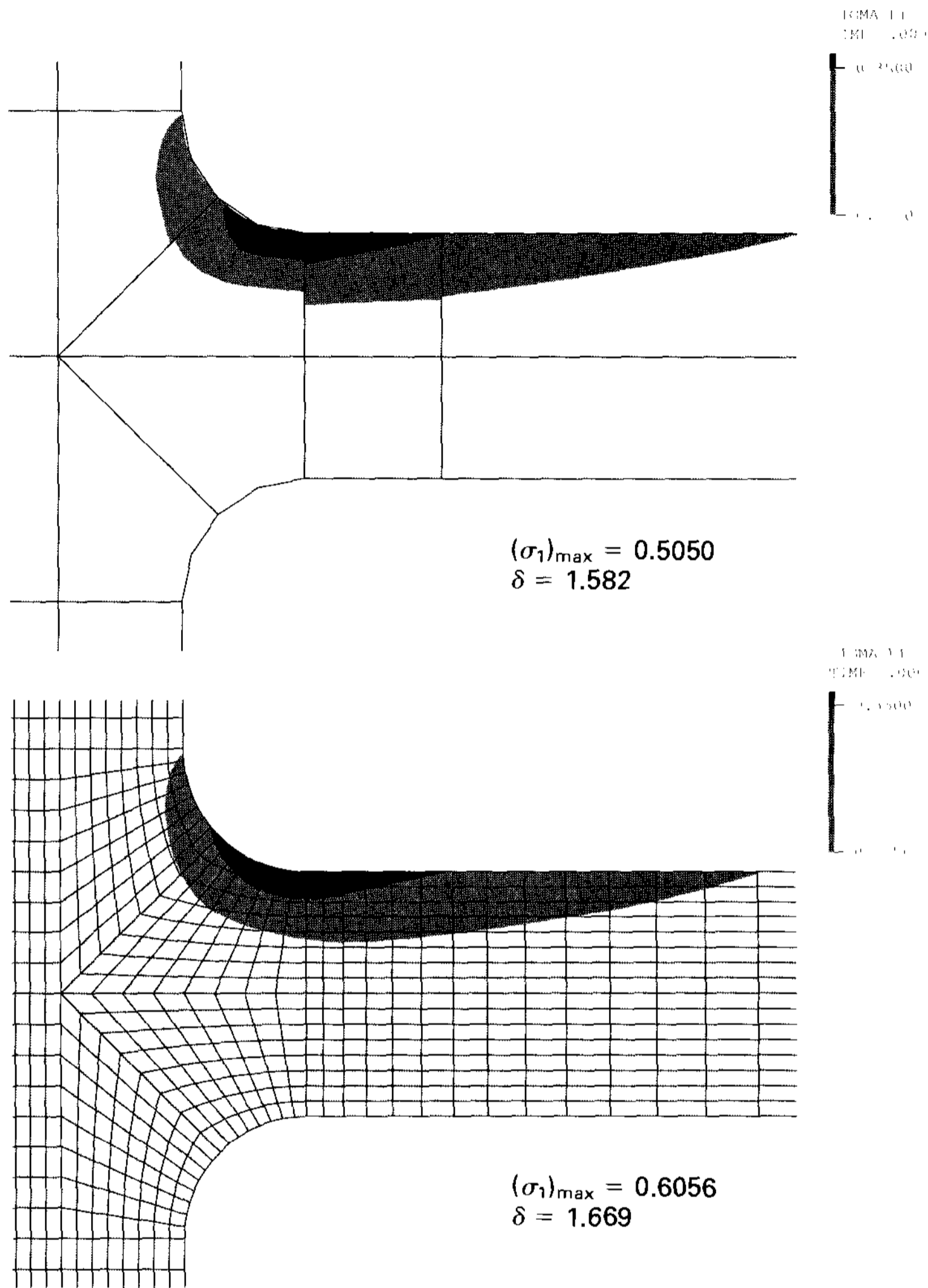
The Finite Element Solution of Almost Incompressible Conditions

The preceding discussion indicates that when pursuing a pure displacement-based finite element analysis of an almost incompressible medium, significant difficulties must be expected. The very small volumetric strain, approaching zero in the limit of total incompressibility, is determined from derivatives of displacements, which are not as accurately predicted as the displacements themselves. Any error in the predicted volumetric strain will appear as a large error in the stresses, and this error will in turn also affect the displacement prediction since the external loads are balanced (using the principle of virtual work) by the stresses. In practice, therefore, a very fine finite element discretization may be required to obtain good solution accuracy.



(a) Geometry, material data, applied loading, and the coarse sixteen element mesh

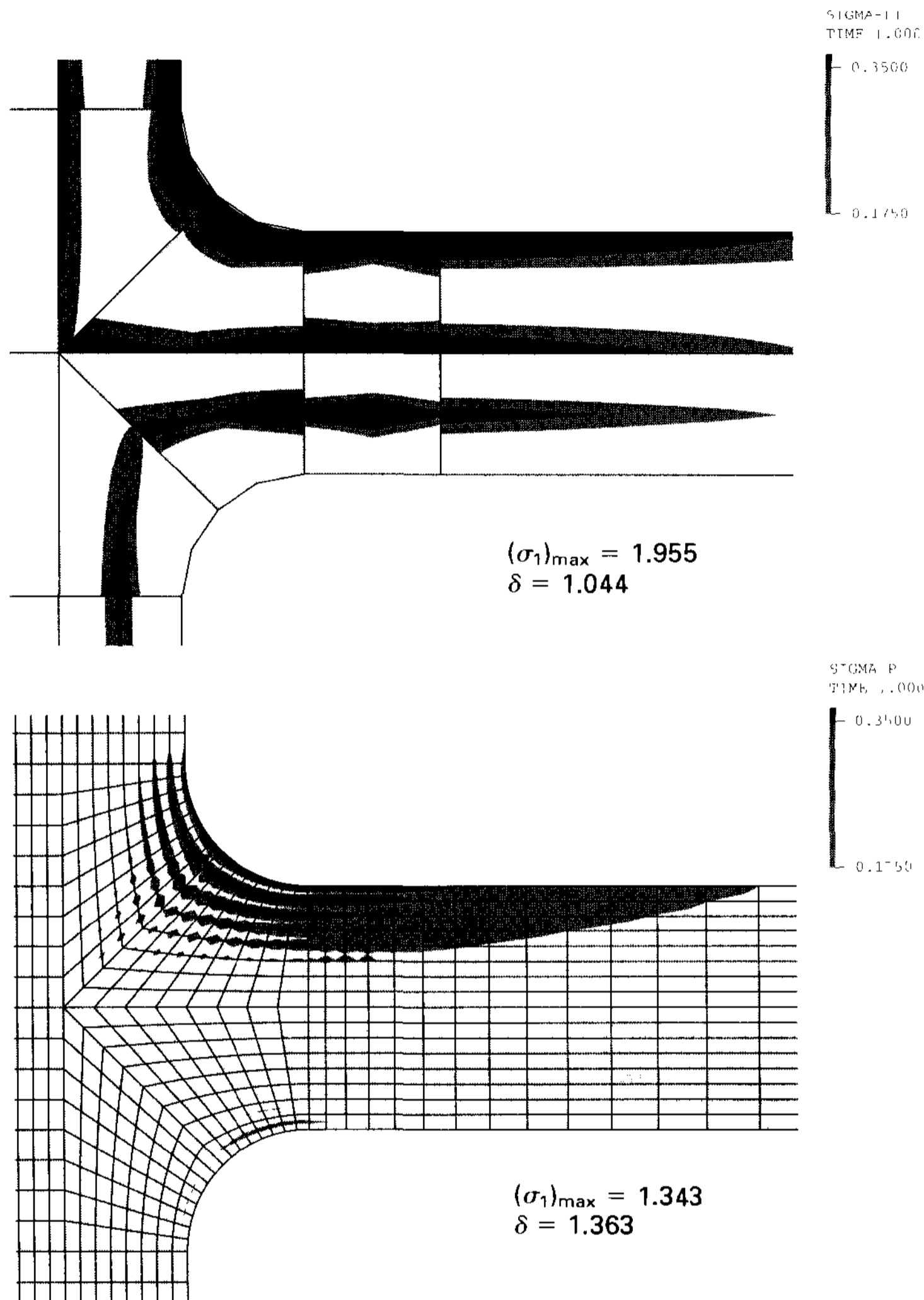
Figure 4.20 Analysis of cantilever bracket in plane strain conditions. Nine-node displacement-based elements are used. The $16 \times 64 = 1024$ -element mesh is obtained by dividing each element of the 16-element mesh into 64 elements. Maximum principal stress results are shown using the band representation of Fig. 4.15. Also, $(\sigma_1)_{\max}$ is the predicted maximum value of the maximum principal stress, and δ is defined in (a).



(b) Displacement-based element solution results for the case Poisson's ratio $\nu = 0.30$. Sixteen element and 16×64 element mesh results

Figure 4.20 (continued)

Figure 4.20 shows some results obtained in the analysis of a cantilever bracket subjected to pressure loading. We consider plane strain conditions and the cases of Poisson's ratio $\nu = 0.30$ and $\nu = 0.499$. In all solutions, nine-node displacement-based elements have been used (with 3×3 Gauss integration; see Section 5.5.5). A coarse mesh and a very fine mesh are used, and Fig. 4.20(a) shows the coarse idealization using only 16 elements. The solution results for the maximum principal stress σ_1 are shown using the isoband representation discussed in Section 4.3.6. Here we have selected the bandwidth so as to be able to see the rather poor performance of the displacement-based element when the Poisson ratio is close to 0.5. Figure 4.20(b) shows that when $\nu = 0.30$, the element stresses are reasonably smooth across boundaries for the coarse mesh and very smooth for the fine mesh. Indeed, the coarse idealization gives a quite reasonable stress prediction. However,



(c) Displacement-based element solution results for the case Poisson's ratio $\nu = 0.499$. Sixteen element and 16×64 element mesh results

Figure 4.20 (continued)

when $\nu = 0.499$, the same meshes of nine-node displacement-based elements result into poor stress predictions [see Fig. 4.20(c)]. Large stress fluctuations are seen in the individual elements of the coarse mesh *and* the fine mesh.¹⁶ Hence, in summary, we see here that the displacement-based element used in the analysis is effective when $\nu = 0.3$, but as ν approaches 0.5, the stress prediction becomes very inaccurate.

This discussion indicates what is very desirable, namely, a finite element formulation which gives essentially the same accuracy in results for a given mesh irrespective of what Poisson's ratio is used, even when ν is close to 0.5. Such behavior is observed if for the finite

¹⁶ We discuss briefly in Section 5.5.6 the use of "reduced integration." If in this analysis the reduced integration of 2×2 Gauss integration is attempted, the solution cannot be obtained because the resulting stiffness matrix is singular.

element formulation the predictive capability of displacements and stresses is independent of the bulk modulus used.

We refer to finite element formulations with this desirable behavior as *nonlocking*, whereas otherwise the finite elements are *locking*.

The term “locking” is based upon experiences in the analysis of beams, plates, and shells (see Section 5.4.1), where an inappropriate formulation—one that locks—results in displacements very much smaller than those intuitively expected for a given mesh (and calculated with an appropriate formulation; see, for example, Fig. 5.20). In the analysis of almost incompressible behavior, using a formulation that locks, the displacements are not necessarily that much in error but the stresses (the pressure) are very inaccurate. We note that the pure displacement formulation generally locks in almost incompressible analysis. These statements are discussed more precisely in Section 4.5.

Effective finite element formulations for the analysis of almost incompressible behavior that do not lock are obtained by interpolating displacements and pressure. Figure 4.21 shows the results obtained in the analysis of the cantilever bracket in Fig. 4.20 with a displacement/pressure formulation referred to as *u/p* formulation using the 9/3 element (see below for the explanation of the formulation and the element). We see that the isobands of the maximum principal stress have in all cases the desirable degree of smoothness and that the stress prediction does not deteriorate when Poisson’s ratio ν approaches 0.5.

To introduce the displacement/pressure formulations, we recall that in a pure displacement formulation, the evaluation of the pressure from the volumetric strain is difficult when κ is large (in comparison to G) and that when a totally incompressible condition is considered, the pressure must be used as a solution variable [see (4.133)]. It therefore appears reasonable to work with the unknown displacements *and* pressure as solution variables when almost incompressible conditions are analyzed. Such analysis procedures, if properly formulated, should then also be directly applicable to the limit of incompressible conditions.

The basic approach of displacement/pressure finite element formulations is therefore to interpolate the displacements and the pressure. This requires that we express the principle of virtual work in terms of the independent variables \mathbf{u} and p , which gives

$$\int_V \bar{\boldsymbol{\epsilon}}'^T \mathbf{S} \, dV - \int_V \bar{\epsilon}_v p \, dV = \mathcal{R} \tag{4.140}$$

where, as usual, the overbar indicates virtual quantities, \mathcal{R} corresponds to the usual external virtual work [\mathcal{R} is equal to the right-hand side of (4.7)], and \mathbf{S} and $\boldsymbol{\epsilon}'$ are the deviatoric stress and strain vectors,

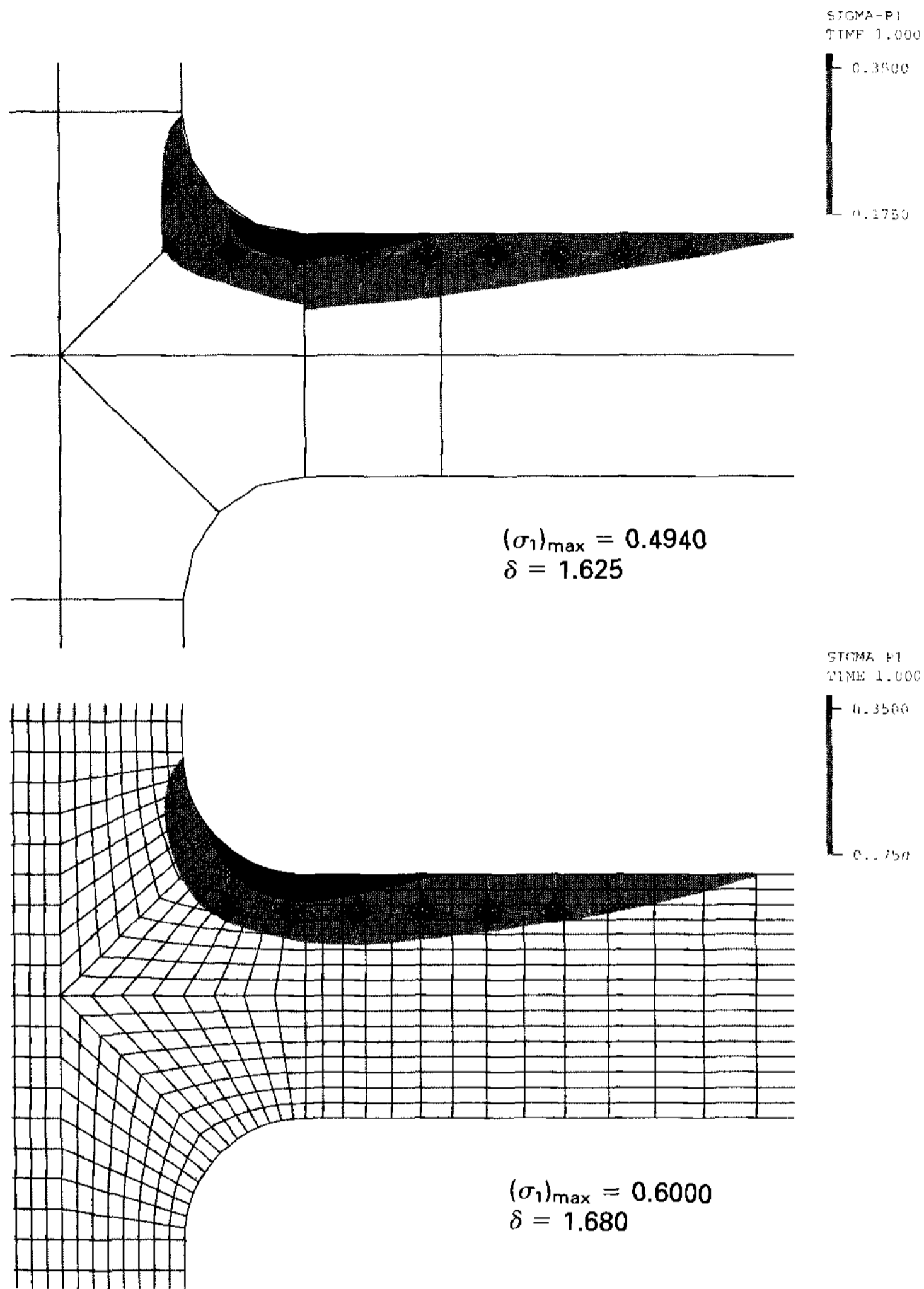
$$\mathbf{S} = \boldsymbol{\tau} + p \boldsymbol{\delta} \tag{4.141}$$

$$\boldsymbol{\epsilon}' = \boldsymbol{\epsilon} - \frac{1}{3} \epsilon_v \boldsymbol{\delta} \tag{4.142}$$

where $\boldsymbol{\delta}$ is a vector of the Kronecker delta symbol [see (4.128)].

Note that using the definition of p in (4.131), a uniform compressive stress gives a positive pressure and that in the simple example in Fig. 4.19, only the volumetric part of the internal virtual work contributed.

In (4.140) we have separated and then summed the deviatoric strain energy and the bulk strain energy. Since the displacements and pressure are considered independent vari-



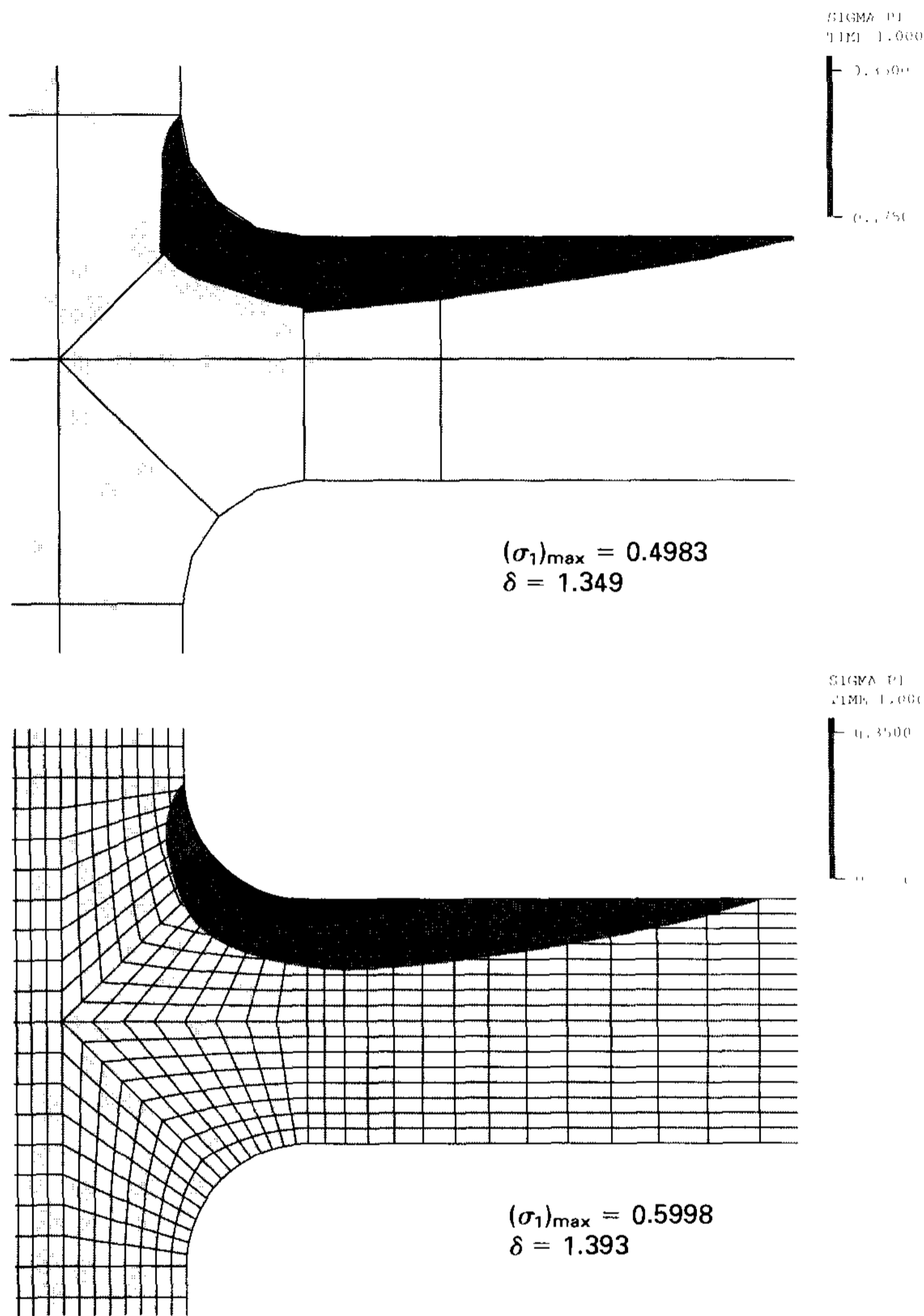
(a) Bands of maximum principal stress. Case of Poisson's ratio $\nu = 0.30$. Sixteen and 16×64 element mesh results

Figure 4.21 Analysis of cantilever bracket in plane strain conditions. Bracket is shown in Fig. 4.20(a). Same meshes as in Fig. 4.20 are used but with the nine-node mixed interpolated element (the 9/3 element). Compare the results shown with those given in Fig. 4.20.

ables, we need another equation to connect these two solution variables. This equation is provided by (4.131) written in integral form (see Example 4.31),

$$\int_V \left(\frac{p}{\kappa} + \epsilon_v \right) \bar{p} \, dV = 0 \tag{4.143}$$

These basic equations can also be derived more formally from variational principles (see L. R. Herrmann [A] and S. W. Key [A]). We derive the basic equations in the following example from the Hu-Washizu functional.



(b) Bands of maximum principal stress. Case of Poisson's ratio $\nu = 0.499$. Sixteen and 16×64 element mesh results

Figure 4.21 (continued)

EXAMPLE 4.31: Derive the u/p formulation from the Hu-Washizu variational principle.

The derivation is quite analogous to the presentation in Example 4.30 where we considered a mixed interpolation for a beam element.

We start by letting $\tau = \mathbf{C}\epsilon$ in (4.114) to obtain the Hellinger-Reissner functional,

$$\Pi_{\text{HR}}^*(\mathbf{u}, \epsilon) = - \int_V \frac{1}{2} \epsilon^T \mathbf{C} \epsilon \, dV + \int_V \epsilon^T \mathbf{C} \partial_\epsilon \mathbf{u} \, dV - \int_V \mathbf{u}^T \mathbf{f}^B \, dV - \int_{S_f} \mathbf{u}^{S_f T} \mathbf{f}^{S_f} \, dS \quad (\text{a})$$

where we assume that the displacement boundary conditions are satisfied exactly (hence, also the displacement variations will be zero on the surface of prescribed displacements).

Next we establish the deviatoric and volumetric contributions and postulate that the deviatoric contribution will be evaluated from the displacements. Hence, we can specialize (a) into

$$\tilde{\Pi}_{HR}^*(\mathbf{u}, p) = \int_V \frac{1}{2} \boldsymbol{\epsilon}'^T \mathbf{C}' \boldsymbol{\epsilon}' dV - \int_V \frac{1}{2} \frac{p^2}{\kappa} dV - \int_V p \epsilon_v dV - \int_V \mathbf{u}^T \mathbf{f}^B dV - \int_{S_f} \mathbf{u}^{S_f T} \mathbf{f}^{S_f} dS \quad (b)$$

where the prime denotes deviatoric quantities, ϵ_v is the volumetric strain evaluated from the displacements, p is the pressure, and κ is the bulk modulus. Note that whereas in (a) the independent variables are \mathbf{u} and $\boldsymbol{\epsilon}$, in (b) the independent variables are \mathbf{u} and p .

Invoking the stationarity of $\tilde{\Pi}_{HR}^*$ with respect to the displacements and the pressure, we obtain

$$\int_V \delta \boldsymbol{\epsilon}'^T \mathbf{C}' \boldsymbol{\epsilon}' dV - \int_V p \delta \epsilon_v dV = \mathcal{R}$$

and

$$\int_V \left(\frac{p}{\kappa} + \epsilon_v \right) \delta p dV = 0$$

where \mathcal{R} corresponds to the virtual work of the externally applied loading [see (4.7)].

It is interesting to note that we may also think of (b) as the total potential in terms of the displacements and the pressure plus a Lagrange multiplier term that enforces the constraint between the volumetric strains and the pressure,

$$\begin{aligned} \tilde{\Pi}_{HR}^* = & - \int_V \frac{1}{2} \boldsymbol{\epsilon}'^T \mathbf{C}' \boldsymbol{\epsilon}' dV + \int_V \frac{1}{2} \frac{p^2}{\kappa} dV - \int_V \mathbf{u}^T \mathbf{f}^B dV \\ & - \int_{S_f} \mathbf{u}^{S_f T} \mathbf{f}^{S_f} dS - \int_V \lambda \left(\epsilon_v + \frac{p}{\kappa} \right) dV \end{aligned} \quad (c)$$

In (c) the last integral represents the Lagrange multiplier constraint, and we find $\lambda = p$.

To arrive at the governing finite element equations, we can now use (4.140) and (4.143) as in Section 4.2.1, but in addition to interpolating the displacements we also interpolate the pressure p . The discussion in Section 4.2.1 showed that we need to consider the formulation of only a single element; the matrices of an assemblage of elements are then formed in a standard manner.

Using, as in Section 4.2.1,

$$\mathbf{u} = \mathbf{H} \hat{\mathbf{u}} \quad (4.144)$$

we can calculate

$$\boldsymbol{\epsilon}' = \mathbf{B}_D \hat{\mathbf{u}}; \quad \epsilon_v = \mathbf{B}_V \hat{\mathbf{u}} \quad (4.145)$$

The additional interpolation assumption is

$$p = \mathbf{H}_p \hat{\mathbf{p}} \quad (4.146)$$

where the vector $\hat{\mathbf{p}}$ lists the pressure variables [(see the discussion following (4.148))].

Substituting from (4.144) to (4.146) into (4.140) and (4.143), we obtain

$$\begin{bmatrix} \mathbf{K}_{uu} & \mathbf{K}_{up} \\ \mathbf{K}_{pu} & \mathbf{K}_{pp} \end{bmatrix} \begin{bmatrix} \hat{\mathbf{u}} \\ \hat{\mathbf{p}} \end{bmatrix} = \begin{bmatrix} \mathbf{R} \\ \mathbf{0} \end{bmatrix} \quad (4.147)$$

where

$$\mathbf{K}_{uu} = \int_V \mathbf{B}_D^T \mathbf{C}' \mathbf{B}_D dV$$

$$\mathbf{K}_{up} = \mathbf{K}_{pu}^T = - \int_V \mathbf{B}_V^T \mathbf{H}_p dV \tag{4.148}$$

$$\mathbf{K}_{pp} = - \int_V \mathbf{H}_p^T \frac{1}{\kappa} \mathbf{H}_p dV$$

and \mathbf{C}' is the stress-strain matrix for the deviatoric stress and strain components.

The relations in (4.144) to (4.148) give the basic equations for formulating elements with displacements and pressure as variables. The key question for the formulation is now, What pressure and displacement interpolations should be used to arrive at effective elements? For example, if the pressure interpolation is of too high a degree compared to the displacement interpolation, the element may again behave as a displacement-based element and not be effective.

Considering for the moment only the pressure interpolation, the following two main possibilities exist and we label them differently.

The u/p formulation. In this formulation, the pressure variables pertain only to the specific element being considered. In the analysis of almost incompressible media (as so far discussed), the element pressure variables can be statically condensed out prior to the element assemblage. Continuity of pressure is not enforced between elements but will be a result of the finite element solution if the mesh used is fine enough.

The u/p-c formulation. The letter “c” denotes continuity in pressure.

In this formulation, the element pressure is defined by nodal pressure variables that pertain to adjacent elements in the assemblage. The pressure variables therefore cannot be statically condensed out prior to the element assemblage. Continuity of pressure between elements is directly enforced and will therefore always be a result of the solution irrespective of whether the mesh used is fine or coarse.

Consider the following two elements, one corresponding to each of the formulations.

EXAMPLE 4.32: For the four-node plane strain element shown, assume that the displacements are interpolated using the four nodes and assume a constant pressure. Evaluate the matrix expressions used for the u/p formulation.

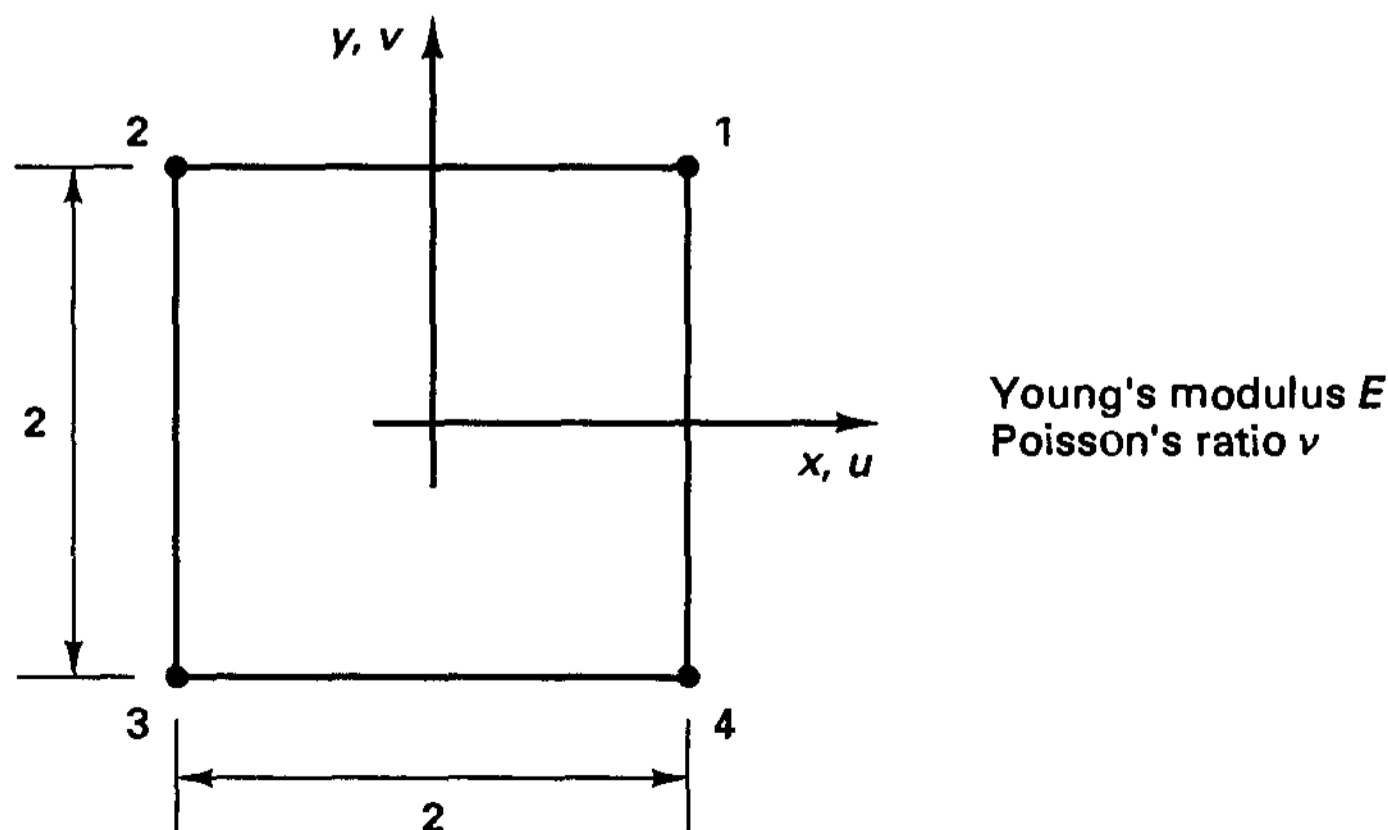


Figure E4.32 A 4/1 element

This element is referred to as the u/p 4/1 element. In plane strain analysis we have

$$\boldsymbol{\epsilon}' = \begin{bmatrix} \epsilon_{xx} - \frac{1}{3}(\epsilon_{xx} + \epsilon_{yy}) \\ \epsilon_{yy} - \frac{1}{3}(\epsilon_{xx} + \epsilon_{yy}) \\ \gamma_{xy} \\ -\frac{1}{3}(\epsilon_{xx} + \epsilon_{yy}) \end{bmatrix} = \begin{bmatrix} \frac{2}{3} \frac{\partial u}{\partial x} - \frac{1}{3} \frac{\partial v}{\partial y} \\ \frac{2}{3} \frac{\partial v}{\partial y} - \frac{1}{3} \frac{\partial u}{\partial x} \\ \frac{\partial u}{\partial y} + \frac{\partial v}{\partial x} \\ -\frac{1}{3} \left(\frac{\partial u}{\partial x} + \frac{\partial v}{\partial y} \right) \end{bmatrix}; \quad \epsilon_v = \epsilon_{xx} + \epsilon_{yy} \quad (a)$$

and $\mathbf{S} = \mathbf{C}' \boldsymbol{\epsilon}'$, where

$$\mathbf{C}' = \begin{bmatrix} 2G & 0 & 0 & 0 \\ 0 & 2G & 0 & 0 \\ 0 & 0 & G & 0 \\ 0 & 0 & 0 & 2G \end{bmatrix}; \quad G = \frac{E}{2(1 + \nu)}$$

The displacement interpolation is as in Example 4.6,

$$\mathbf{u} = \mathbf{H} \hat{\mathbf{u}}$$

with $\mathbf{u}(x, y) = \begin{bmatrix} u(x, y) \\ v(x, y) \end{bmatrix}; \quad \hat{\mathbf{u}}^T = [u_1 \quad u_2 \quad u_3 \quad u_4 \quad ; \quad v_1 \quad v_2 \quad v_3 \quad v_4]$

$$\mathbf{H} = \begin{bmatrix} h_1 & h_2 & h_3 & h_4 & ; & 0 & 0 & 0 & 0 \\ 0 & 0 & 0 & 0 & ; & h_1 & h_2 & h_3 & h_4 \end{bmatrix} \quad (b)$$

$$h_1 = \frac{1}{4}(1+x)(1+y); \quad h_2 = \frac{1}{4}(1-x)(1+y)$$

$$h_3 = \frac{1}{4}(1-x)(1-y); \quad h_4 = \frac{1}{4}(1+x)(1-y)$$

Using (a) and (b), the strain-displacement interpolation matrices are

$$\mathbf{B}_D = \begin{bmatrix} \frac{2}{3} h_{1,x} & \frac{2}{3} h_{2,x} & \dots & ; & -\frac{1}{3} h_{1,y} & -\frac{1}{3} h_{2,y} & \dots \\ -\frac{1}{3} h_{1,x} & -\frac{1}{3} h_{2,x} & \dots & ; & \frac{2}{3} h_{1,y} & \frac{2}{3} h_{2,y} & \dots \\ h_{1,y} & h_{2,y} & \dots & ; & h_{1,x} & h_{2,x} & \dots \\ -\frac{1}{3} h_{1,x} & -\frac{1}{3} h_{2,x} & \dots & ; & -\frac{1}{3} h_{1,y} & -\frac{1}{3} h_{2,y} & \dots \end{bmatrix}$$

and $\mathbf{B}_V = [h_{1,x} \quad h_{2,x} \quad \dots \quad ; \quad h_{1,y} \quad h_{2,y} \quad \dots]$

For a constant pressure assumption we have

$$\mathbf{H}_p = [1]; \quad \hat{\mathbf{p}} = [p_0]$$

Since the degree of freedom $\hat{\mathbf{p}} = [p_0]$ pertains only to this element and not to the adjacent elements, we can use static condensation to obtain from (4.147) the element stiffness matrix corresponding to the nodal point displacement degrees of freedom only;

$$\mathbf{K} = \mathbf{K}_{uu} - \mathbf{K}_{up} \mathbf{K}_{pp}^{-1} \mathbf{K}_{pu}$$

The element is further discussed in Example 4.38.

EXAMPLE 4.33: Consider the nine-node plane strain element shown in Fig. E4.33. Assume that the displacements are interpolated using the nine nodes and that the pressure is interpolated using only the four corner nodes. Refer to the information given in Example 4.32 and discuss the additional considerations for the evaluation of the matrix expressions of this element.

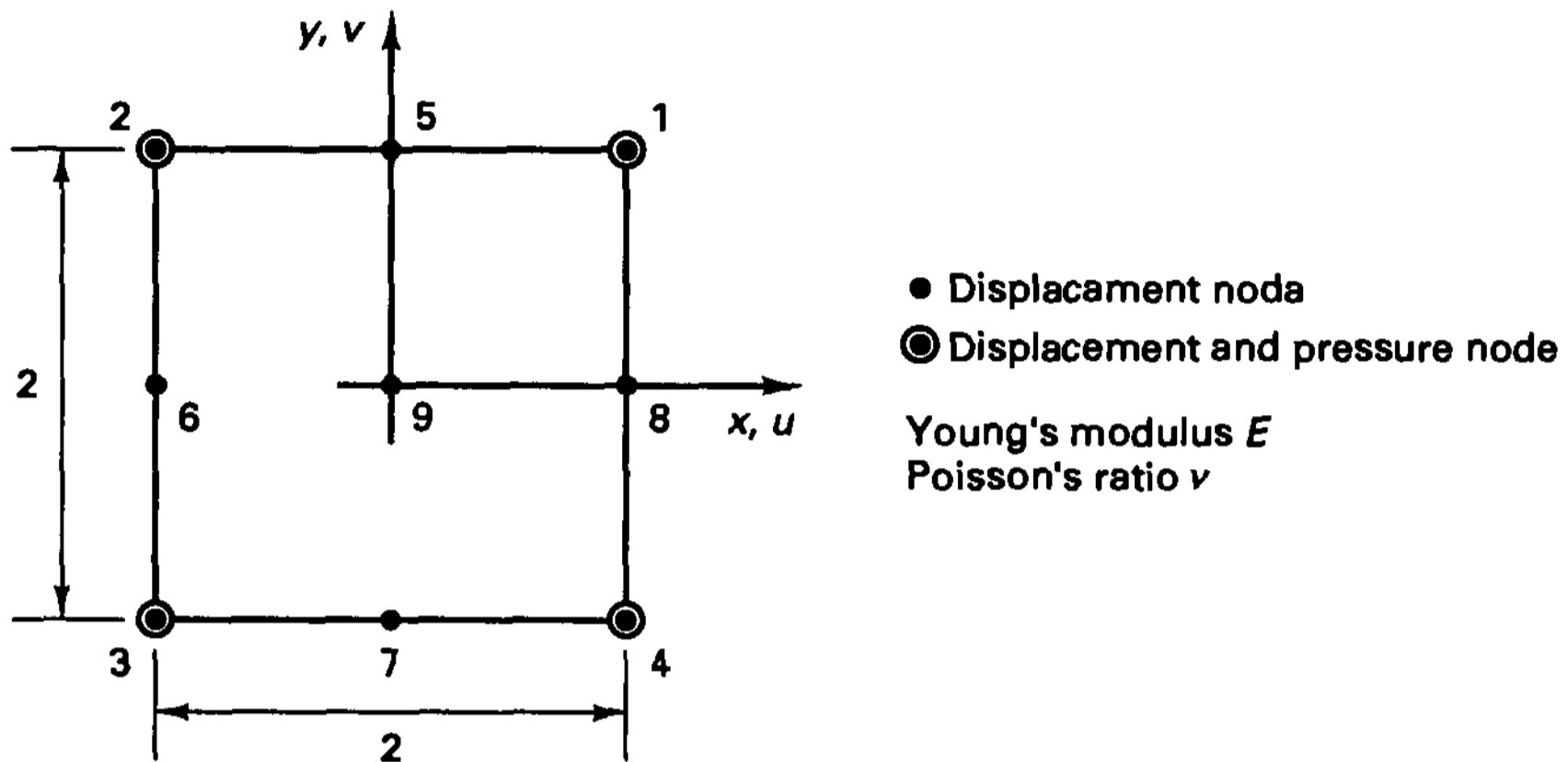


Figure E4.33 A 9/4-c element

This element was proposed by P. Hood and C. Taylor [A]. In the formulation the nodal pressures pertain to adjacent elements, and according to the above element nomination we refer to it as a *u/p-c* element (it is the 9/4-c element).

The deviatoric and volumetric strains are as given in (a) in Example 4.32. The displacement interpolation corresponds to the nine nodes of the element,

$$\begin{bmatrix} u(x, y) \\ v(x, y) \end{bmatrix} = \begin{bmatrix} h_1^* & \dots & h_9^* & \vdots & 0 & \dots & 0 \\ 0 & \dots & 0 & \vdots & h_1^* & \dots & h_9^* \end{bmatrix} \begin{bmatrix} u_1 \\ \vdots \\ u_9 \\ \dots \\ v_1 \\ \vdots \\ v_9 \end{bmatrix} \quad (a)$$

where the interpolation functions h_i^* are constructed as explained in Section 4.2.3 (or see Section 5.3 and Fig. 5.4).

The deviatoric and volumetric strain-displacement matrices are obtained as in Example 4.32. The pressure interpolation is given by

$$p = [h_1 \quad h_2 \quad h_3 \quad h_4] \begin{bmatrix} p_1 \\ p_2 \\ p_3 \\ p_4 \end{bmatrix}$$

where the h_i are those given in (b) in Example 4.32.

A main computational difference between this element and the four-node element discussed in Example 4.32 is that the pressure degrees of freedom cannot be statically condensed out on the element level because the variables p_1, \dots, p_4 pertain to the element we are considering here *and* to the adjacent elements, thus describing a continuous pressure field for the discretization.

Let us now return to the discussion of what pressure and displacement interpolations should be used in order to have an effective element.

For instance, in Example 4.32, we used four nodes to interpolate the displacements and assumed a constant pressure, and we may ask whether a constant pressure is the appropriate choice for the four-node element. Actually, for this element, it is a somewhat natural choice because the volumetric strain calculated from the displacements contains linear variations in x and y and our pressure assumption should be of lower order.

When higher-order displacement interpolations are used, the choice of the appropriate pressure interpolation is not obvious and indeed much more difficult: the pressure should not be interpolated at too low a degree because then the pressure prediction could be of higher order and hence be more accurate, but the pressure should also not be interpolated at too high a degree because then the element would behave like the displacement-based elements and lock. Hence, we want to use the highest degree of pressure interpolation that does not introduce locking into the element.

For example, considering the u/p formulation and biquadratic displacement interpolation (i.e., nine nodes for the description of the displacements), we may naturally try the following cases:

1. Constant pressure, $p = p_0$ (9/1 element)
2. Linear pressure, $p = p_0 + p_1x + p_2y$ (9/3 element)
3. Bilinear pressure, $p = p_0 + p_1x + p_2y + p_3xy$ (9/4 element)

and so on, up to a quadratic pressure interpolation (which corresponds to the 9/9 element).

These elements have been analyzed theoretically and by use of numerical experiments. Studies of the elements show that the 9/1 element does not lock, but the rate of convergence of pressure (and hence stresses) as the mesh is refined is only of $o(h)$ because a constant pressure is assumed in each nine-node element. The poor quality of the pressure prediction can of course also have a negative effect on the prediction of the displacements.

Studies also show that the 9/3 element is most attractive because it does not lock and the stress convergence is of $o(h^2)$. Hence, the predictive capability is optimal since if a biquadratic displacement expansion is used, no higher-order convergence in stresses can be expected. Also, the 9/3 element is effective for any Poisson's ratio up to 0.5 (but the static condensation of the pressure degrees of freedom is possible only for values of $\nu < 0.5$).

Hence, we may be tempted to always use the 9/3 element (instead of the displacement-based nine-node element). However, we find in practice that the 9/3 element is computationally slightly more expensive than the nine-node displacement-based element, and when ν is less than 0.48, the additional terms in the pressure expansion of the displacement-based element allow a slightly better prediction of stresses.

The next u/p element of interest is the 9/4 element, and studies show that this element locks when ν is close to 0.50; hence it cannot be recommended for almost incompressible analysis.

In an analogous manner, other u/p elements can be constructed, and Table 4.6 summarizes some choices. Regarding these elements, we may note that the four-node two-dimensional and eight-node three-dimensional elements are extensively used in practice. However, the nine-node two-dimensional and 27-node three-dimensional elements are frequently more powerful.

As indicated in Table 4.6, the $Q_2 - P_1$ and $P_2^+ - P_1$ elements are the first members of two families of elements that may be used. That is, the quadrilateral elements $Q_n - P_{n-1}$, and the triangular elements $P_n^+ - P_{n-1}$, $n > 2$, are also effective elements.

In Table 4.6 we refer to the inf-sup condition, which we will discuss in Section 4.5.

From a computational point of view, the u/p elements are attractive because the element pressure degrees of freedom can be statically condensed out before the elements are assembled (assuming $\nu < 0.5$ but possibly very close to 0.5). Hence, the degrees of freedom for the assemblage of elements are only the same nodal point displacements that are also the degrees of freedom in the pure displacement-based solution.

However, the u/p -c formulation has the advantage that a continuous pressure field is always calculated. Table 4.7 lists some effective elements.

The Finite Element Solution of Totally Incompressible Conditions

If we want to consider the material to be totally incompressible, we can still use (4.140) and (4.143), but we then let $\kappa \rightarrow \infty$. For this reason, we refer to this case as the *limit problem*. Then (4.143) becomes

$$\int_V \epsilon_v \bar{p} \, dV = 0 \quad (4.149)$$

and (4.147) becomes, correspondingly,

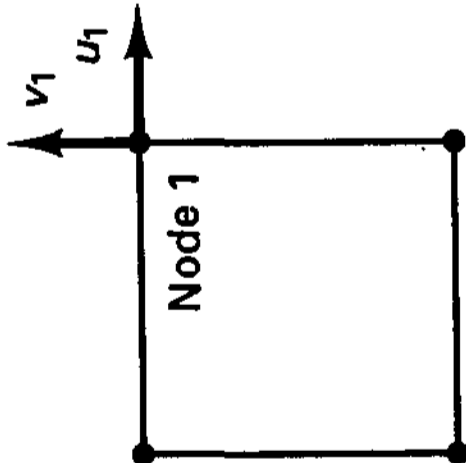
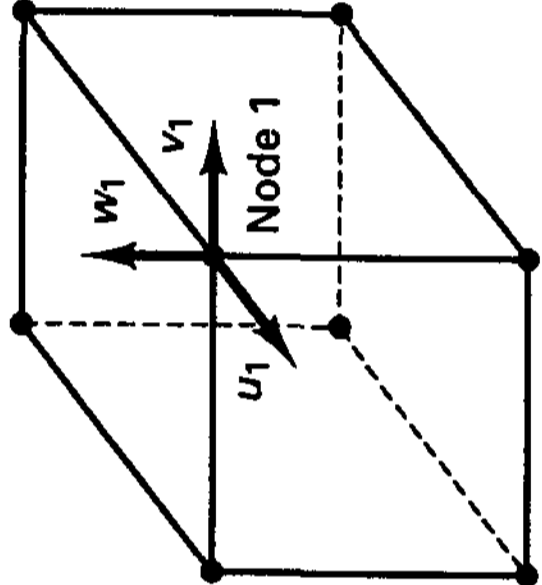
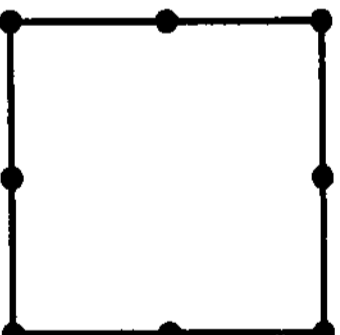
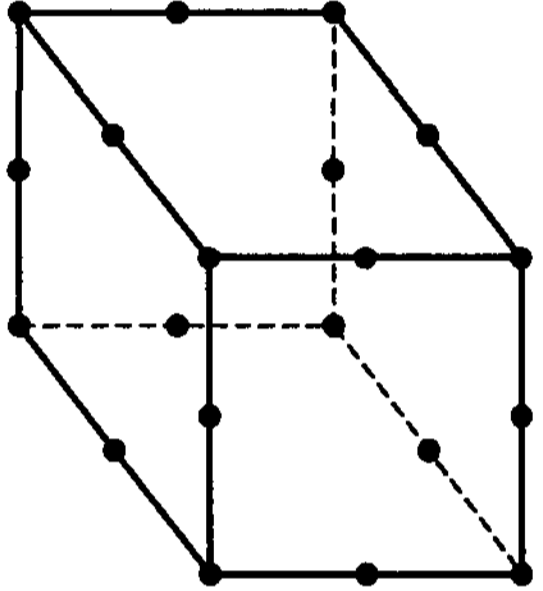
$$\begin{bmatrix} \mathbf{K}_{uu} & \mathbf{K}_{up} \\ \mathbf{K}_{pu} & \mathbf{0} \end{bmatrix} \begin{bmatrix} \hat{\mathbf{u}} \\ \hat{\mathbf{p}} \end{bmatrix} = \begin{bmatrix} \mathbf{R} \\ \mathbf{0} \end{bmatrix} \quad (4.150)$$

Hence, in the coefficient matrix, the diagonal elements corresponding to the pressure degrees of freedom are now zero. It follows that a static condensation of the element pressure degrees of freedom in the u/p formulation is no longer possible and that the solution of the equations of the complete assemblage of elements needs special considerations (beyond those required in the pure displacement-based solution) to avoid encountering a zero pivot element (see Section 8.2.5).

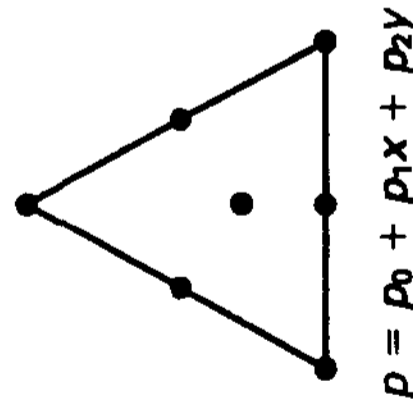
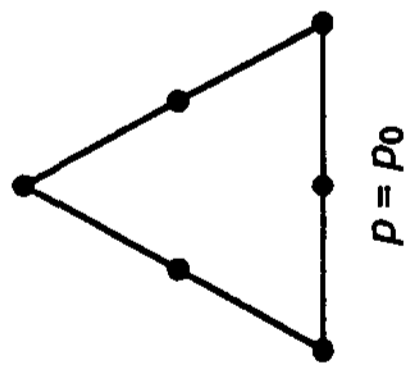
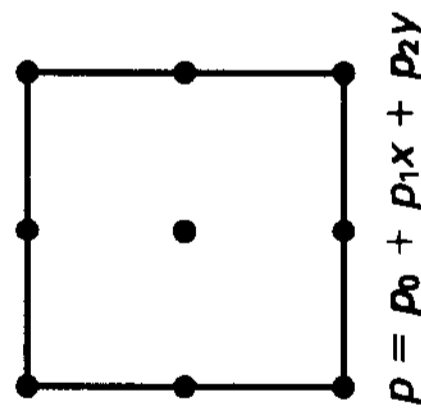
Suitable elements for solution are listed in Tables 4.6 and 4.7. These elements are effective (except for the $Q_1 - P_0$ elements) because they have good predictive capability irrespective of how close the behavior of the medium is to a situation of total incompressibility (but the procedure for solving the governing finite element equations must take into account that the elements in \mathbf{K}_{pp} become increasingly smaller as total incompressibility is approached).

As already noted earlier, we refer to the inf-sup condition in Tables 4.6 and 4.7. This condition is the basic mathematical criterion that determines whether a mixed finite element discretization is stable and convergent (and hence will yield a reliable solution). The condition was introduced as *the* fundamental test for mixed finite element formulations by I. Babuška [A] and F. Brezzi [A] and since then has been used extensively in the analysis of mixed finite element formulations. In addition to the inf-sup condition, there is also the ellipticity condition which has not received as much attention because frequently—as in the analysis of almost incompressible media—the ellipticity condition is automatically satisfied.

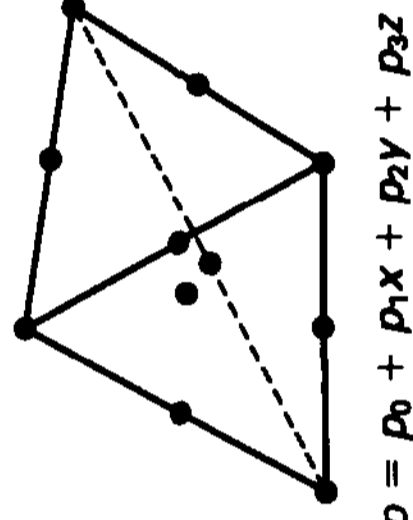
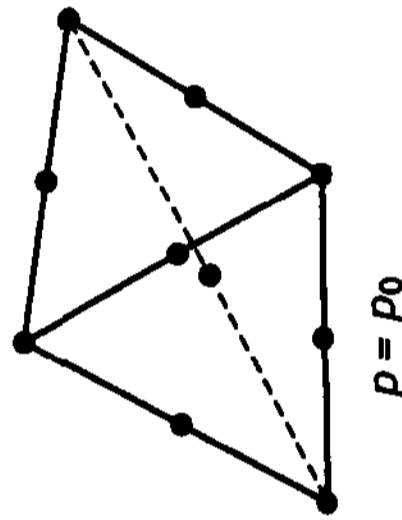
TABLE 4.6 Various effective u/p elements (displacements between elements are continuous and pressure variables pertain to individual elements)[†]

Element	Nodal points		Remarks
	2-D element	3-D element	
$Q_1 - P_0$ in 2-D: 4/1 in 3-D: 8/1	 <p style="text-align: center;">$P = P_0$</p>	 <p style="text-align: center;">$P = P_0$</p>	The element predicts reasonably good displacements, but stresses may be inaccurate because of the constant pressure assumption and possible pressure fluctuations. The element does not satisfy the inf-sup condition (see discussion of element in Section 4.5.5).
$Q_2^1 - P_0; Q_2^2 = Q_2 \cap P_3$ in 2-D: 8/1 in 3-D: 20/1	 <p style="text-align: center;">$P = P_0$</p>	 <p style="text-align: center;">$P = P_0$</p>	

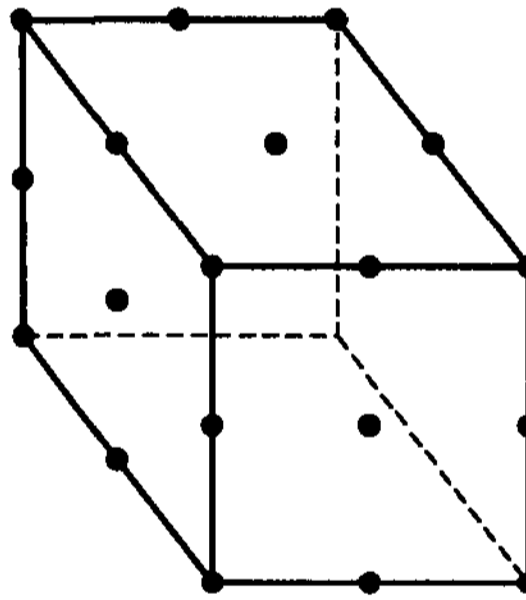
$Q_2 - P_1$
in 2-D: 9/3
in 3-D: 27/4



$P_2 - P_0$
in 2-D: 6/1
in 3-D: 10/1

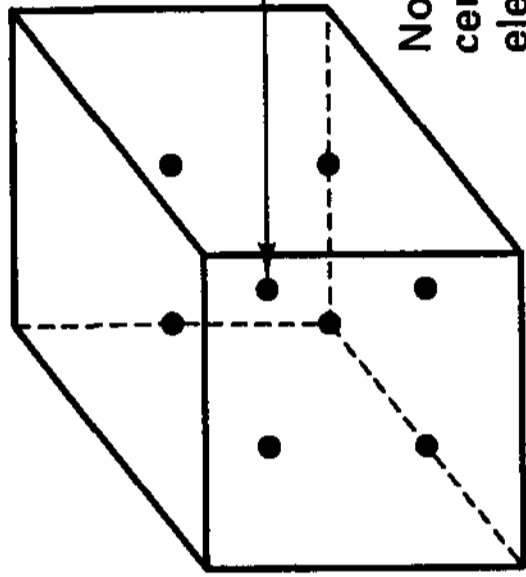


Only the visible 18 of
the total 27 nodes are
shown



$p = p_0 + p_1x + p_2y + p_3z$

Only the 8 non-
visible nodes are
shown



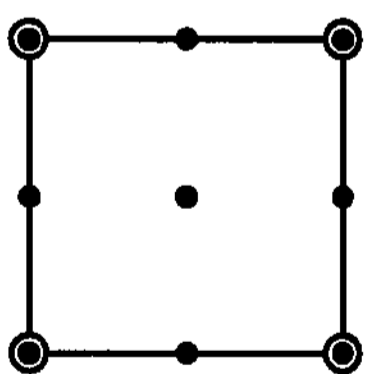
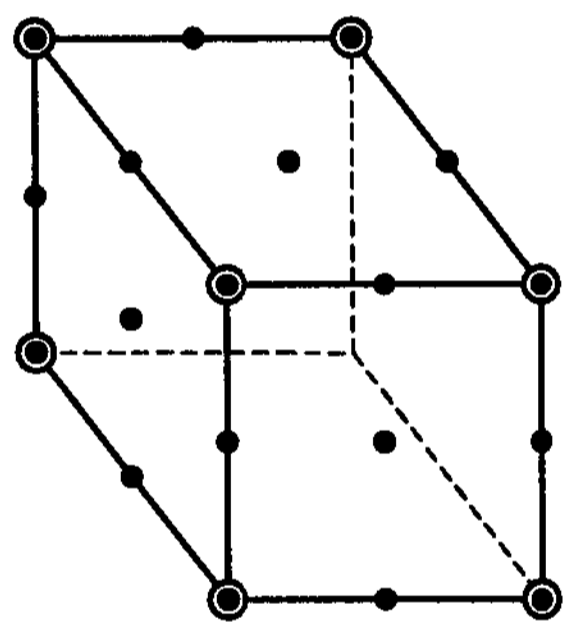
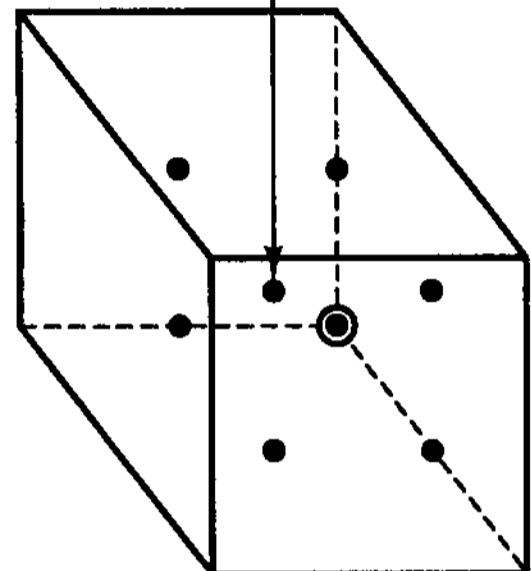
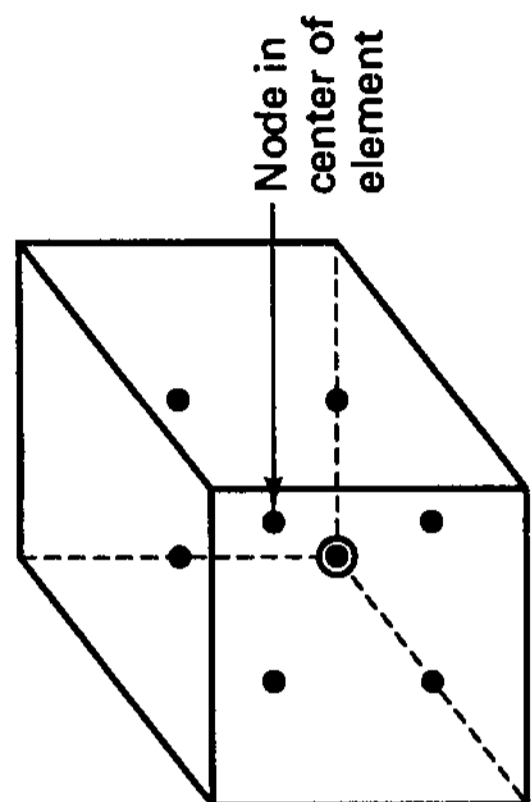
The optimal quadrilateral element using a biquadratic displacement expansion. The largest number of pressure variables is used subject to the condition that the inf-sup condition is to be satisfied. The first member of the family of quadrilateral elements $Q_n - P_{n-1}$, $n \geq 2$. All these elements satisfy the inf-sup condition (see Example 4.36).

See M. Crouzeix and P.-A. Raviart [A]. The element satisfies the inf-sup condition, but the constant pressure assumption may require fine discretization.

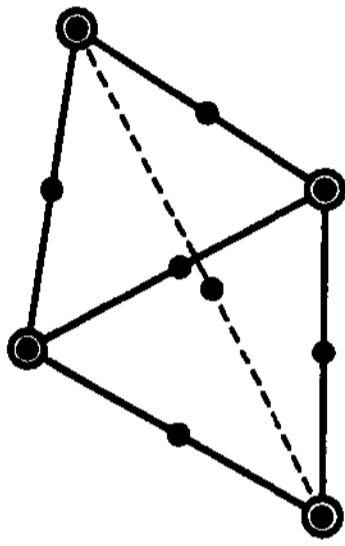
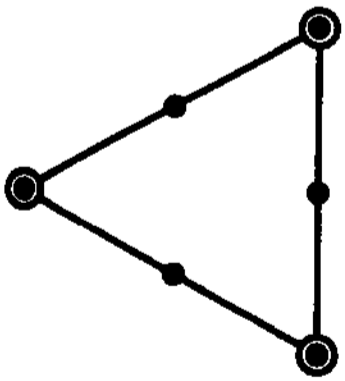
See M. Crouzeix and P.-A. Raviart [A]. The optimal triangular element using a quadratic displacement expansion (with a cubic bubble). P_2^\dagger denotes the space of polynomials P_2 enriched by the cubic bubble. The largest number of pressure variables is used subject to the condition that the inf-sup condition is to be satisfied. The first member of the family of triangular elements $P_n^\dagger - P_{n-1}$, $n \geq 2$. All these elements satisfy the inf-sup condition.

† For the interpolation functions, see Figs. 4.13, 5.4, 5.5, 5.11, and 5.13.

TABLE 4.7 Various effective u/p -c elements (displacements and pressure are continuous and all elements satisfy the inf-sup condition)[†]

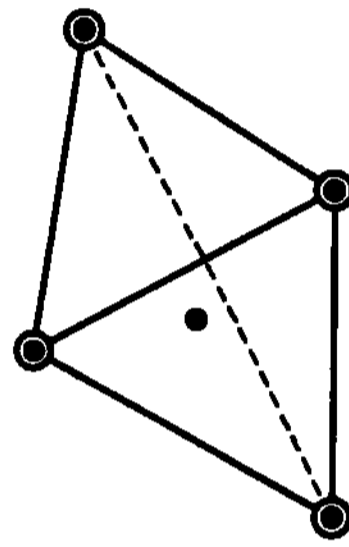
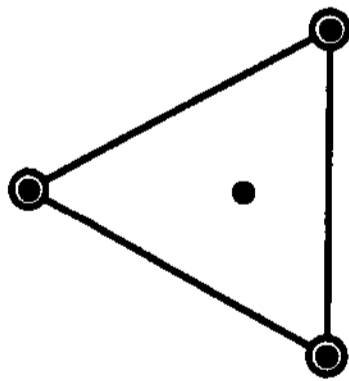
Element	Nodal points		Remarks
	2-D element	3-D element	
$Q_2 - Q_1$ in 2-D: 9/4-c in 3-D: 27/8-c			Only the visible 19 of the total 27 nodes are shown
			Only the 8 non-visible nodes are shown
			See P. Hood and C. Taylor [A]. The first member of the $Q_n - Q_{n-1}$ family of quadrilateral elements, $n \geq 2$.

$P_2 - P_1$
 in 2-D: 6/3-c
 in 3-D: 10/4-c



See P. Hood and C. Taylor [A]. The first member of the $P_n - P_{n-1}$ family of triangular elements, $n \geq 2$.

$P_1^+ - P_1$
 in 2-D: 4/3-c
 in 3-D: 5/4-c



See D. N. Arnold, F. Brezzi, and M. Fortin [A]. P_1^+ denotes the space of polynomials P_1 enriched by the cubic bubble. Also referred to as MINI elements.

- Node with displacement variables
- ⊙ Node with displacement and pressure variables

† For the interpolation functions, see Figs. 4.13, 5.4, 5.5, 5.11, and 5.13.

We may ask whether in practice it is really important to satisfy the inf-sup condition, that is, whether perhaps this condition is too strong and elements that do not satisfy it can still be used reliably. Our experience is that if the inf-sup condition is satisfied, the element will be, for the interpolations used, as effective as we can reasonably expect and in that sense optimal. For example, the 9/3 element for plane strain analysis in Table 4.6 is based on a parabolic interpolation of displacements and a linear interpolation of pressure. The element does not lock, and the order of convergence of displacements is always $o(h^3)$, and of stresses, $o(h^2)$, which is surely the best behavior we can obtain with the interpolations used.

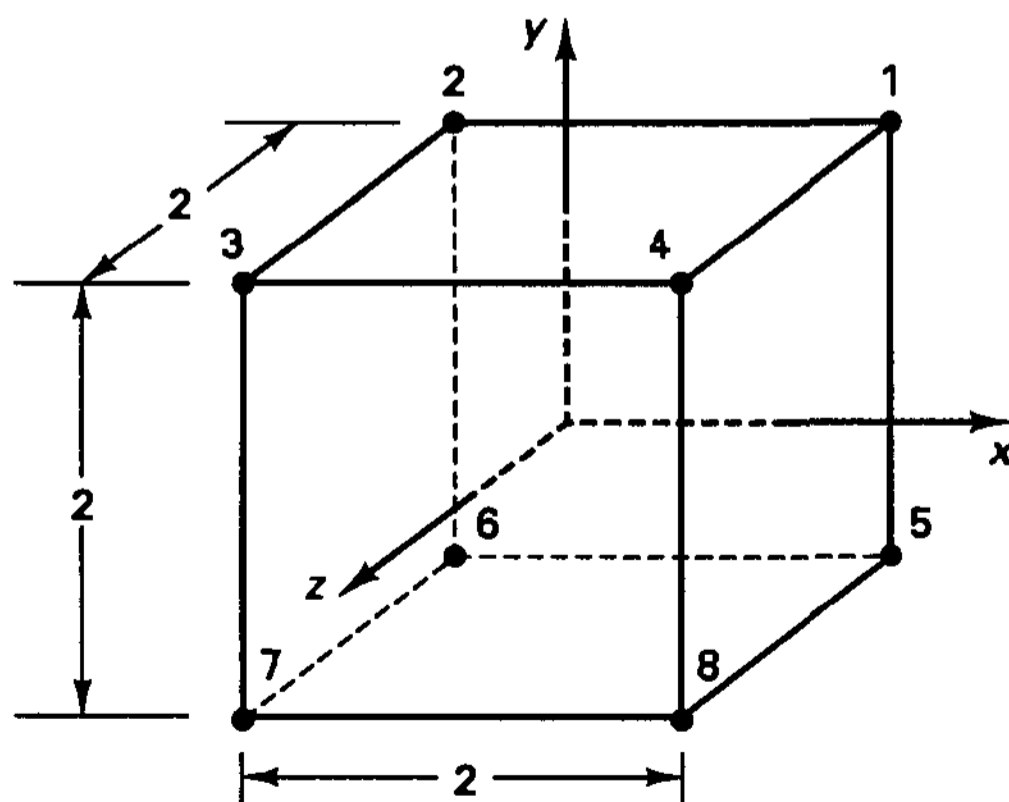
On the other hand, if the inf-sup condition is not satisfied, the element will not always display for all analysis problems (pertaining to the mathematical model considered) the convergence characteristics that we would expect and indeed require in practice. The element is therefore not robust and reliable.

Since the inf-sup condition is of great fundamental importance, we present in the following section a derivation that although not mathematically complete does yield valuable insight. In this discussion we will also encounter and briefly exemplify the ellipticity condition. For a mathematically complete derivation of the ellipticity and inf-sup conditions and many more details, we refer the reader to the book by F. Brezzi and M. Fortin [A].

In the derivation in the next section we examine the problem of incompressible elasticity, but our considerations are also directly applicable to the problem of incompressible fluid flow, and as shown in Section 4.5.7, to the formulations of structural elements.

4.4.4 Exercises

- 4.33. Use the four-node and eight-node shell elements available in a finite element program and perform the patch tests in Fig. 4.17.
- 4.34. Consider the three-dimensional eight-node element shown. Design the patch test and identify analytically whether it is passed for the element.



$$\begin{aligned}
 u &= \sum_{i=1}^8 h_i u_i + \alpha_1 \phi_1 + \alpha_2 \phi_2 + \alpha_3 \phi_3 \\
 v &= \sum_{i=1}^8 h_i v_i + \alpha_4 \phi_1 + \alpha_5 \phi_2 + \alpha_6 \phi_3 \\
 w &= \sum_{i=1}^8 h_i w_i + \alpha_7 \phi_1 + \alpha_8 \phi_2 + \alpha_9 \phi_3 \\
 h_i &= \frac{1}{8} (1 + x_i x)(1 + y_i y)(1 + z_i z) \\
 \phi_1 &= 1 - x^2; \phi_2 = 1 - y^2; \phi_3 = 1 - z^2
 \end{aligned}$$

Displacement interpolation functions

4.35. Consider the Hu-Washizu functional Π_{HW} in (4.114) and derive in detail the equations (4.116) to (4.121).

4.36. The following functional is referred to as the Hellinger-Reissner functional¹⁷

$$\begin{aligned} \Pi_{\text{HR}}(\mathbf{u}, \boldsymbol{\tau}) = & \int_V -\frac{1}{2} \boldsymbol{\tau}^T \mathbf{C}^{-1} \boldsymbol{\tau} dV + \int_V \boldsymbol{\tau}^T \boldsymbol{\partial}_\epsilon \mathbf{u} dV \\ & - \int_V \mathbf{u}^T \mathbf{f}^B dV - \int_{S_f} \mathbf{u}^{S_f T} \mathbf{f}^{S_f} dS - \int_{S_u} \mathbf{f}^{S_u T} (\mathbf{u}^{S_u} - \mathbf{u}_p) dS \end{aligned}$$

where the prescribed (not to be varied) quantities are \mathbf{f}^B in V , \mathbf{u}_p on S_u , and \mathbf{f}^{S_f} on S_f .

Derive this functional from the Hu-Washizu functional by imposing $\boldsymbol{\epsilon} = \mathbf{C}^{-1} \boldsymbol{\tau}$. Then invoke the stationarity of Π_{HR} and establish all remaining differential conditions for the volume and surface of the body.

4.37. Consider the functional

$$\Pi_1 = \Pi - \int_{S_u} \mathbf{f}^{S_u T} (\mathbf{u}^{S_u} - \mathbf{u}_p) dS$$

where Π is given in (4.109) and \mathbf{u}_p are the displacements to be prescribed on the surface S_u . Hence, the vector \mathbf{f}^{S_u} represents the Lagrange multipliers (surface tractions) used to enforce the surface displacement conditions. Invoke the stationarity of Π_1 and show that the Lagrange multiplier term will enforce the displacement boundary conditions on S_u .

4.38. Consider the three-node truss element in Fig. E4.29. Use the Hu-Washizu variational principle and establish the stiffness matrices for the following assumptions:

(a) Parabolic displacement, linear strain, and constant stress

(b) Parabolic displacement, constant strain, and constant stress

Discuss your results in terms of whether the choices of interpolations are sensible (see Example 4.29).

4.39. Show that the following stress-strain expressions of an isotropic material are equivalent.

$$\tau_{ij} = \kappa \epsilon_V \delta_{ij} + 2G \epsilon'_{ij} \tag{a}$$

$$\tau_{ij} = C_{ijrs} \epsilon_{rs} \tag{b}$$

$$\boldsymbol{\tau} = \mathbf{C} \boldsymbol{\epsilon} \tag{c}$$

where κ is the bulk modulus, G is the shear modulus,

$$\kappa = \frac{E}{3(1 - 2\nu)}; \quad G = \frac{E}{2(1 + \nu)}$$

E is Young's modulus, ν is Poisson's ratio, ϵ_V is the volumetric strain, and ϵ'_{ij} are the deviatoric strain components,

$$\epsilon_V = \epsilon_{kk}; \quad \epsilon'_{ij} = \epsilon_{ij} - \frac{\epsilon_V}{3} \delta_{ij}$$

Also,

$$C_{ijrs} = \lambda \delta_{ij} \delta_{rs} + \mu (\delta_{ir} \delta_{js} + \delta_{is} \delta_{jr})$$

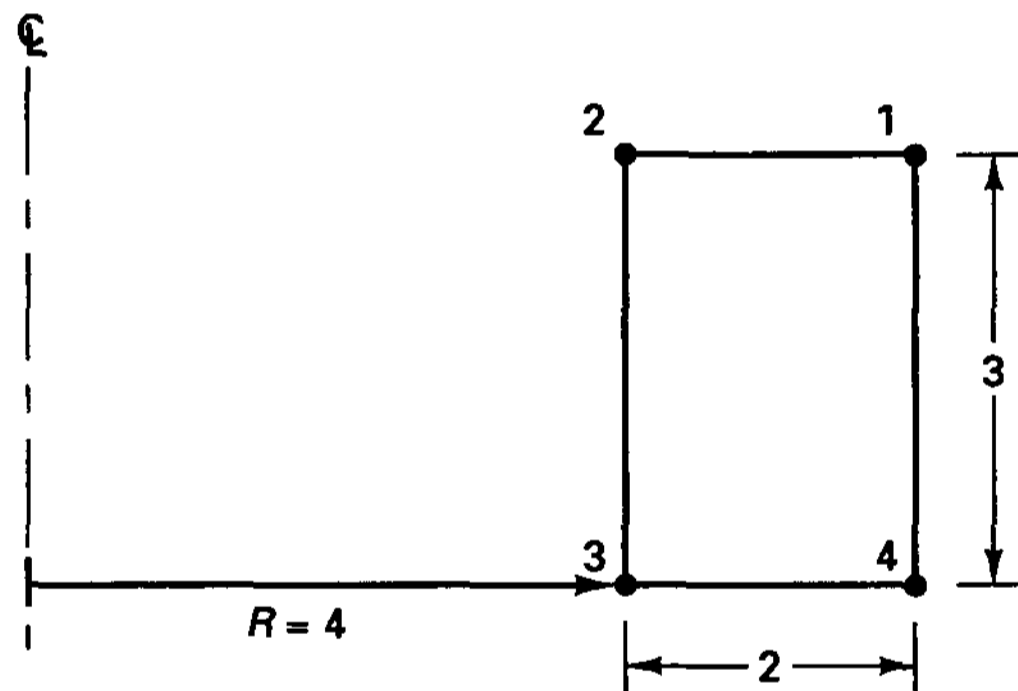
¹⁷ This functional is sometimes given in a different form by applying the divergence theorem to the second term.

where λ and μ are the Lamé constants,

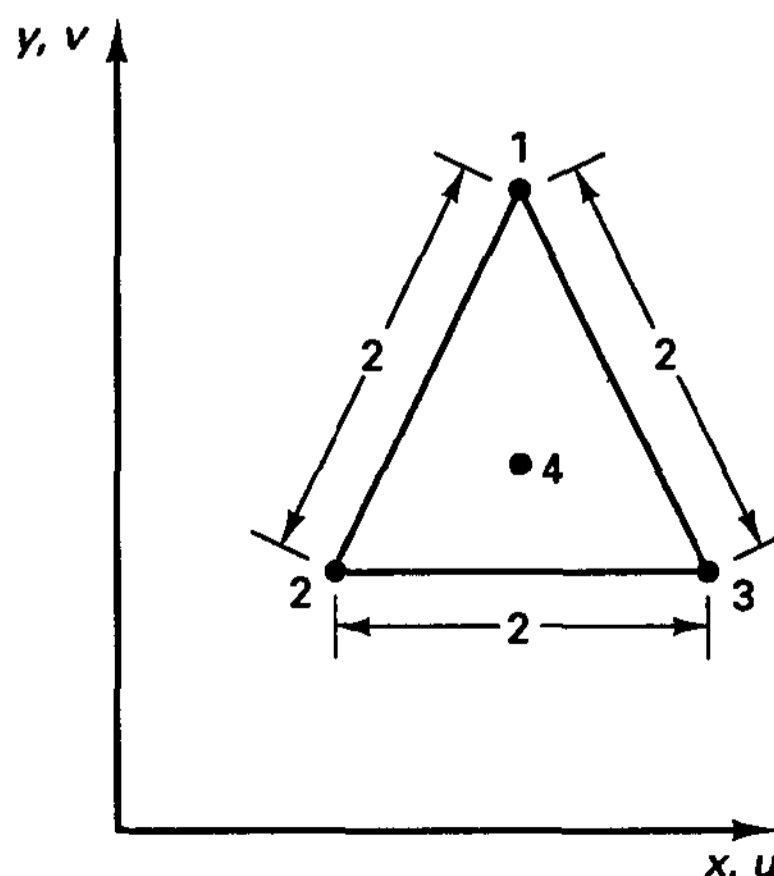
$$\lambda = \frac{E\nu}{(1 + \nu)(1 - 2\nu)}; \quad \mu = \frac{E}{2(1 + \nu)}$$

In (a) and (b) tensorial quantities are used, whereas in (c) the vector of strains contains the engineering shear strains (which are equal to twice the tensor components; e.g., $\gamma_{xy} = \epsilon_{12} + \epsilon_{21}$). Also, the stress-strain matrix \mathbf{C} in (c) is given in Table 4.3.

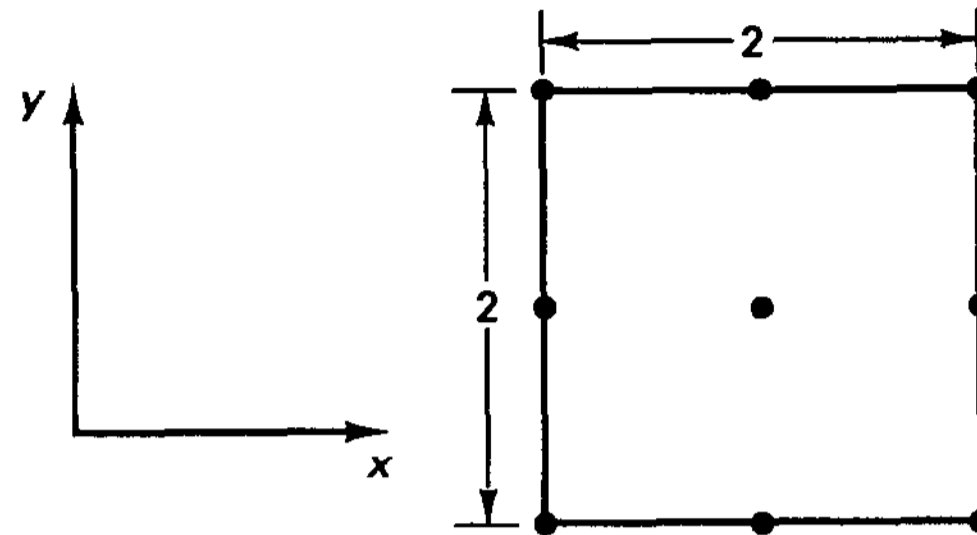
- 4.40. Identify the order of pressure interpolation that should be used in the u/p formulation in order to obtain the same stiffness matrix as in the pure displacement formulation. Consider the following elements of 2×2 geometry.
- (a) Four-node element in plane strain
 - (b) Four-node element in axisymmetric conditions
 - (c) Nine-node element in plane strain.
- 4.41. Consider the 4/1 element in Example 4.32 and assume that the displacement boundary condition to be imposed is $u_1 = \bar{u}$. Show formally that imposing this boundary condition prior to or after the static condensation of the pressure degree of freedom, yields the same element contribution to the stiffness matrix of the assemblage.
- 4.42. Consider the axisymmetric 4/1 u/p element shown. Construct the matrices \mathbf{B}_D , \mathbf{B}_V , \mathbf{C}' , and \mathbf{H}_p for this element.



- 4.43. Consider the 4/3-c element in plane strain conditions shown. Formulate all displacement and strain interpolation matrices for this element (see Table 4.7).

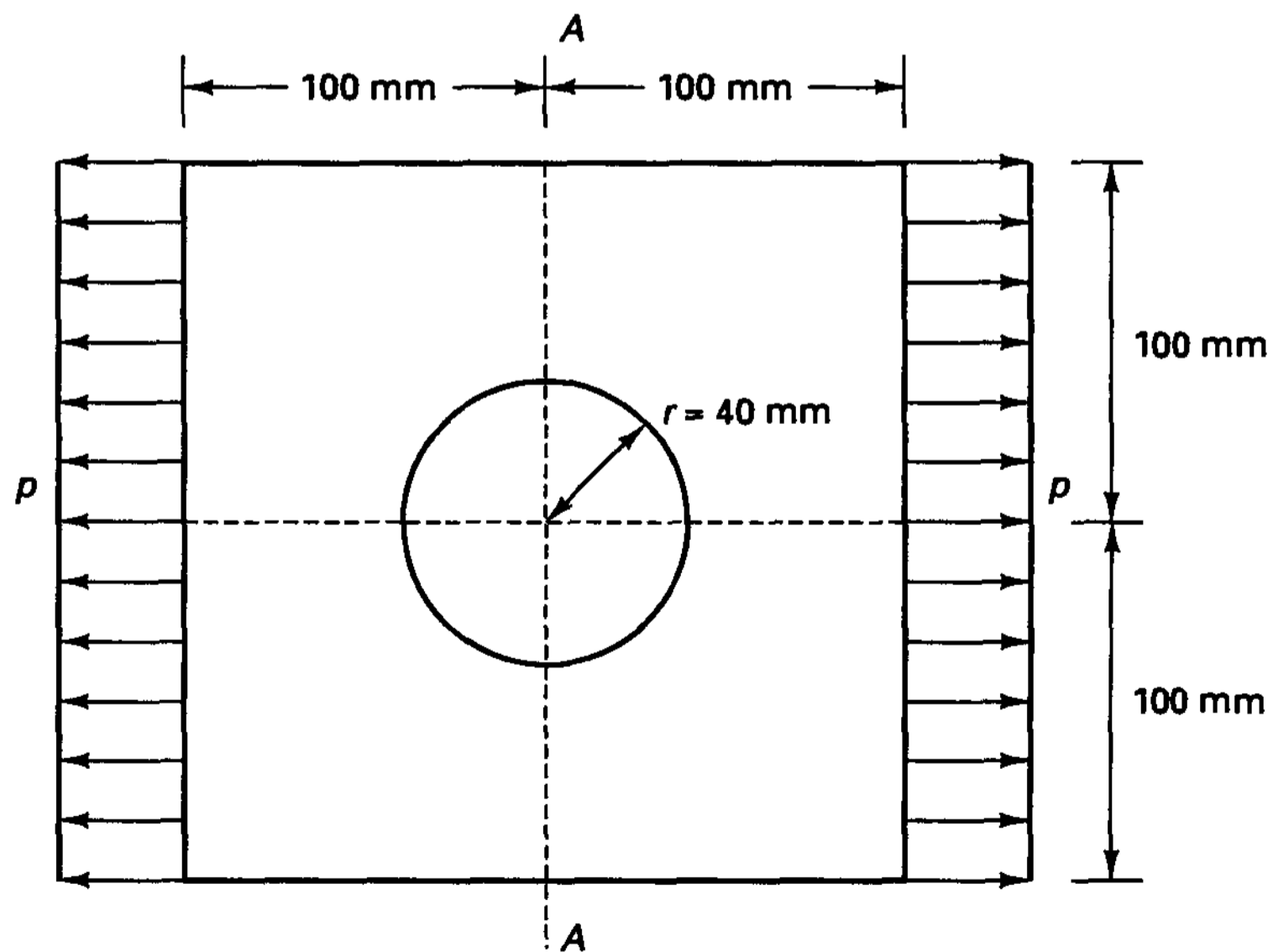


4.44. Consider the 9/3 plane strain u/p element shown. Calculate the matrix K_{pp} .



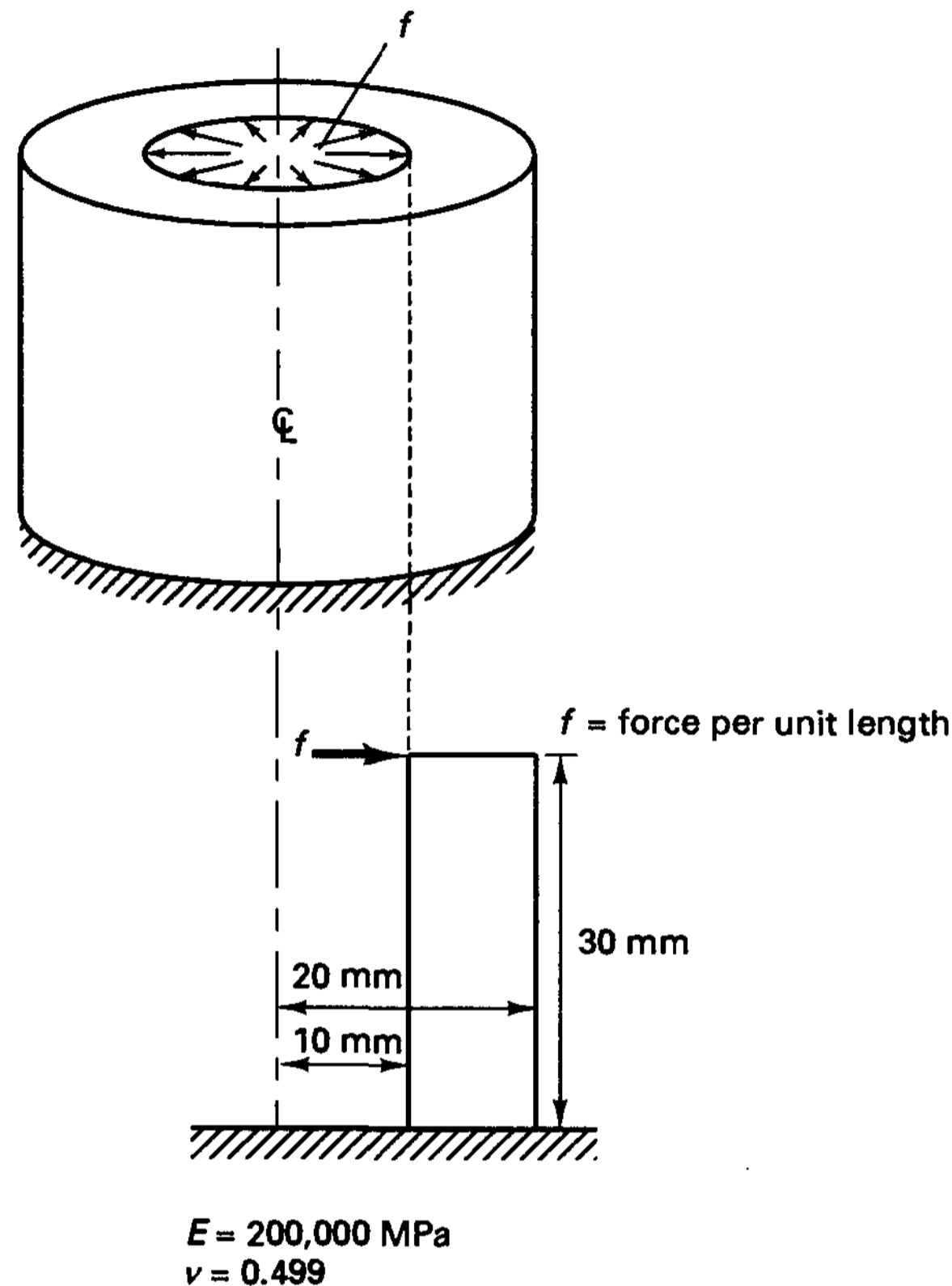
Young's modulus E
 Poisson's ratio $\nu = 0.49$

4.45. Consider the plate with the circular hole shown. Use a finite element program to solve for the stress distribution along section AA for the two cases of Poisson's ratios $\nu = 0.3$ and $\nu = 0.499$. Assess the accuracy of your results by means of an error measure. (*Hint: For the analysis with $\nu = 0.499$, the 9/3 element is effective.*)



Plane strain condition
 Young's modulus $E = 200,000$ MPa

4.46. The static response of the thick cylinder shown is to be calculated with a finite element program.



Use idealizations based on the following elements to analyze the cylinder.

- (a) Four-node displacement-based element
- (b) Nine-node displacement-based element
- (c) 4/1 u/p element.
- (d) 9/3 u/p element.

In each case use a sequence of meshes and identify the convergence rate of the strain energy.

4.5 THE INF-SUP CONDITION FOR ANALYSIS OF INCOMPRESSIBLE MEDIA AND STRUCTURAL PROBLEMS

As we pointed out in the previous section, it is important that the finite element discretization for the analysis of almost, and of course totally, incompressible media satisfy the inf-sup condition. The objective in this section is to present this condition. We first consider the pure displacement formulation for the analysis of solids and then the displacement/pres-

sure formulations. Finally, we also briefly discuss the inf-sup condition as applicable to structural elements.

In our discussion we apply the displacement and displacement/pressure formulations to a solid medium. However, the basic observations and conclusions are also directly applicable to the solution of incompressible fluid flows if velocities are used instead of displacements (see Section 7.4).

4.5.1 The Inf-Sup Condition Derived from Convergence Considerations

We want to solve a general linear elasticity problem (see Section 4.2.1) in which a body is subjected to body forces \mathbf{f}^B , surface tractions \mathbf{f}^{S_f} on the surface S_f , and displacement boundary conditions \mathbf{u}^{S_u} on the surface S_u . Without loss of generality of the conclusions that we want to reach in this section, we can assume that the prescribed displacements \mathbf{u}^{S_u} and prescribed tractions \mathbf{f}^{S_f} are zero. Of course, we assume that the body is properly supported, so that no rigid body motions are possible. We can then write our analysis problem as a problem of minimization,

$$\min_{\mathbf{v} \in V} \left\{ \frac{1}{2} a(\mathbf{v}, \mathbf{v}) + \frac{\kappa}{2} \int_{\text{Vol}} (\text{div } \mathbf{v})^2 d\text{Vol} - \int_{\text{Vol}} \mathbf{f}^B \cdot \mathbf{v} d\text{Vol} \right\} \quad (4.151)$$

where using indicial notation and tensor quantities (see Sections 4.3.4 and 4.4.3),

$$\begin{aligned} a(\mathbf{u}, \mathbf{v}) &= 2G \int_{\text{Vol}} \sum_{i,j} \epsilon'_{ij}(\mathbf{u}) \epsilon'_{ij}(\mathbf{v}) d\text{Vol} \\ \epsilon'_{ij}(\mathbf{u}) &= \epsilon_{ij}(\mathbf{u}) - \frac{1}{3} \text{div } \mathbf{u} \delta_{ij} \\ \epsilon_{ij}(\mathbf{u}) &= \frac{1}{2} \left(\frac{\partial u_i}{\partial x_j} + \frac{\partial u_j}{\partial x_i} \right); \quad \text{div } \mathbf{v} = v_{i,i} \end{aligned} \quad (4.152)$$

where $\kappa = E/[3(1 - 2\nu)]$ (bulk modulus), $G = E/[2(1 + \nu)]$ (shear modulus), $E =$ Young's modulus, $\nu =$ Poisson's ratio.

$$V = \left\{ \mathbf{v} \mid \frac{\partial v_i}{\partial x_j} \in L^2(\text{Vol}), i, j = 1, 2, 3; v_i|_{S_u} = 0, i = 1, 2, 3 \right\}$$

In these expressions we use the notation defined earlier (see Section 4.3) and we denote by "Vol" the domain over which we integrate so as to avoid any confusion with the vector space V . Also, we use for the vector \mathbf{v} and scalar q the norms

$$\|\mathbf{v}\|_V^2 = \sum_{i,j} \left\| \frac{\partial v_i}{\partial x_j} \right\|_{L^2(\text{Vol})}^2; \quad \|q\|_0^2 = \|q\|_{L^2(\text{Vol})}^2 \quad (4.153)$$

where the vector norm $\|\cdot\|_V$ is somewhat easier to work with but is equivalent to the Sobolev norm $\|\cdot\|_1$ defined in (4.76) (by the Poincaré-Friedrichs inequality).

In the following discussion we will not explicitly give the subscripts on the norms but always imply that a vector \mathbf{w} has norm $\|\mathbf{w}\|_V$ and a scalar γ has norm $\|\gamma\|_0$.

Let \mathbf{u} be the minimizer of (4.151) (i.e., the exact solution to the problem) and let V_h be a space of a sequence of finite element spaces that we choose to solve the problem. These spaces are defined in (4.84). Of course, each discrete problem,

$$\lim_{v_h \in V_h} \left\{ \frac{1}{2} a(v_h, v_h) + \frac{\kappa}{2} \int_{\text{Vol}} (\text{div } v_h)^2 d\text{Vol} - \int_{\text{Vol}} \mathbf{f}^B \cdot v_h d\text{Vol} \right\} \quad (4.154)$$

has a unique finite element solution \mathbf{u}_h . We considered the properties of this solution in Section 4.3.4, and in particular we presented the properties (4.95) and (4.101). However, we also stated that the constants c in these relations are dependent on the material properties. The important point now is that when the bulk modulus κ is very large, the relations (4.95) and (4.101) are no longer useful because the constants are too large. Therefore, we want our finite element space V_h to satisfy another property, still of the form (4.95) but in which the constant c , in addition to being independent of h , is also independent of κ .

To state this new desired property, let us first define the "distance" between the exact solution \mathbf{u} and the finite element space V_h (see Fig. 4.22),

$$d(\mathbf{u}, V_h) = \inf_{v_h \in V_h} \|\mathbf{u} - v_h\| = \|\mathbf{u} - \tilde{\mathbf{u}}_h\| \quad (4.155)$$

where $\tilde{\mathbf{u}}_h$ is an element in V_h but is in general not the finite element solution.

The Basic Requirements

In engineering practice, the bulk modulus κ may vary from values of the order of G to very large values, and indeed to infinity when complete incompressibility is considered. Our objective is to use finite elements that are uniformly effective irrespective of what value κ

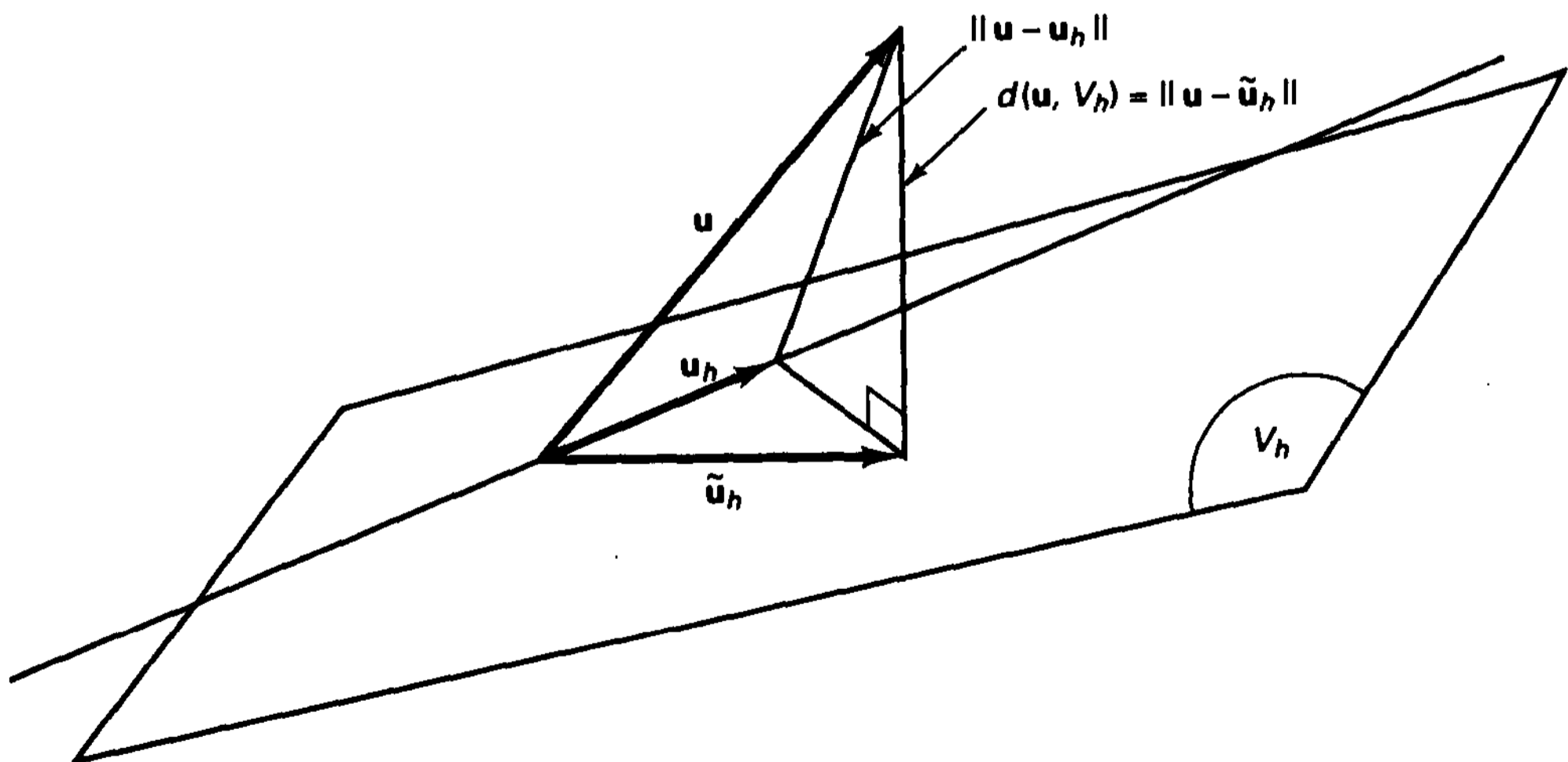


Figure 4.22 Schematic representation of solutions and distances; for optimal convergence $\|\mathbf{u} - \mathbf{u}_h\| \leq c d(\mathbf{u}, V_h)$ with c independent of h and κ .

takes. Mathematically, therefore, our purpose is to find conditions on V_h such that

$\ \mathbf{u} - \mathbf{u}_h\ \leq c d(\mathbf{u}, V_h)$ <p><i>with a constant c independent of h and κ.</i></p>

(4.156)

These conditions shall guide us in our choice of effective finite elements and discretizations.

The inequality (4.156) means that the distance between the continuous solution \mathbf{u} and the finite element solution \mathbf{u}_h will be smaller than a (reasonably sized) constant c times $d(\mathbf{u}, V_h)$ and that this relationship will be satisfied with the *same* constant c irrespective of the bulk modulus used. Note that this *independence* of c from the bulk modulus is the key property we did not have in Section 4.3.4 when we derived a relation such as (4.156) [see (4.95)].

Assume that the condition (4.156) holds (with a reasonably sized constant c). Then if $d(\mathbf{u}, V_h)$ is $o(h^k)$, we know that $\|\mathbf{u} - \mathbf{u}_h\|$ is also $o(h^k)$, and since c is reasonably sized and independent of κ , we will in fact observe the same solution accuracy and improvement in accuracy as h is decreased irrespective of the bulk modulus in the problem. In this case the finite element spaces have good approximation properties for any value of κ , and the finite element discretization is reliable (see Section 1.3).

The relationship in (4.156) expresses our fundamental requirement for the finite element discretization, and finite element formulations that satisfy (4.156) do not lock (see Section 4.4.3). In the following discussion, we write (4.156) only in forms with which we can work more easily in choosing effective finite elements. One of these forms uses an inf-sup value and is the celebrated inf-sup condition.

To proceed further, we define the spaces K and D ,

$$K(q) = \{\mathbf{v} \mid \mathbf{v} \in V, \operatorname{div} \mathbf{v} = q\} \tag{4.157}$$

$$D = \{q \mid q = \operatorname{div} \mathbf{v} \text{ for some } \mathbf{v} \in V\} \tag{4.158}$$

and the corresponding spaces for our discretizations,

$$K_h(q_h) = \{\mathbf{v}_h \mid \mathbf{v}_h \in V_h, \operatorname{div} \mathbf{v}_h = q_h\} \tag{4.159}$$

$$D_h = \{q_h \mid q_h = \operatorname{div} \mathbf{v}_h \text{ for some } \mathbf{v}_h \in V_h\} \tag{4.160}$$

Hence the space $K_h(q_h)$, for a given q_h , corresponds to all the elements \mathbf{v}_h in V_h that satisfy $\operatorname{div} \mathbf{v}_h = q_h$. Also, the space D_h corresponds to all the elements q_h with $q_h = \operatorname{div} \mathbf{v}_h$ that are reached by the elements \mathbf{v}_h in V_h ; that is, for any q_h an element of D_h there is at least one element \mathbf{v}_h in V_h such that $q_h = \operatorname{div} \mathbf{v}_h$. Similar thoughts are applicable to the spaces K and D .

We recall that when κ is large, the quantity $\|\operatorname{div} \mathbf{u}_h\|$ will be small; the larger κ , the smaller $\|\operatorname{div} \mathbf{u}_h\|$, and it is difficult to obtain an accurate pressure prediction $p_h = -\kappa \operatorname{div} \mathbf{u}_h$. In the limit $\kappa \rightarrow \infty$ we have $\operatorname{div} \mathbf{u}_h = 0$, but the pressure p_h is still finite (and of course of order of the applied tractions) and therefore $\kappa(\operatorname{div} \mathbf{u}_h)^2 = 0$.

Before developing the inf-sup condition, let us state the ellipticity condition for the problem of total incompressibility: there is a constant α greater than zero and independent of h such that

$$a(\mathbf{v}_h, \mathbf{v}_h) \geq \alpha \|\mathbf{v}_h\|^2 \quad \forall \mathbf{v}_h \in K_h(0) \quad (4.161)$$

This condition in essence states that the deviatoric strain energy is to be bounded from below, a condition that is clearly satisfied. We further refer to and explain the ellipticity condition for the incompressible elasticity problem in Section 4.5.2.

Let us emphasize that in this finite element formulation the only variables are the displacements.

Obtaining the Inf-Sup Condition

The inf-sup condition—which when satisfied ensures that (4.156) holds—can now be developed as follows. Since the condition of total incompressibility clearly represents the most severe constraint, we consider this case. Then $q = 0$, \mathbf{u} belongs to $K(q)$ for $q = 0$ [that is, $K(0)$], and the continuous problem (4.151) becomes

$$\min_{\mathbf{v} \in K(0)} \left\{ \frac{1}{2} a(\mathbf{v}, \mathbf{v}) - \int_{\text{Vol}} \mathbf{f}^B \cdot \mathbf{v} \, d\text{Vol} \right\} \quad (4.162)$$

with the solution \mathbf{u} , while the discrete problem is

$$\min_{\mathbf{v}_h \in K_h(0)} \left\{ \frac{1}{2} a(\mathbf{v}_h, \mathbf{v}_h) - \int_{\text{Vol}} \mathbf{f}^B \cdot \mathbf{v}_h \, d\text{Vol} \right\} \quad (4.163)$$

with the solution \mathbf{u}_h .

Now consider condition (4.156). We notice that in this condition we compare distances. In the following discussion we characterize a distance as “small” if it remains of the same order of magnitude as $d(\mathbf{u}, V_h)$ as h decreases. Similarly, we will say that a vector is small if its length satisfies this definition and that a vector is “close” to another vector if the vector difference in the two vectors is small.

Since $\mathbf{u}_h \in K_h(0)$, and therefore always $\|\mathbf{u} - \mathbf{u}_h\| \leq \tilde{c} d[\mathbf{u}, K_h(0)]$ (see Exercise 4.47), we can also write condition (4.156) in the form

$$\boxed{d[\mathbf{u}, K_h(0)] \leq c d(\mathbf{u}, V_h)} \quad (4.164)$$

which means that we want the distance from \mathbf{u} to $K_h(0)$ to be small. This relation expresses the requirement that if the distance between \mathbf{u} and V_h (the complete finite element displacement space) decreases at a certain rate as $h \rightarrow 0$, then the distance between \mathbf{u} and the space in which the actual solution lies [because $\mathbf{u}_h \in K_h(0)$] decreases at the same rate.

Figure 4.23 shows schematically the spaces and vectors that we use. Let \mathbf{u}_{h0} be a vector of our choice in $K_h(0)$ and let \mathbf{w}_h be the corresponding vector such that

$$\tilde{\mathbf{u}}_h = \mathbf{u}_{h0} + \mathbf{w}_h \quad (4.165)$$

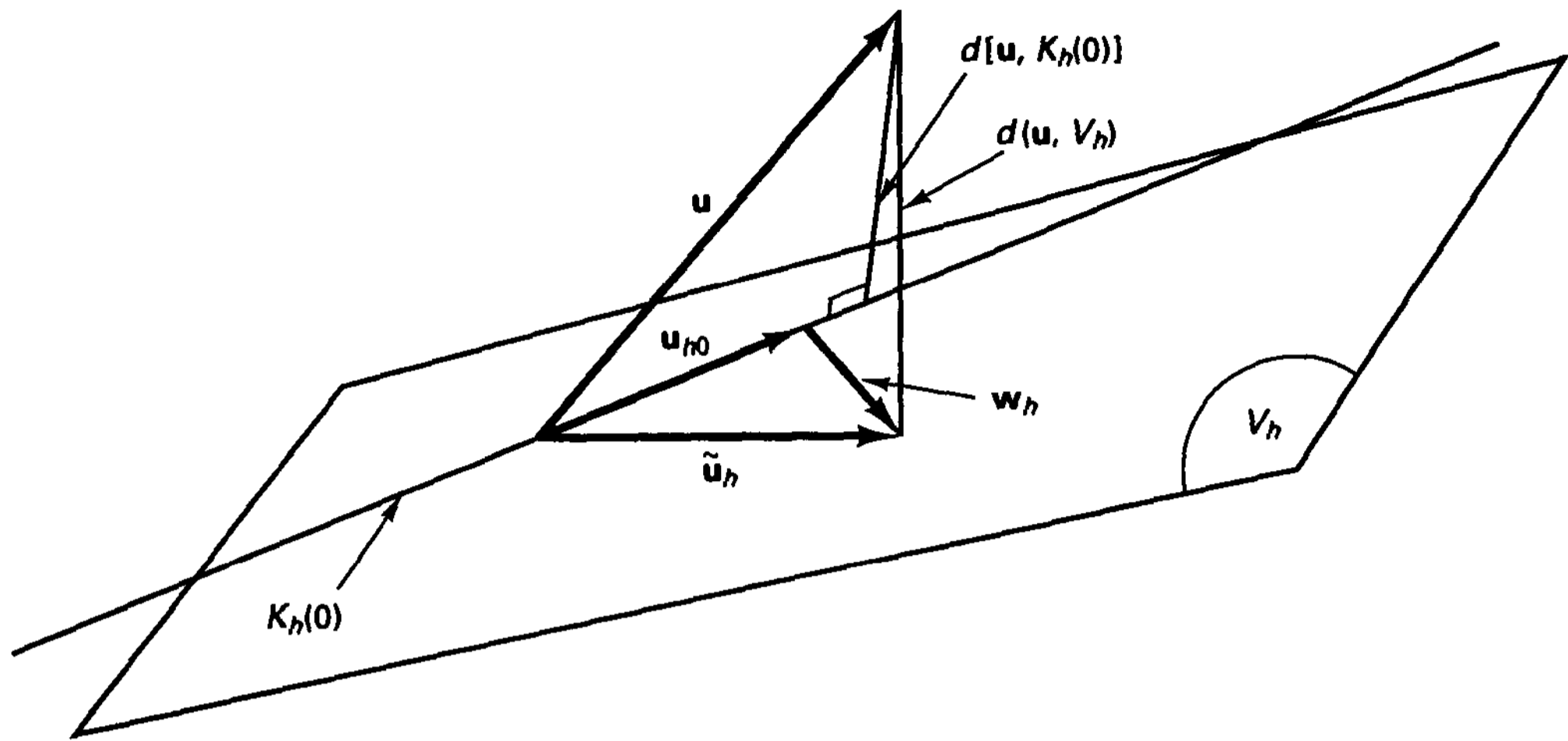


Figure 4.23 Spaces and vectors considered in deriving the inf-sup condition

We can then prove that the condition in (4.164) is fulfilled provided that

<p>for all $q_h \in D_h$, there is a $w_h \in K_h(q_h)$ such that</p> $\ w_h\ \leq c' \ q_h\ $ <p>where c' is independent of h and the bulk modulus κ.</p>	(4.166)
---	---------

First, we always have (see Exercise 4.48)

$$\|\operatorname{div}(\mathbf{u} - \tilde{\mathbf{u}}_h)\| \leq \alpha \|\mathbf{u} - \tilde{\mathbf{u}}_h\| \tag{4.167}$$

and hence,

$$\|\operatorname{div} \tilde{\mathbf{u}}_h\| \leq \alpha d(\mathbf{u}, V_h) \tag{4.168}$$

where α is a constant and we used $\operatorname{div} \mathbf{u} = 0$.

Second, we consider

$$\begin{aligned} \|\mathbf{u} - \mathbf{u}_{h0}\| &= \|\mathbf{u} - \tilde{\mathbf{u}}_h + w_h\| \\ &\leq \|\mathbf{u} - \tilde{\mathbf{u}}_h\| + \|w_h\| \end{aligned}$$

Now assume that (4.166) holds with $q_h = \operatorname{div} \tilde{\mathbf{u}}_h$. Because $\operatorname{div} \mathbf{u}_{h0} = 0$, we have $\operatorname{div} \tilde{\mathbf{u}}_h = \operatorname{div} w_h$, where we note that $\tilde{\mathbf{u}}_h$ is fixed by (4.155) and therefore q_h is fixed, but by choosing different values of \mathbf{u}_{h0} different values of w_h are also obtained. Then it follows that

$$\begin{aligned} \|\mathbf{u} - \mathbf{u}_{h0}\| &\leq d(\mathbf{u}, V_h) + c' \|q_h\| \\ &= d(\mathbf{u}, V_h) + c' \|\operatorname{div} \tilde{\mathbf{u}}_h\| \\ &\leq d(\mathbf{u}, V_h) + c' \alpha d(\mathbf{u}, V_h) \end{aligned} \tag{4.169}$$

We emphasize that we have used the condition (4.166) in this derivation and have assumed that \mathbf{u}_{h0} is an element in $K_h(0)$ such that w_h satisfies (4.166). Also, note that (4.168) established only that $\|\operatorname{div} \tilde{\mathbf{u}}_h\|$ is small, but then (4.169) established that $\|\mathbf{u} - \mathbf{u}_{h0}\|$ is small.

Third, since $\mathbf{u}_{ho} \in K_h(0)$, we obtain from (4.169),

$$d[\mathbf{u}, K_h(0)] \leq \|\mathbf{u} - \mathbf{u}_{ho}\| \leq (1 + \alpha c') d(\mathbf{u}, V_h) \quad (4.170)$$

which is (4.164) with $c = 1 + \alpha c'$, and we note that c is independent of h and the bulk modulus.

The crucial step in the derivation of (4.164) is that using (4.166) with $q_h = \operatorname{div} \tilde{\mathbf{u}}_h$, we can choose a vector \mathbf{w}_h that is small [which follows by using (4.166) and (4.168)]. We note that (4.166) is the only condition we need in order to prove (4.164) and is therefore the fundamental requirement to be satisfied in order to have a finite element discretization that will give an optimal rate of convergence.

The optimal rate of convergence requires in (4.164) that the constant c' in (4.166) be independent of h . Assume, for example, that instead of (4.166) we have $\|\mathbf{w}_h\| \leq (1/\beta_h)\|q_h\|$ with β_h decreasing with h . Then (4.170) will read

$$d[\mathbf{u}, K_h(0)] \leq \left(1 + \frac{\alpha}{\beta_h}\right) d(\mathbf{u}, V_h) \quad (4.171)$$

and hence the distance between \mathbf{u} and $K_h(0)$ will not decrease at the same rate as $d(\mathbf{u}, V_h)$. However, convergence, although not optimal, will still occur if $d(\mathbf{u}, V_h)$ decreases faster than β_h . This shows that the condition in (4.166) is a strong guarantee for good convergence properties of our discretization.

Let us now rewrite (4.166) in the form of the inf-sup condition. From (4.166) we obtain, with q_h and \mathbf{w}_h variables, $\mathbf{w}_h \in K_h(q_h)$, the condition

$$\|\mathbf{w}_h\| \|q_h\| \leq c' \|q_h\|^2 = c' \int_{\text{Vol}} q_h \operatorname{div} \mathbf{w}_h d\text{Vol} \quad (4.172)$$

or the condition is that for all $q_h \in D_h$, there is a $\mathbf{w}_h \in K_h(q_h)$ such that

$$\frac{1}{c'} \|q_h\| \leq \frac{\int_{\text{Vol}} q_h \operatorname{div} \mathbf{w}_h d\text{Vol}}{\|\mathbf{w}_h\|} \quad (4.173)$$

Hence, we want

$$\frac{1}{c'} \|q_h\| \leq \sup_{\mathbf{v}_h \in V_h} \frac{\int_{\text{Vol}} q_h \operatorname{div} \mathbf{v}_h d\text{Vol}}{\|\mathbf{v}_h\|} \quad (4.174)$$

and the inf-sup condition follows,

$$\inf_{q_h \in D_h} \sup_{\mathbf{v}_h \in V_h} \frac{\int_{\text{Vol}} q_h \operatorname{div} \mathbf{v}_h d\text{Vol}}{\|\mathbf{v}_h\| \|q_h\|} \geq \beta > 0$$

with β a constant independent of κ and h

(4.175)

We note that $\beta = 1/c'$.

Therefore, (4.166) implies (4.175), and it can also be proven that (4.175) implies (4.166) (see Example 4.42). (We will not present this proof until later because we must first discuss certain additional basic facts.) Hence, we may also refer to (4.166) as one form of the inf-sup condition.

The inf-sup condition says that for a finite element discretization to be effective, we must have that, for a sequence of finite element spaces, if we take any $q_h \in D_h$, there must be a $\mathbf{v}_h \in V_h$ such that the quotient in (4.175) is $\geq \beta > 0$. If the inf-sup condition is satisfied by the sequence of finite element spaces, then our finite element discretization scheme will exhibit the good approximation property that we seek, namely, (4.156) will be fulfilled.

Note that if β is dependent on h , say (4.175) is satisfied with β_h instead of β , then the expression in (4.171) will be applicable (for an example, see the three-node isoparametric beam element in Section 4.5.7).

Whether the inf-sup condition is satisfied depends, in general, on the specific finite element we use, the mesh topology, and the boundary conditions. If a discretization using a specific finite element always satisfies (4.175), for any mesh topology and boundary conditions, we simply say that the element satisfies the inf-sup condition. If, on the other hand, we know of one mesh topology and/or one set of (physically realistic) boundary conditions for which the discretization does not satisfy (4.175), then we simply say that the element does not satisfy the inf-sup condition.

Another Form of the Inf-Sup Condition

To analyze whether an element satisfies the inf-sup condition (4.175), another form of this condition is very useful, namely

For all \mathbf{u} there is a $\mathbf{u}_I \in V_h$ (a vector that interpolates \mathbf{u}) such that

$$\int_{\text{Vol}} \text{div}(\mathbf{u} - \mathbf{u}_I) q_h \, d\text{Vol} = 0 \quad \text{for all } q_h \in D_h \tag{4.176}$$

$$\|\mathbf{u}_I\| \leq c \|\mathbf{u}\|$$

with the constant c independent of \mathbf{u} , \mathbf{u}_I , and h .

The equivalence of (4.176) and (4.175) [and hence (4.166)] can be formally proven (see F. Brezzi and M. Fortin [A] and F. Brezzi and K. J. Bathe [A, B]), but to simply relate the statements in (4.176) to our earlier discussion, we note that two fundamental requirements emerged in the derivation of the inf-sup condition; namely, that there is a vector \mathbf{w}_h such that (see Figure 4.23)

$$\text{div } \mathbf{w}_h = \text{div } \tilde{\mathbf{u}}_h \tag{4.177}$$

and [see (4.166) and (4.168)]

$$\|\mathbf{w}_h\| \leq c^* d(\mathbf{u}, V_h) \tag{4.178}$$

where c^* is a constant.

We note that (4.176) corresponds to (4.177) and (4.178) if we consider the vector $\tilde{\mathbf{u}}_h - \mathbf{u}$ (the vector of difference between the best approximation in V_h and the exact solution) the *solution vector* and the vector \mathbf{w}_h the *interpolation vector*.

Hence, the conditions are that the interpolation vector \mathbf{w}_h shall satisfy the above divergence and “small-size” conditions *for and measured on* the vector $(\tilde{\mathbf{u}}_h - \mathbf{u})$ in order to have an effective discretization scheme.

The three expressions of the inf-sup condition, (4.166), (4.175), and (4.176), are useful in different ways but of course all express the same requirement. In mathematical analyses the forms (4.166) and (4.175) are usually employed, whereas (4.176) is frequently most easily used to prove whether a specific element satisfies the condition (see Example 4.36).

Considering the inf-sup condition, we recognize that the richer the space $K_h(0)$, the greater the capacity to satisfy (4.175) [that is, (4.164)]. However, unfortunately, using the standard displacement-based elements, the constraint is generally too strong for the elements and meshes (i.e., spaces V_h) of interest and the discretizations lock (see Fig. 4.20). We therefore turn to mixed formulations that do not lock and that exhibit the desired rates of convergence. Excellent candidates are the displacement/pressure formulations already introduced in Section 4.4.3. However, whereas the pure displacement formulation is (always) stable but generally locks, for any mixed formulation, a main additional concern is that it be stable. We shall see in the following discussion that the conditions of no locking and stability are fulfilled if by appropriate choice of the displacement and pressure interpolations the inf-sup condition is satisfied, and the desired (optimal) convergence rate is also obtained if the interpolations for the displacements and pressure are chosen appropriately.

Weakening the Constraint

Let us consider the u/p formulation. The variational discrete problem in the u/p formulation [corresponding to (4.140) and (4.143)] is

$$\min_{\mathbf{v}_h \in V_h} \left\{ \frac{1}{2} a(\mathbf{v}_h, \mathbf{v}_h) + \frac{\kappa}{2} \int_{\text{Vol}} [P_h(\text{div } \mathbf{v}_h)]^2 d\text{Vol} - \int_{\text{Vol}} \mathbf{f}^B \cdot \mathbf{v}_h d\text{Vol} \right\} \quad (4.179)$$

where the projection operator P_h is defined by

$$\int_{\text{Vol}} [P_h(\text{div } \mathbf{v}_h) - \text{div } \mathbf{v}_h] q_h d\text{Vol} = 0 \quad \text{for all } q_h \in Q_h \quad (4.180)$$

and Q_h is a “pressure space” to be chosen. We see that Q_h always contains $P_h(D_h)$ but that Q_h is sometimes larger than $P_h(D_h)$, which is a case that we shall discuss later.

To recognize that (4.179) and (4.180) are indeed equivalent to the u/p formulation, we rewrite (4.179) and (4.180) as

$$2G \int_{\text{Vol}} \boldsymbol{\epsilon}'_{ij}(\mathbf{u}_h) \boldsymbol{\epsilon}'_{ij}(\mathbf{v}_h) d\text{Vol} - \int_{\text{Vol}} p_h \text{div } \mathbf{v}_h d\text{Vol} = \int_{\text{Vol}} \mathbf{f}^B \cdot \mathbf{v}_h d\text{Vol} \quad \forall \mathbf{v}_h \in V_h \quad (4.181)$$

$$\int_{\text{Vol}} \left(\frac{p_h}{\kappa} + \text{div } \mathbf{u}_h \right) q_h d\text{Vol} = 0 \quad \forall q_h \in Q_h \quad (4.182)$$

These equations are (4.140) and (4.143) in Section 4.4.3, and we recall that they are valid for any value of $\kappa > 0$. The key point in the u/p formulation is that (4.180) [i.e., (4.182)] is applied individually for each element and, provided κ is finite, the pressure variables can be statically condensed out on the element level (before assembly of the element stiffness matrix into the global structure stiffness matrix).

Consider the following example.

EXAMPLE 4.34: Derive $P_h(\text{div } \mathbf{v}_h)$ for the 4/1 element shown in Fig. E4.34. Hence, evaluate the term $(\kappa/2) \int_{\text{Vol}} [P_h(\text{div } \mathbf{v}_h)]^2 d\text{Vol}$ in (4.179).

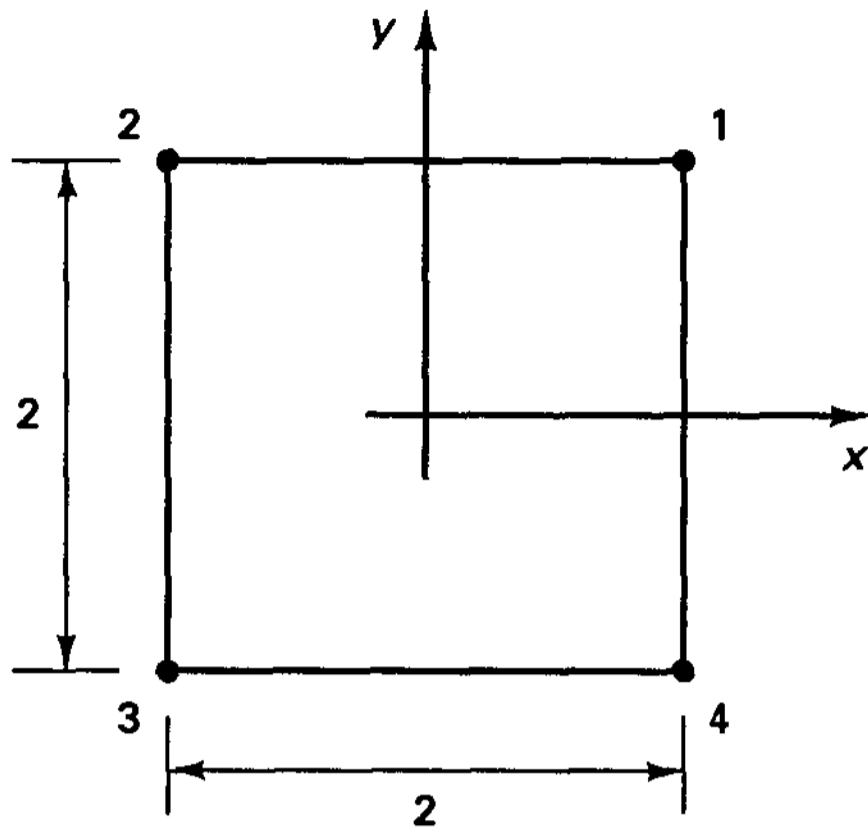


Figure E4.34 A 4/1 plane strain element

We have

$$\text{div } \mathbf{v}_h = [h_{1,x} \dots h_{4,x} \quad ; \quad h_{1,y} \dots h_{4,y}] \hat{\mathbf{u}}$$

where

$$\hat{\mathbf{u}}^T = [u_1 \dots u_4 \quad ; \quad v_1 \dots v_4]$$

We now use (4.180), with q_h an arbitrary nonzero constant (say $q_h = \alpha$), because here Q_h is the space of constant pressures. Since $P_h(\text{div } \mathbf{v}_h)$ is also constant, we have from (4.180),

$$4P_h(\text{div } \mathbf{v}_h)\alpha = \alpha \int_{\text{vol}} \text{div } \mathbf{v}_h \, d\text{Vol}$$

which gives

$$P_h(\text{div } \mathbf{v}_h) = \frac{1}{4}[1 \quad -1 \quad -1 \quad 1 \quad ; \quad 1 \quad 1 \quad -1 \quad -1] \hat{\mathbf{u}} = \mathbf{D}\hat{\mathbf{u}}$$

Hence,

$$\frac{\kappa}{2} \int_{\text{vol}} [P_h(\text{div } \mathbf{v}_h)]^2 \, d\text{Vol} = \frac{\kappa}{2} \hat{\mathbf{u}}^T \mathbf{G}_h \hat{\mathbf{u}}$$

where

$$\mathbf{G}_h = 4\mathbf{D}^T \mathbf{D}$$

Note that although we have used the pressure space Q_h , the stiffness matrix obtained from (4.179) will correspond to nodal point displacements only.

Also, we may note that the term $P_h(\text{div } \mathbf{v}_h)$ is simply $\text{div } \mathbf{v}_h$ at $x = y = 0$.

EXAMPLE 4.35: Consider the nine-node element shown in Fig. E4.35 and assume that \mathbf{v}_h is given by the nodal point displacements $u_1 = 1, u_5 = 0.5, u_8 = 0.5, u_9 = 0.25$ with all other nodal point displacements equal to zero. Let Q_h be the space corresponding to $\{1, x, y\}$. Evaluate $P_h(\text{div } \mathbf{v}_h)$.

To evaluate $P_h(\text{div } \mathbf{v}_h)$ we use the general relationship

$$\int_{\text{vol}} (P_h(\text{div } \mathbf{v}_h) - \text{div } \mathbf{v}_h)q_h \, d\text{Vol} = 0 \quad \forall q_h \in Q_h \tag{a}$$

In this example,

$$\text{div } \mathbf{v}_h = \frac{\partial u_h}{\partial x} + \frac{\partial v_h}{\partial y}$$

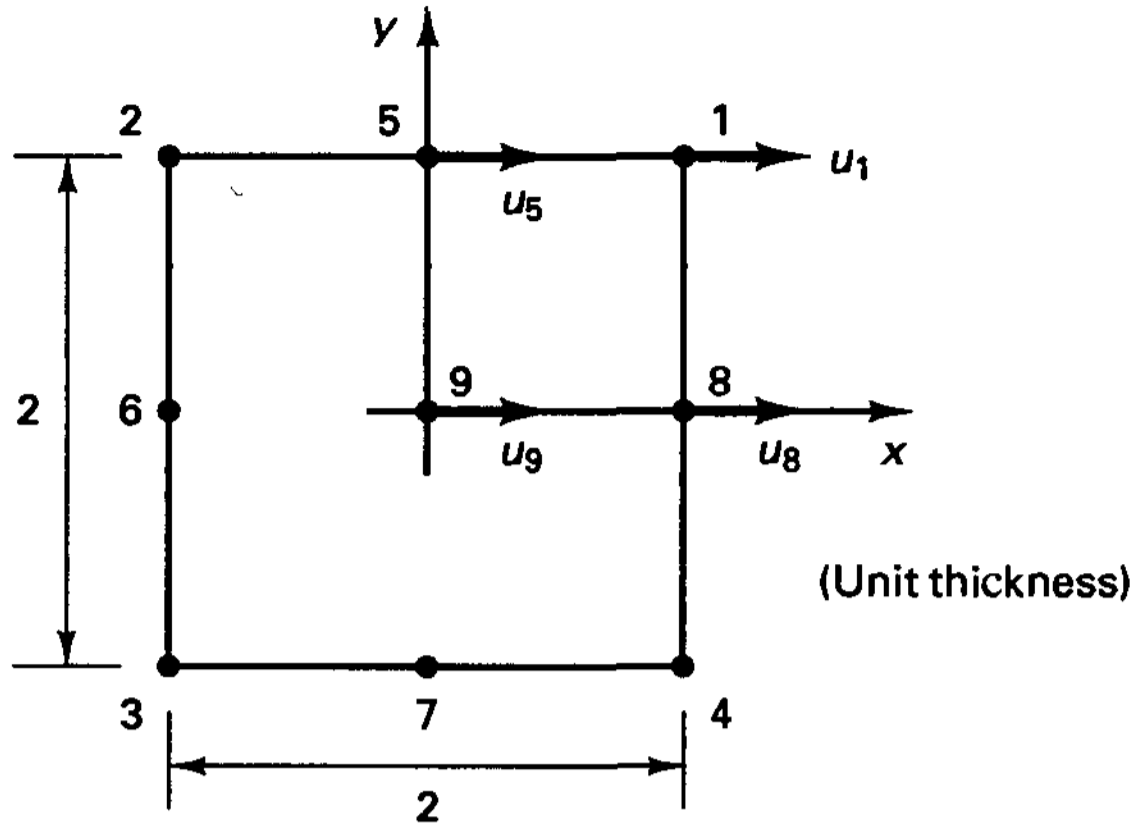


Figure E4.35 A 9/3 element subjected to nodal point displacements

where u_h and v_h are given by the element nodal point displacements. Hence,

$$u_h = \frac{1}{4}(1 + x)(1 + y)$$

$$v_h = 0$$

and

$$\text{div } \mathbf{v}_h = \frac{1}{4}(1 + y)$$

Let

$$P_h(\text{div } \mathbf{v}_h) = a_1 + a_2x + a_3y$$

then (a) gives
$$\int_{\text{Vol}} \left[(a_1 + a_2x + a_3y) - \frac{1}{4}(1 + y) \right] q_h dx dy = 0 \tag{b}$$

for $q_h = 1, x,$ and y . Hence, (b) gives the set of equations

$$\begin{bmatrix} \int_{\text{Vol}} dx dy & \int_{\text{Vol}} x dx dy & \int_{\text{Vol}} y dx dy \\ \int_{\text{Vol}} x^2 dx dy & \int_{\text{Vol}} xy dx dy & \\ \text{Symmetric} & \int_{\text{Vol}} y^2 dx dy & \end{bmatrix} \begin{bmatrix} a_1 \\ a_2 \\ a_3 \end{bmatrix} = \begin{bmatrix} \int_{\text{Vol}} \frac{1}{4}(1 + y) dx dy \\ \int_{\text{Vol}} \frac{1}{4}(1 + y) x dx dy \\ \int_{\text{Vol}} \frac{1}{4}(1 + y) y dx dy \end{bmatrix}$$

or

$$\begin{bmatrix} 4 & 0 & 0 \\ & \frac{4}{3} & 0 \\ \text{Sym.} & & \frac{4}{3} \end{bmatrix} \begin{bmatrix} a_1 \\ a_2 \\ a_3 \end{bmatrix} = \begin{bmatrix} 1 \\ 0 \\ \frac{1}{3} \end{bmatrix} \tag{c}$$

The solution of (c) gives $a_1 = \frac{1}{4}, a_2 = 0, a_3 = \frac{1}{4}$, and hence,

$$P_h(\text{div } \mathbf{v}_h) = \frac{1}{4}(1 + y)$$

This result is correct because $\text{div } \mathbf{v}_h$ can be represented exactly in Q_h and in such a case the projection gives of course the value of $\text{div } \mathbf{v}_h$.

The inf-sup condition corresponding to (4.179) is now like the inf-sup condition we discussed earlier but using the term $P_h(\text{div } \mathbf{v}_h)$ instead of $\text{div } \mathbf{v}_h$. Hence our condition is now

$$\inf_{q_h \in P_h(D_h)} \sup_{\mathbf{v}_h \in V_h} \frac{\int_{\text{Vol}} q_h \operatorname{div} \mathbf{v}_h \, d\text{Vol}}{\|\mathbf{v}_h\| \|q_h\|} \geq \beta > 0 \tag{4.183}$$

In other words, the inf-sup condition now corresponds to any element in V_h and $P_h(D_h)$. Hence, when applying (4.166), (4.175), or (4.176) to the mixed interpolated u/p elements, we now need to consider the finite element spaces V_h and $P_h(D_h)$, where $P_h(D_h)$ is used instead of D_h .

EXAMPLE 4.36: Prove that the inf-sup condition is satisfied by the 9/3 two-dimensional u/p element presented in Section 4.4.3.

For this proof we use the form of the inf-sup condition given in (4.176) (see F. Brezzi and K. J. Bathe [A]). Given \mathbf{u} smooth we must find an interpolation, $\mathbf{u}_I \in V_h$, such that for each element m ,

$$\int_{\text{Vol}^{(m)}} (\operatorname{div} \mathbf{u} - \operatorname{div} \mathbf{u}_I) q_h \, d\text{Vol}^{(m)} = 0 \tag{a}$$

for all q_h polynomials of degree ≤ 1 in $\text{Vol}^{(m)}$. To define \mathbf{u}_I we prescribe the values of each displacement at the nine element nodes (corner nodes, midside nodes, and the center node). We start with the corner nodes and require for these nodes $i = 1, 2, 3, 4$,

$$\mathbf{u}_I|_i = \mathbf{u}|_i \quad \text{eight conditions} \tag{b}$$

Then we adjust the values at the midside nodes $j = 5, 6, 7, 8$ in such a way that

$$\int_{S_j} (\mathbf{u} - \mathbf{u}_I) \cdot \mathbf{n} \, dS = \int_{S_j} (\mathbf{u} - \mathbf{u}_I) \cdot \boldsymbol{\tau} \, dS = 0 \quad \text{eight conditions} \tag{c}$$

for every edge S_1, \dots, S_4 of the element with \mathbf{n} the unit normal vector and $\boldsymbol{\tau}$ the unit tangential vector to the edge.

Next we note that (a) in particular implies, for every constant q_h ,

$$\int_{\text{Vol}^{(m)}} \operatorname{div}(\mathbf{u} - \mathbf{u}_I) q_h \, d\text{Vol}^{(m)} = q_h \sum_{S_1, \dots, S_4} \int_{S_j} (\mathbf{u} - \mathbf{u}_I) \cdot \mathbf{n} \, dS \tag{d}$$

We are left to use the two degrees of freedom at the element center node. We choose these in such a way that

$$\int_{\text{Vol}^{(m)}} \operatorname{div}(\mathbf{u} - \mathbf{u}_I) x \, d\text{Vol}^{(m)} = \int_{\text{Vol}^{(m)}} \operatorname{div}(\mathbf{u} - \mathbf{u}_I) y \, d\text{Vol}^{(m)} = 0 \tag{e}$$

We note now that (d) and (e) imply (a) and that \mathbf{u}_I , constructed element by element through (b) and (c), will be continuous from element to element. Finally, note that clearly if \mathbf{u} is a (vector) polynomial of degree ≤ 2 on the element, we obtain $\mathbf{u}_I \equiv \mathbf{u}$ and this ensures optimal bounds for $\|\mathbf{u} - \mathbf{u}_I\|$ and implies the condition $\|\mathbf{u}_I\| \leq c \|\mathbf{u}\|$ in (4.176) for all \mathbf{u} .

While in the u/p formulation the projection (4.180) is carried out for each element individually, in the u/p -c formulation a continuous pressure interpolation is assumed and then (4.181) and (4.182) are applied. The relation (4.182) with the continuous pressure interpolation gives a set of equations coupling the displacements and pressures for adjacent

elements. In this case the inf-sup condition is still given by (4.183), but now the pressure space corresponds to the nodal point continuous pressure interpolations.

In dealing with the inf-sup condition, we recognize that the ability to satisfy the condition depends on how the space $P_h(D_h)$ relates to the space of displacements V_h . Here again, P_h is the projection operator onto the space Q_h [see (4.180) and (4.182)], and, in general, the smaller the space Q_h , the easier it is to satisfy the condition. Of course, if for a given space V_h the inf-sup condition is satisfied with Q_h smaller than necessary, we have a stable element but the predictive capability is not as high as possible (namely, as high as it would be using the larger space Q_h but still satisfying the inf-sup condition).

For example, consider the nine-node isoparametric element (see Section 4.4.3). Using the u/p formulation with $P_h = I$ (the identity operator), the displacement-based formulation is obtained and the element locks. Reducing the constraint to obtain the 9/3 element, the inf-sup condition is satisfied (see Example 4.36) and optimal convergence rates are obtained for the displacements and the pressure; that is, the convergence rate for the displacements is $o(h^3)$ and for the stress is $o(h^2)$, which is all that we can expect with a parabolic interpolation of displacements and a linear interpolation of pressure. Reducing the constraint further to obtain the 9/1 element, the inf-sup condition is also satisfied, and while the element behavior for the interpolations used is still optimal, the predictive capability of this nine-node element is not the best possible (because a constant element pressure is assumed, whereas a linear pressure variation could be used).

This observation (about the quality of the solution) is explained by the error bounds (see, for example, F. Brezzi and K. J. Bathe [B]). Let $\mathbf{u}_I \in V_h$ be an interpolant of \mathbf{u} satisfying

$$\left. \begin{aligned} \int_{\text{vol}} [\text{div}(\mathbf{u} - \mathbf{u}_I)] q_h \, d\text{Vol} = 0 \quad \forall q_h \in P_h(D_h) \\ \|\mathbf{u}_I\| \leq c \|\mathbf{u}\| \end{aligned} \right\} \quad (4.184)$$

and

$$\|\mathbf{u}_I\| \leq c \|\mathbf{u}\|$$

If (4.184) holds for all possible solutions \mathbf{u} , then

$$\|\mathbf{u} - \mathbf{u}_h\| \leq c_1(\|\mathbf{u} - \mathbf{u}_I\| + \|(I - P_h)p\|) \quad (4.185)$$

and

$$\|p + \kappa P_h(\text{div } \mathbf{u}_h)\| \leq c_2(\|\mathbf{u} - \mathbf{u}_I\| + \|(I - P_h)p\|) \quad (4.186)$$

where $p = -\kappa \text{div } \mathbf{u}$ and c_1, c_2 are constants independent of h and κ . We note of course that (4.184) is the inf-sup condition with the weakened constraint $q_h \in P_h(D_h)$ [see (4.176)] and that the right-hand sides of (4.185) and (4.186) are smaller the closer P_h is to I .

4.5.2 The Inf-Sup Condition Derived from the Matrix Equations

Further insight into the inf-sup condition is obtained by studying the governing algebraic finite element equations. Let us consider the case of total incompressibility (it being the most severe case),

$$\begin{bmatrix} (\mathbf{K}_{uu})_h & (\mathbf{K}_{up})_h \\ (\mathbf{K}_{pu})_h & \mathbf{0} \end{bmatrix} \begin{bmatrix} \mathbf{U}_h \\ \mathbf{P}_h \end{bmatrix} = \begin{bmatrix} \mathbf{R}_h \\ \mathbf{0} \end{bmatrix} \quad (4.187)$$

where \mathbf{U}_h lists all the unknown nodal point displacements and \mathbf{P}_h lists the unknown pressure variables. Since the material is assumed to be totally incompressible, we have a square null

matrix equal in size to the number of pressure variables in the lower right of the coefficient matrix.

The mathematical analysis of the formulation resulting in (4.187) consists of a study of the *solvability* and the *stability* of the equations, where the stability of the equations implies their solvability.

The solvability of (4.187) simply refers to the fact that (4.187) can actually be solved for unique vectors \mathbf{U}_h and \mathbf{P}_h when \mathbf{R}_h is given.

The conditions for solvability (see Exercise 4.54) are

Condition i:

$$\mathbf{V}_h^T (\mathbf{K}_{uu})_h \mathbf{V}_h > 0 \quad \text{for all } \mathbf{V}_h \text{ satisfying } (\mathbf{K}_{pu})_h \mathbf{V}_h = \mathbf{0} \quad (4.188)$$

Condition ii:

$$(\mathbf{K}_{up})_h \mathbf{Q}_h = \mathbf{0} \quad \text{implies that } \mathbf{Q}_h \text{ must be zero} \quad (4.189)$$

The space of displacement vectors \mathbf{V}_h that satisfy $(\mathbf{K}_{pu})_h \mathbf{V}_h = \mathbf{0}$ represents the kernel of $(\mathbf{K}_{pu})_h$.

The *stability* of the formulation is studied by considering a sequence of problems of the form (4.187) with increasingly finer meshes. Let S be the smallest constant such that

$$\frac{\|\Delta \mathbf{u}_h\|_V + \|\Delta p_h\|_0}{\|\mathbf{u}_h\|_V + \|p_h\|_0} \leq S \frac{\|\Delta \mathbf{f}^B\|_{DV}}{\|\mathbf{f}^B\|_{DV}} \quad (4.190)$$

for all $\mathbf{u}_h, p_h, \mathbf{f}^B, \Delta \mathbf{u}_h, \Delta p_h, \Delta \mathbf{f}^B$, where $\|\cdot\|_V$ and $\|\cdot\|_0$ are the norms defined in (4.153), $\|\cdot\|_{DV}$ means the dual norm of $\|\cdot\|_V$ (see Section 2.7), and $\Delta \mathbf{f}^B, \Delta \mathbf{u}_h$, and Δp_h denote a prescribed perturbation on the load function \mathbf{f}^B and the resulting perturbations on the displacement vector \mathbf{u}_h and pressure p_h . Of course, we have

$$\begin{bmatrix} (\mathbf{K}_{uu})_h & (\mathbf{K}_{up})_h \\ (\mathbf{K}_{pu})_h & \mathbf{0} \end{bmatrix} \begin{bmatrix} \Delta \mathbf{U}_h \\ \Delta \mathbf{P}_h \end{bmatrix} = \begin{bmatrix} \Delta \mathbf{R}_h \\ \mathbf{0} \end{bmatrix} \quad (4.191)$$

where $\Delta \mathbf{R}_h$ corresponds to the load variation $\Delta \mathbf{f}^B$ and the norms of the finite element variables in (4.190) are given by the nodal point values listed in the solution vectors. Hence (4.190) expresses that for a given relative perturbation in the load vector, the corresponding relative perturbation in the solution is bounded by S times the relative perturbation in the loads.

For any given fixed mesh, satisfying the conditions of solvability (4.188) and (4.189) implies that (4.190) is satisfied for some S , the value of which depends on the mesh.

The formulation is stable if for any sequence of meshes the stability constant S is uniformly bounded. Hence, our question of stability reduces to asking for the conditions on the matrices $(\mathbf{K}_{uu})_h$ and $(\mathbf{K}_{up})_h$ that ensure that S remains uniformly bounded when using any sequence of meshes.

We considered briefly in Section 2.7 the stability conditions as related to a formulation that leads to a general coefficient matrix \mathbf{A} [see (2.169) to (2.179)]. If we specialize these considerations to the specific coefficient matrix used in the displacement/pressure formulations, we will find a rather natural result (see F. Brezzi and K. J. Bathe [B]), namely, that the stability conditions are an extension of the solvability conditions (4.188) and (4.189) in that stability in the use of these relations with increasingly finer meshes must be preserved.

The stability condition corresponding to the solvability condition (4.188) is that there is an $\alpha > 0$ independent of the mesh size such that

$$\mathbf{V}_h^T (\mathbf{K}_{uu})_h \mathbf{V}_h \geq \alpha \|\mathbf{v}_h\|_V^2 \quad \text{for all } \mathbf{V}_h \in \text{kernel} [(\mathbf{K}_{pu})_h] \quad (4.192)$$

This condition is the ellipticity condition already mentioned briefly in Section 4.5.1. The relation states that, for any fineness of mesh, the Rayleigh quotient obtained with any vector \mathbf{V}_h satisfying $(\mathbf{K}_{pu})_h \mathbf{V}_h = \mathbf{0}$, will be bounded from below by the constant α (which is independent of element mesh size). This ellipticity condition is always (i.e., for any choice of element interpolation) fulfilled by our displacement/pressure formulations. We elaborate upon this fact in the following example.

EXAMPLE 4.37: Consider the ellipticity condition in (4.192) and discuss that it is satisfied for any (practical) displacement/pressure formulation.

To understand that the ellipticity condition is fulfilled, we need to recall that (4.187) is the result of the finite element discretization in (4.179). Hence,

$$\mathbf{V}_h^T (\mathbf{K}_{uu})_h \mathbf{V}_h; \quad \mathbf{V}_h \in \text{kernel} (\mathbf{K}_{pu})_h \quad (a)$$

corresponds to twice the strain energy stored in the finite element discretization when \mathbf{v}_h corresponds to an element in V_h that satisfies $P_h(\text{div } \mathbf{v}_h) = 0$. However, unless we select the pressure space $Q_h = \{0\}$, that is, unless we totally remove the incompressibility constraint and the formulation does not contain strain energy due to compression—an impractical and trivial case—the expression in (a) will always be greater than zero (and bounded from below).

If (4.192) is not satisfied, we could easily stabilize the solution. This is achieved by considering the almost incompressible case and using the variational formulation

$$\min_{\mathbf{v}_h \in V_h} \left\{ \frac{1}{2} a(\mathbf{v}_h, \mathbf{v}_h) + \frac{\kappa^*}{2} \int_{\text{Vol}} (\text{div } \mathbf{v}_h)^2 d\text{Vol} + \frac{\kappa - \kappa^*}{2} \int [P_h(\text{div } \mathbf{v}_h)]^2 d\text{Vol} - \int_{\text{Vol}} \mathbf{f}^B \cdot \mathbf{v}_h d\text{Vol} \right\}$$

where κ^* is a bulk modulus of the order of the shear modulus and does not lead to locking. Of course, we could now assume $(\kappa - \kappa^*) \rightarrow \infty$.

This procedure amounts to evaluating a portion of the bulk energy as in the displacement method and using a projection for the remaining portion. Note that when κ is equal to κ^* , the part to be projected is zero. Hence the essence of the scheme is that a well-behaved part of the term that is difficult to deal with has been moved to be evaluated without the projection. This kind of stabilization to satisfy the ellipticity condition can be important in the design of formulations (see F. Brezzi and M. Fortin [A]). The procedure has been proposed to stabilize a displacement/pressure formulation for the analysis of inviscid fluids (see C. Nitikitpaiboon and K. J. Bathe [A]) and for the development of plate and shell elements (see D. N. Arnold and F. Brezzi [A]). However, the difficulty with this approach can be in selecting the portions of energies to be evaluated with and without projection, in particular when the various kinematic actions are fully coupled as, for instance, in the analysis of shell structures (see Section 5.4.2).

The stability condition corresponding to the solvability condition (4.189) is that there is a $\beta > 0$ independent of the mesh size h such that

$$\inf_{Q_h} \sup_{V_h} \frac{\mathbf{Q}_h^T (\mathbf{K}_{pu})_h \mathbf{V}_h}{\|q_h\| \|\mathbf{v}_h\|} \geq \beta > 0 \quad (4.193)$$

for every problem in the sequence.

Note that here we take the sup using the elements in V_h and the inf using the elements in Q_h . Of course, this relation is our inf-sup condition (4.183) in algebraic form, but we now have $q_h \in Q_h$, where Q_h is not necessarily equal to $P_h(D_h)$.

We note that a simple test consisting of counting displacement and pressure variables and comparing the number of such variables is not adequate to identify whether a mixed formulation is stable. The above discussion shows that such a test is certainly not sufficient to ensure the stability of a formulation and in general does not even ensure that condition (4.189) for solvability is satisfied (see also Exercises 4.60 and 4.64).

4.5.3 The Constant (Physical) Pressure Mode

Let us assume in this section that our finite element discretization contains no spurious pressure modes (which we discuss in the next section) and that the inf-sup condition for $q_h \in P_h(D_h)$ is satisfied.

We mentioned earlier (see Section 4.4.3) that when our elasticity problem corresponds to total incompressibility (i.e., we consider $q = \text{div } \mathbf{u} = 0$) and all displacements normal to the surface of the body are prescribed (i.e., S_u is equal to S), special considerations are necessary. Actually, we can consider the following two cases.

Case i: *All displacements normal to the body surface are prescribed to be zero.* In this case, the pressure is undetermined unless it is prescribed at one point in the body. Namely, assume that p_0 is a constant pressure. Then

$$\int_{\text{Vol}} p_0 \text{div } \mathbf{v}_h \, d\text{Vol} = p_0 \int_S \mathbf{v}_h \cdot \mathbf{n} \, dS = 0 \quad \forall \mathbf{v}_h \in V_h \quad (4.194)$$

where \mathbf{n} is the unit normal vector to the body surface. Hence, if the pressure is not prescribed at one point, we can add an arbitrary constant pressure p_0 to any proposed solution. A consequence is that the equations (4.187) cannot be solved unless the pressure is prescribed at one point, which amounts to eliminating one pressure degree of freedom [one column in $(\mathbf{K}_{up})_h$ and the corresponding row in $(\mathbf{K}_{pu})_h$]. If this pressure degree of freedom is not eliminated, Q_h is larger than $P_h(D_h)$, the solvability condition (4.189) is not satisfied, and the inf-sup value including this pressure mode is zero. For a discussion of the case Q_h larger than $P_h(D_h)$ but pertaining to spurious pressure modes, see Section 4.5.4.

Of course, instead of eliminating one pressure degree of freedom, it may be more expedient in practice to release some displacement degrees of freedom normal to the body surface.

Case ii: *All displacements normal to the body surface are prescribed with some nonzero values.* The difficulty in this case is that the incompressibility condition must be fulfilled

$$\int_{\text{Vol}} \text{div } \mathbf{v}_h \, d\text{Vol} = \int_S \mathbf{v}_h \cdot \mathbf{n} \, dS = 0 \quad \forall \mathbf{v}_h \in V_h \quad (4.195)$$

A constant pressure mode will also be present, which can be eliminated as discussed for Case i. If the body geometry is complex, it can be difficult to satisfy exactly the surface integral condition in (4.195). Since any error in fulfilling this condition can result in a large error in pressure prediction, it may be best in practice to leave the displacement(s) normal to the surface free at some node(s).

Let us next consider that the body is only almost incompressible, that κ is large but finite, and that the u/p formulation is used. In Case i, the arbitrary constant pressure p_0 will then automatically be set to zero (in the same way as spurious modes are set to zero; see Section 4.5.4). This is a most convenient result because we do not need to be concerned with the elimination of a pressure degree of freedom. Of course, in practice we could also leave some nodal point displacement degree(s) of freedom normal to the body surface free, which would eliminate the constant pressure mode.

With the constant pressure mode present in the model, Q_h is (by one basis vector) larger than $P_h(D_h)$ and the inf-sup value corresponding to this mode is zero. Nevertheless, we can solve the algebraic equations and obtain a reliable solution (unless κ is so large that the ill-conditioning of the coefficient matrix results in significant round-off errors, see Section 8.2.6).

In Case ii, it is probably best to proceed as recommended above, namely, to leave some nodal displacement(s) normal to the surface free, in order to give the material the freedom to satisfy the constraint of near incompressibility. Then the constant pressure mode is not present in the finite element model.

An important point in these considerations is that if all displacements normal to the surface of the body are prescribed, the pressure space will be larger than $P_h(D_h)$, but only by the constant pressure mode. This mode is of course a physical phenomenon and not a spurious mode. If the inf-sup condition for $q_h \in P_h(D_h)$ is satisfied, then the solution is rendered stable and accurate by simply eliminating the constant pressure mode (or using the u/p formulation with a not too large value of κ to automatically set the value of the constant pressure to zero). We consider in the next section the case of Q_h larger than $P_h(D_h)$ as a result of spurious pressure modes.

4.5.4 Spurious Pressure Modes—The Case of Total Incompressibility

We consider in this section the condition of total incompressibility and, merely for simplicity of discussion, that the physical constant pressure mode mentioned earlier is not present in the model. If it were actually present, the considerations given above would apply in addition to those we shall now present.

With this provision, we recall that in our discussion of the inf-sup condition we assumed that the space Q_h is equal to the space $P_h(D_h)$ [see (4.183)], whereas in (4.193) we have no such restriction. In an actual finite element solution we may well have $P_h(D_h) \subsetneq Q_h$, and it is important to recognize the consequences.

If the space Q_h is larger than the space $P_h(D_h)$, the solution will exhibit spurious pressure modes. These modes are a result of the numerical solution procedure only, namely, the specific finite elements and mesh patterns used, and have no physical explanation.

We define a spurious pressure mode as a (nonzero) pressure distribution p_s that satisfies the relation

$$\int_{\text{Vol}} p_s \operatorname{div} \mathbf{v}_h \, d\text{Vol} = 0 \quad \forall \mathbf{v}_h \in V_h \quad (4.196)$$

In the matrix formulation (4.187) a spurious pressure mode corresponds to the case

$$(\mathbf{K}_{up})_h \mathbf{P}_s = \mathbf{0} \quad (4.197)$$

where \mathbf{P}_s is the (nonzero) vector of pressure variables corresponding to p_s . Hence, the solvability condition (4.189) is not satisfied when spurious pressure modes are present, and of course the inf-sup value when testing over the complete space Q_h in (4.193) is zero.

Let us show that if Q_h is equal to $P_h(D_h)$, there can be no spurious pressure mode. Assume that \hat{p}_h is proposed to be a spurious pressure mode. If $Q_h = P_h(D_h)$, there is always a vector $\hat{\mathbf{v}}_h$ such that $\hat{p}_h = -P_h(\text{div } \hat{\mathbf{v}}_h)$. However, using $\hat{\mathbf{v}}_h$ in (4.196), we obtain

$$-\int_{\text{Vol}} \hat{p}_h \text{div } \hat{\mathbf{v}}_h d\text{Vol} = -\int_{\text{Vol}} \hat{p}_h P_h(\text{div } \hat{\mathbf{v}}_h) d\text{Vol} = \int_{\text{Vol}} \hat{p}_h^2 d\text{Vol} > 0 \quad (4.198)$$

meaning that (4.196) is not satisfied. On the other hand, if Q_h is greater than $P_h(D_h)$, notably $P_h(D_h) \subsetneq Q_h$, then we can find a pressure distribution in the space orthogonal to $P_h(D_h)$, and hence for that pressure distribution (4.196) is satisfied (see Example 4.38).

Hence, we now recognize that in essence we have two phenomena that may occur when testing a specific finite element discretization using displacements and pressure as variables:

1. The *locking phenomenon*, which is detected by the smallest value of the inf-sup expression not being bounded from below by a value $\beta > 0$ [see discussion following (4.156)]
2. The *spurious modes phenomenon*, which corresponds to a zero value of the inf-sup expression when we test with $q_h \in Q_h$.

Of course, when a discretization with spurious modes is considered, we might still be interested in the smallest nonzero value of the inf-sup expression, and we can focus on this value by only testing with $q_h \in P_h(D_h)$, in other words, by ignoring all spurious pressure modes.

The numerical inf-sup test described in Section 4.5.6 actually gives the smallest nonzero value of the inf-sup expression and also evaluates the number of spurious pressure modes.

Let us note here, as a side remark, that the spurious pressure modes have no relationship to the spurious zero energy modes mentioned in Section 5.5.6 (and which are a result of using reduced or selective numerical integration in the evaluation of element stiffness matrices). In the displacement/pressure formulations considered here, each element stiffness matrix is accurately calculated and exhibits only the correct physical rigid body modes. The spurious pressure modes in the *complete* mesh are a result of the specific displacement and pressure spaces used for the *complete* discretization.

One way to gain more insight into the relation (4.193) is to imagine the matrix $(\mathbf{K}_{up})_h$ [or $(\mathbf{K}_{pu})_h = (\mathbf{K}_{up})_h^T$] in diagonalized form (choosing the appropriate basis for displacements

and pressure variables), in which case we would have

$$\begin{array}{c}
 \begin{array}{|c|} \hline \text{Kernel } (\mathbf{K}_{up})_h \\ \hline \sqrt{\lambda_n} \\ \sqrt{\lambda_{n-1}}^\dagger \\ \vdots \\ \sqrt{\lambda_k} \\ \hline 0 \\ \vdots \\ 0 \\ \hline \text{Kernel } (\mathbf{K}_{pu})_h \\ \hline 0 \\ \vdots \\ 0 \\ \hline \end{array} \\
 (\mathbf{K}_{up})_h = \\
 \begin{array}{|c|} \hline \text{Elements} \\ \text{not shown} \\ \text{are zeros} \\ \hline \end{array} \\
 \begin{array}{|c|} \hline n_p \\ \hline \end{array} \\
 \begin{array}{|c|} \hline n_u \\ \hline \end{array} \\
 \end{array} \tag{4.199}$$

[†] We call the elements $\sqrt{\lambda_i}$ in anticipation of our discussion in Section 4.5.6.

In this representation the zero columns define the kernel of $(\mathbf{K}_{up})_h$ and each zero column corresponds to a spurious pressure mode. Also, since for any displacement vector $\hat{\mathbf{U}}_h$ we need

$$(\mathbf{K}_{pu})_h \hat{\mathbf{U}}_h = \mathbf{0} \tag{4.200}$$

and $(\mathbf{K}_{pu})_h = (\mathbf{K}_{up})_h^T$, the size of the kernel of $(\mathbf{K}_{pu})_h$ determines whether the solution is overconstrained. Whereas, on one hand, we want the kernel of $(\mathbf{K}_{up})_h$ to be zero (no spurious pressure modes), on the other hand, we want the kernel of $(\mathbf{K}_{pu})_h$ to be large so as to admit many linearly independent vectors $\hat{\mathbf{U}}_h$ that satisfy (4.200). Our actual displacement solution to the problem (4.187) will lie in the subspace spanned by these vectors, and if that subspace is too small, as a result of the pressure space Q_h being too large, the solution will be overconstrained. The theory on the inf-sup condition [see the discussion in Section 4.5.1 and (4.193)] showed that this overconstraint is detected by $\sqrt{\lambda_k}$ decreasing to zero as the mesh is refined. Vice versa, if $\sqrt{\lambda_k} \geq \beta > 0$, for any mesh, as the size of the elements is decreased, with β independent of the mesh, the solution space is not overconstrained and the discretization yields a reliable solution (with the optimal rate of convergence in the displacements and pressure, provided the pressure space is largest without violating the inf-sup condition; see Section 4.5.1).

4.5.5 Spurious Pressure Modes—The Case of Near Incompressibility

In the above discussion we assumed conditions of total incompressibility, and the use of either the u/p or the u/p -c formulation. Consider now that we have a finite (but large) κ and that the u/p formulation with static condensation on the pressure degrees of freedom (as is typical) is used. In this case, the governing finite element equations are, for a typical element,

(or the complete mesh),

$$\begin{bmatrix} (\mathbf{K}_{uu})_h & (\mathbf{K}_{up})_h \\ (\mathbf{K}_{pu})_h & (\mathbf{K}_{pp})_h \end{bmatrix} \begin{bmatrix} \mathbf{U}_h \\ \mathbf{P}_h \end{bmatrix} = \begin{bmatrix} \mathbf{R}_h \\ \mathbf{0} \end{bmatrix} \quad (4.201)$$

or
$$[(\mathbf{K}_{uu})_h - (\mathbf{K}_{up})_h(\mathbf{K}_{pp})_h^{-1}(\mathbf{K}_{pu})_h]\mathbf{U}_h = \mathbf{R}_h \quad (4.202)$$

So far we have assumed that no nonzero displacements are prescribed. It is an important observation that in this case any spurious pressure mode has no effect on the predicted displacements and pressure. The reason can be shown by considering $(\mathbf{K}_{up})_h$ in (4.199) with some zero columns. Since $(\mathbf{K}_{pp})_h$ is, in the same basis, diagonal with the bulk modulus $-\kappa^{-1}$ as diagonal elements and the corresponding right-hand-side is a zero vector, the solution for the spurious pressure mode values is zero (see also Example 4.39).

A different observation is that the coefficient matrix in (4.201) contains a large bulk modulus which, when κ^{-1} is close to zero, results in ill-conditioning—but this ill-conditioning is observed whether or not spurious pressure modes are present.

The spurious pressure modes can, however, have a drastic effect when nonzero displacements are prescribed. In this case, we recognize that the right-hand side corresponding to the pressure degrees of freedom may not be zero (see Section 4.2.2 on how nonzero displacements are imposed), and a large spurious pressure may be generated.

Clearly, a reliable element should not lock and ideally should not lead to any spurious pressure mode in any chosen mesh.

The elements listed in Tables 4.6 and 4.7 are of such a nature—except for the 4/1 two-dimensional u/p element (and the analogous 8/1 three-dimensional element). Using the 4/1 element, specific meshes with certain boundary conditions exhibit a spurious pressure mode, and the 4/1 element does not satisfy the inf-sup condition (4.183) unless used in special geometric arrangements of macroelements (see P. Le Tallec and V. Ruas [A] for an example). However, because of its simplicity, the 4/1 element is quite widely used in practice. We examine this element in more detail in the following example.

EXAMPLE 4.38: Consider the finite element discretization of 4/1 elements shown in Fig. E4.38 and show that the spurious checkerboard mode of pressure indicated in the figure exists.

We note that for this model all tangential displacements on the boundary are set to zero. In order to show that the pressure distribution indicated in Fig. E4.38 corresponds to a spurious pressure mode, we need to prove that (4.196) holds. Consider a single element as shown in Fig. E4.38(a). We have

$$\int_{\text{Vol}} p^{e_i} \text{div } \mathbf{v}_h^e d\text{Vol} = p^{e_i} [1 \quad -1 \quad -1 \quad 1 \quad \vdots \quad 1 \quad 1 \quad -1 \quad -1] \hat{\mathbf{u}}$$

where p^{e_i} is the constant pressure in the element and

If a patch of four adjacent elements is then considered, we note that for the displacement u_i shown in Fig. E4.38(b) we have

$$\int_{\text{Vol}} p \text{div } \mathbf{v}_h d\text{Vol} = [p^{e_1}(1) + p^{e_2}(1) + p^{e_3}(-1) + p^{e_4}(-1)] u_i = 0 \quad (a)$$

provided the pressure distribution corresponds to $p^{e_1} = -p^{e_2} = p^{e_3} = -p^{e_4}$. Similarly, for any displacement v_i we have

$$\int_{\text{Vol}} p \text{div } \mathbf{v}_h d\text{Vol} = [p^{e_1}(-1) + p^{e_2}(1) + p^{e_3}(1) + p^{e_4}(-1)] v_i = 0 \quad (b)$$

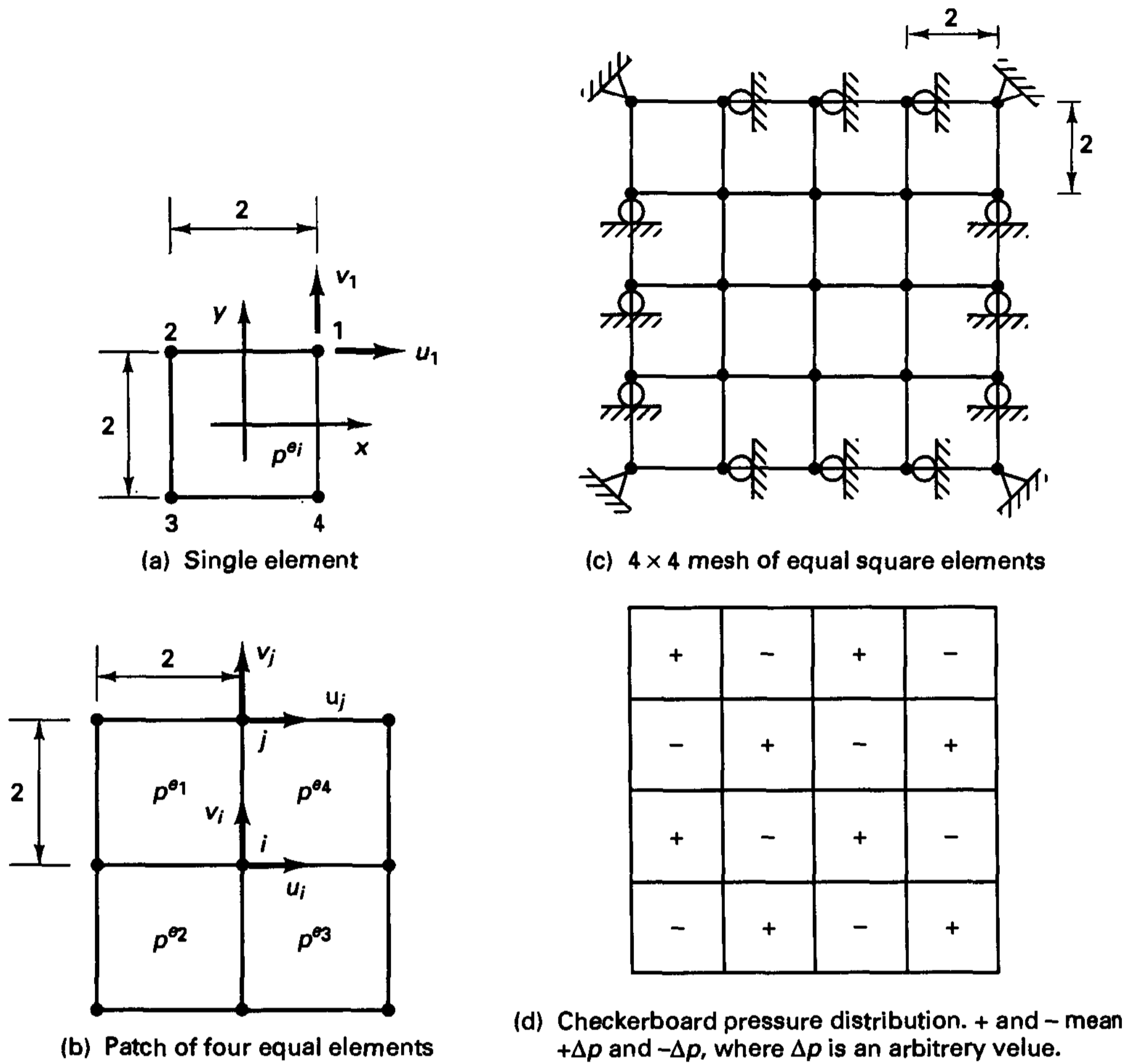


Figure E4.38 4/1 elements

For the normal displacement v_j on an edge of the patch, we similarly obtain

$$\int_{\text{Vol}} p \operatorname{div} \mathbf{v}_h d\text{Vol} = [p^{e1}(1) + p^{e2}(1)]v_j = 0 \quad (c)$$

On the other hand, for a tangential displacement u_j , the integral

$$\int_{\text{Vol}} p \operatorname{div} \mathbf{v}_h d\text{Vol} \neq 0$$

However, in the model in Fig. E4.38(c) all tangential displacements are constrained to zero. Hence, by superposition, using expressions (a) to (c), the relation (4.196) is satisfied for any nodal point displacements when the pressure distribution is the indicated checkerboard pressure.

Note that the same checkerboard pressure distribution is also a spurious pressure mode when more nodal point displacements than those given in Fig. E4.38(c) are constrained to zero. Also note that the (assumed) pressure distribution in Fig. E4.38(d) cannot be obtained by any nodal point displacements, hence this pressure distribution does not correspond to an element in $P_h(D_h)$.

In the above example, we showed that a spurious pressure mode is present when the 4/1 element is used in discretizations of equal-size square elements with certain boundary

conditions. The spurious pressure mode no longer exists when nonhomogeneous meshes are employed or at least one tangential displacement on the surface is released to be free.

Consider now that a force is applied to any one of the free degrees of freedom in Fig. E4.38(c). The solution is then obtained by solving (4.201) and, as pointed out before, the spurious pressure mode will not enter the solution (it will not be observed).

The spurious pressure mode, however, has a very significant effect on the calculated stresses when, for example, one tangential boundary displacement is prescribed to be nonzero while all other tangential boundary displacements are kept at zero.¹⁸ In this case the prescribed nodal point displacement results in a nonzero forcing vector for the pressure degrees of freedom, and the spurious pressure mode is excited. Hence, in practice, it is expedient to not constrain all tangential nodal point displacements on the body considered.

Let us conclude this section by considering the following example because it illustrates, in a simple manner, some of the important general observations we have made.

EXAMPLE 4.39:¹⁹ Assume that the governing equations (4.187) are

$$\begin{bmatrix} \alpha_1 & 0 & 0 & \beta_1 & 0 \\ 0 & \alpha_2 & 0 & 0 & \beta_2 \\ 0 & 0 & \alpha_3 & 0 & 0 \\ \beta_1 & 0 & 0 & 0 & 0 \\ 0 & \beta_2 & 0 & 0 & 0 \end{bmatrix} \begin{bmatrix} u_1 \\ u_2 \\ u_3 \\ p_1 \\ p_2 \end{bmatrix} = \begin{bmatrix} r_1 \\ r_2 \\ r_3 \\ g_1 \\ g_2 \end{bmatrix} \quad (a)$$

Of course, such simple equations are not obtained in practical finite element analysis, but the essential ingredients are those of the general equations (4.187). We note that the coefficient matrix corresponds to a fully incompressible material condition and that the entries g_1 and g_2 correspond to prescribed boundary displacements.

These equations can also be written as

$$\alpha_i u_i + \beta_i p_i = r_i; \quad \beta_i u_i = g_i; \quad i = 1, 2; \quad \alpha_3 u_3 = r_3$$

Assume that $\alpha_i > 0$ for all i (as we would have in practice). Then, $u_3 = r_3/\alpha_3$, and we need only consider the typical equations

$$\alpha u + \beta p = r; \quad \beta u = g \quad (b)$$

(where we have dropped the subscript i).

When the material is considered almost incompressible, u_3 is unchanged but (b) becomes

$$\alpha u_\epsilon + \beta p_\epsilon = r; \quad \beta u_\epsilon - \epsilon p_\epsilon = g \quad (c)$$

where $\epsilon = 1/\kappa$ (ϵ is very small when the bulk modulus κ is very large) and u_ϵ, p_ϵ is the solution sought. Equations (c) give

$$u_\epsilon = \frac{\epsilon r + \beta g}{\epsilon \alpha + \beta^2}; \quad p_\epsilon = \frac{\beta r - \alpha g}{\epsilon \alpha + \beta^2} \quad (d)$$

We can now make the following observations.

First, we consider the case of a spurious pressure mode, i.e., $\beta = 0$.

Case i: $\beta = g = 0$

This case corresponds to a spurious pressure mode and zero prescribed displacements.

The solution of (b) gives $u = r/\alpha$, with p undetermined.

The solution of (c) gives $u_\epsilon = r/\alpha, p_\epsilon = 0$.

¹⁸ We may note that these analysis conditions and results are similar to the conditions and results obtained when all displacements normal to the surface of a body are constrained to zero, except for one, at which a normal displacement is prescribed [see (4.195)].

¹⁹ This example was presented by F. Brezzi and K. J. Bathe [B].

Hence, we notice that the use of a finite bulk modulus allows us to solve the equations and suppresses the spurious pressure.

Case ii: $\beta = 0, g \neq 0$

This case corresponds to a spurious pressure mode and nonzero prescribed displacements (corresponding to this mode).

Now (b) has no solution for u and p .

The solution of (c) is $u_\epsilon = r/\alpha, p_\epsilon = -g/\epsilon$.

Hence, the spurious pressure becomes large as κ increases.

Next we consider the case of β very small.

Hence, we have no spurious pressure mode. Of course, the inf-sup condition is not passed if $\beta \rightarrow 0$.

Case iii: β is small

Let us also assume that $g = 0$.

Now (b) gives the solution $u = 0, p = r/\beta$.

The solution of (c) is $u_\epsilon \rightarrow 0$ and $p_\epsilon \rightarrow r/\beta$ for $\epsilon \rightarrow 0$ (β fixed, and hence we have $\beta^2 \gg \epsilon\alpha$), which is consistent with the solution of (b). Hence, the displacement approaches zero and the pressure becomes large when β is small and the bulk modulus increases. Of course, we test for this behavior with the inf-sup condition. For an actual finite element solution, this observation may be interpreted as taking a fixed mesh (β is fixed) and increasing κ . The result is that the pressure in the mode for which β is small increases while the displacements in this mode decrease.

However, (c) also gives $u_\epsilon \rightarrow r/\alpha$ and $p_\epsilon \rightarrow 0$ for $\beta \rightarrow 0$ (ϵ fixed, and hence we have $\beta^2 \ll \epsilon\alpha$), which is the behavior noted earlier in Case i. For an actual finite element solution this observation may be interpreted as taking a fixed κ and increasing the fineness of the mesh. As β is decreased as a result of mesh refinement, the pressure corresponding to this mode becomes small. Hence, the behavior of this pressure mode is when β is sufficiently small (which may mean a very fine mesh when κ is large) like the behavior of a spurious mode.

4.5.6 The Inf-Sup Test

The results of analytical studies of the inf-sup characteristics of various displacement/pressure elements are summarized in Tables 4.6 and 4.7 (see also F. Brezzi and M. Fortin [A]). However, an analytical proof of whether the inf-sup condition is satisfied by a specific element can be difficult, and for this reason a numerical test is valuable. Such a test can be applied to newly proposed elements and also to discretizations with elements of distorted geometries (recall that analytical studies assume homogeneous meshes of square elements). Of course, a numerical test cannot be completely affirmative (as an analytical proof is), but if a properly designed numerical test is passed, the formulation is very likely to be effective. The same idea is used when performing the patch test only in numerical form (to study incompatible displacement formulations and the effect of element geometric distortions) because an analytical evaluation is not achieved (see Section 4.4.1).

In the following discussion we present the numerical inf-sup test proposed by D. Chapelle and K. J. Bathe [A].

First consider the u/p formulation. In this case the inf-sup condition (4.183) can be written in the form

$$\inf_{\mathbf{w}_h \in V_h} \sup_{\mathbf{v}_h \in V_h} \frac{\int_{\text{Vol}} P_h(\text{div } \mathbf{w}_h) \text{div } \mathbf{v}_h d \text{Vol}}{\|P_h(\text{div } \mathbf{w}_h)\| \|\mathbf{v}_h\|} \geq \beta > 0 \quad (4.203)$$

or
$$\inf_{\mathbf{w}_h \in V_h} \sup_{\mathbf{v}_h \in V_h} \frac{b'(\mathbf{w}_h, \mathbf{v}_h)}{[b'(\mathbf{w}_h, \mathbf{w}_h)]^{1/2} \|\mathbf{v}_h\|} \geq \beta > 0 \tag{4.204}$$

where
$$b'(\mathbf{w}_h, \mathbf{v}_h) = \int_{\text{Vol}} P_h(\text{div } \mathbf{w}_h) P_h(\text{div } \mathbf{v}_h) d\text{Vol} = \int_{\text{Vol}} P_h(\text{div } \mathbf{w}_h) \text{div } \mathbf{v}_h d\text{Vol} \tag{4.205}$$

The relation (4.204) is in matrix form

$$\inf_{\mathbf{W}_h} \sup_{\mathbf{V}_h} \frac{\mathbf{W}_h^T \mathbf{G}_h \mathbf{V}_h}{[\mathbf{W}_h^T \mathbf{G}_h \mathbf{W}_h]^{1/2} [\mathbf{V}_h^T \mathbf{S}_h \mathbf{V}_h]^{1/2}} \geq \beta > 0 \tag{4.206}$$

where \mathbf{W}_h and \mathbf{V}_h are vectors of the nodal displacement values corresponding to \mathbf{w}_h and \mathbf{v}_h , and $\mathbf{G}_h, \mathbf{S}_h$ are matrices corresponding to the operator b' and the norm $\|\cdot\|_V$, respectively. The matrices \mathbf{G}_h and \mathbf{S}_h are, respectively, positive semidefinite and positive definite (for the problem we consider, see Section 4.5.1).

EXAMPLE 4.40: In Example 4.34 we calculated the matrix \mathbf{G}_h of a 4/1 element. Now also establish the matrix \mathbf{S}_h of this element.

To evaluate \mathbf{S}_h we recall that the norm of \mathbf{w} is given by [see (4.153)]

$$\|\mathbf{w}\|_V^2 = \sum_{i,j} \left\| \frac{\partial w_i}{\partial x_j} \right\|_{L^2(\text{Vol})}^2$$

Hence, for our case

$$\|\mathbf{w}_h\|_V^2 = \int_{-1}^{+1} \int_{-1}^{+1} \left[\left(\frac{\partial u}{\partial x} \right)^2 + \left(\frac{\partial u}{\partial y} \right)^2 + \left(\frac{\partial v}{\partial x} \right)^2 + \left(\frac{\partial v}{\partial y} \right)^2 \right] dx dy \tag{a}$$

where u, v are the components $w_i, i = 1, 2$.

Let us order the nodal point displacements in $\hat{\mathbf{u}}$ as in Example 4.34,

$$\hat{\mathbf{u}}^T = [u_1 \quad u_2 \quad u_3 \quad u_4 \quad \vdots \quad v_1 \quad v_2 \quad v_3 \quad v_4]$$

By definition, $\|\mathbf{w}_h\|_V^2 = \hat{\mathbf{u}}^T \mathbf{S}_h \hat{\mathbf{u}}$. Also, we have

$$\frac{\partial u}{\partial x} = \sum_{i=1}^4 h_{i,x} u_i; \quad \frac{\partial u}{\partial y} = \sum_{i=1}^4 h_{i,y} u_i \tag{b}$$

and we write in (a)

$$\begin{aligned} \left(\frac{\partial u}{\partial x} \right)^2 &= \left(\frac{\partial u}{\partial x} \right)^T \left(\frac{\partial u}{\partial x} \right) \\ \left(\frac{\partial u}{\partial y} \right)^2 &= \left(\frac{\partial u}{\partial y} \right)^T \left(\frac{\partial u}{\partial y} \right) \end{aligned} \tag{c}$$

Substituting from (c) and (b) into (a) we obtain

$$\begin{aligned} \mathbf{S}_h(1, 1) &= \int_{-1}^{+1} \int_{-1}^{+1} [(h_{1,x})^2 + (h_{1,y})^2] dx dy = \frac{2}{3} \\ \mathbf{S}_h(1, 2) &= \int_{-1}^{+1} \int_{-1}^{+1} [h_{1,x} h_{2,x} + h_{1,y} h_{2,y}] dx dy = -\frac{1}{6} \end{aligned}$$

and so on.

Similarly, the terms corresponding to the v_i degrees of freedom are calculated, and we obtain

$$\mathbf{S}_h = \begin{bmatrix} \tilde{\mathbf{S}}_h & \mathbf{0} \\ \mathbf{0} & \tilde{\mathbf{S}}_h \end{bmatrix}; \quad \tilde{\mathbf{S}}_h = \frac{1}{6} \begin{bmatrix} 4 & -1 & -2 & -1 \\ -1 & 4 & -1 & -2 \\ -2 & -1 & 4 & -1 \\ -1 & -2 & -1 & 4 \end{bmatrix}$$

Let us now consider the u/p -c formulation. In this case the same expression as in (4.206) applies, but we need to use $\mathbf{G}_h = (\mathbf{K}_{pu})_h^T \mathbf{T}_h^{-1} (\mathbf{K}_{pu})_h$, where \mathbf{T}_h is the matrix of the L^2 -norm of p_h (see Exercise 4.59); i.e., for any vector of pressure nodal values \mathbf{P}_h , we have $\|p_h\| = \mathbf{P}_h^T \mathbf{T}_h \mathbf{P}_h$.

The form (4.206) of the inf-sup condition is effective because we can numerically evaluate the inf-sup value of the left-hand side and do so for a sequence of meshes. If the left-hand-side inf-sup value approaches (asymptotically) a value greater than zero (and there are no spurious pressure modes, further discussed below), the inf-sup condition is satisfied. In practice, only a sequence of about three meshes needs to be considered (see examples given below).

The key is the evaluation of the inf-sup value of the expression in (4.206). We can show that this value is given by the square root of the smallest nonzero eigenvalue of the problem

$$\mathbf{G}_h \boldsymbol{\phi}_h = \lambda \mathbf{S}_h \boldsymbol{\phi}_h \quad (4.207)$$

Hence, if there are $(k - 1)$ zero eigenvalues (because \mathbf{G}_h is a positive semidefinite matrix) and we order the eigenvalues in ascending order, we find that the inf-sup value of the expression in (4.206) is $\sqrt{\lambda_k}$. We prove this result in the following example.

EXAMPLE 4.41: Consider the function $f(\mathbf{U}, \mathbf{V})$ defined as

$$f(\mathbf{U}, \mathbf{V}) = \frac{\mathbf{U}^T \mathbf{G} \mathbf{V}}{(\mathbf{U}^T \mathbf{G} \mathbf{U})^{1/2} (\mathbf{V}^T \mathbf{S} \mathbf{V})^{1/2}} \quad (a)$$

where \mathbf{G} is an $n \times n$ symmetric positive semidefinite matrix, \mathbf{S} is an $n \times n$ positive definite matrix, and \mathbf{U}, \mathbf{V} are vectors of order n . Show that

$$\inf_{\mathbf{U}} \sup_{\mathbf{V}} f(\mathbf{U}, \mathbf{V}) = \sqrt{\lambda_k} \quad (b)$$

where λ_k is the smallest nonzero eigenvalue of the problem

$$\mathbf{G} \boldsymbol{\phi} = \lambda \mathbf{S} \boldsymbol{\phi} \quad (c)$$

Let the eigenvalues of (c) be

$$\lambda_1 = \lambda_2 = \dots = \lambda_{k-1} = 0 < \lambda_k \leq \lambda_{k+1} \dots \leq \lambda_n$$

and the corresponding eigenvectors be $\boldsymbol{\phi}_1, \boldsymbol{\phi}_2, \dots, \boldsymbol{\phi}_n$.

To evaluate $f(\mathbf{U}, \mathbf{V})$, we represent \mathbf{U} and \mathbf{V} as

$$\mathbf{U} = \sum_{i=1}^n \tilde{u}_i \boldsymbol{\phi}_i; \quad \mathbf{V} = \sum_{i=1}^n \tilde{v}_i \boldsymbol{\phi}_i$$

Therefore, for any \mathbf{U} ,

$$\begin{aligned} \sup_{\mathbf{V}} f(\mathbf{U}, \mathbf{V}) &= \sup_{\tilde{v}_i} \frac{\sum_{i=1}^n \lambda_i \tilde{u}_i \tilde{v}_i}{\left(\sum_{i=1}^n \lambda_i \tilde{u}_i^2\right)^{1/2} \left(\sum_{i=1}^n \tilde{v}_i^2\right)^{1/2}} \\ &= \frac{1}{\left(\sum_{i=1}^n \lambda_i \tilde{u}_i^2\right)^{1/2}} \sup_{\tilde{v}_i} \frac{\sum_{i=1}^n \lambda_i \tilde{u}_i \tilde{v}_i}{\left(\sum_{i=1}^n \tilde{v}_i^2\right)^{1/2}} \end{aligned} \tag{d}$$

To evaluate the supremum value in (d), let us define $\alpha_i = \lambda_i \tilde{u}_i$; then we note that

$$\sum_{i=1}^n \lambda_i \tilde{u}_i \tilde{v}_i = \sum_{i=1}^n \alpha_i \tilde{v}_i \leq \sqrt{\sum_{i=1}^n \alpha_i^2 \sum_{i=1}^n \tilde{v}_i^2} \tag{e}$$

(by the Schwarz inequality), and equality is reached when $\tilde{v}_i = \alpha_i$. Substituting from (e) into (d) and using $\lambda_1 = \dots = \lambda_{k-1} = 0$, we thus obtain

$$\sup_{\mathbf{V}} f(\mathbf{U}, \mathbf{V}) = \sqrt{\frac{\sum_{i=1}^n \lambda_i^2 \tilde{u}_i^2}{\sum_{i=1}^n \lambda_i \tilde{u}_i^2}} = \sqrt{\frac{\sum_{i=k}^n \lambda_i^2 \tilde{u}_i^2}{\sum_{i=k}^n \lambda_i \tilde{u}_i^2}}$$

If we now let $\sqrt{\lambda_i} \tilde{u}_i = \beta_i$, we can write

$$\inf_{\mathbf{U}} \sup_{\mathbf{V}} f(\mathbf{U}, \mathbf{V}) = \inf_{(\tilde{u}_i)_{i=1}^n} \sqrt{\frac{\sum_{i=k}^n \lambda_i^2 \tilde{u}_i^2}{\sum_{i=k}^n \lambda_i \tilde{u}_i^2}} = \inf_{(\beta_i)_{i=k}^n} \sqrt{\frac{\sum_{i=k}^n \lambda_i \beta_i^2}{\sum_{i=k}^n \beta_i^2}} \tag{f}$$

The last expression in (f) has the form of a Rayleigh quotient (see Section 2.6), and we know that the smallest value is $\sqrt{\lambda_k}$, achieved for $\beta_k \neq 0$ and $\beta_i = 0$, for $i \neq k$, which gives the required result.

In practice, to calculate the inf-sup value $\sqrt{\lambda_k}$ an eigenvalue solution routine should be used that can skip over all zero eigenvalues and then calculate λ_k . A Sturm sequence test (see Section 11.4.3) will then also give the value of k , and then we can conclude directly whether the model contains spurious pressure modes. Namely, let n_p be the number of pressure degrees of freedom and n_u be the number of displacement degrees of freedom. Then the number of pressure modes, k_{pm} , is

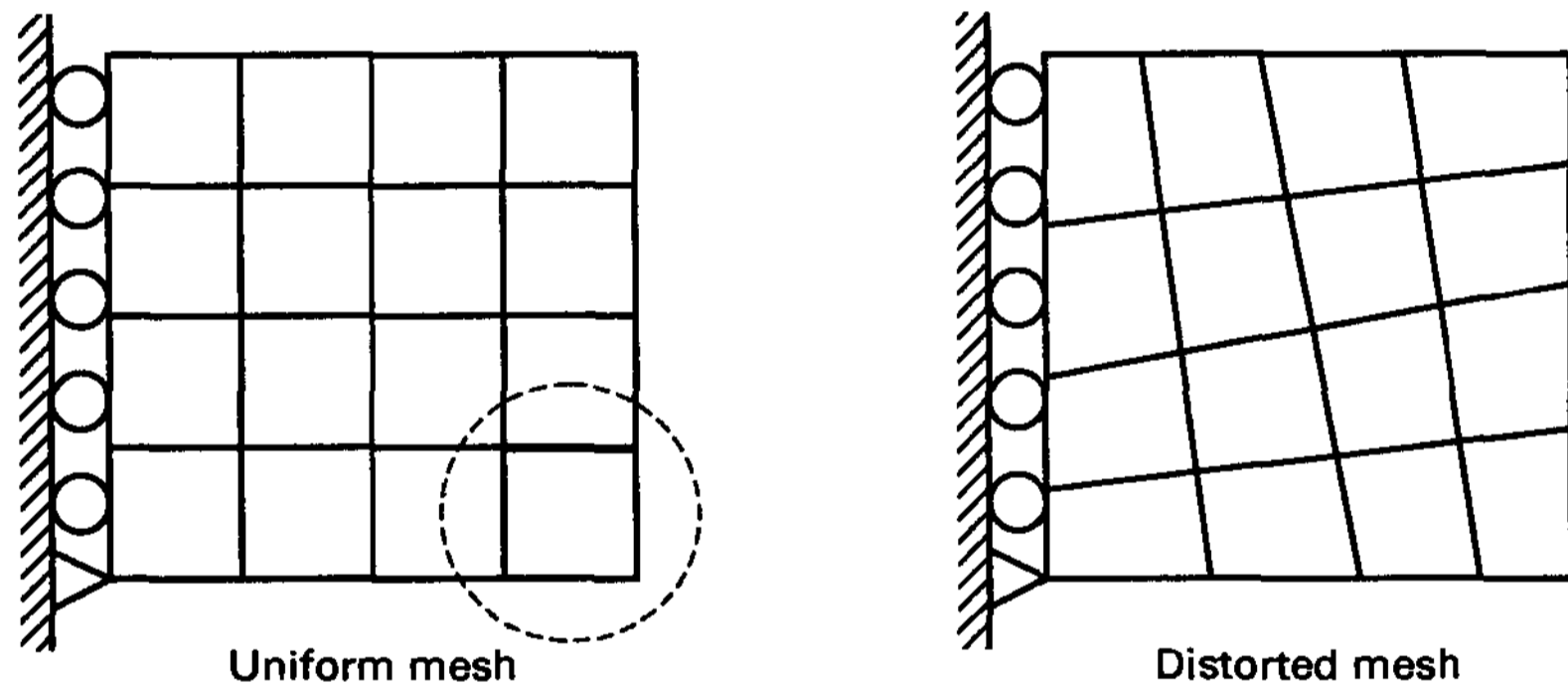
$$k_{pm} = k - (n_u - n_p + 1)$$

If $k_{pm} > 0$, the finite element discretization contains the constant pressure mode or spurious pressure modes [the inf-sup value in (4.193) is zero, although λ_k (the first nonzero

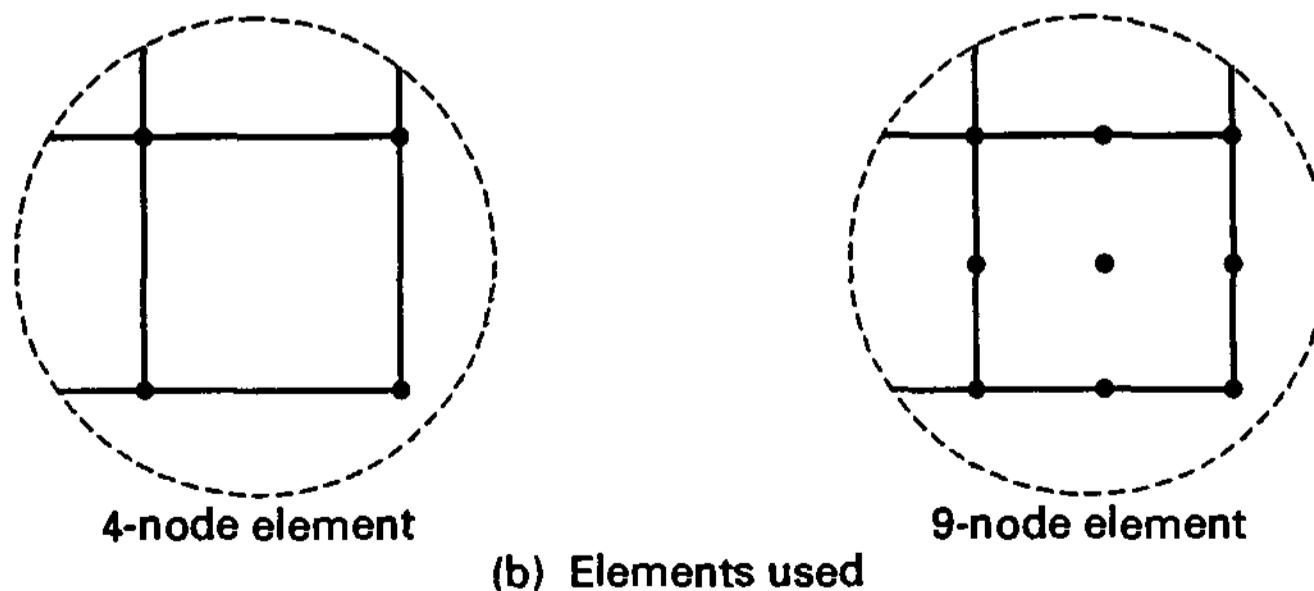
eigenvalue) may asymptotically approach a value greater than zero]. This formula follows because for there to be no pressure mode, the kernel $(\mathbf{K}_{up})_h$ must be zero [see (4.199)].

To demonstrate this inf-sup test, we show in Fig. 4.24 results obtained for the four-node and nine-node elements. We see that a sequence of three meshes used to calculate $\sqrt{\lambda_k}$ for each discretization was, in these cases, sufficient to identify whether the element locks. We note that, clearly, the four-node and the nine-node displacement-based elements do not satisfy the inf-sup condition and that the distortions of elements have a negligible effect on the results. In each of these tests k_{pm} was zero, hence, as expected, the idealizations do not contain any pressure modes. Of course, a spurious pressure mode would be found for the 4/1 element if the boundary conditions of Example 4.38 were used. That is, in the general testing of elements for spurious modes the condition of zero displacements on the complete boundary should be considered [the smaller the dimension of V_h , for a given Q_h , the greater the possibility that (4.196) is satisfied].

The solutions in Fig. 4.24 are numerical results pertaining to only one problem and one mesh topology. However, if the inf-sup condition is not satisfied in these results, then we can conclude that it is not satisfied in general.

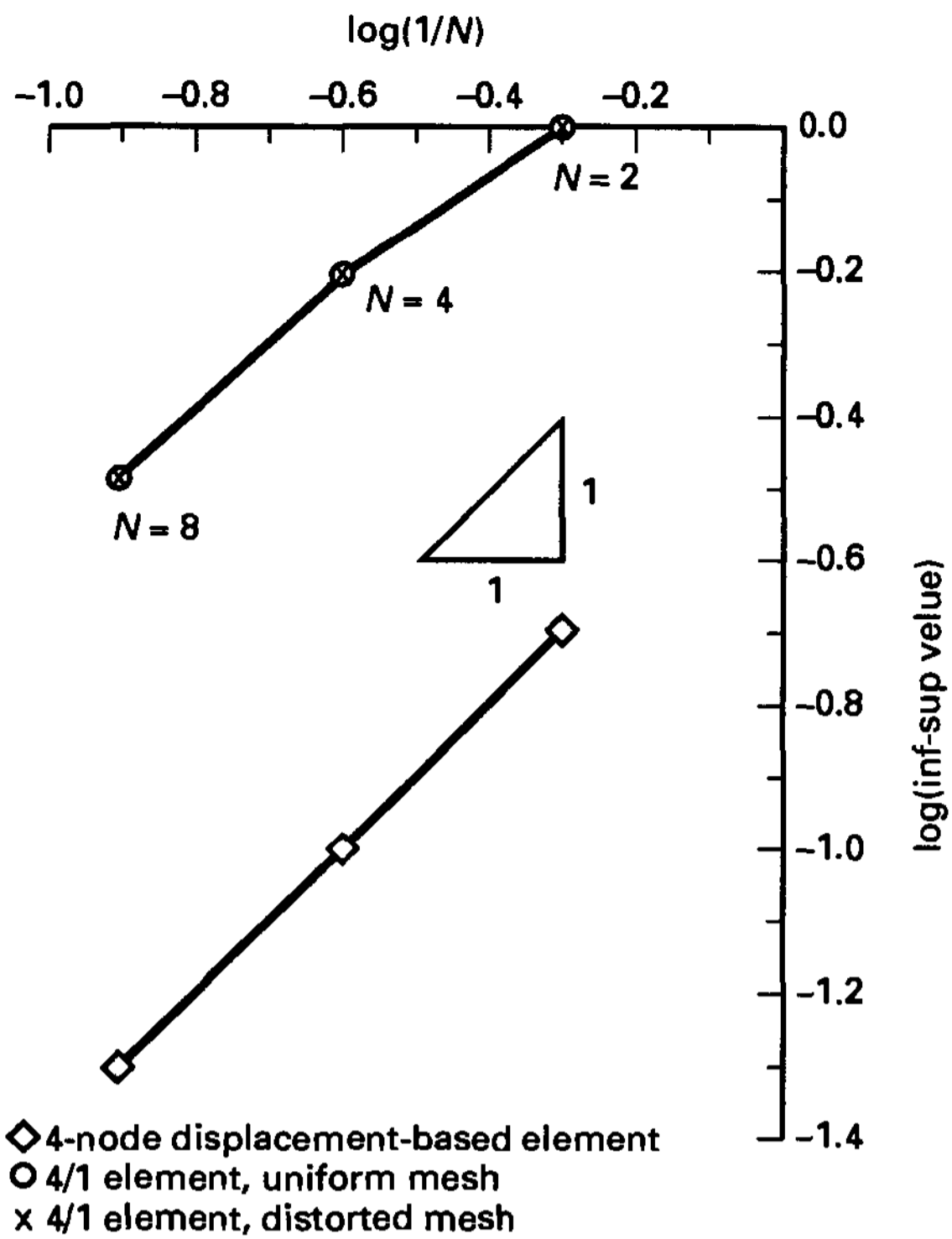


(a) Problem considered in inf-sup test. $N =$ number of elements along each side; we show $N = 4$, plane strain case

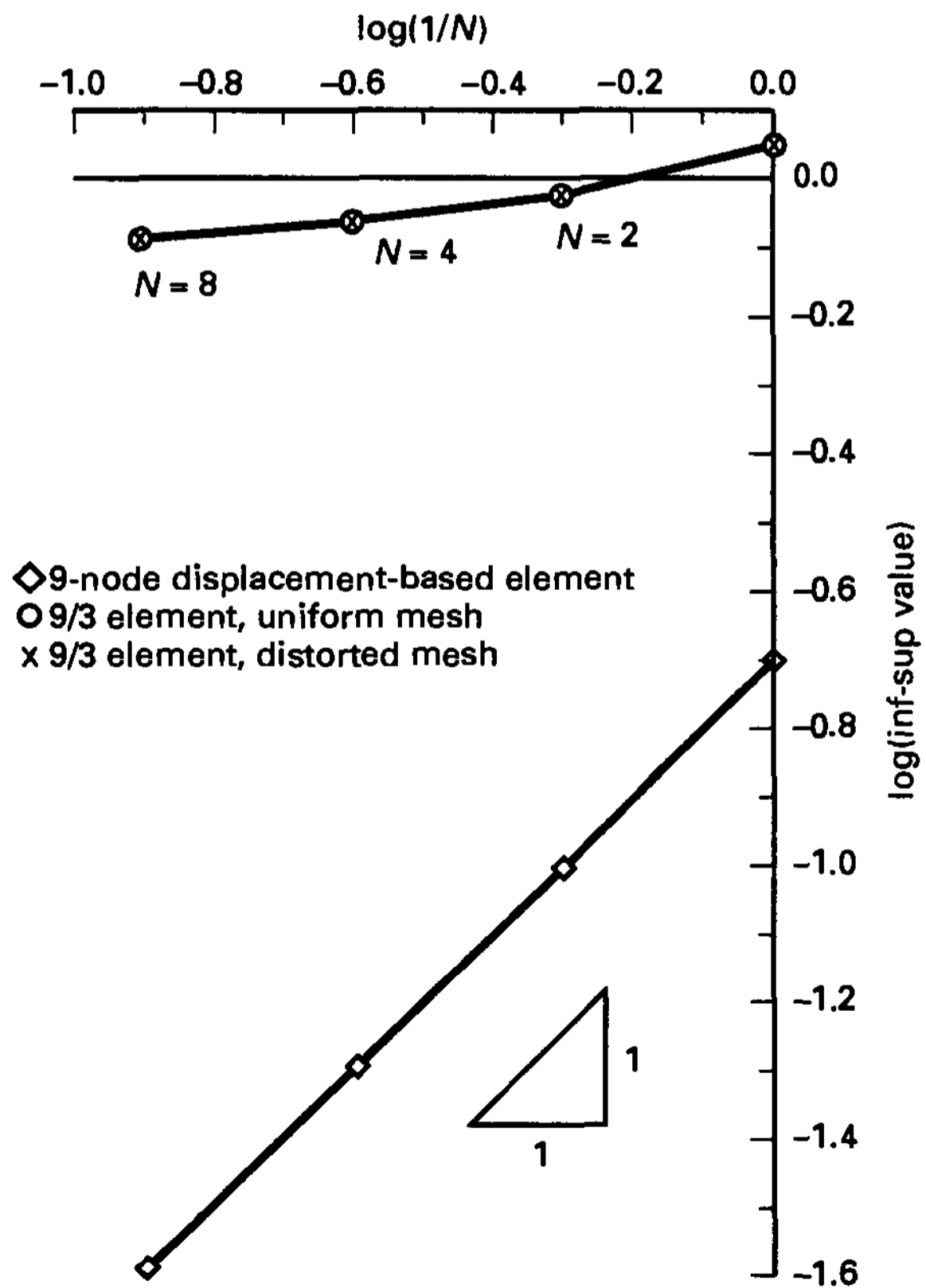


(b) Elements used

Figure 4.24 The inf-sup test applied in a simple problem



(c) 4-node elements



(d) 9-node elements

Figure 4.24 (continued)

Figure 4.25 shows results pertaining to the three-node triangular constant pressure element, formulated as a u/p element (see Exercise 4.50). The results show that the inf-sup condition is not satisfied by this element. Further, it is interesting to note that the meshes with pattern B do not contain spurious pressure modes, whereas the other meshes in general do contain spurious pressure modes.

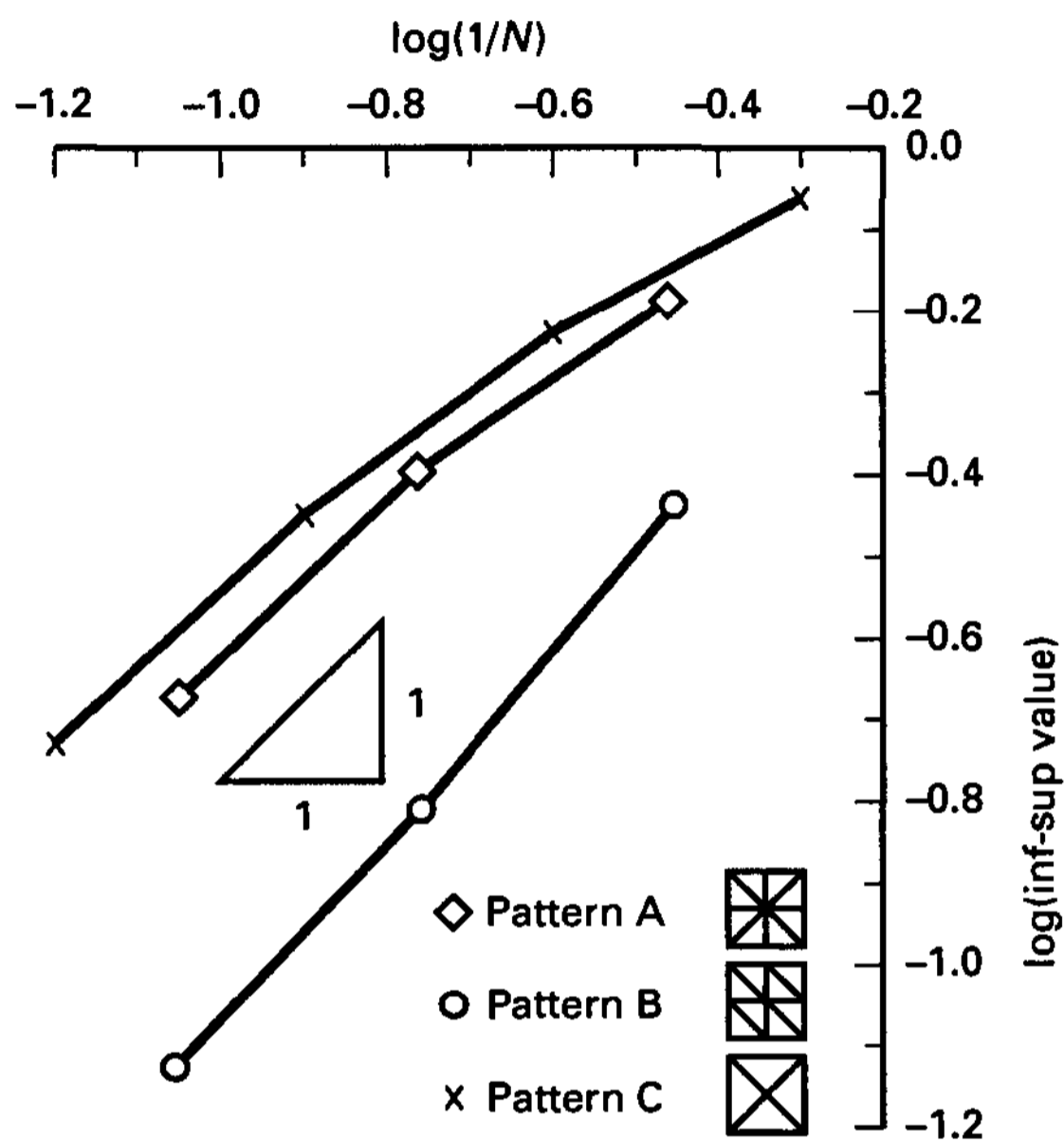


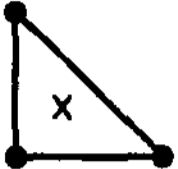
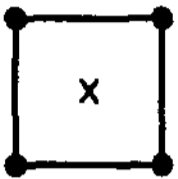
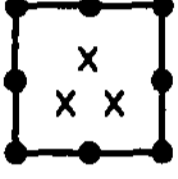
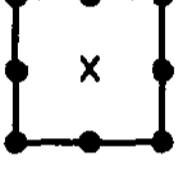
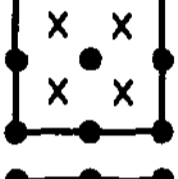
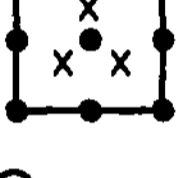
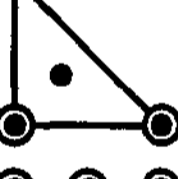
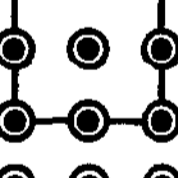
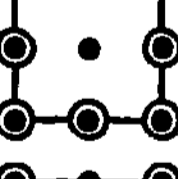
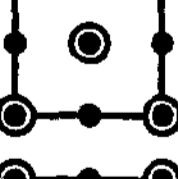
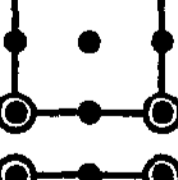
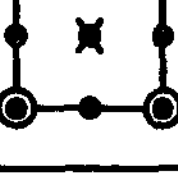
Figure 4.25 Inf-sup test of triangular elements, using problem of Fig.4.24(a). The patterns A and C result in spurious modes.

Additional results are given in Table 4.8 (see D. Chapelle and K. J. Bathe [A]). This table gives a summary of the results of the numerical evaluations of the inf-sup condition and analytical results, given, for example, by F. Brezzi and M. Fortin [A]. The numerical evaluation is useful because the same procedure applies to all u/p and $u/p-c$ elements, in uniform or distorted meshes, and elements can be evaluated for which no analytical results are (yet) available. Also, the effects of constructing macroelements from the basic elements can be easily evaluated (see D. Chapelle and K. J. Bathe [A] for some results regarding the 4/1 element used in a macroelement).

A similar numerical evaluation of the inf-sup condition for other constraint problems, in particular mixed formulations, can be performed (see, for example, Exercise 4.63).

Finally, we recall that in the derivation of the inf-sup condition (see Section 4.5.1), we showed that if (4.166) holds, then the inf-sup condition (4.175) follows. However, as we pointed out, the equivalence of (4.166) and (4.175) also requires that we prove that if (4.175) holds, then (4.166) follows. We deferred this proof to Example 4.42, which we present next.

TABLE 4.8 *Inf-sup numerical predictions*

Element [†]	Inf-sup condition		Remarks	
	Analytical proof	Numerical prediction		
	3/1 [‡]	Fail	Fail	See Fig. 4.25
	4/1 [‡]	Fail	Fail	See Fig. 4.24
	8/3	Fail	Fail	
	8/1	Pass	Pass	
	9/4	Fail	Fail	
	9/3	Pass	Pass	See Example 4.36, Fig. 4.24
	4/3-c	Pass	Pass	
	9/9-c	Fail	Fail	
	9/8-c	Fail	Fail	
	9/5-c	?	Fail	
	9/4-c	Pass	Pass	
	9/(4-c + 1)	?	Pass	For the element see P. M. Gresho, R. L. Lee, S. T. Chan, and J. M. Leone, Jr. [A]

[†] O, Continuous pressure degree of freedom; X, discontinuous pressure degree of freedom.

[‡] 3/1 and 4/1 element discretizations can contain spurious pressure modes.

EXAMPLE 4.42: Assume that the inf-sup condition (4.175) holds. Prove that (4.166) follows.

Let the eigenvectors and corresponding eigenvalues of (4.207) with \mathbf{G}_h corresponding to D_h [and not $P_h(D_h)$ because in (4.175) we consider D_h] be ϕ_i and λ_i , $i = 1, \dots, n$. The vectors ϕ_i form an orthonormal basis of V_h . Then we can write any vector \mathbf{w}_h in V_h as

$$\mathbf{w}_h = \sum_{i=1}^n w_h^i \phi_i \quad (a)$$

and we have by use of the eigenvalue and vector properties (see Section 2.5)

$$\|\operatorname{div} \mathbf{w}_h\|^2 = \sum_{i=1}^n \lambda_i (w_h^i)^2 \quad (b)$$

Let us now pick any q_h and any $\tilde{\mathbf{w}}_h$ satisfying $\operatorname{div} \tilde{\mathbf{w}}_h = q_h$. We can decompose $\tilde{\mathbf{w}}_h$ in the form of (a),

$$\tilde{\mathbf{w}}_h = \sum_{i=1}^{k-1} \tilde{w}_h^i \phi_i + \sum_{i=k}^n \tilde{w}_h^i \phi_i \quad (b)$$

The first summation sign in (b) defines a vector that belongs to $K_h(0)$ and may be a large component. However, we are concerned only with the component that is not an element of $K_h(0)$, which we call \mathbf{w}_h ,

$$\mathbf{w}_h = \sum_{i=k}^n \tilde{w}_h^i \phi_i$$

With this \mathbf{w}_h , we have

$$\begin{aligned} \frac{\|q_h\|^2}{\|\mathbf{w}_h\|^2} &= \frac{\sum_{i=k}^n \lambda_i (\tilde{w}_h^i)^2}{\sum_{i=k}^n (\tilde{w}_h^i)^2} \\ &\geq \lambda_k \\ &= \beta_h^2 \\ &\geq \beta^2 \end{aligned}$$

and (4.166) follows with $c' = 1/\beta$.

4.5.7 An Application to Structural Elements: The Isoparametric Beam Elements

In the above discussion we considered the general elasticity problem (4.151) and the corresponding variational discrete problem (4.154) subject to the constraint of (near or total) incompressibility. However, the ellipticity and inf-sup conditions are also the basic conditions to be considered in the development of beam, plate, and shell elements that are subject to shear and membrane strain constraints (see Section 5.4). We briefly introduced a mixed two-node beam element in Example 4.30 and we consider this and higher-order elements of the same kind in Section 5.4.1. Let us briefly discuss the ellipticity and inf-sup conditions for mixed interpolated and pure displacement-based beam elements.

General Considerations

The variational discrete problem of the displacement-based formulation is

$$\min_{\mathbf{v}_h \in V_h} \left\{ \frac{EI}{2} \int_0^L (\beta_h')^2 dx + \frac{GAk}{2} \int_0^L (\gamma_h)^2 dx - \int_0^L p w_h dx \right\} \quad (4.208)$$

where EI and GAk are the flexural and shear rigidities of the beam (see Section 5.4.1), L is the length of the beam, p is the transverse load per unit length, β_h is the section rotation, γ_h is the transverse shear strain,

$$\gamma_h = \frac{\partial w_h}{\partial x} - \beta_h \quad (4.209)$$

w_h is the transverse displacement, and an element of V_h is

$$\mathbf{v}_h = \begin{bmatrix} w_h \\ \beta_h \end{bmatrix} \quad (4.210)$$

The constraint to be dealt with is now the shear constraint,

$$\gamma_h = \frac{\partial w_h}{\partial x} - \beta_h \rightarrow 0 \quad (4.211)$$

In practice, γ_h is usually very small and can of course also be zero. Hence we have, using our earlier notation, the spaces

$$K_h(q_h) = \{\mathbf{v}_h \mid \mathbf{v}_h \in V_h, \gamma_h(\mathbf{v}_h) = q_h\} \quad (4.212)$$

$$D_h = \{q_h \mid q_h = \gamma_h(\mathbf{v}_h) \text{ for some } \mathbf{v}_h \in V_h\} \quad (4.213)$$

and the norms

$$\|\mathbf{v}_h\|^2 = \int_{\text{Vol}} \left[\left(\frac{\partial w_h}{\partial x} \right)^2 + L^2 \left(\frac{\partial \beta_h}{\partial x} \right)^2 \right] d\text{Vol}; \quad \|\gamma_h\|^2 = \int_{\text{Vol}} (\gamma_h)^2 d\text{Vol} \quad (4.214)$$

The ellipticity condition is satisfied in this problem formulation because

$$EI \int_0^L (\beta_h')^2 dx \geq \alpha \|\mathbf{v}_h\|^2 \quad \forall \mathbf{v}_h \in K_h(0) \quad (4.215)$$

with $\alpha > 0$ and independent of h . To prove this relation we need only to note that

$$\int_0^L \left(\frac{\partial w_h}{\partial x} \right)^2 dx = \int_0^L (\beta_h)^2 dx \leq \int_0^L L^2 \left(\frac{\partial \beta_h}{\partial x} \right)^2 dx \quad (4.216)$$

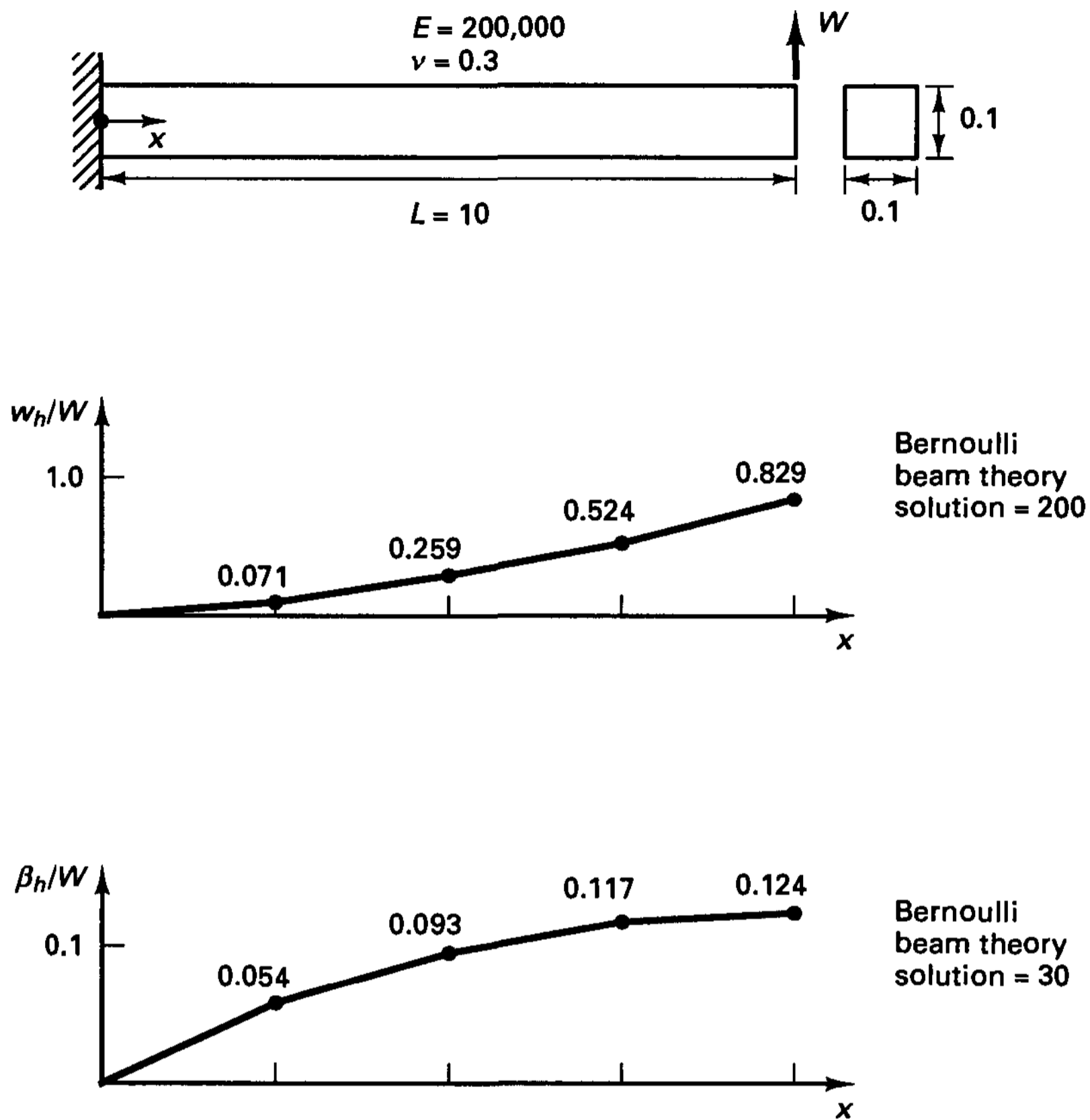
and therefore,
$$\|\mathbf{v}_h\|^2 \leq 2L^2 \int_{\text{Vol}} \left(\frac{\partial \beta_h}{\partial x} \right)^2 d\text{Vol} \quad (4.217)$$

giving $\alpha = EI/2L^2$.

The inf-sup condition for this formulation is

$$\inf_{\gamma_h \in D_h} \sup_{\mathbf{v}_h \in V_h} \frac{\int_{\text{Vol}} \gamma_h [(\partial w_h / \partial x) - \beta_h] d\text{Vol}}{\|\gamma_h\| \|\mathbf{v}_h\|} \geq c > 0 \quad (4.218)$$

in which the constant c is independent of h .

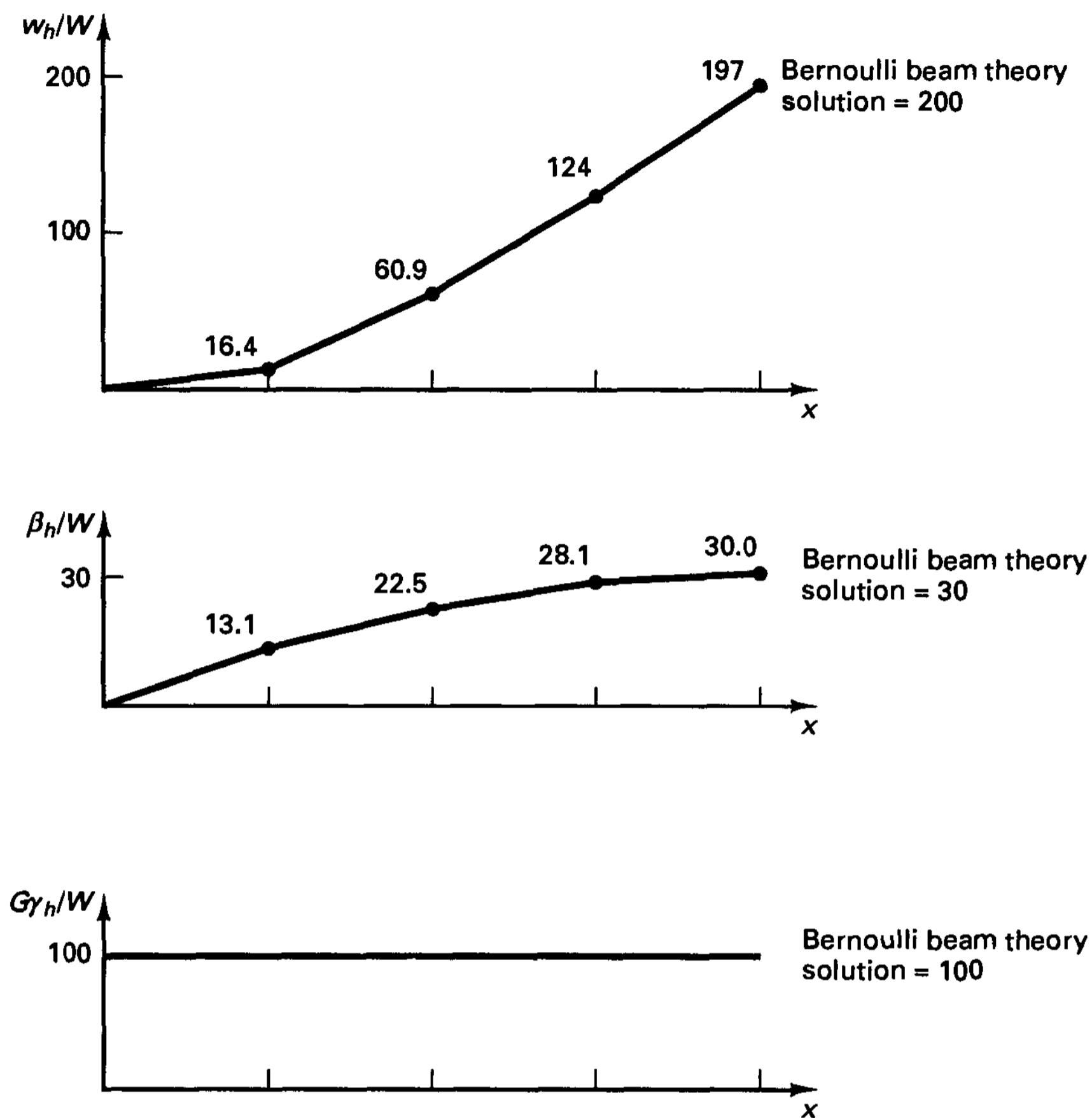


(a) Analysis with pure displacement-based element: w_h and β_h vary linearly over each element, and $\gamma_h = (\partial w_h / \partial x) - \beta_h$; since the values of w_h and β_h are very inaccurate, the shear strains are so too

Figure 4.26 Analysis of cantilever beam using two-node beam elements. Four equal length elements are used. (Shear correction factor k of (5.57) is taken equal to 1.0.)

The two-node element. Let us first consider the two-node displacement-based element for which w_h and β_h are assumed linear over each element [see Fig. 4.26(a) for an example solution]. A comparison of the computed results with the Bernoulli beam theory solution given in Fig. 4.26 shows that the element performs quite badly. In this case $K_h(0) = \{0\}$, and so the inf-sup condition in (4.218) is not satisfied. Referring to (4.164), we can also see that a good convergence behavior is not possible; namely, $d(\mathbf{u}, V_h) \rightarrow 0$ as we increase the space V_h , whereas $d[\mathbf{u}, K_h(0)] = \|\mathbf{u}\|$ (a constant value).

Next, consider the two-node mixed interpolated element for which w_h and β_h are linear and γ_h is constant over each element. Figure 4.26(b) shows the results obtained in the cantilever analysis and indicates the good predictive capability of this element. The ellipticity condition is again satisfied (see Exercise 4.61), and in addition we now need to investi-



(b) Analysis with mixed interpolated element; w_h and β_h vary linearly over each element, and γ_h is constant in each element

Figure 4.26 (continued)

gate whether the following inf-sup condition is satisfied:

$$\inf_{\gamma_h \in P_h(D_h)} \sup_{\mathbf{v}_h \in \mathbf{V}_h} \frac{\int_{\text{Vol}} \gamma_h [(\partial w_h / \partial x) - \beta_h] d\text{Vol}}{\|\gamma_h\| \|\mathbf{v}_h\|} \geq c > 0 \quad (4.219)$$

Now $K_h(0) \neq \{0\}$, and we test for the inf-sup condition by considering a typical γ_h (where γ_h is thought of as a variable). Then with a typical γ_h given, we choose

$$\hat{\mathbf{v}}_h = \begin{bmatrix} \hat{w}_h \\ \hat{\beta}_h \end{bmatrix} \quad (4.220)$$

with $\hat{\beta}_h = 0$ and $\partial \hat{w}_h / \partial x = \gamma_h$.

Now consider

$$\frac{\int_{\text{Vol}} \gamma_h [(\partial \hat{w}_h / \partial x) - \hat{\beta}_h] d\text{Vol}}{\|\hat{\mathbf{v}}_h\|} = \sqrt{\int_{\text{Vol}} (\gamma_h)^2 d\text{Vol}} \quad (4.221)$$

Hence, we have

$$\begin{aligned} \sup_{\mathbf{v}_h \in V_h} \frac{\int_{\text{Vol}} \gamma_h [(\partial w_h / \partial x) - \beta_h] d\text{Vol}}{\|\mathbf{v}_h\|} &\geq \frac{\int_{\text{Vol}} \gamma_h [(\partial \hat{w}_h / \partial x) - \hat{\beta}_h] d\text{Vol}}{\|\hat{\mathbf{v}}_h\|} \\ &= \sqrt{\int_{\text{Vol}} (\gamma_h)^2 d\text{Vol}} \end{aligned} \tag{4.222}$$

with γ_h still a variable. Therefore, for the two-node mixed interpolated beam element we have

$$\inf_{\gamma_h \in P_h(D_h)} \sup_{\mathbf{v}_h \in V_h} \frac{\int_{\text{Vol}} \gamma_h [(\partial w_h / \partial x) - \beta_h] d\text{Vol}}{\|\gamma_h\| \|\mathbf{v}_h\|} \geq 1 \tag{4.223}$$

and the inf-sup condition is satisfied.

We can also apply the inf-sup eigenvalue test to the two-node beam elements. The equations used are those presented for the elasticity problem, but we use the spaces of the beam elements (see Exercise 4.63). Figure 4.27 shows the results obtained. We note that in (4.207) the smallest nonzero eigenvalue of the pure displacement-based discretization approaches zero as the mesh is refined, whereas the mixed interpolated beam element meshes give an eigenvalue that equals 1.0 for all meshes [which corresponds to the equal sign in (4.223)].

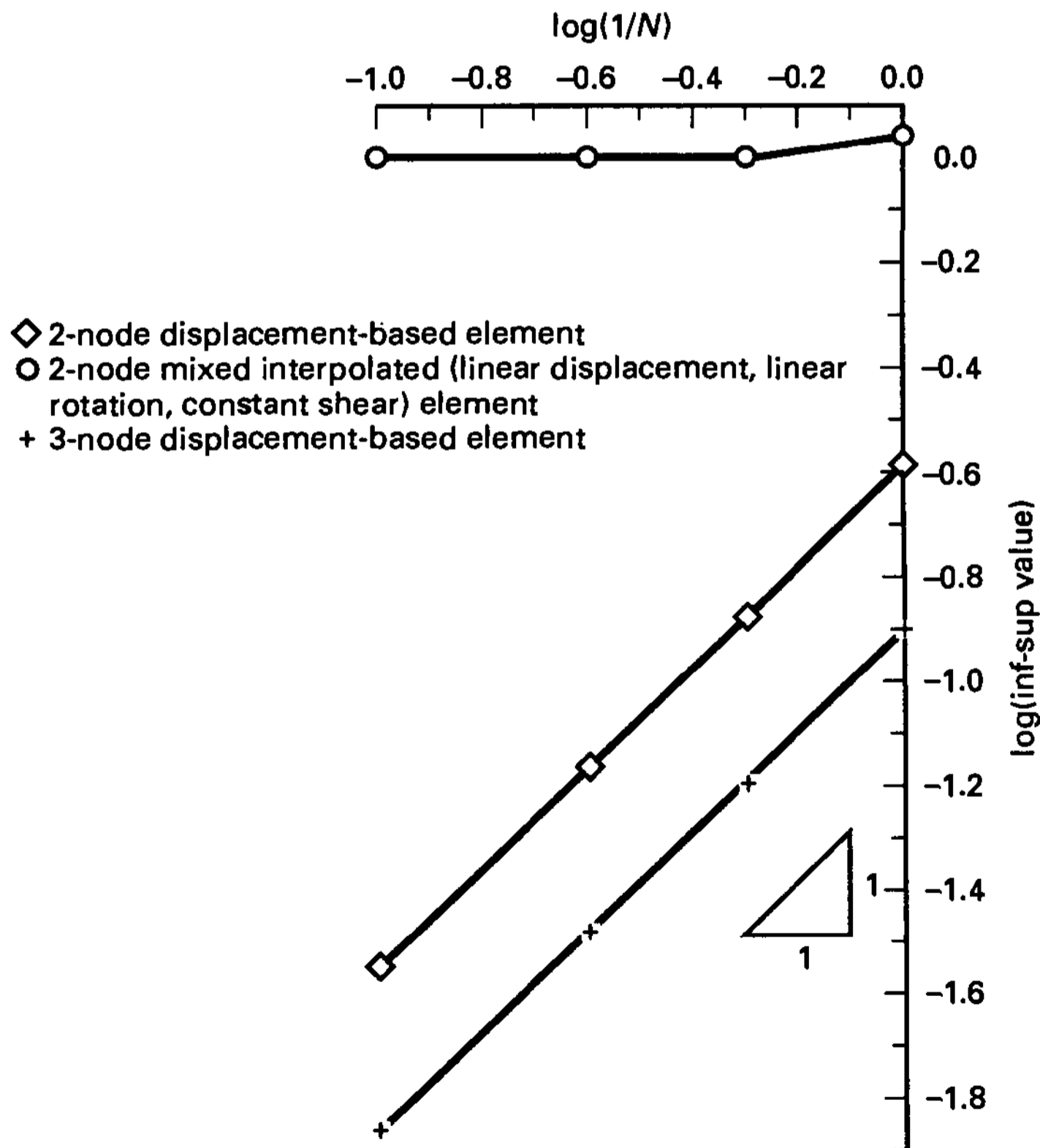


Figure 4.27 Inf-sup test of beam elements (a cantilever beam is considered)

Higher-order mixed interpolated beam elements can be analyzed in the same way as the two-node elements (see Exercise 4.62). Figure 4.27 also shows the results obtained for the three-node pure displacement-based element with the numerical inf-sup test.

4.5.8 Exercises

4.47. Prove that $\| \mathbf{u} - \mathbf{u}_h \| \leq \bar{c} d[\mathbf{u}, K_h(0)]$ is always true, where \mathbf{u}_h is the finite element solution and $K_h(0)$ is defined in (4.159). Use that

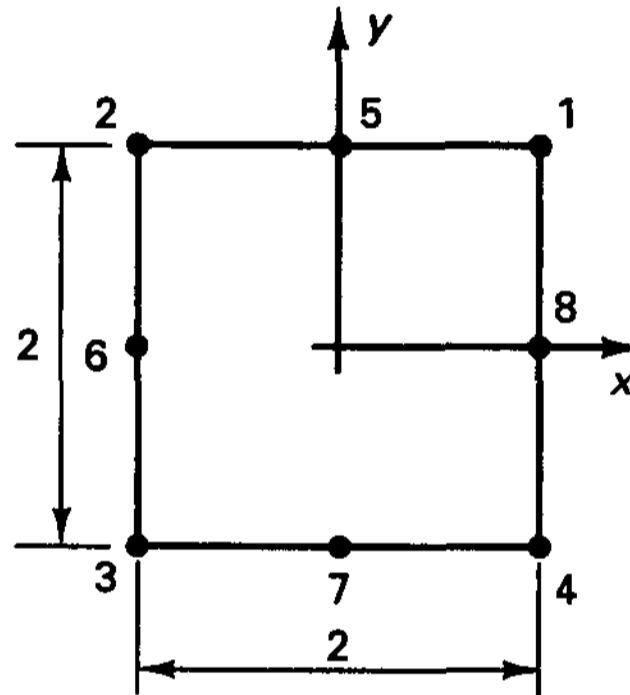
$$\exists \alpha > 0 \text{ such that } \forall \mathbf{v}_h \in K_h(0), a(\mathbf{v}_h, \mathbf{v}_h) \geq \alpha \| \mathbf{v}_h \|^2$$

$$\exists M > 0 \text{ such that } \forall \mathbf{v}_{h1}, \mathbf{v}_{h2} \in V_h, |a(\mathbf{v}_{h2}, \mathbf{v}_{h1})| \leq M \| \mathbf{v}_{h1} \| \| \mathbf{v}_{h2} \|$$

and the approach in (4.94). Note that the constant \bar{c} is independent of the bulk modulus.

4.48. Prove that $\| \text{div}(\mathbf{v}_1 - \mathbf{v}_2) \|_0 \leq c \| \mathbf{v}_1 - \mathbf{v}_2 \|_V$. Here $\mathbf{v}_1, \mathbf{v}_2 \in V_h$ and c is a constant.

4.49. Evaluate $P_h(\text{div} \mathbf{v}_h)$ for the eight-node element shown assuming a constant pressure field over the element.



4.50. Evaluate the stiffness matrix of a general 3/1 triangular u/p element for two-dimensional analysis. Hence, the element has three nodes and a constant discontinuous pressure is assumed. Use the data in Fig. E4.17 and consider plane stress, plane strain, and axisymmetric conditions.

- (a) Establish all required matrices using the general procedure for the u/p elements (see Example 4.32) but do not perform any matrix multiplications. Consider the case κ finite.
- (b) Compare the results obtained in Example 4.17 with the results obtained in part (a).
- (c) Give the u/p element matrix when total incompressibility is assumed (hence static condensation on the pressure degree of freedom cannot be performed).

(Note: This element is not a reliable element for practical analysis of (almost) incompressible conditions but is merely used here in an exercise.)

4.51. Consider the 4/1 element in Example 4.32. Show that using the term $P_h(\text{div} \mathbf{v}_h)$ (evaluated in Example 4.34) in (4.179), we obtain the same element stiffness matrix as that found in Example 4.32.

4.52. Consider the 9/3 element in Example 4.36; i.e., assume that $Q_h = [1, x, y]$. Assume that corresponding to \mathbf{v}_h the nodal point displacements are

$$\begin{aligned} u_1 &= 1; & u_2 &= -1; & u_3 &= -1; & u_4 &= 1; & u_6 &= -1; & u_8 &= 1 \\ v_1 &= 1; & v_2 &= -1; & v_3 &= -1; & v_4 &= 1; & v_6 &= -1; & v_8 &= 1 \end{aligned}$$

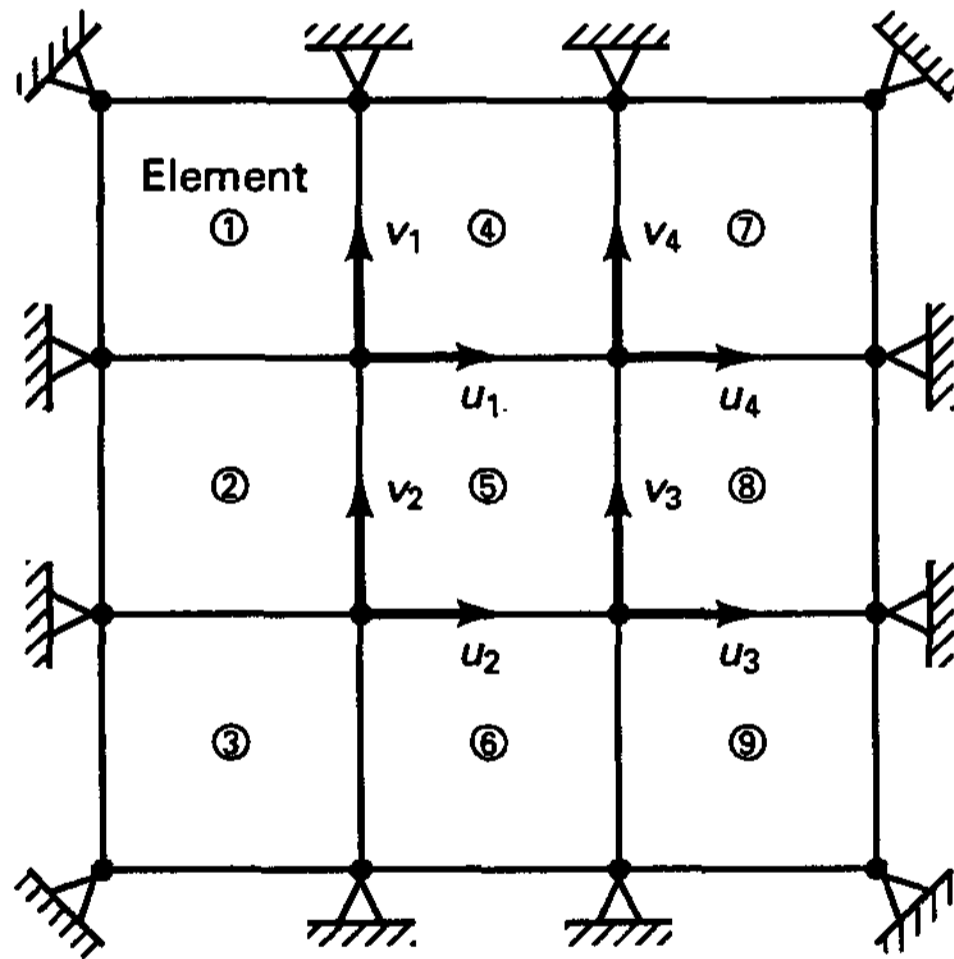
with all other nodal point displacements zero. Calculate the projection $P_h(\text{div} \mathbf{v}_h)$.

- 4.53. Show that the 8/1 u/p element satisfies the inf-sup condition (and hence discretizations using this element will not display a spurious pressure mode). For the proof refer to Example 4.36.
- 4.54. Consider the solution of (4.187) and show that the conditions i and ii in (4.188) and (4.189) are necessary and sufficient for a unique solution.
- 4.55. Consider the ellipticity condition in (4.192). Prove that this condition is satisfied for the 4/1 element in two-dimensional plane stress and plane strain analyses.
- 4.56. The constant pressure mode, $p_0 \in Q_h$, in a two-dimensional square plane strain domain of an incompressible material modeled using four 9/3 elements with all boundary displacements set to zero is not a spurious mode (because it physically should exist). Show that this mode is not an element of $P_h(D_h)$.
- 4.57. Consider the 4/1 element. Can you construct a two-element model with appropriate boundary conditions that contains a spurious pressure mode? Explain your answer.
- 4.58. Consider the nine 4/1 elements shown. Assume that all boundary displacements are zero.
 - (a) Pick a pressure distribution \hat{p}_h for which there exists a vector \mathbf{v}_h such that

$$\int_{\text{Vol}} \hat{p}_h \operatorname{div} \mathbf{v}_h \, d\text{Vol} > 0$$

- (b) Pick a pressure distribution \hat{p}_h for which any displacement distribution \mathbf{v}_h in V_h will give

$$\int_{\text{Vol}} \hat{p}_h \operatorname{div} \mathbf{v}_h \, d\text{Vol} = 0$$



- 4.59. Consider the u/p -c formulation.
 - (a) Show that the inf-sup condition can be written as in (4.206) but that $\mathbf{G}_h = (\mathbf{K}_{up})_h \mathbf{T}_h^{-1} (\mathbf{K}_{pu})_h$.
 - (b) Also, show that, alternatively, the eigenproblem

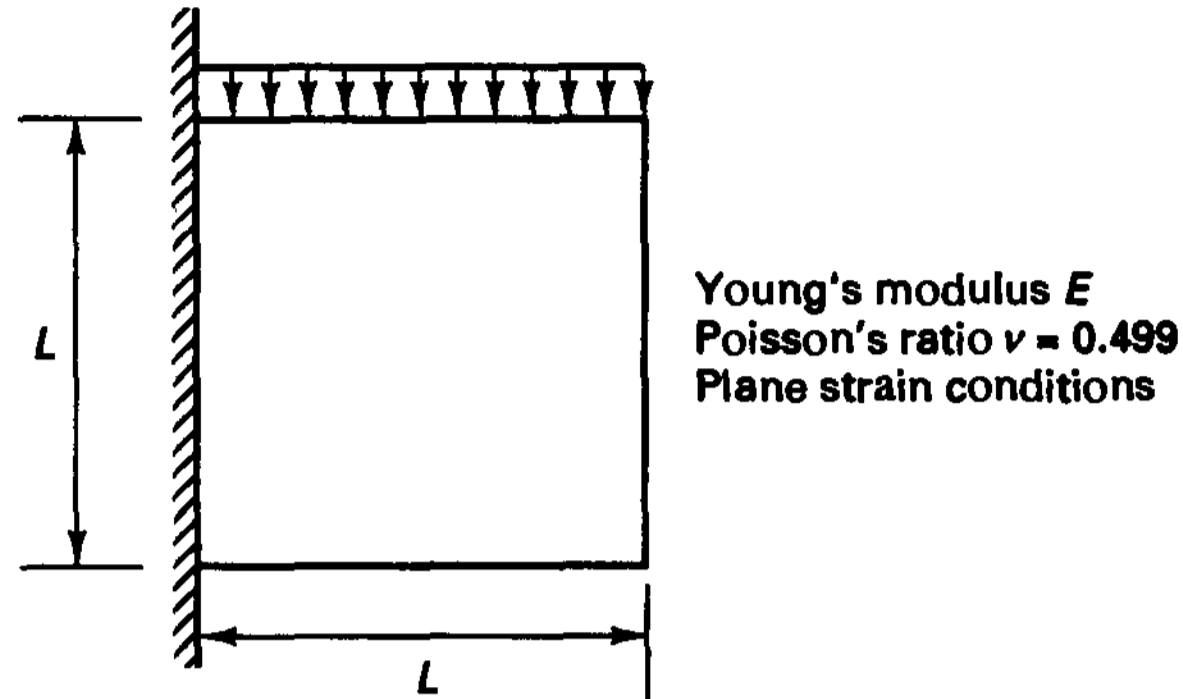
$$\mathbf{G}'_h \mathbf{Q}_h = \lambda' \mathbf{T}_h \mathbf{Q}_h \tag{a}$$

can be considered, where $\mathbf{G}'_h = (\mathbf{K}_{pu})_h \mathbf{S}_h^{-1} (\mathbf{K}_{up})_h$, and that the smallest nonzero eigenvalues of (a) and (4.207) are the same.

Here \mathbf{T}_h is the matrix of the L^2 -norm of p_h ; that is, for any vector of nodal pressures \mathbf{P}_h , we have $\|p_h\| = \mathbf{P}_h^T \mathbf{T}_h \mathbf{P}_h$; hence $\mathbf{T}_h = -\kappa(\mathbf{K}_{pp})_h$.

- 4.60. Consider the analysis of the cantilever plate in plane strain conditions shown. Assume that the 3/1 u/p element is to be used in a sequence of uniform mesh refinements. Let n_u be the number

of nodal point displacements and n_p the number of pressure variables. Show that as the mesh is refined, the ratio n_u/n_p approaches 1. (This clearly indicates solution difficulties.)



Calculate the same ratio when the 9/3 and 9/8-c elements are used (the 9/8-c element is defined in Table 4.8) and discuss your result.

- 4.61. Show that the mixed interpolated two-, three-, and four-node beam elements satisfy the ellipticity condition. The two-node element was considered in Section 4.5.7, and the three- and four-node elements are discussed in Section 5.4.1 (see also Exercise 4.62).
- 4.62. Show analytically that the inf-sup condition is not satisfied for the three- and four-node displacement-based beam elements and that the condition is satisfied for the mixed interpolated beam elements with γ_h varying, respectively, linearly and parabolically (see Section 5.4.1).
- 4.63. Establish the eigenvalue problem of the numerical inf-sup test for the beam elements considered in Section 4.5.7. Use the form (4.207) and define all matrices in detail.
- 4.64. Consider the problem in Fig. 4.24 and the elements mentioned in Table 4.8. Calculate, for each of these elements, the constraint ratio defined as the number of displacement degrees of freedom divided by the number of pressure degrees of freedom as the mesh is refined, that is, as $h \rightarrow 0$. Hence note that this constraint ratio alone does not show whether or not the inf-sup condition is satisfied.